An investigation of elbow loading in one-handed tennis backhand groundstrokes using computer simulation

AN INVESTIGATION OF ELBOW LOADING IN ONE-HANDED TENNIS BACKHAND GROUNDSTROKES USING COMPUTER SIMULATION

by

Jonathan Alexander Glynn

A Doctoral Thesis

Submitted in partial fulfilment of the requirements for the award of Doctor of Philosophy of Loughborough University

April 2007

ABSTRACT

An investigation of elbow loading in one-handed tennis backhand groundstrokes using computer simulation

Jonathan Alexander Glynn, Loughborough University, 2007

A 3D subject-specific computer simulation model of a ball-racket system linked to an upper-limb and torso was developed to investigate factors which may result in adverse loading at the elbow during one-handed backhand groundstrokes. Rigid hand, forearm, upper-arm and torso segments were driven by joint angle time histories obtained from backhand performances. Wobbling mass segments were incorporated to represent soft tissue motion. The upper-limb model was attached to a forward dynamics model of the racket-ball system using spring-dampers at the thenar and hypothenar eminences of the hand. The racket frame was represented using two rigid bodies with two torsional spring-dampers to allow motion in and out of the racket plane. The stringbed was represented by nine point masses connected using elastic springs. A point mass representation of the tennis ball allowed normal and oblique impacts at the nine locations on the stringbed. Inertia parameters for the elite tennis player and the rackets and visco-elastic parameters for the rackets and ball were determined from independent experimental tests. Visco-elastic parameters for the hand and wobbling masses were determined within the matching process of six backhand trials. Excellent agreement between performance and matching simulations was obtained with a mean RMS difference of 1.3% based on racket kinematics, outbound ball velocity and time of ball contact. Simulation results suggest that the inertia and stiffness parameters of the racket frame and the stringbed tension have a relatively small influence on elbow loading within current design ranges. In contrast, the off-centre ball impact simulations resulted in an 11% increase in peak internal elbow joint force, a 22% increase in peak pronation-supination net torque and a 19% increase in peak elbow-flexion extension net torque around the elbow joint. This research suggests that racket frame vibration is an unlikely mechanism for tennis elbow and that an accumulation of peak loads from off-centre hits is a more likely cause.

PUBLICATIONS

Conference Presentations:

Glynn, J. A., King, M. A., and Mitchell, S. R. (2006). *Investigating elbow loading using a computer simulation model of a one-handed tennis backhand.* In M. Hiley, M. King, M. Pain, F. Yeadon (Ed.), Proceedings of the Biomechanics Interest Group, Number 22 (pp.7). Loughborough, UK: Loughborough University.

Glynn, J. A., King, M. A., and Mitchell, S. R. (2006). *Determining subject-specific parameters for a computer simulation model of a one-handed tennis backhand.* In H. Schwameder, G. Strutzenberger, V. Fastenbauer, S. Lindinger, E. Müller (Ed.), XXIV International Symposium on Biomechanics in Sports, Volume 2 (pp.14-18). Salzburg, Austria: University of Salzburg.

Glynn, J. A., King, M. A., and Mitchell, S. R. (2006). *The effect of tennis ball impact location on forces at the elbow during one-handed backhand strokes.* In J. Vanrenterghem, A. Lees (Ed.), Proceedings of the Biomechanics Interest Group, Number 23 (pp.12). Liverpool, UK: Liverpool John Moores University.

ACKNOWLEDGEMENTS

My research experience here at Loughborough has been a very enjoyable one. I would like to express my gratitude to my supervisors Dr Mark King and Dr Sean Mitchell for making this possible and for their support and guidance. I would also like to acknowledge the financial support of the School of Sport and Exercise Sciences and Head AG.

I wish to thank my friends and colleagues, past and present, in the sports biomechanics research group (Fred, Mike, Matt, Lesley, Veni, Chris, Emma, Behzat, Andy, Sam, Pete, Steph, Felix, Adaffi and Helen) and everyone else who comes for coffee (Jo, Sarah, Alec and George). All of you have helped at some point during the course of my studies. Particular thanks must go to Jim'll for his assistance in making the computer graphics, to Jim May who kindly agreed to be my subject in this study and to Andy Statham who helped during the performance data collection process.

Special mention must go to my family for their love and encouragement throughout my years here at Loughborough. Finally, I must refer to the most important person in my life. Even writing a thesis did not seem daunting with her love and support. Thanks for being the best girlfriend in the world Cec.

DEDICATION

To my beautiful Prin'Cec

and

my family

TABLE OF CONTENTS

LIST OF FIGURES

LIST OF TABLES

CHAPTER 1

INTRODUCTION

1.1 CHAPTER OVERVIEW

This chapter provides a general overview of the area of study focussing on loading at the elbow when performing one-handed backhand groundstrokes. Previous research relevant to this field, both experimental and theoretical, is summarised. The statement of purpose and specific research questions to be addressed are presented.

1.2 THE AREA OF STUDY

In recent years, tennis injuries and in particular 'tennis elbow' (TE), have become a primary concern for tennis equipment manufacturers as the application of science and research has pushed technology to its limits. TE is an umbrella term describing medial and lateral elbow pain caused by a variety of activities from plumbing to shaking hands (McLaughlin & Miller, 1980). In 1902, Clado found lateral epicondylitis in top French tennis players, and for the first time the condition was connected with the name 'tennis elbow'. Interestingly, Roetert et al. (1995) suggest that 40 to 50% of recreational tennis players will be affected at some stage, although it is generally acknowledged that elite tennis players do not suffer from this condition (Blackwell & Cole, 1994).

Most teaching professionals attribute TE among the population of recreational players to poorly performed backhand strokes (McLaughlin & Miller, 1980). In particular, research has found that more than 90% of TE results from 'improper movements' of the one-handed backhand groundstoke (Ellenbecker, 1995). The process of co-ordinating multiple body parts is further complicated by ball and stringbed deformations and subsequent vibrations of the racket frame.

Although there is general agreement as to its pathology, citations for the aetiology of TE are many and varied. Biomechanical evidence would appear to suggest that the initial impact shock wave is the most likely cause of TE (Knudson, 2004). However, there is relatively little known about the effects of

perturbing racket parameters and ball impact characteristics on loading at the elbow joint and the associated potential for injury to the performer.

1.3 PREVIOUS RESEARCH

Previous research concerning the tennis one-handed backhand groundstroke has been both experimental (the collection of data from an actual performance) and theoretical (mathematical and computer simulation models). In the past, experimental studies have used high-speed cinematography (e.g. Elliott et al., 1989) and more recently automatic tracking systems (e.g. Wang, 1998). Measurement inaccuracy in kinematic studies due to low frame rates and insufficient camera numbers has typically prevented the derivation of joint torques and forces (Wu et al., 2001). To examine factors such as hand forces (Knudson, 1991a), force sensing resistors have been used whilst tennis racket accelerations have been monitored using accelerometers attached to the racket frame (e.g. Hennig et al., 1992).

The major difficulties of studying the upper extremity kinetics have been the measurement of impact forces during actual performances (Wu et al., 2001) and the understanding of how impact force is distributed throughout the hand-arm system (Roetert et al., 1995). Experimental research in tennis has been hampered by the complexity of strokes and the short contact phase of the ball on the stringbed (Schlarb et al., 1998). Researchers have been unable to draw firm conclusions on the effect of perturbing racket parameters under experimental conditions as changes to one variable, such as racket mass, have inadvertently introduced changes to another, such as technique.

To overcome these problems, mathematical models (e.g. Hatze, 1976) and more recently computer simulation models (e.g. Glitsch et al., 1999) have been developed. The tennis player was typically modelled as a series of rigid bodies linked by simple pin joints (e.g. Nesbit et al., 2006). The racket frame has been modelled with differing levels of complexity depending on the number of dimensions used and whether the human has been considered as part of the system. Stringbed and balls have typically been modelled as flexible bodies when human interaction with the racket handle has been ignored (e.g. Casolo & Lorenzi, 2000). Where the tennis player has also been considered as part of the system, the racket has often been fixed

to the hand segment and not actively gripped (e.g. Nesbit et al., 2006) resulting in unrealistic inputs to the arm.

Nesbit et al. (2006) have suggested racket inertia parameters and the location of ball impact may appreciably affect loading at the elbow, whilst racket frame vibration is sensitive to its stiffness and the aforementioned variables. However, the predicted relative effects of these parameters must be treated with caution as model features such as racket frame vibration, variable grip pressure and anatomical damping in the system have been neglected. Further research is needed to obtain a clearer understanding of how loading from tennis ball impacts during a one-handed backhand groundstroke is transmitted to the upper-limb system.

1.4 STATEMENT OF PURPOSE

The intention of this study is to achieve a better understanding of the factors which may increase the loading at the elbow joint when performing one-handed tennis backhand groundstrokes. In particular, it is hoped to advance knowledge concerning the aetiology of TE. It is of interest to know how the joint reaction forces and the net joint torques experienced at the wrist and elbow joints are affected by the inertia and visco-elastic properties of the tennis racket frame. The effects of perturbing the ball impact location on the stringbed and the stringbed stiffness on the loading transmitted to the upper limb are also of concern. To facilitate this a computer simulation model of one-handed backhand groundstrokes was developed. Following satisfactory evaluation, the model was used to address the following research questions.

1.5 RESEARCH QUESTIONS

Q1. How do the inertia and the stiffness and damping properties of the tennis racket frame affect elbow loading in one-handed tennis backhand groundstrokes?

Research into tennis injuries has been hampered by the difficulty of isolating racket parameters, to measure the effect of changing them, when the player is also involved. "No one has done any real experiments to determine a racket's influence on injury. Until someone comes up with a way of measuring it, we're stuck with anecdotal evidence." (Brody, 1997)

Theoretical approaches (e.g. Nesbit et al., 2006) have suggested that racket mass centre inertia values may noticeably affect the torques experienced at the elbow although such results must be treated with caution due to the omission of potentially important model features such as racket frame vibration.

In a review of modern tennis equipment, Miller (2006) notes that a link has been proposed between the increased stiffness of modern rackets causing faster racket frame vibration and an increased susceptibility to TE. Segesser (1985) suggested that vibrations of the racket frame in the region of 80 to 200 Hz are likely to contribute to the development of TE. Whilst manufacturers are keen to point out that their rackets dampen out frame vibrations quickly, the vibrations are damped out significantly faster when the racket is hand-held (Brody, 1989).

Q2. How does the location of the ball impact on the stringbed and the stringbed stiffness affect elbow loading in one-handed tennis backhand groundstrokes?

The forces generated by ball-racket impact, especially off-centre impacts, have been identified as a factor that may contribute to the development of TE (Hennig et al., 2002). When the impact of the ball on the racket is not along the longitudinal axis of the racket frame, the racket will rotate around that axis. This creates a moment around the wrist which must be resisted by the forearm musculature. Knudson (1991a) suggests rackets that minimise the effects of off-centre impacts should be considered as an intervention to reduce the risk of TE.

It is widely accepted that an increase in string tension results in a decrease in ball contact time and outbound velocity with the advantage of greater hitting accuracy. Increased string tension is likely to contribute to an increase in the initial shock after ball impact due to the shorter ball-stringbed contact time (Hennig, 1992). String tension may also affect off-centre impacts since rackets strung at a higher tension rotate less on impact (Brody et al., 2002).

Q3. Does the rigid body recoil of the racket or its modal response have the greater influence on the loading components at the elbow?

This is an important question as it may indicate the mechanism of injury. If initial forces and torques from impulsive loading are dominant, this would support

research suggesting that high eccentric loading of the wrist extensor muscles may be the cause of TE (Blackwell & Cole, 1994). If vibration forces are dominant, the vibration of the racket frame could be the primary cause of TE (Knudson, 2004). To address this question the model needs to incorporate the modal response of the racket frame, variable grip force, and anatomical damping (Nesbit et al., 2006).

1.6 CHAPTER ORGANISATION

Chapter 2 critically reviews the literature relating to studies on the analysis of one-handed tennis backhand groundstrokes. There is also a review of the literature relating to the techniques of investigation within the field of performance related sports biomechanics, relevant to this study.

Chapter 3 describes the features of the computer simulation model that has been developed. Details of how the racket frame, the stringbed and the tennis ball were modelled are included. The human upper-limb model is described and details of the wobbling mass models and racket-hand interface are presented. Features of the angle-driven model are then introduced.

Chapter 4 describes the equipment and protocol that was used to collect kinematic and kinetic data for an elite subject performing one-handed tennis backhand groundstrokes. The techniques used to obtain the subject-specific inertia and gripping parameters for the elite subject, required as input to the simulation model, are also detailed.

Chapter 5 details the methods used to calculate the stiffness and damping properties of the tennis ball, stringbed and racket frame models. There is also a description of how the inertia parameters of the tennis racket were obtained.

Chapter 6 outlines the procedure used for the evaluation of the angle-driven simulation model including the results of this process. The results from simulations using the model are presented and direct comparisons are made between trials matched to actual performances. A sensitivity analysis is then performed to examine the effects of model parameters on the observed output.

Chapter 7 discusses the results of this study and applies them to answering the research questions posed in this chapter. A discussion of the limitations of the study and suggestions for future research are included.

CHAPTER 2

LITERATURE REVIEW

2.1 CHAPTER OVERVIEW

This chapter comprises two main sections. Firstly, there is a review of the literature that has focussed on the one-handed tennis backhand groundstroke. Appraisals of injury to the upper extremity of tennis players and key aspects of the ball-racket-arm system with a view to creating a computer simulation model are given. Secondly, the techniques of investigation required to develop a subject-specific computer simulation model of one-handed tennis backhand groundstrokes are discussed. The associated sub-sections include reviews of simulation modelling processes, parameter determination and image analysis.

2.2 THE TENNIS BACKHAND

The backhand, together with the forehand and service, form the cornerstone of tennis stroke production (Elliott et al., 1989). Historically, the tennis backhand has been defined as the stroke that causes the back of one's hand to be facing the opponent when striking the ball (Roetert & Groppel, 2001). The emergence and popularity of the two-handed backhand have forced some reconsideration of that definition. To account for the vastly different position of the hands on the racket, a more general definition is that a backhand is the stroke where the ball approaches to the left side of a right-handed player.

It is widely accepted that the one-handed backhand requires greater strength on the part of the performer than in the two-handed case (Giangarra et al., 1993). This is due to only one upper-limb being used to generate force when swinging the racket and a decreased rotation of the trunk when compared to the two-handed case (Groppel, 1984). Despite considerable debate as to why, researchers agree that there is a link between poorly performed one-handed backhand groundstrokes and an increased susceptibility to elbow injury.

2.2.1 One-handed backhand technique

Both the slice and topspin one-handed backhand groundstrokes can be broken down into three distinct phases (Figure 2.1):

Phase 1: a racket preparation phase which begins with the first motion of the backswing and ends with the first forward motion of the racket.

Phase 2: an acceleration phase which begins with a forward swing of the racket towards the ball and ends with ball impact.

Phase 3: a follow through phase, beginning with ball impact and followed by a continuous forward movement of the racket following the ball.

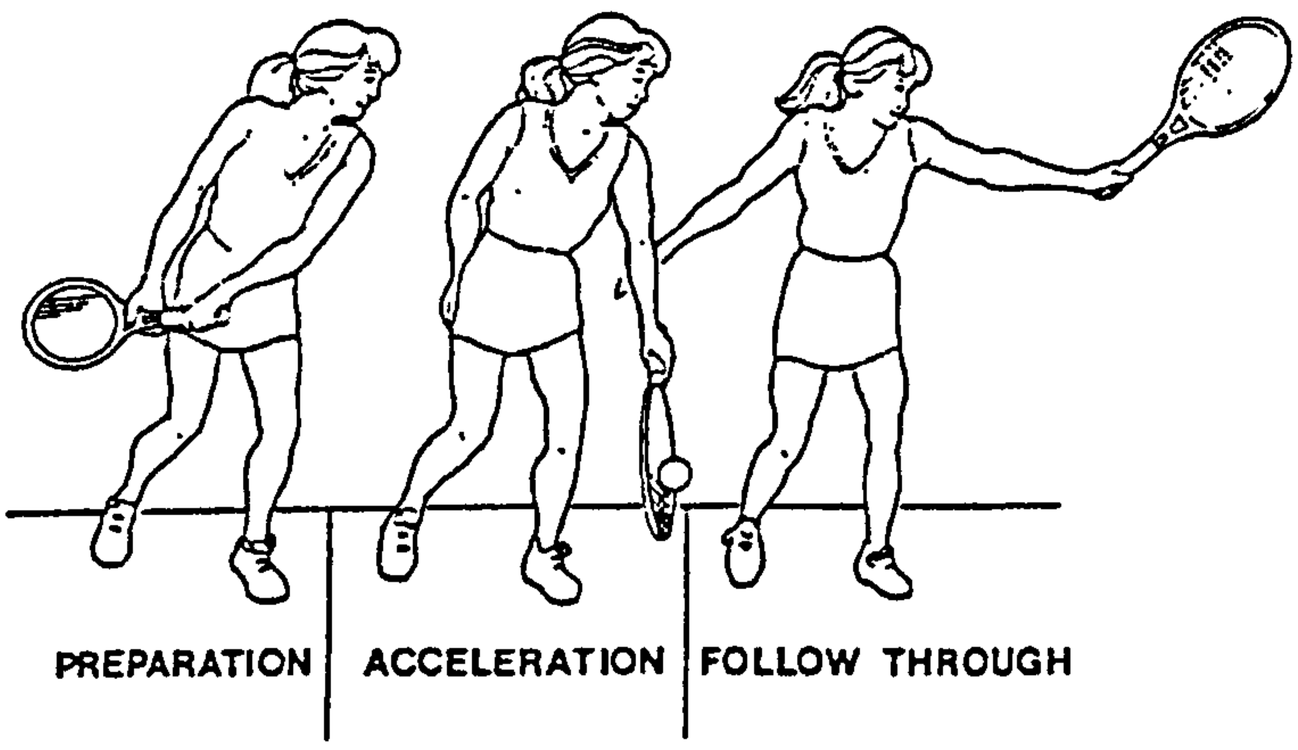

Figure 2.1. Phases of the one-handed tennis backhand groundstroke (adapted from Giangarra et al., 1993, pg. 395)

Traditionally, a player will adopt a closed stance with the body turned sideways to the net. This allows a full backswing and the racket to hit through the line of the ball in the contact zone (Tilmanis, 1975). When the player steps towards the incoming ball, the hips turn slightly, transferring momentum to the trunk, which begins rotating. The upper-arm then moves about the shoulder initiating slight forearm movement, which in turn causes the hand and racket to be correctly positioned for ball contact (Groppel, 1984). Due to the difficulty involved in coordinating the body parts, a recreational player will often rely on the forearm musculature as a power source (Nirschl, 1974).

2.2.2 Upper extremity injuries to tennis players

The upper extremity is thought to be particularly susceptible to injury in tennis because of the repetitive muscular contractions needed to accelerate and stabilise the

dominant limb (Jobe & Nuber, 1986). Due to the relatively low occurrence of wrist injuries amongst tennis players, this area has received little attention in the literature. Wrist injury may occur due to repetitive forceful stroke play or less commonly from the sudden direct impact of the racket handle (Osterman et al., 1988). Wrist tendonitis (inflammation and degeneration of the tendon sheath) is uncommon in tennis, but may occur in novice players with poor stroke mechanics or in advanced players who have excessive wrist motion (Kibler & Chandler, 1994). Shoulder pain is a common complaint amongst tennis players, particularly in the region of the anterior rotator cuff muscles (McCann & Bigliani, 1994). Injury can occur from the adverse stresses during the serve and overhead motions, where the acromion bone on top of the shoulder impinges on the rotator cuff. However, elbow injury in tennis has received by far the most attention.

2.2.3 A specific injury: Tennis elbow

Epidemiology of tennis elbow

Tennis elbow (TE) is an umbrella term that describes pain localised on the inside or outside of the elbow from a variety of repetitive motions (McLaughlin & Miller, 1980). Approximately 50% of tennis players can expect to get TE at some time during their tennis lifetime (Kamien, 1992; Priest et al., 1980). Its prevalence in recreational players is well reported (Priest et al., 1980; Roetert et al., 1995) whilst the incidence amongst elite tennis players is extremely low considering their frequency and intensity of play (Blackwell & Cole, 1994). The condition is most common amongst individuals over 35 years of age and cases are generally equal between genders (Renstrom, 1994).

Pain on the medial side of the elbow results from irritation of the common wrist flexor attachment on the medial epicondyle that is usually associated with the vigorous wrist flexion actions in serving or the forehand drive groundstroke (Roussopoulos & Cooke, 2000). Pain on the outside of the elbow is from irritation of the common wrist extensor attachment (lateral epicondyle) that is usually associated with errors in one-handed backhand groundstroke technique (Bernhang et al., 1974; Blackwell & Cole, 1994; Giangarra et al., 1993; Roetert et al., 1995). Due to its relatively high incidence and chronic nature, lateral epicondylitis has received most attention and the term is often used interchangeably with TE.

Tennis players using a two-handed backhand groundstroke rarely develop TE since there are two body parts to coordinate (Roetert et al., 1995) and another arm to absorb more energy from the impact (McCue, 1982). A player with poor one-handed technique will use the wrist stabilising muscles rather than the posterior shoulder musculature to generate power (Akuthota, 2004). This 'leading elbow technique' can cause overuse of the wrist extensors and supinators.

Pathology of tennis elbow

Within the forearm, there are several muscles originating from the lateral epicondyle, which function to extend the wrist. Although any of the common extensor origin tendons may be affected by overuse and repetitive stress, the extensor carpi radialis brevis (ECRB) muscle is most commonly cited. The tendon of the ECRB muscle is comparatively short and wide (Blackwell & Cole, 1994) and may have a poor biomechanical design with respect to the other wrist extensor muscles (Ljung et al., 1999). Micro-tears and scarring occur, although inflammatory cells are rarely found in chronic cases (Akuthota, 2004). The ECRB muscle inserts into the base of the third metacarpal at the centre of the hand (Figure 2.2).

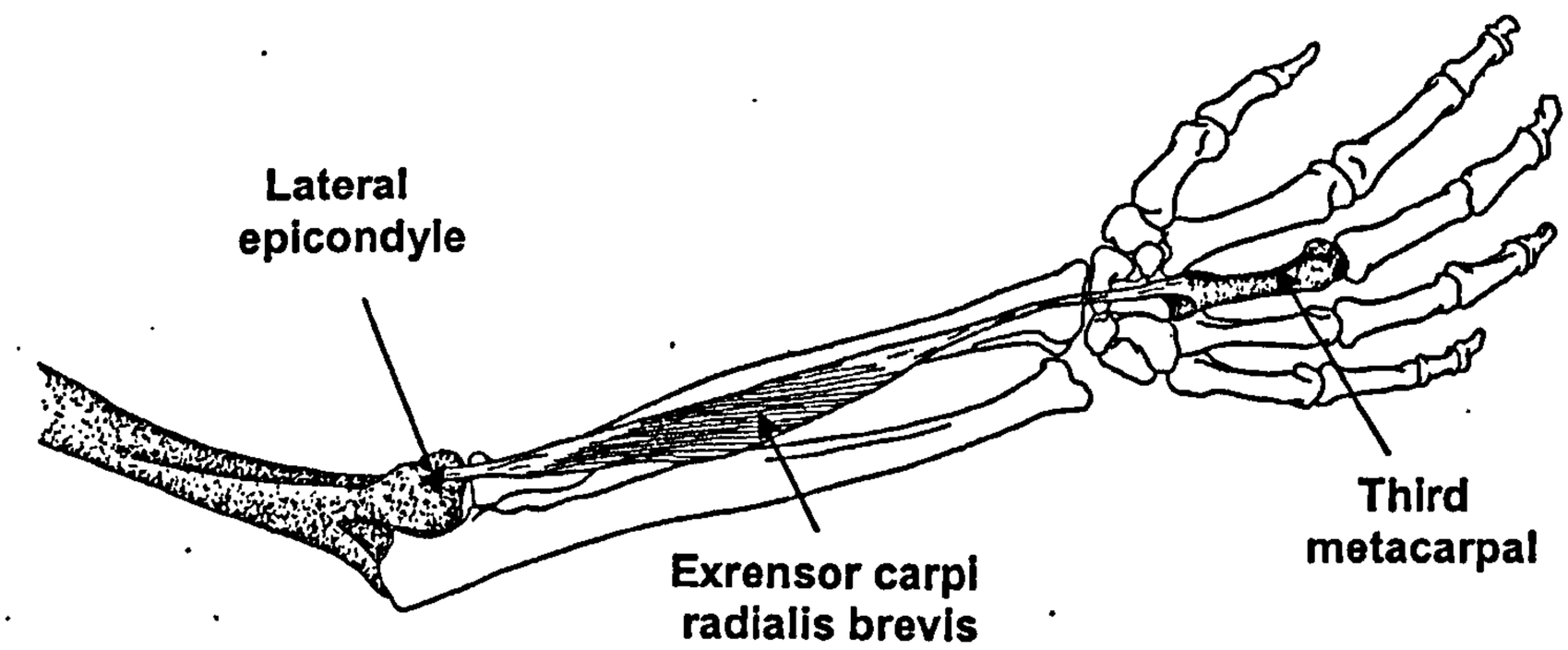

Figure 2.2. Extensor carpi radialis brevis muscle
(adapted from Stone & Stone, 2003, pg. 134)

Aetiology of tennis elbow

Of all tennis injuries, TE has received by far the most attention. However, there appear to be large gaps in the knowledge of its aetiology. The search for the cause of TE has focused on loading from the initial shock wave and the frame

vibrations caused by impact (Knudson, 2004). Roussopoulos and Cooke (2000) suggest the physical stimuli which alone, or in combination, may cause injury:

- A single sharp impulsive stress and strain to the muscles, as from a badly hit ball
- An accumulation of 'normal' or slightly high stresses, from prolonged playing
- A sharp vibration in the loaded muscle, as from a badly hit ball
- An accumulation of many vibrations, each one not in itself dangerous

Published research has been unable to establish whether any or all of these stimuli are responsible. Segesser (1985) suggested that tennis racket oscillations in the range of 80 to 200 Hz are likely to contribute to the development of TE. In contrast, Knudson (1991a) argues that impulsive loading (initial shock) in tennis is the likely mechanism of injury since only these large forces can create the recoil of the racket that rapidly stretches the muscles of the forearm. Studies have demonstrated that muscle damage and muscle soreness are greater after exercise that involves eccentric contractions (Enoka, 1996; Lieber et al., 1991). Alternatively, repetitive concentric contraction of the wrist muscles, shortening as they maintain tension to stabilise the wrist, may produce chronic overload (Roetert et al., 1995). Collectively, the biomechanical and clinical studies would appear to support the impulsive loading theory of tennis elbow as opposed to the vibration theory (Miller, 2006). The factors that may increase the likelihood of injury are more numerous:

Table 2.1. Factors that may increase the likelihood of injury

Racket parameters	Technique	Physiology
Sweet spot size	Grip tightness	Mode of contraction (eccentric)
Stringbed stiffness	Ball impact location	Genetic predisposition
Frame stiffness and damping	Wrist over-extension	Ageing and / or illness
Frame vibration modes and frequencies	Wrist snap	Fatigue induced strength reduction
Frame inertia parameters	Fatigue induced stroke degeneration	Inadequate muscle, bone, and / or tendon development

2.2.4 Modelling the equipment

Numerous researchers have examined the interaction between the equipment and the tennis player with a view to understanding TE. Whilst some have focused on biomechanical aspects of the ball-racket-arm system, including the grip on the racket and the effect of the ball-racket impact on the player's arm, others have examined the physical mechanics of tennis rackets. The following is a review of the literature that has implications for creating a subject-specific computer simulation model of one-handed tennis backhand groundstrokes.

In recent years, the modelling of an impact between a tennis ball and racket has been attempted by many, although few models incorporate the human system as well. The majority have modelled the ball, stringbed and racket frame components separately and then combined them to create a complete model of the system.

The tennis ball

The impact of a tennis ball with strings has been simplified tremendously (e.g. Brannigan & Adali, 1981) and is typically studied for cases where the ball is incident normally on the strings, with ball rotation being neglected (Brody, 1997; Cross, 2000c; Goodwill & Haake, 2000a). The ball has previously been modelled as a point mass to which a spring-damper system is attached (e.g. Goodwill & Haake, 2003; Leigh & Lu, 1992). These viscoelastic models (Nigg & Herzog, 1999) assume that the surface of contact between the ball and strings is simply a plane that intersects the spherical ball. The theory implies that if a spring is displaced a distance x from its equilibrium position and moves with velocity $\dot{x}$, then the restoring force (F) from the spring is governed by Equation 2.1 where k is the spring constant (N/m) and c is the damping coefficient (Ns/m).

$$F = -kx - c\dot{x} \tag{2.1}$$

Arguing that the natural frequency of the ball's vibration has an effect on the coefficient of restitution (COR), Matsuhisa et al. (2004) modelled the ball as two point masses connected by a spring.

Recently, more complex Finite Element (FE) models were developed (e.g. Casolo et al., 1999). The weakness of this approach was that the computational

requirements related to modelling the ball limited the complexity with which the racket frame could then be modelled.

The oblique impact of a tennis ball onto a rigid horizontal surface has previously been modelled using relatively simple Newtonian mechanics (e.g. Brody, 1984) and applying a COR in the vertical direction to account for energy losses in rebound. An assumption of these models was that neither the ball nor the surface deform and the COR is constant. The more complex model by Haake et al. (2003) incorporates features of viscoelastic, impulsive and Newtonian force models. A non-linear spring and damper was used to model the stiffness and energy loss in the shell whilst the model simulates impulsive forces at the front and rear of the ball due to mass in the shell coming to rest. Friction forces acting upon the ball were also accounted for which allowed ball rotation (spin) to be reversed.

The tennis racket

The tennis racket consisting of stringbed and frame sections has been modelled theoretically at various levels of sophistication depending on the number of dimensions used and whether the tennis player was considered as part of the dynamic system.

The stringbed

Viscoelastic models have been used extensively in the modelling of the stringbed (e.g. Goodwill & Haake, 2003; Leigh & Lu, 1992; Maeda & Okauchi, 2002). In the one-dimensional model of Leigh and Lu (1992), the interwoven strings formed a membrane where the tension in each string was the same and did not change with the deflection of the string. In reality, the string becomes stiffer with increasing deflection and the stiffness varies across the face of the racket, being lower at the centreline than the rim. A damping term was considered only as a hypothetical possibility since the strings absorb the incoming ball energy by deforming and returning 95% of that energy back to the ball (Brody, 1995).

In the FE models of Widing and Moeinzadeh (1990) and Casolo et al. (2000), a mesh of two-node cable elements was used to represent the strings. To simplify the models, strings were assumed to be connected at the contact points although this may not always be the case under deformation as strings move relative to each other. Modelling the strings discretely as opposed to a membrane gave the flexibility to

change the string pattern and string tensions. However, this extension limited the models to a static analysis due to the difficulty in constructing and solving a complex model of a dynamic system.

Brody (1988) used a laser and high-speed electronic equipment to determine the effect of string tension on the dwell time (time between ball contact with the strings and separation) for a range of impact speeds. Figure 2.3 shows that with increasing string tension and ball-racket relative speeds, the dwell time decreased. In agreement with other studies (e.g. Cross, 2000a) the impact of the ball with the strings was a very short event, lasting between 4 and 8 ms. Increased string tension is likely to contribute to an increase in the initial shock after ball impact as the increased impulse at ball contact occurs in a shorter time (Hennig, 1992).

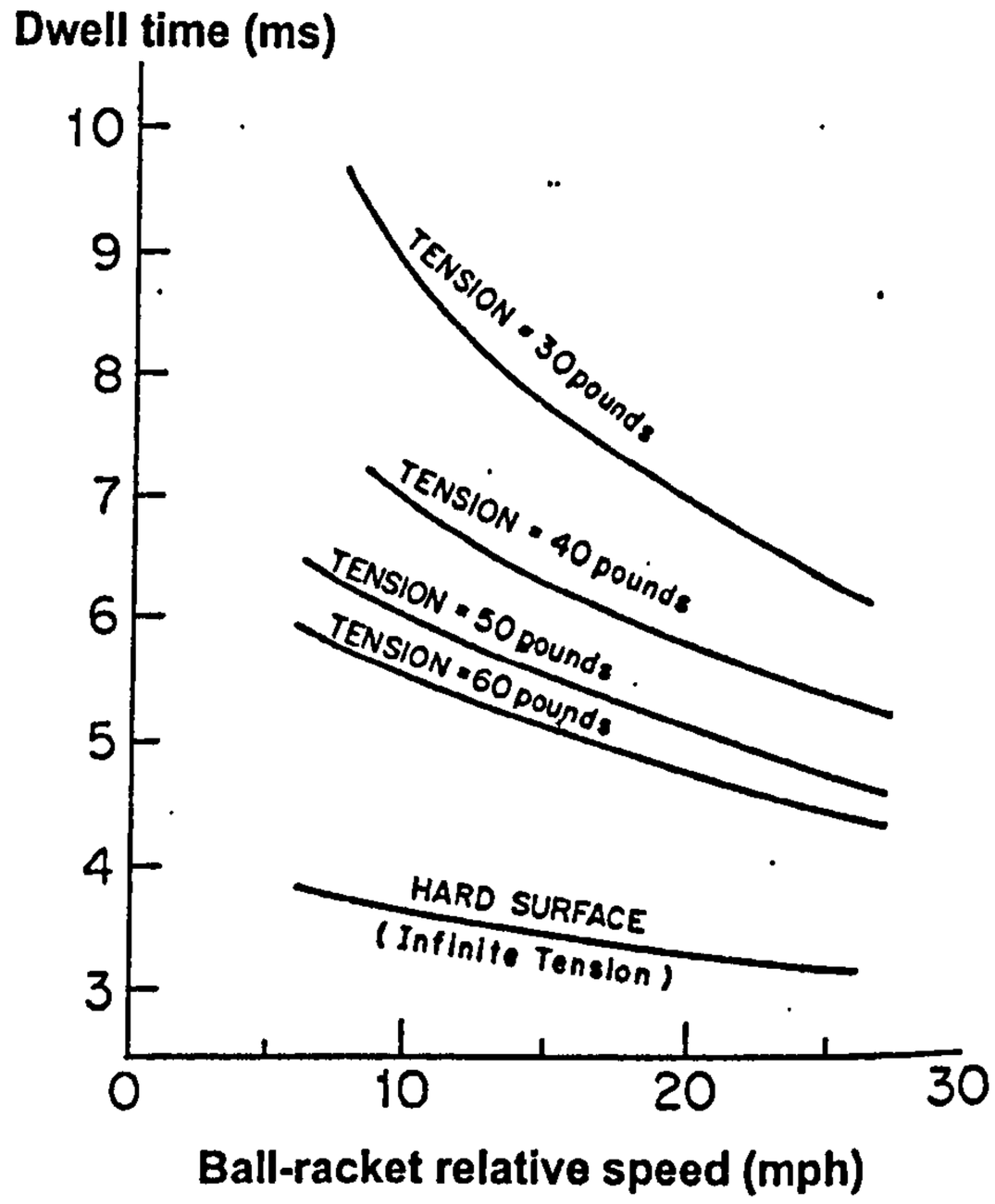

Figure 2.3. Dwell time of the ball on the strings for a range of impact conditions (adapted from Brody, 1988, pg. 12)

Studies have shown (Brannigan & Adali, 1981; Brody, 1979; Groppel et al., 1987; Knudson, 1988) that the rebound velocity of the ball increases with a decrease in string tension, the so-called 'trampoline effect'. Experimental research by Goodwill and Haake (2004) supports a decrease in the dwell time for an increase in

string tension, but results suggest that for the same shot, rebound velocity and ball spin were not dependent on string tension. A simple theoretical model of planar forehand groundstrokes (Kawazoe et al., 2003) suggests that there is no appreciable increase in the predicted shock vibration transmitted to the wrist joint for an increase in initial string tension from 45 to 65 lbs.

The racket frame

The modelling of a tennis racket frame can be divided into two broad sections: rigid beam models and flexible beam models. A rigid beam model has the advantage of requiring fewer parameters. Since modern rackets are so stiff, they can be modelled by treating the frame as a rigid body enclosing a flexible string membrane (Brody, 1997). A major limitation of this approach is that the vibrations of the frame and the associated energy losses are not accounted for. Goodwill and Haake (2003) showed that for impacts along the longitudinal axis, close to the geometric stringbed centre, the rigid beam model agrees well with experimental data, but given a range of impact locations, a flexible beam model offers a closer match (Figure 2.4). Another limitation of rigid beam models is that the effect of altering the material from which the frame is made cannot be observed.

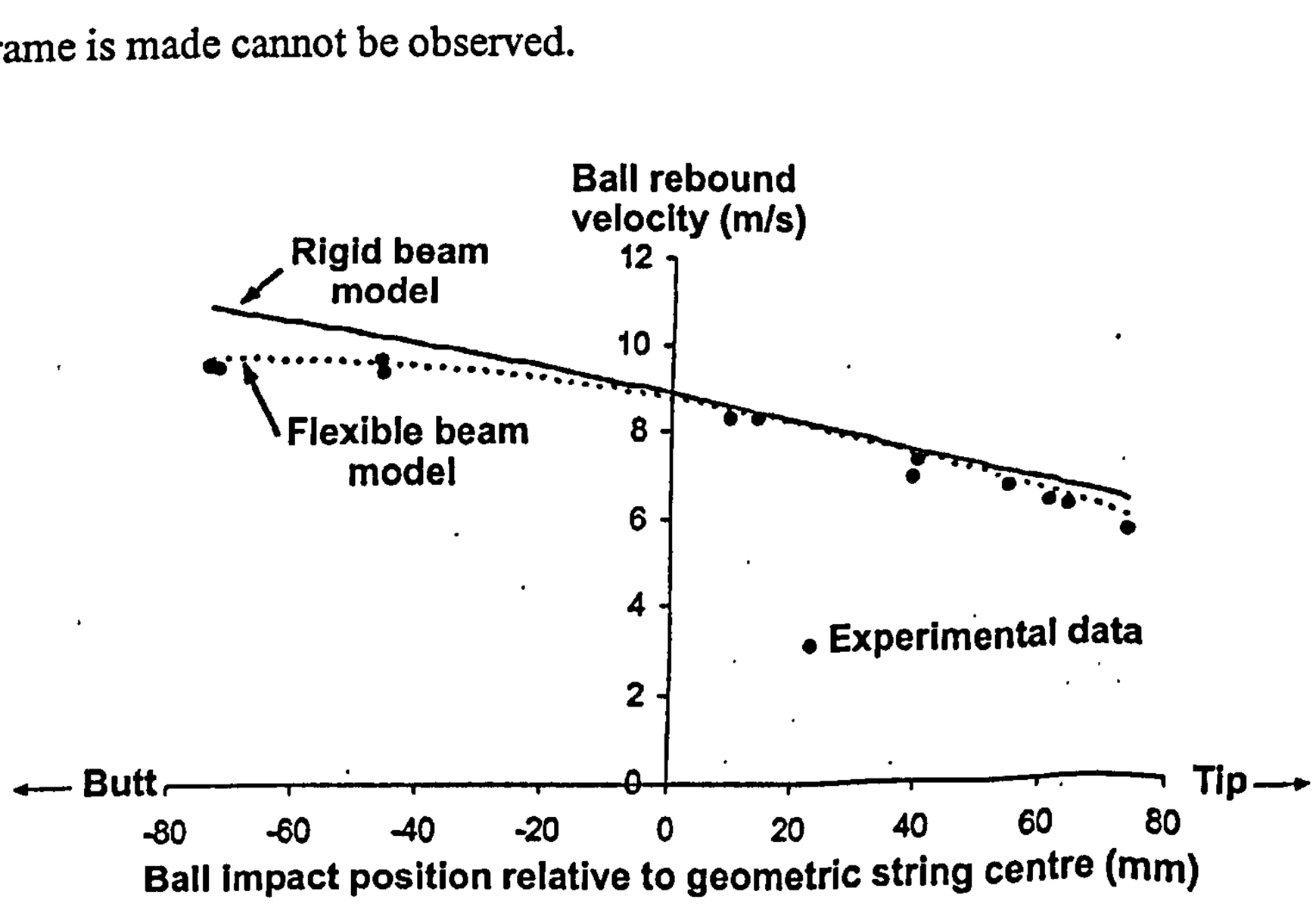

Figure 2.4. Comparison of rigid and flexible beam models in calculating ball rebound velocity (adapted from Goodwill & Haake, 2003, pg. 84)

Most beam models (e.g. Goodwill & Haake, 2000b) have been one-dimensional, modelling only collisions on the longitudinal axis. Two-dimensional models (e.g. Cross, 2000a) have typically assumed that the beam undergoes rigid body rotation about the longitudinal axis when the ball impacts off-centre. Cross argued that this assumption was justified since it had been shown experimentally (Kawazoe, 1997) that the fundamental frequency for torsional oscillations is much higher than that for transverse oscillations. However, Cross is referring to the motion of the ball post-impact and torsional oscillations may be important for the transmission of vibration and forces to the human arm system.

Mathematical models exist (Hatze, 1976; Missavage & Baker, 1984), which are similar in complexity and assume the racket frame to be a flexible beam of non-uniform cross-section. The force acting between the ball and racket is considered to be greatest at the centre of the head decreasing steadily towards the boundary. Brannigan and Adali (1981) developed a more complex FE model that included the parameters of string tension and string configuration although they neglect the deformation of the ball in their equations. Based on the experimental results of Hatze (1976) they modelled the impact force N(t) between the ball and racket as a sine function (Equation 2.2) of ball-stringbed contact time (r).

$$N(t) = F\sin(\pi t/r), F > 0, 0 \le t \le r \qquad (2.2)$$

The FE model of Brannigan and Adali (1981) used elastic beam elements (78 nodes) with a constant cross-sectional area, as well as homogenous mass distribution (Figure 2.5).

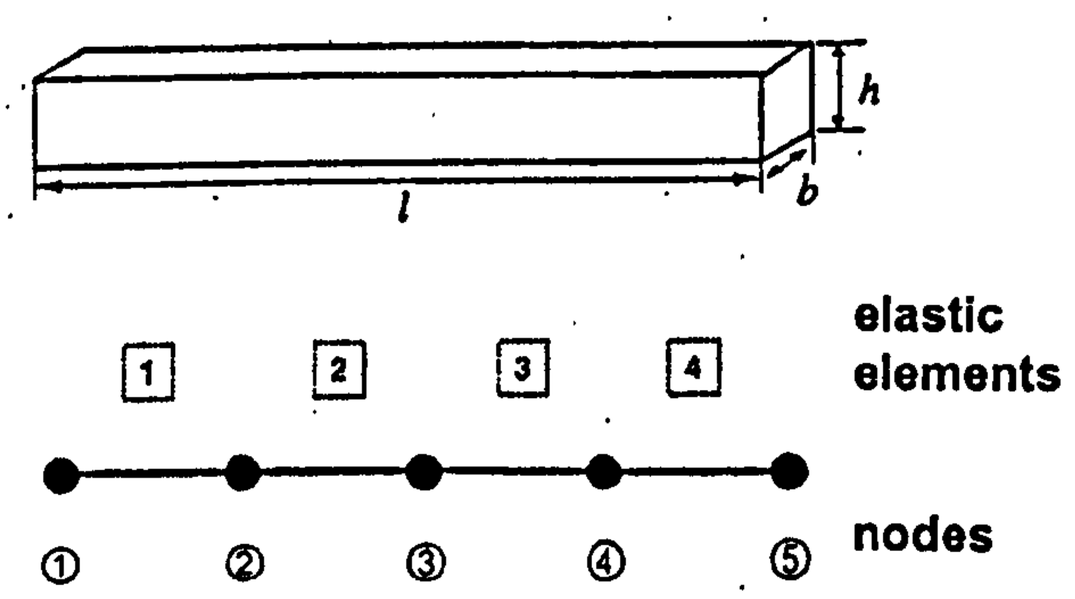

Figure 2.5. Example of an elastic beam used in FE modelling (adapted from Schlarb et al., 1998, pg. 380)

Assuming the frame undergoes small deformations, Casolo et al. (2000) developed a racket frame model using three-dimensional linear beam elements (no mid-side nodes) with two nodes. Other researchers (Glitsch et al., 1999; Widing & Moeinzadeh, 1990) have modelled the racket frame with curved beam elements.

The weakness of the FE approach is that researchers have been forced to use an unrealistic boundary condition (a clamped handle). This restriction is necessary due to the difficulty in modelling dynamic interactions with other bodies. These simulations have typically led to results that do not correspond to the real stroke situation (Schlarb et al., 1998). In an attempt to combine the two approaches, Schlarb et al. (1998) used the results of a FE analysis as input for a flexible racket forward dynamics model. The planar computer model was based on a multiple pendulum consisting of upper-arm, lower arm, hand and racket. Comparison of acceleration profiles at the racket handle (Figure 2.6) showed that the simulation output closely matched the experimental data.

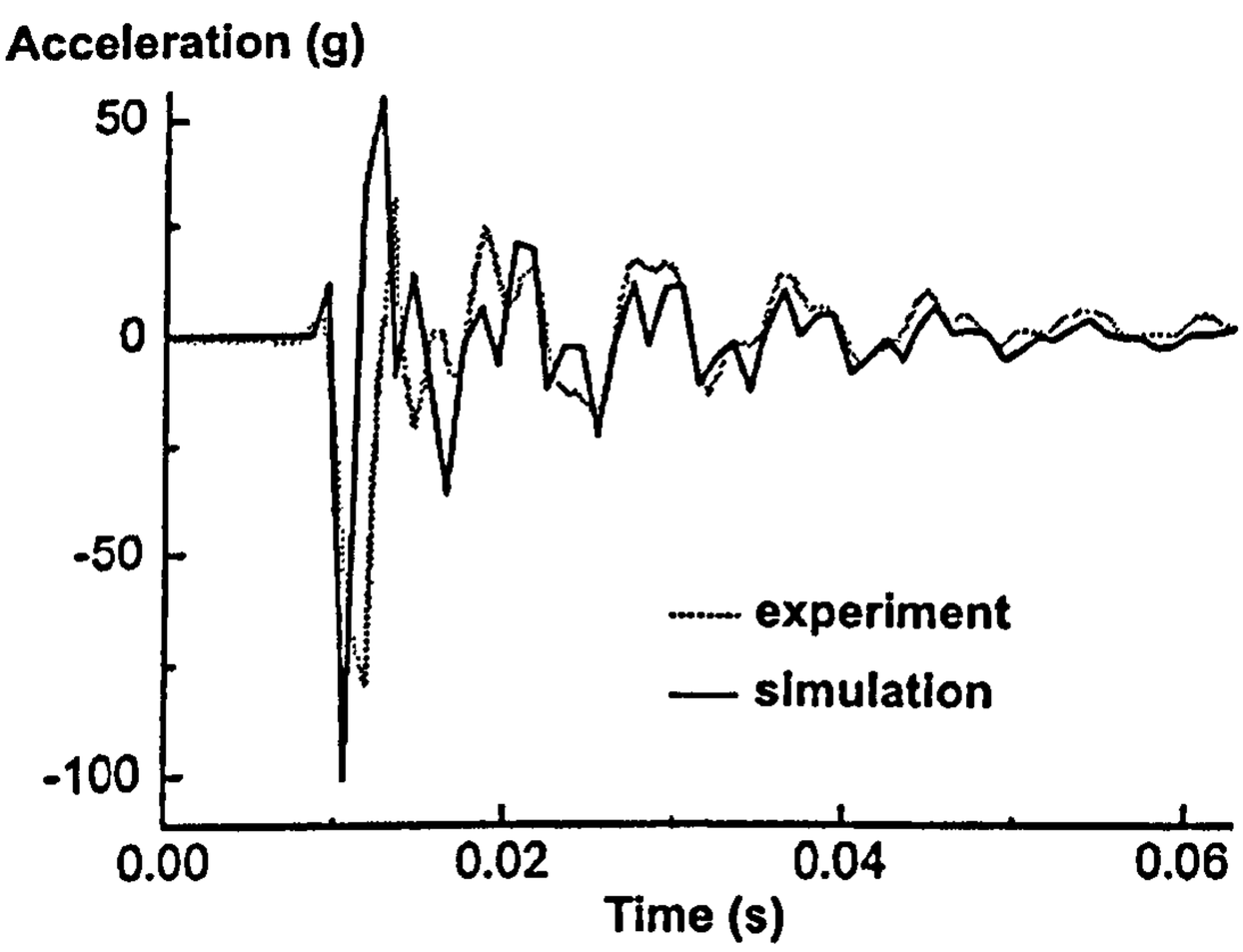

Figure 2.6. Comparison of acceleration profiles at the racket handle (adapted from Schlarb et al., 1998, pg. 381)

2.2.5 Modelling the grip

On the basis of experimental vibration patterns (e.g. Brody, 1989) and computer simulations (e.g. Schlarb et al., 1998), it has been suggested that the 'freely gripped' racket best approximates real play results. The main arguments presented to support this model are that (a) the hand has only a small effect on racket vibration, and (b) the ball will leave the strings before the impulse is transmitted along the

racket frame to the hand (Brody, 1997; Cross, 1998). However, only the combination of this racket with a suitable hand-racket connection can simulate a real tennis stroke and the inputs to the human system. No definitive conclusions have emerged as yet on how to properly interconnect human and racket models (Nesbit et al., 2006).

The mechanical coupling of the racket handle with the body is changed with each modification of grip force (Nab et al., 1998). Consequently, there have been few attempts to model the interaction between the human hand and the handle of the tennis racket in any detail. Based on the assumption that the ball impacts a stationary racket undergoing rigid body rotation, Kawazoe (1997) modelled the hand-held grip as a simple pin joint. The input to the human arm in terms of force and vibration is therefore assumed to be unrealistic. This can also be said for the model of Nesbit et al. (2006) as the connection between the racket and the hand was perfectly rigid with no damping. The authors acknowledge that the model lacks the soft tissue elasticity that would absorb and dissipate the impact energy.

In the dynamic simulation of a forehand groundstroke, Schlarb et al. (1998) used a bushing (finite) element (Figure 2.7), which enabled the researchers to define a stiffness matrix between the two nodes. Although simulations with other hand-racket-connections (e.g. fixed) were tried, only the combination of a freely vibrating racket model with a loose, moveable hand-racket-connection (using a bushing element) was found to adequately simulate the accelerations of a real tennis stroke.

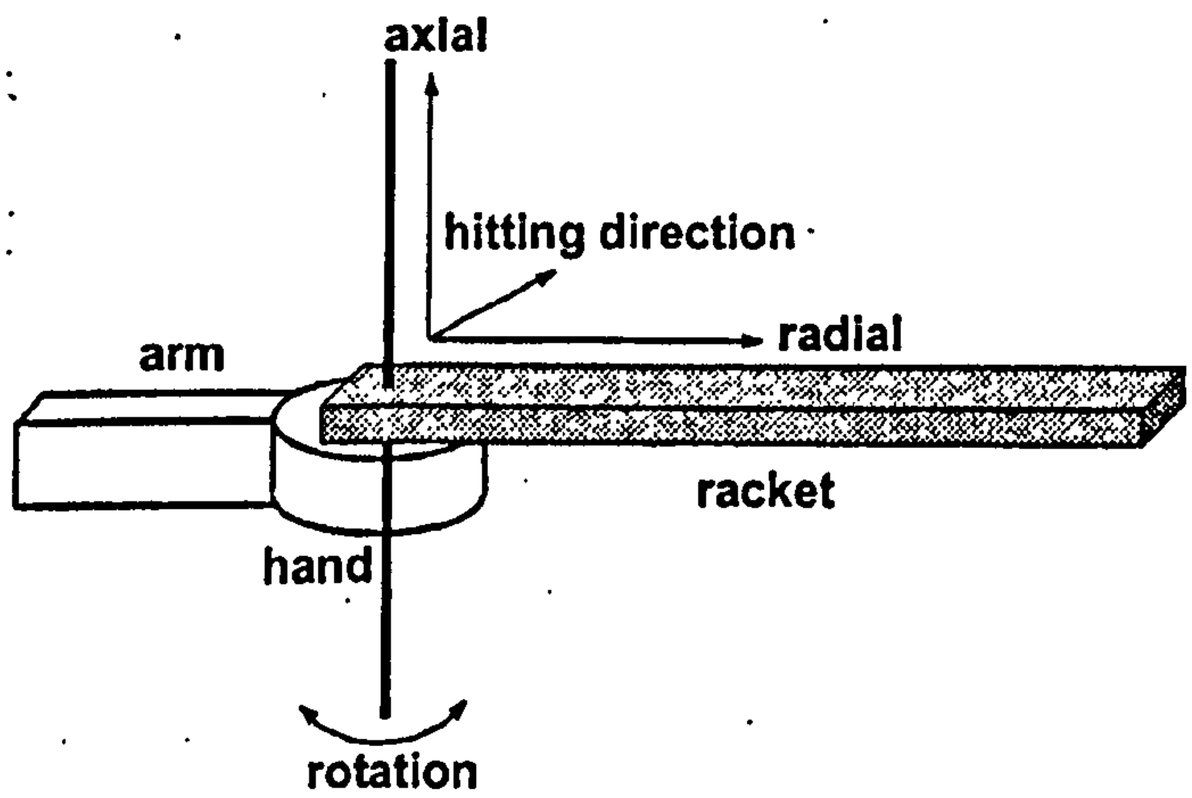

Figure 2.7. Bushing element used to model the hand-racket handle interaction (adapted from Schlarb et al., 1998, pg. 381)

2.2.6 Modelling the upper-limb

Human joint motion consists mainly of rotation and small amounts of translation are typically ignored in human body models (e.g. Alexander, 1990). To model the tennis player, chains of rigid bodies linked by pin joints have typically been used in planar simulation models (e.g. Casolo & Ruggieri, 1991; Glitsch et al., 1999; Schlarb et al., 1998). Bahamonde and Knudson (2003) modelled the stroking arm using a three-segment rigid body inverse dynamics model to examine the kinetics of the upper-limb during a forehand groundstroke. The model included a racket / hand segment, forearm and upper-arm. It is anticipated that in the modelling of a one-handed backhand groundstroke, the hand and racket will need to be modelled in isolation to account for movement between the two.

The wrist joint

Wrist motion is the result of a complex interaction of carpal kinematics occurring at different levels of the joint (Riek et al., 1999). However, during normal wrist motion, there is very little movement between individual bones and they can be thought of as a functional unit (Savelberg et al., 1993). The movements occurring at the joint are flexion / extension and radial / ulnar deviation (Figure 2.8). It has been shown that there is a small separation between the flexion / extension axis and the radial / ulnar axis (Andrews & Youm, 1979) but that torque about the wrist is insensitive to changes in the separation of the two axes over a range of 0 - 2.0 cm (Buchanan et al., 1993). As a result, the wrist has been modelled (Gohner et al., 1998; Riek et al., 1999) as a simple two DOF hinge joint with coincident axes of rotation.

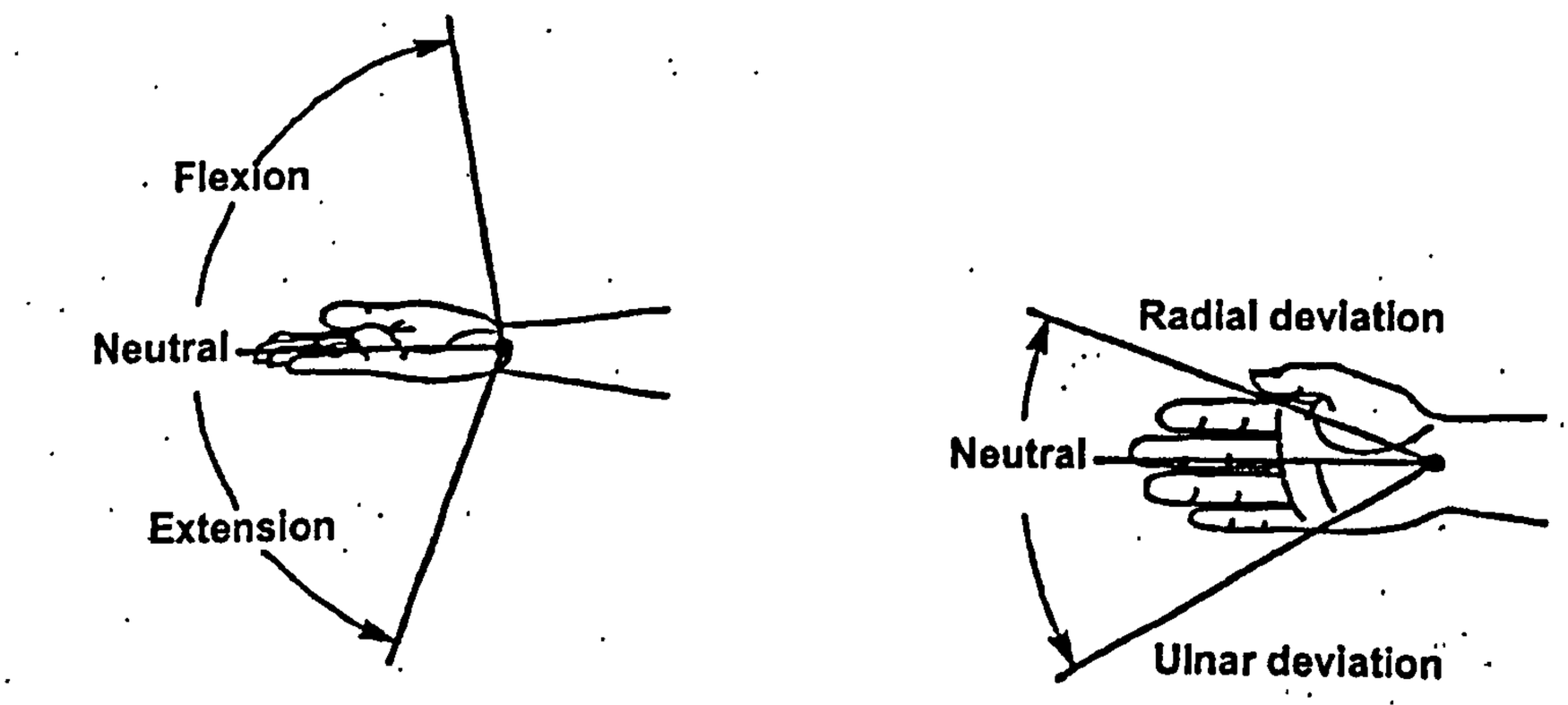

Figure 2.8. Movements of the wrist joint (adapted from *Cybex Norm Testing & Rehabilitation System, 1996, pg. 36)*

For half a second either side of ball impact, Wang et al. (1998) determined the major movements occurring at the wrist joint during a one-handed tennis backhand to be flexion / extension (39.6 ± 20.8 deg) and radial / ulnar deviation (46.8 ± 18.3 deg).

The elbow joint

The major movements occurring at the elbow joint (Figure 2.9) during a one-handed tennis backhand are flexion / extension (35.3 ± 14.4 deg) and pronation / supination (71.2 ± 20.8 deg) (Wang et al., 1998). However, the geometry of the joint and the ligamentous constraints result in the additional motion of abduction / adduction which creates a 'carrying angle' (Challis, 1991). There have been contradictory reports as to how the carrying angle varies and simulation models have typically neglected this third DOF. Gohner et al. (1998) used two hinge joints at the elbow to represent forearm flexion / extension and forearm pronation / supination in their model of forehand groundstrokes. Hummel and Hubbard (2001) modelled a revolute joint at the humeral-ulnar articulation to produce elbow flexion. Separate segments were used for the ulna and radius bones and a single DOF was used to describe the pronation of the ulna-radius pair as in Lemay (1996).

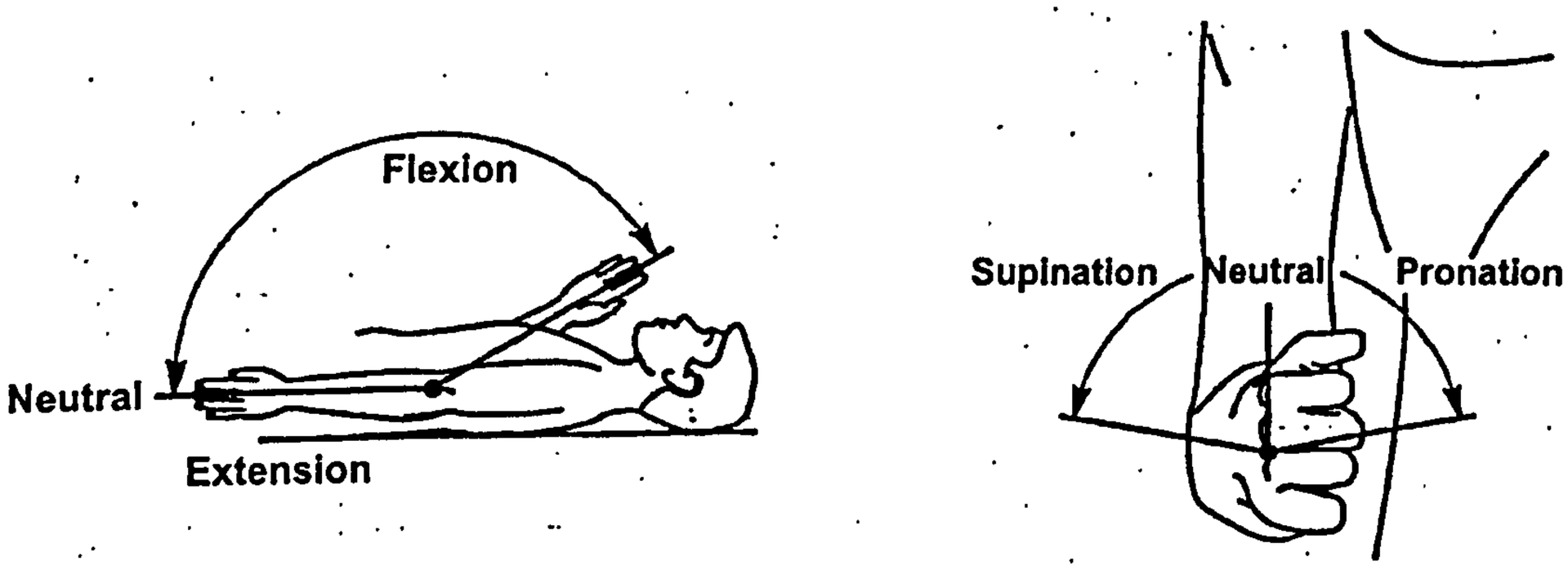

Figure 2.9. Movements of the elbow joint (adapted from *Cybex Norm Testing & Rehabilitation System, 1996, pg. 41)*

Shoulder joint

The shoulder mechanism, consisting of the thorax, clavicle, scapula and humerus, is because of its complexity one of the most challenging systems to model (Helm, 1994). As a consequence, 2D models (e.g. Luca & Forrest, 1973) that neglect the movement of the scapula, have dominated the research. In reality, the scapula will move, but motion studies have shown that a fixed and reproducible relation exists

between motions of the scapula and the humerus (Helm, 1994). Elliott et al. (1989) observed that the shoulder angle (due to the external rotation of the humerus) and the resultant end point velocity remain relatively stable throughout the forward swing of the one-handed backhand groundstroke to maintain control of the racket at impact.

The results of Wang et al. (1998) showed that the major movements of the shoulder joint (Figure 2.10) for a one-handed backhand groundstroke are adduction / abduction (-73.6 ± 11.5 deg), flexion / extension (45.7 ± 20.2 deg), and internal / external rotation (46.3 ± 13.7 deg). Gohner et al. (1998) represented each of these shoulder joint movements by using three hinges.

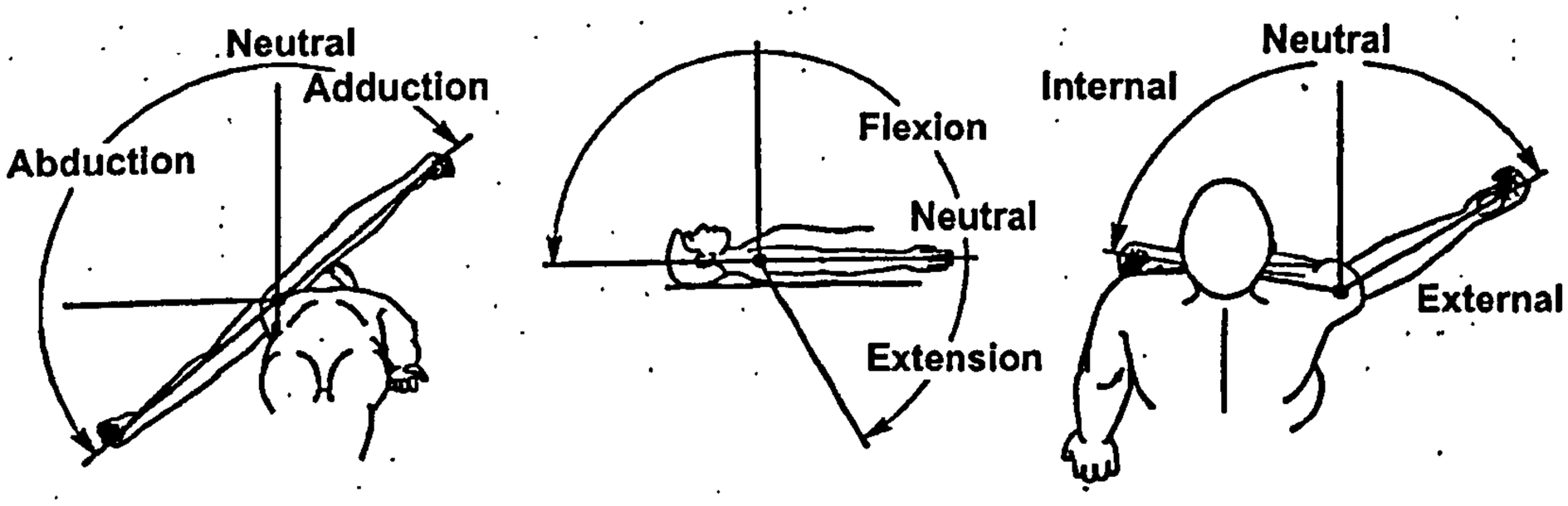

Figure 2.10. Movements of the shoulder joint (adapted from *Cybex Norm Testing & Rehabilitation System, 1996, pg. 50)*

2.2.7 Racket arm kinematics

In the one-handed backhand groundstroke the wrist joint is extending up to impact, and is often forced into a rapid flexion indicating a short, violent eccentric muscle stretch (Knudson, 2004). There has been research into how the kinematics of the wrist joint differ between novice and advanced players (e.g. Blackwell & Cole, 1994; Riek et al., 1999) to try and explain the disparity in the incidences of TE for both groups. Blackwell and Cole (1994) found that expert players struck the tennis ball with their wrists extended by an average of -23 deg from neutral alignment; moreover, their wrists were moving further into extension at impact. In contrast, novice players struck the ball with their wrists flexed 13 deg from neutral alignment whilst moving their wrists further into flexion. Riek et al. (1999) used experimental results as input to a computer simulation model.

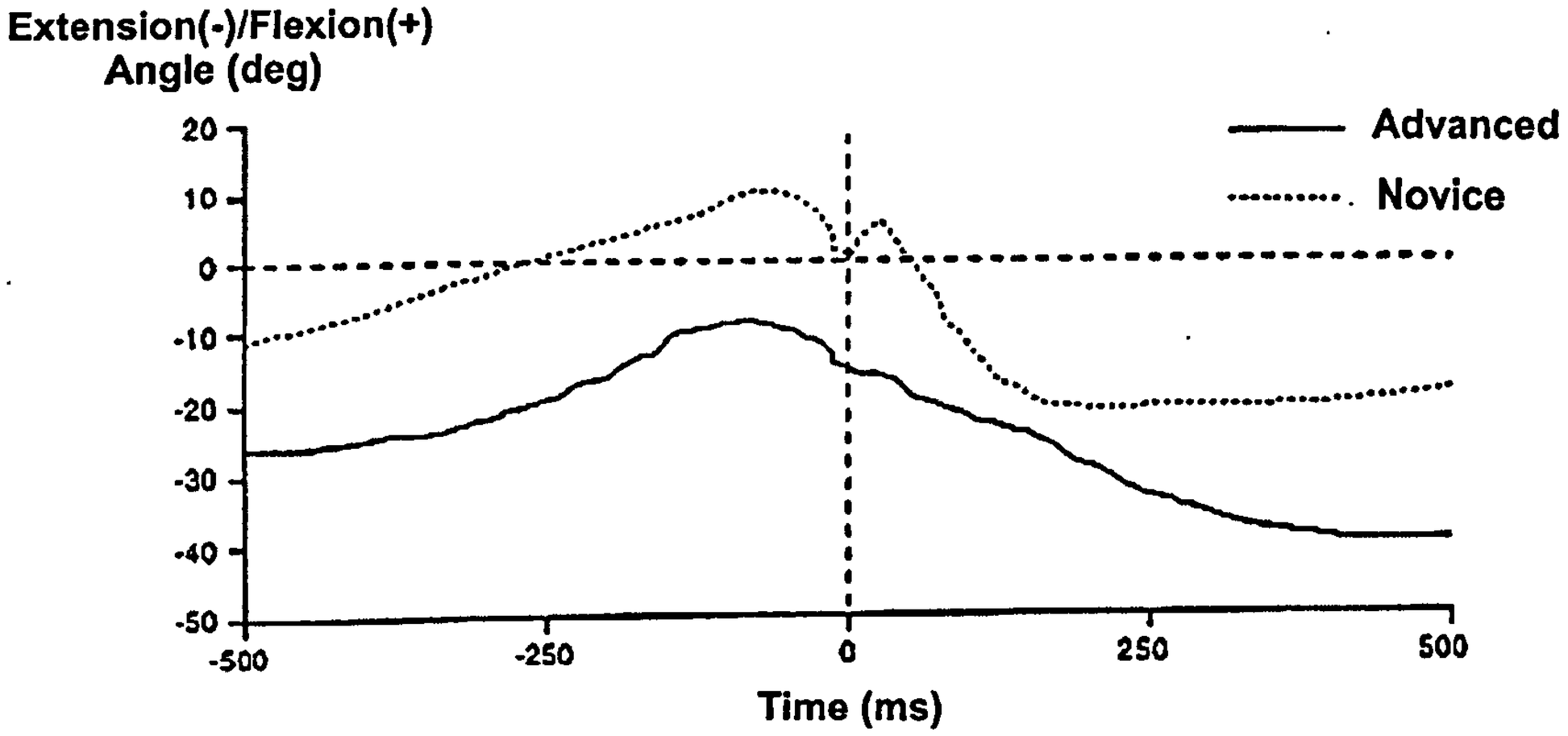

Figure 2.11. Flexion / extension wrist joint angles of novice and advanced players performing a backhand stroke (adapted from Riek et al., 1999, pg. 479)

In agreement with the trend reported by Blackwell and Cole (1994) the advanced group reached a minimum extension angle of –10 deg from neutral alignment approximately 100 ms before impact and then moved their wrists further into extension. The model predicted that the novice group would begin movement toward wrist flexion well before ball impact and reach a peak wrist flexion angle of approximately 10 deg from neutral alignment around 100 ms before ball impact. Shortly after impact, the wrists of the novice players moved into more flexion in agreement with the experimental results of Blackwell and Cole (1994), before extending the wrist once more.

Riek et al. (1999) found that the angular position about the radial deviation axis showed differences between the advanced and novice groups. Novice players began the stroke with the wrist ulnar deviated. The advanced group exhibited a similar kinematic pattern but began the movement with the wrist radially deviated.

By means of a cinematographic analysis (two phase-locked cameras operating at 200 Hz), Elliott and Christmass (1995) calculated pre- and post-impact mean joint angular velocities from the displacement data of different backhand groundstrokes.

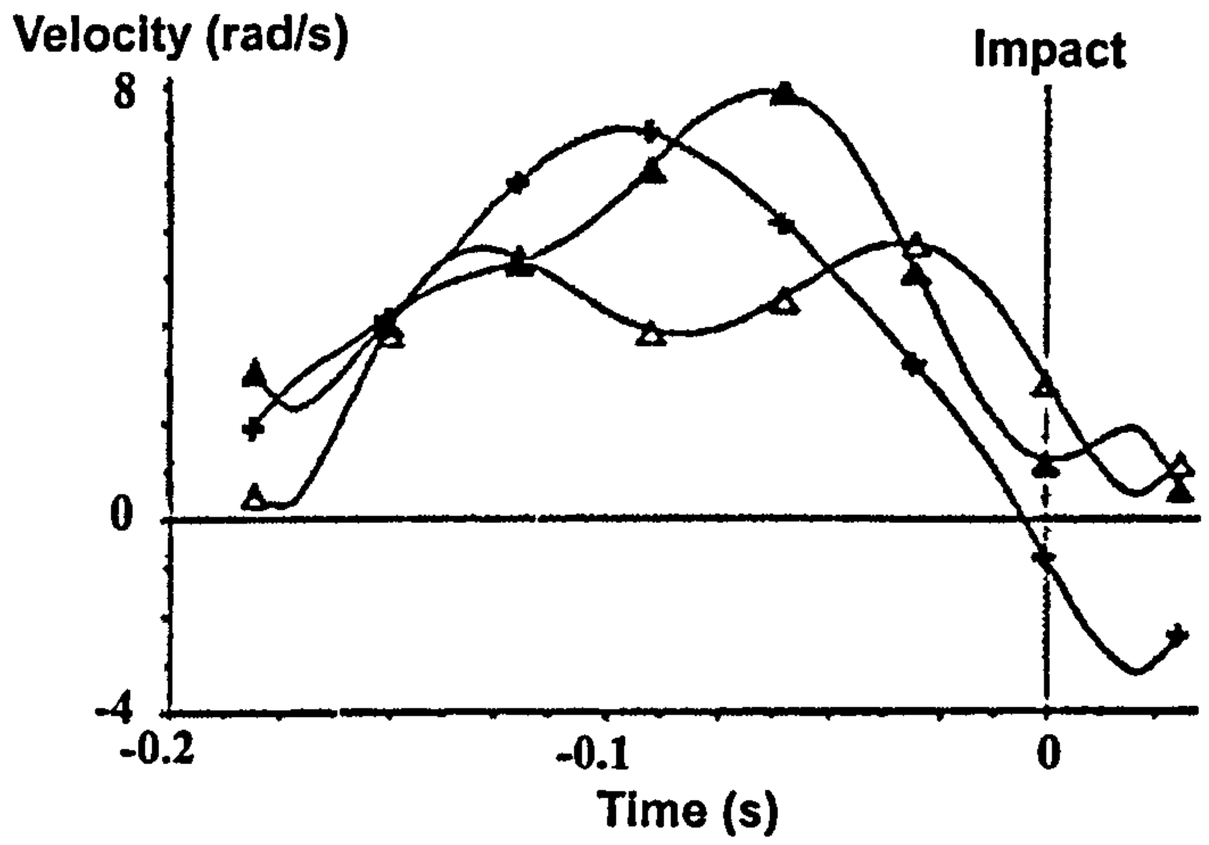

Figure 2.12. Mean angular velocities for the low backspin backhand stroke at the shoulder (+), elbow (Δ) and wrist (Δ) joints (adapted from Elliott & Christmass, 1995, pg. 150)

A comparison of joint angular velocities for the upper-limb showed that racket head speed was derived from the summation of forward movement of the body, trunk rotation and rotations about the shoulder, elbow and wrist joints. However, the external rotation of the upper-arm and forearm supination would also appear to play integral roles in the generation of racket-head speed (Elliott & Christmass, 1995). As illustrated by Figure 2.12, the body segments slowed down just prior to contact. The subsequent negative acceleration of the hitting limb during the follow through phase may be important in reducing the chance of injury (Elliott et al., 1986). However, before making such statements, it must be first shown that the negative acceleration is not a consequence of over smoothing the large negative acceleration of impact (Knudson, 2001).

Wang et al. (1998) used an automatic tracking system operating at 60 Hz to analyse the 3D kinematics for performances of one-handed backhand groundstrokes. The validity of the results obtained is questionable due to the relatively low frame rate of the six cameras used, for a movement which lasted less than a second. The experiment found that the movement of the shoulder was small for the acceleration phase immediately prior to impact. The maximum angular velocities of the shoulder external rotation, elbow flexion and wrist extension occurred in the instant prior to impact, then immediately decreased as in the study by Elliott and Christmass (1995).

2.2.8 Hand forces

Studies measuring forces on key hand locations have found a wide variability in peak forces transmitted to the hand during one-handed backhand groundstrokes (Hatze, 1976; Knudson, 1991a; Knudson & White, 1989). Peak forces due to the impulsive loading from ball impact have ranged from 5 to 311 N with the largest influencing factor appearing to be how far off-centre the ball impacts the racket face.

Knudson has published extensively his work into forces induced in the hand by the tennis racket for the forehand (Knudson, 1991b; Knudson & White, 1989) and backhand groundstrokes (Knudson, 1989, 1991a). The results obtained from force sensing resistors showed that all subjects tightened their grips immediately before impact by increasing the forces at the hypothenar sensor for the forehand and at the thenar sensor for the backhand (Figure 2.13).

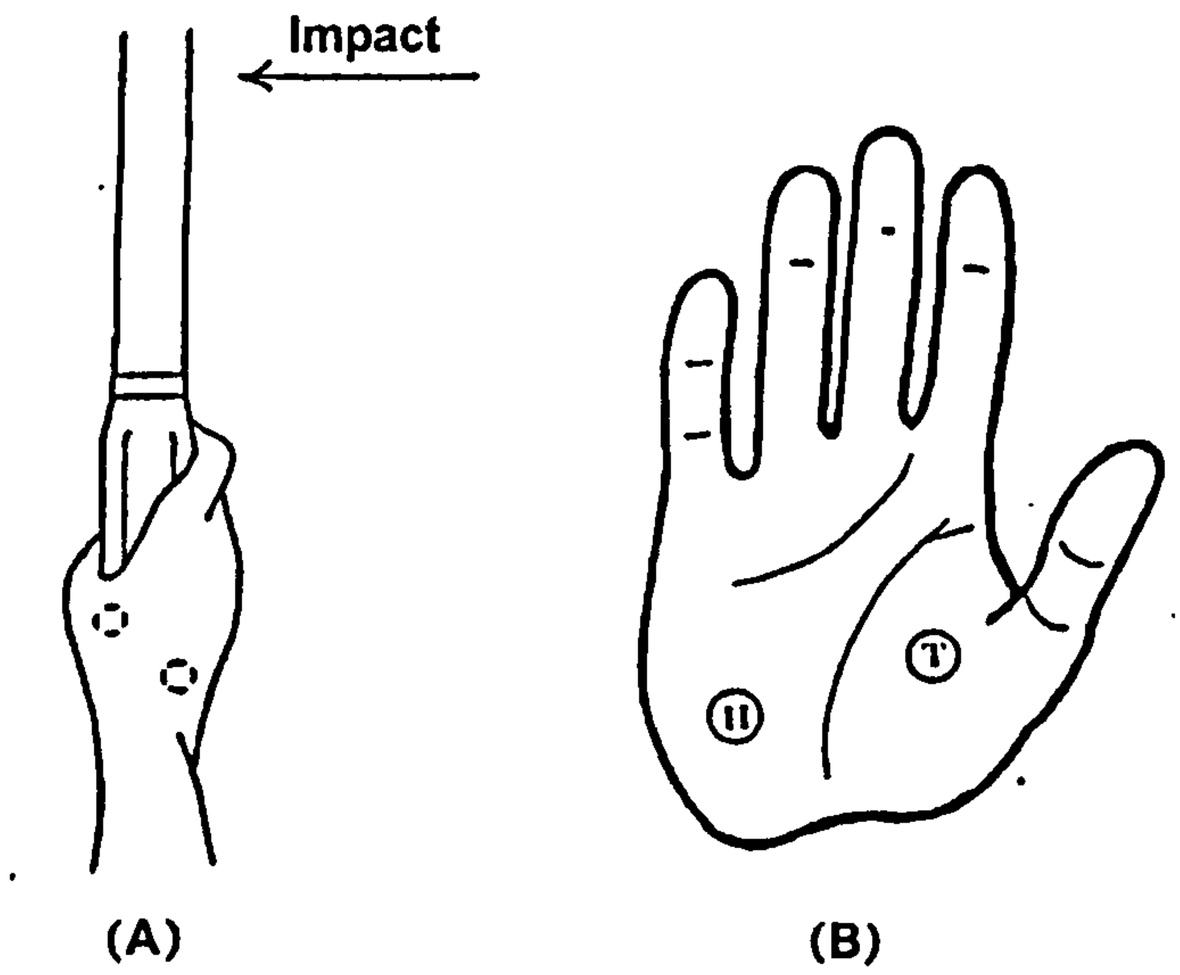

Figure 2.13. Superior view of hand placement on the racket in a backhand grip (A), and the corresponding sensor locations on the palm of the hand (B); where H and T are the approximate locations of the hypothenar and thenar eminences respectively (adapted from Knudson, 1991a, pg. 284)

Although pre-impact forces showed a consistent pattern, peak post-impact forces were highly variable ranging from 4 to 309 N and from 6 to 124 N for the forehand and backhand respectively. Interestingly, the intermediate subjects used had much lower thenar forces (20N as opposed to 40N for advanced subjects) during the backhand, in preparation for impact. According to Knudson, this provides less resistance to the

acceleration of the racket. Large impact acceleration may be related to a rapid stretch of the wrist extensors, which has been hypothesised to be the cause of tennis elbow (Knudson, 1991a).

The considerable variability in the magnitude of the impulsive forces observed by Knudson was attributed to variations in impact location and racket velocity during the experiments. Cross (1998) minimised this problem by measuring forces at selected impact locations and using a stationary racket to keep the initial racket velocity constant at zero. The results were consistent with those of Knudson and White (1989) who found that for the forehand groundstroke, the force increases at the base of the index finger and decreases at the hypothenar eminence during the impact. On the basis that the force on the middle finger remained constant at all times, Cross (1998) suggests that the axis of rotation within the hand is located almost exactly in the middle of the hand.

2.2.9 Racket arm kinetics

A simple analytical model developed by McLaughlin and Miller (1980) was the first to calculate internal forces and moments during one-handed tennis backhand gorundstrokes. They formulated a linear objective function and minimised the weighted sums of the muscle stresses, joint moments, and joint reaction forces on structures in the forearm through optimisation. The results correlated reasonably well with observed patterns of muscle electromyogram (EMG) signals for the nine selected forearm muscles. However, there was no attempt to estimate or scale muscle parameters to their subjects. Instead, input parameters were taken from the literature.

An investigation into the dynamics of the extensor carpi radialis brevis (ECRB) muscle during one-handed backhand groundstrokes was undertaken by Riek et al. (1999). Their simulation model predicted that the advanced group would exhibit a considerably larger peak force (89.9 N) when compared with the novice group (65.3 N). In the advanced group, impact occurred well before (128 ms) the peak force but for the novice group impact nearly coincided (32 ms after) with the peak force. As a result, it is likely that the muscle was in a less advantageous state to deal with the sudden stretch, just after impact (Riek et al., 1999). It can be inferred that a higher force in the ECRB muscle is associated with increased loads in tendon attaching it to the lateral epicondyle at the elbow. However, it is unknown what the critical loads are which may cause micro-tears within the tendon.

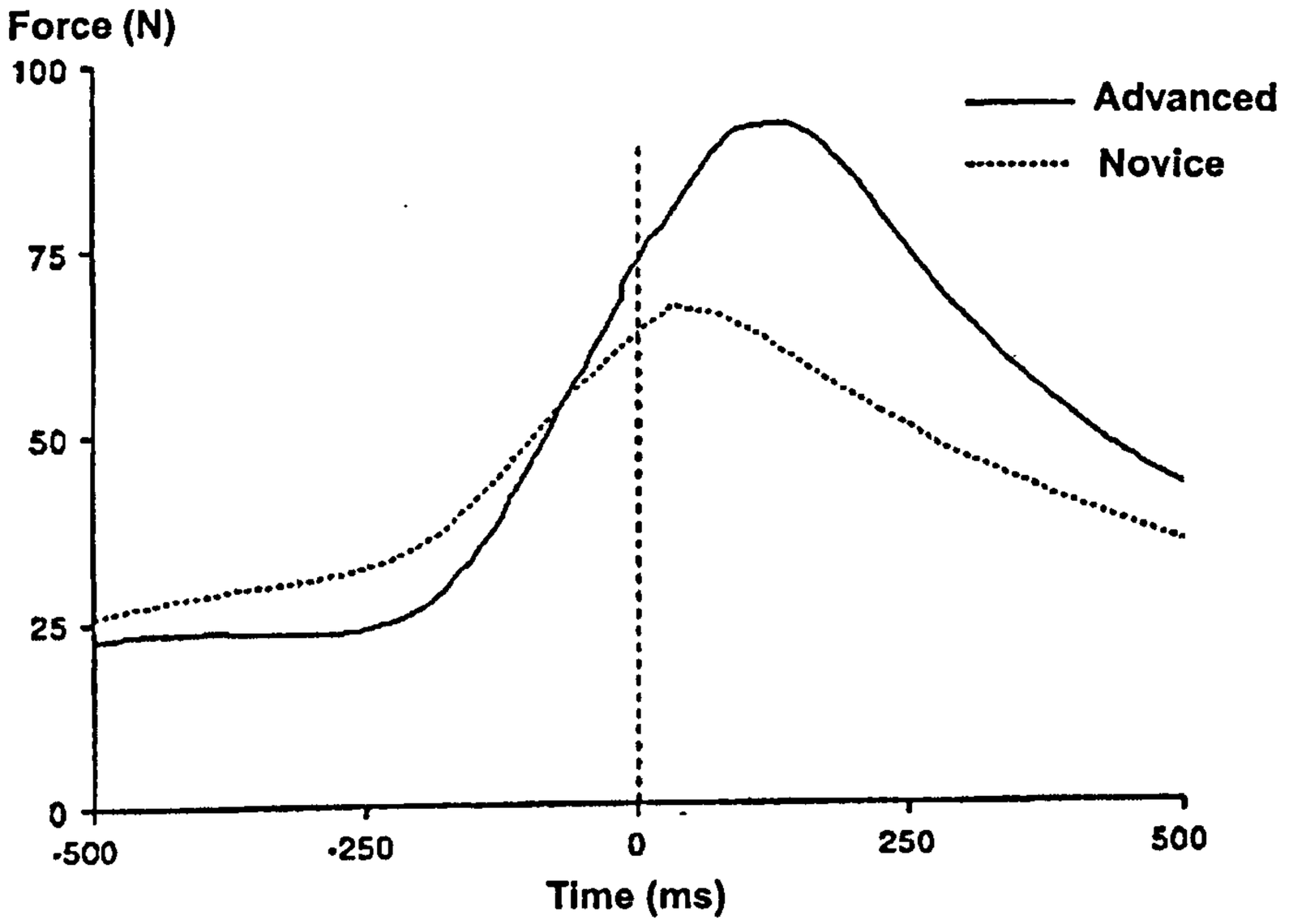

Figure 2.14. Muscle force in ECRB predicted by the model for advanced and novice groups (adapted from Riek et al., 1999, pg. 480)

Wu et al. (2001) developed a mathematical model to estimate ball contact duration on the stringbed (dwell time) and the peak impact force on the racket for two tennis backhand techniques. Data was only collected at 60 Hz and this may explain why the errors in predicted dwell time are similar to the actual dwell times calculated in other studies (e.g. Cross, 2000a). For the advanced subjects, a one-handed backhand groundstroke with a short backswing had a significantly shorter dwell time (0.008 ± 0.003 s) and a greater peak resultant force (330.0 ± 141 N) than that with a long backswing (0.016 ± 0.004 s and 180.8 ± 49 N). The explanation provided is that a long backswing allows the racket to follow the ball after initial ball and racket contact, which increases the ball and racket contact duration. However, the relative ball-racket velocities at impact are not given and the reason for an increase in dwell time is not clear.

2.2.10 Muscle activation of the upper-limb

Electromyography (EMG) has been widely employed to examine the muscular demands of tennis strokes with particular attention given to the wrist extensors during the one-handed backhand groundstroke (Li et al., 2004). The high level of muscular activity of the wrist extensors may be one of the reasons for the predisposition of these muscles to injury (Morris et al., 1989; Giangarra et al., 1993).

Ryu et al. (1988) used EMG signals to analyse the complex sequences of muscle activity occurring at the shoulder in tennis players. The middle deltoid, supraspinatus, and infraspinatus (Figure 2.15) were found to be most active in the acceleration and follow-through stages (see Figure 2.1) of the one-handed backhand groundstroke, whilst some activity was noted in the biceps brachii, latissimus dorsi and serratus anterior. The follow-through phase was characterised by moderate activity of the biceps brachii, middle deltoid, supraspinatus, and infraspinatus.

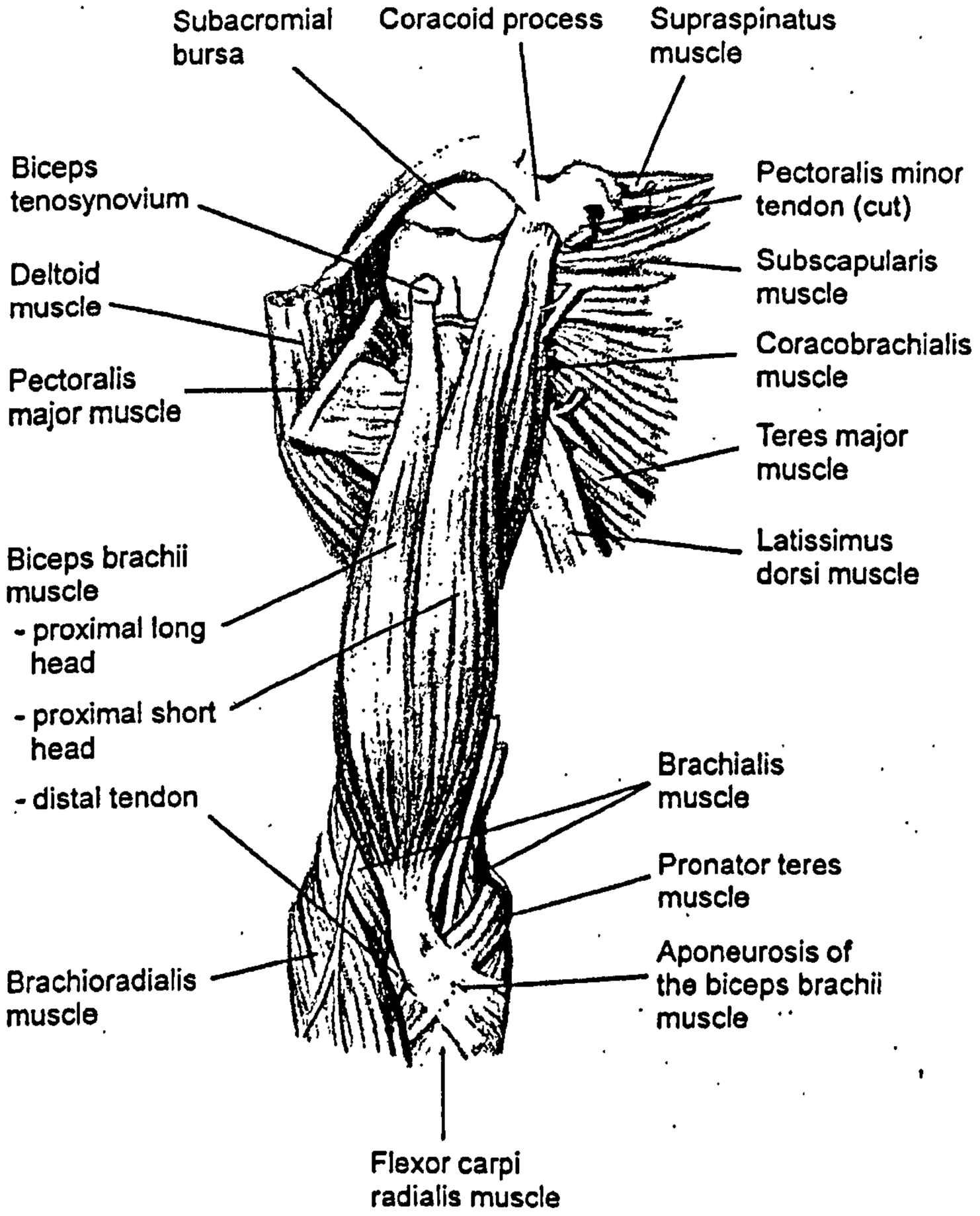

Figure 2.15. Anterior view of the muscles and tendons of the upper-arm (adapted from Jozsa & Kannus, 1997, pg. 54)

Blackwell and Cole (1994) examined the EMG signals from the ECRB muscle and for the flexor carpi radialis (FCR) muscle during the one second interval centred on the time of ball-racket impact. The activity of the ECRB muscle increased during the post-impact period for the expert players consistent with the wrist extension they

produced following ball-racket impact. Activity of the FCR remained unchanged (expressed as a percentage of maximal voluntary contraction) from pre- to post-impact intervals in both groups.

The simulation model of Riek et al. (1999) predicted that advanced players display increasing activation levels of the ECRB muscle up to, and just after, ball impact. Thereafter, the activation level drops (Figure 2.16) in contrast to the aforementioned study.

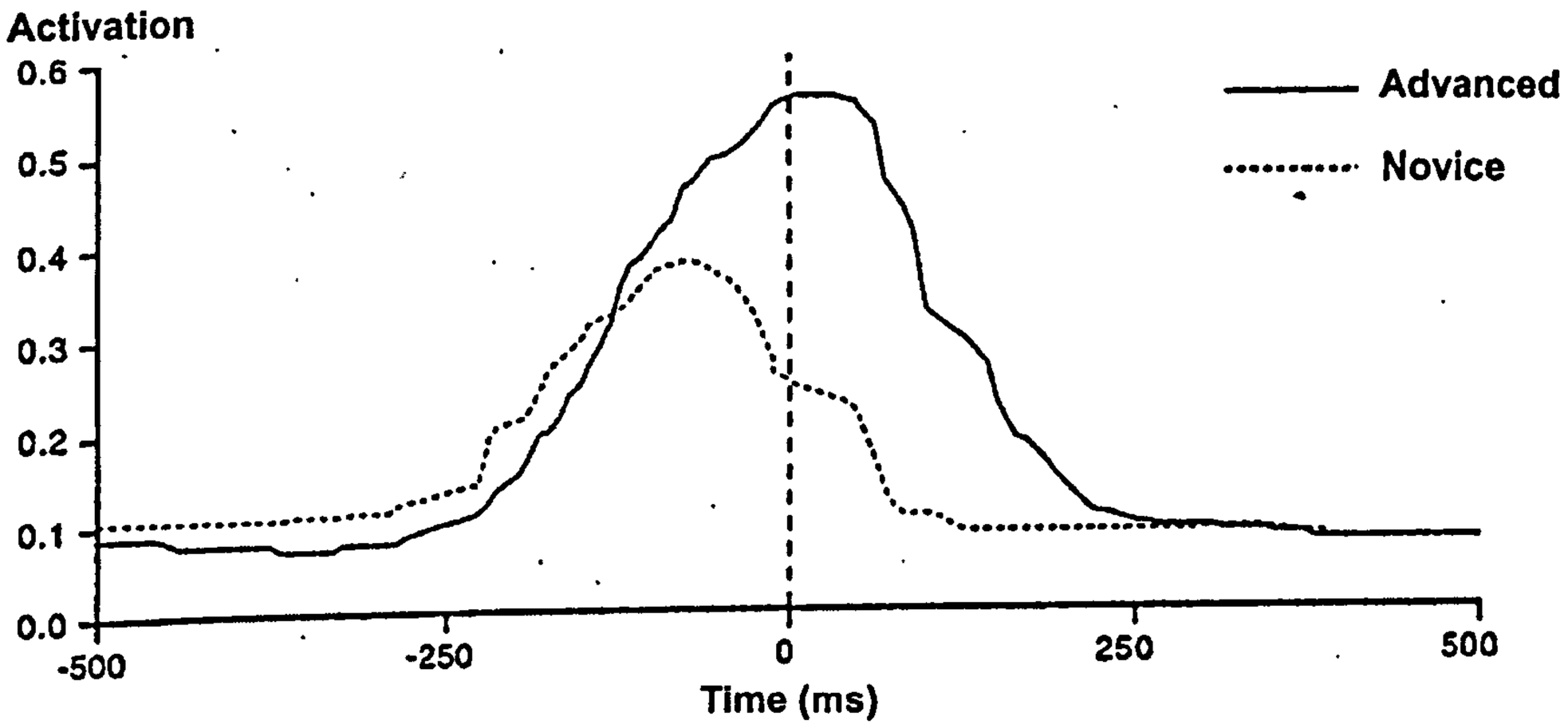

Figure 2.16. Simulated activation of the ECRB muscle
(adapted from Riek et al., 1999, pg. 479)

EMG analyses of the one-handed backhand groundstroke (Bauer, 1997; Knudson & Blackwell, 1997) revealed that groups of healthy players and players suffering from tennis elbow exhibited different activation patterns of the racket arm musculature with respect to similar ball-racket impacts. The data of Bauer (1997) indicated that the wrist extensor muscles were activated significantly earlier for the injured subjects than the uninjured ones (-0.39 s as opposed to –0.24 s) and were also activated for longer after impact (0.39 s as opposed to 0.24 s). Muscles were considered active if the magnitude of the EMG reached 20% or greater of that recorded during maximum voluntary muscle contractions.

2.2.11 Length, mass and moment of inertia of tennis rackets

Kneib et al. (1998) used a computer simulation model to study the influence of racket length on the tennis stroke. The model was based on 2D multiple pendulums

consisting of upper-arm and forearm, hand and racket segments. The arm segments were linked by hinge joints and the viscoelastic properties of the racket, strings and ball were combined in an overall spring-damper system according to Leigh and Lu (1992). A racket with an elongated grip but the same mass and moment of inertia as a conventional racket resulted in increased loads in the wrist (16%), elbow (17%) and particularly the grip joint (212%). Kneib concluded that the advantage of a higher rebound velocity (2%) is attained at an unacceptable cost to the recreational player.

Depending on where additional mass is added, altering the total mass of a racket will affect the balance point and the total weight of the racket as well as the moments of inertia (MOIs) and the vibration response (Cross, 2001). Cross found that mass added at the tip of the racket is effective at increasing racket power and that the point of maximum power is shifted towards the tip of the racket. Both Kamien (1990) and Renstrom (1994) state that there is no definitive or consistent evidence that any particular weight of racket or type of racket frame material will decrease or increase the risk of arm injury.

Mitchell et al. (2000) investigated the effect of racket inertia values upon the head speed generated by tennis players during the serve. The results indicated that a decrease in racket inertia, within realistic limits, can significantly increase the head speed achieved by skilled players although it is noted that this result may not be independent of the weight of the racket. Brody (1985) talks about the 'swingweight' of the racket which is the MOI about the transverse axis through the handle.

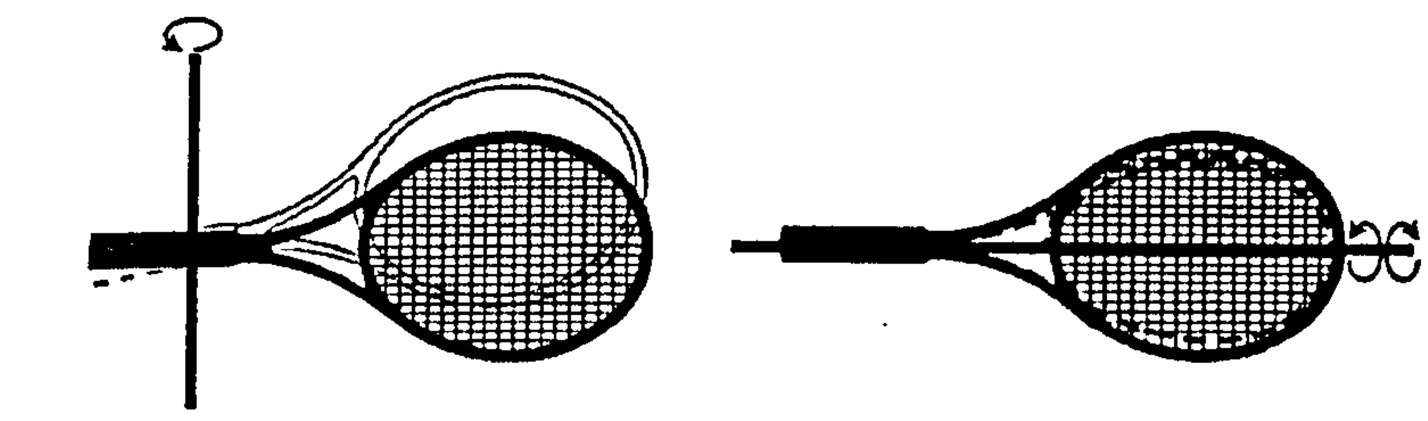

Figure 2.17. Swingweight and longitudinal axes of a tennis racket

The swingweight determines the racket's 'hitting mass' when the ball is struck and is a matter of preference for the tennis player. Also of importance to the tennis player is the MOI about the longitudinal axis through the handle of the racket as this determines the racket's resistance to twisting when the ball is hit 'off-centre'. Using their computer simulation model of a tennis forehand groundstroke, Nesbit et al.

(2006) suggest that the MOI about the longitudinal axis of the tennis racket noticeably influences the pronation / supination torque at the elbow. However, the simplicity with which the hand interacts with the racket in this model raises questions as to the extent to which it can predict the relative effect of perturbations of racket MOI values. The MOI about the frontal axis perpendicular to the plane of the racket is of concern only when spin is being applied to the ball as in a 'slice' groundstroke (Brody, 1985).

2.2.12 The sweet spots

Professor Howard Brody has written many articles concerning the physics of tennis. He observes that there are three definitions of the sweet spot on the strings of the racket, each based on a different physical principle. The first definition of the sweet spot is the point giving the maximum coefficient of restitution (COR), which is where the greatest return velocity is generated. The second definition relates to the point at which the impact gives no reaction impulse at the racket handle, the centre of percussion (COP). The third definition connects the sweet spot to a point on the racket face along the longitudinal axis (the node) at which being struck by the ball results in minimal vibrations on the racket handle. This spot is actually a curved line which extends from the middle of the strings to points at about two and ten o'clock on the frame (Brody et al., 2002). The node refers to the point where the curved line intersects with the longitudinal axis of the racket. Cross (1997) also defines a dead spot, which is the point on a racket where an incident ball stops dead on a stationary racket (Figure 2.18A).

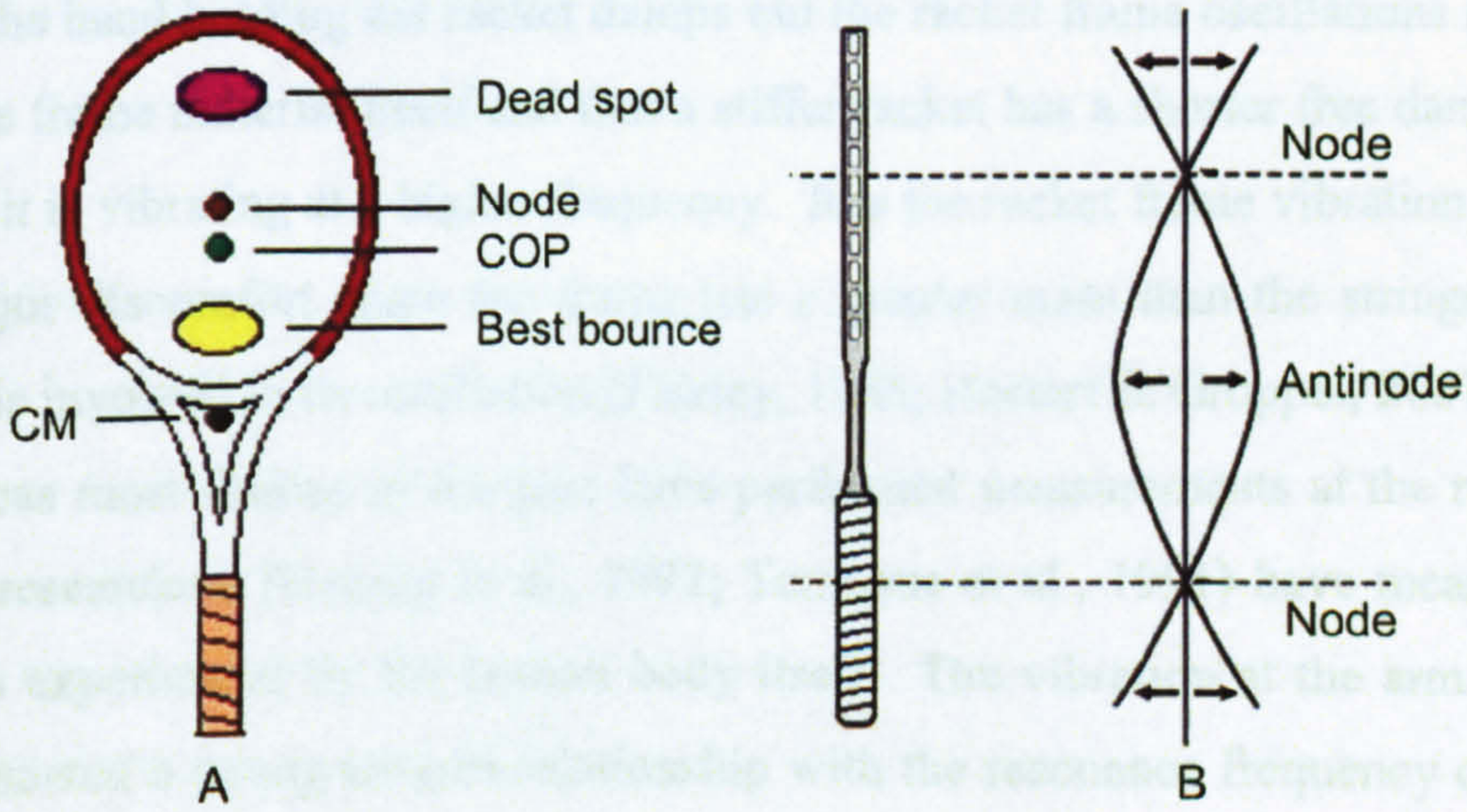

Figure 2.18. The sweet spots of a tennis racket (A) and its fundamental mode of vibration (B) (adapted from Brody, 1988, pg. 25)

2.2.13 Off-centre impacts

Forces on the hand arise from rotation, translation and vibration of the racket handle (Cross, 1998). The initial shock your hand feels can be minimised by hitting the ball at the COP (Roetert & Groppel, 2001) whilst for an impact at the node, the vibration component is zero (Brody, 1981). The forces generated by ball-racket impact, especially off-centre impacts, have been identified as a factor that may contribute to the development of tennis elbow (Hennig et al., 1992). When the impact of the ball is not along the longitudinal axis of the racket frame, the racket will rotate around that axis. This creates a moment around the wrist which must be resisted by the forearm musculature. Although modern rackets are more forgiving in terms of performance they have also led to an increased shock transmission from the racket to the player (Miller, 2006). Knudson (1991a) suggests rackets that minimise the effects of off-centre impacts should be considered as an intervention to reduce the risk of tennis elbow.

2.2.14 Vibration of racket frame

The system of tennis racket and strings is elastic with little damping and is therefore prone to vibrations. When the ball strikes the racket, energy is imparted to the strings. Some of this energy goes to vibrating the structure at a characteristic resonance frequency typically in the range 100 - 200 Hz (Brody, 1995; Cooke et al., 2002). The strings will vibrate at a frequency of about 400 Hz at a low string tension and up to 600 Hz at a high string tension (Brody et al., 2002). Brody (1989) also showed that the hand holding the racket damps out the racket frame oscillations much faster than the frame material itself and that a stiffer racket has a shorter free damping time because it is vibrating at a higher frequency. It is the racket frame vibrations that cause the major discomfort since the frame has a greater mass than the strings and more energy is involved in its oscillation (Fairley, 1985; Roetert & Groppel, 2001).

Whereas most studies in the past have performed measurements at the racket frame, some researchers (Hennig et al., 1992; Tomosue et al., 1991) have measured the vibrations experienced by the human body itself. The vibration at the arm after ball impact showed a strong inverse relationship with the resonance frequency of the racket frame (Hennig et al., 1992). When the ball impacted off-centre, almost a threefold increase in load onto the arm was observed. The data indicate that the vibrations in the wrist were only one tenth of those in the racket handle and that

vibration levels in the elbow were approximately a third of those experienced at the wrist. The attenuation in the amplitude of vibration from the racket to the elbow is to be expected. However, since the measurements were taken externally with accelerometers clamped to bony protrusions at the wrist and elbow, the accuracy to which this reflects the oscillating loads transmitted through the muscle / tendon system is unknown.

A very tight grip has been shown to increase the magnitude of the transmitted vibration due to an increase in the impulsive force at the point of impact (Hatze, 1976). Vibration at frequencies below 40 Hz can be effectively transmitted through the arm to the shoulder whereas the absorption of vibration energy from frequencies above 60 Hz takes place almost entirely in the hand (Dong et al., 2004; Sorensson & Burstrom, 1997). Studies which focussed on hand-forearm vibration have found that discomfort due to vibration applied to the hand decreased as frequencies exceeded 180 Hz (Li et al., 2004). However, as uncomfortable as these oscillations may feel, there is no clinical evidence that vibrations are (or are not) a source of injury to the hand or arm (Brody, 1995; Roetert & Groppel, 2001).

2.2.15 Summary of tennis literature

Mathematical models of varying complexity have been used for tennis simulation. To model the human, chains of rigid bodies have typically been used whilst the strings / impact surfaces and balls are mostly taken as flexible bodies. The tennis racket frame has been modelled using both rigid and flexible beams. Few simulation models have incorporated the human and ball-racket systems and those that did made assumptions which reduce the confidence that can be placed in the model output.

The research on the impact dynamics of tennis rackets demonstrates that the ball, racket and string system are subject to very large forces and vibration. Experiments and theoretical models have attempted to shed light on these phenomena, but as yet it is unclear what effect these forces and vibrations have on the upper-limb of the tennis player. No mention has been made of a suitable biomechanical model of the one-handed backhand groundstroke capable of predicting this. Such a model, customised to an individual performer, could permit analysis of the relative effects of racket parameters and technique on loading at the elbow.

2.3 TECHNIQUES OF INVESTIGATION

Research into dynamic activities can be divided into two categories: experimental and theoretical. However, the most effective approach encompasses both types of research (Yeadon & Challis, 1994).

Whereas experiments measure what happens in the real world to real objects, a mathematical model forms a similar basis for a computer experiment (Bartlett, 1999). The advantage of this is that quantities of interest can be systematically and independently varied, whereas experimentally it is sometimes difficult to represent a system physically so that its behaviour throughout a range of conditions can be examined. Computer simulation allows complete reproducibility at an arbitrary time resolution (Kneib et al., 1998). Problems arise when the theoretical model is found to be an inadequate representation of the movement being studied. This can generally be avoided by basing simulations on appropriate experimental data as part of the scientific method (Yeadon & Challis, 1994).

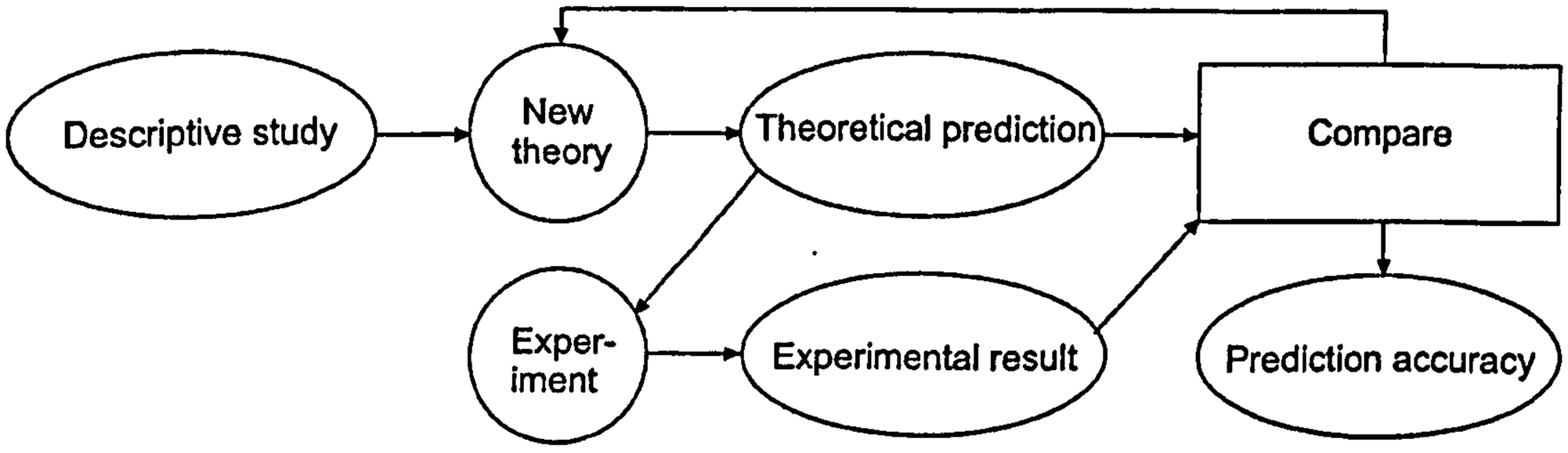

Figure 2.19. The theory-experiment cycle of the scientific method

Experimental difficulties in tennis research caused by the complexity of the strokes and the short contact phase demand the development of computer simulation models (Schlarb et al., 1998). An investigation of the one-handed tennis backhand groundstroke requires knowledge of a number of different techniques. In the following sections, a review of simulation modelling, parameter determination and image analysis is provided.

2.4 SIMULATION MODELLING

2.4.1 Overview of simulation model development

There are four distinct phases in simulation modelling: the development of the model, the evaluation of the model, the optimisation of a performance using the model and a sensitivity analysis.

2.4.2 Development of simulation model

Model complexity

Previous models involving the human body have been very complex (e.g. Hatze, 1981) although there are those who advocate the use of simpler models (e.g. Alexander, 1992; Hubbard, 1993). An advantage of a simpler approach is that it is easier to discover the effect of perturbing model parameters (Alexander, 1995; Pandy, 2003) although the accuracy of the model may be poor and important features may be omitted (Yeadon & Challis, 1994). With highly complex models, the derivation of the equations of motion and the model parameters is challenging, whilst the interpretation and evaluation of the results is more difficult (Yeadon & King, 2002). However, a complex model can be made to simulate a simple model by the use of suitable constraints (Yeadon & Challis, 1994). The challenge for the investigator appears to be the selection of an appropriate level of complexity, bearing in mind the purpose of the model.

Formulation of equations of motion - software packages

The development of a simulation model requires the formulation of the equations of motion. Whilst some researchers have chosen to develop their models from first principles (e.g. Brannigan & Adali, 1981; Hatze, 1976), more recent models have successfully made use of the availability of special computer programs such as DADS (Schlarb et al., 1998) and AUTOLEV^{TM}3 (Hummel & Hubbard, 2001).

The development of computer code is relatively quick and the chance of making a mistake in the code is reduced. Also, the researcher is not concerned with the numerical methods used and can focus on the biomechanical problem in question. However, although software packages can reduce the complexity of producing a model, they cannot help with the selection of the structure of the model (Yeadon & Challis, 1994).

2.4.3 Evaluation

Only when a model has been shown to accurately represent the real life situation can the researcher be confident in its capabilities (Hubbard, 1993). A simulation model may be customised to the individual performer by calculating subject-specific parameters. This allows the simulated performance of the model to be compared with the same athlete's actual performance. Although most models are evaluated with respect to kinematic data, if the model is being used to evaluate forces, a kinetic comparison of simulation and performance is also required (Yeadon & King, 2002).

2.4.4 Optimisation

Since modern computers allow many simulations to be run one after each other, a special type of experimentation, optimisation, becomes feasible (Nigg & Herzog, 1999). The optimisation process is used to determine the minimum or maximum value of a given objective function which comprises one or more independent variables. Weightings must be determined for each variable so that an optimal solution can be reached. There are many algorithms, varying in complexity, that are capable of maximising or minimising a given function. When the objective function is multi-dimensional and is dependent on more than one variable, a process called 'Simulated Annealing' has often been used (e.g. King, 1998; Wilson, 2003).

Simulated Annealing Algorithm

Presented by Corana et al. (1987) the Simulated Annealing Algorithm (SAA) is based on how liquids cool to form solids. The analogy is that when molten metal is allowed to cool slowly (anneal) the molecules within will align themselves to form pure crystals. The pure crystals are in a state of minimum energy since there has been ample time for the atoms to lose energy during redistribution. The algorithm starts at some 'high' temperature given by the user and creates a sequence of points, choosing which to accept and reject. The process will accept uphill (to move away from local optima) as well as the usual downhill moves in search of a global minimum. After a specified number of points have been tried, the temperature is reduced. This procedure continues until a temperature is reached whereby no more useful energy can be expected.

Corona et al. (1987) and Goffe et al. (1994) tested the SAA on a number of functions and compared the results with other optimisation algorithms such as the Simplex Method (Nelder & Mead, 1965) which is a local optimisation method. The process of Simulated Annealing was found to be costly in terms of function evaluations for a single run when compared to other methods. However, when compared to multiple runs needed by other algorithms to test different starting values, the SAA becomes effective (Goffe et al., 1994). A major advantage of the SAA over other optimisation methods is that by exploring the function's entire surface, the process is largely independent of the starting value (Goffe et al., 1994).

2.4.5 Sensitivity analysis

A sensitivity analysis is needed to enable the researcher to place complete confidence in the results of the simulation study. The problem lies in the uncertainty associated with the values given to the model parameters not included in the optimisation procedure (Yeadon & Challis, 1994). A sensitivity analysis investigates the effect that such uncertainties have on a calculated optimum. High sensitivity implies that small deviations from the theoretical optimum will result in values that are appreciably below optimum whilst the converse is also true.

2.4.6 Summary of simulation models

The stages involved in the development, evaluation and optimisation of a simulation model have been discussed with reference to the literature. The next section details the parameters required and the techniques used to obtain them.

2.5 PARAMETER DETERMINATION

2.5.1 Overview of parameter determination

For a simulation model to accurately represent real life activity, parameters must be determined directly from experiments or indirectly through an optimisation process when direct measurements are not possible. This section will review the possible methods of determination for the inertia parameters of the human and for the parameters of the tennis ball and tennis racket.

2.5.2 Inertia parameters

In studies of human movement, the segments of the human body are idealised as rigid bodies. It is necessary to know the mass, mass centre location, and the principal moments of inertia (MOIs) about the mass centre of the rigid body. One of the earliest methods of determining segmental inertia parameters was using cadavers (e.g. Dempster, 1955). Later, this cadaver data was used within regression equations as a means of expressing the segmental inertia parameters as functions of anthropometric measurements. This approach has been linear (e.g. Hinrichs, 1985) and non-linear (e.g. Yeadon & Morlock, 1989) with the latter yielding more accurate estimates. The obvious disadvantage of cadaver data is that it is not subject-specific and therefore of little value in a subject-specific computer simulation model.

A number of techniques are needed to calculate inertia parameters by direct measurement. Water immersion techniques have been used to calculate segment volumes (Clauser et al., 1969), reaction board measurements for mass centre locations (Drillis et al., 1964) and oscillation techniques for MOIs (Hatze, 1975). Some of these experimental methods are restricted to certain body segments and there is the difficulty of obtaining inertia parameters for central segments (Yeadon & Challis, 1994).

Magnetic Resonance Imaging (MRI) circumvents the reliance on cadaver data and can distinguish between various soft tissues (Mungiole, 1990). At present, the impracticality of this technique, being expensive and not widely available, appears to outweigh its apparent accuracy in providing estimates of segmental inertia parameters. For determination of the MOIs of the upper-limb, Challis and Kerwin (1992) showed that geometric modelling techniques gave acceptable accuracy and offered a relatively simple alternative to statistical methods.

Geometric modelling

In these mathematical models, body segments are represented by a series of geometric solids of different shapes, the size of which are determined by anthropometric measurements. The inertial properties of the body segments are determined by assuming that the segments have the same volumes as the geometric solids. The densities of the segments are taken from cadaver data introducing uncertainty in the estimated values. Although geometric models are all based on the same principles, their complexity has differed amongst researchers. For instance,

Hatze (1980) developed a 17-segment model requiring 242 direct measurements from the subject. In contrast, the inertia model of Yeadon (1990a) comprises 11 segments and 40 geometric solids, specified by 95 anthropometric measurements. The maximum error of the total body mass estimates was found to be 2.3% as opposed to 0.32% which Hatze (1980) records. However, the time needed to take these measurements is approximately 20 to 30 minutes compared to over an hour when using Hatze's earlier model.

Inertia parameters of a tennis racket

The MOIs of a tennis racket about its principal axes through the centre of mass (COM) and about parallel axes are needed as input to a 3D simulation model. Brody (1985) describes simple experiments that can be performed to achieve this. By suspending a racket on a wire and measuring the period of the torsional oscillations (T), the MOI of the racket can be calculated using the following Equation 2.3:

$$I = kT^2/4\pi^2 \qquad (2.3)$$

The value k is the torsional constant of the wire which can be determined by measuring T for a calibration block of known MOI and similar mass to the racket. The parallel axis theorem ($I_d = I_{cm} + md^2$) can then be used to connect the MOI about any axis (I_d) with the MOI about the COM of the racket (I_{cm}) as long as the distance between the axes (d) is known.

2.5.3 Generating joint motion

As input to a simulation model, information regarding the forces acting on the system are needed. When the technique has not required maximum effort by the performer and the forces created by the muscles are not of great importance (e.g. Yeadon et al., 1990c) then joint angle time histories have been used as input. However, if the performer reaches a state of maximum effort a muscle model is required that will adequately describe the forces / torques produced during dynamic one-handed backhand groundstrokes so that techniques can be limited to those within the capabilities of the performer.

The parameters of many muscle-driven simulation models have been taken from the literature which means that the model cannot be customised to an individual

(Yeadon & Challis, 1994). In order to obtain subject-specific strength parameters to limit techniques in angle-driven models and for torque-driven simulation models, joint torques have been measured using an isovelocity dynamometer (e.g. King & Yeadon, 2002; Kong, 2005).

Isovelocity dynamometry

Isovelocity dynamometers, such as the KinCom and Cybex control the angular velocity through a specified range of movement (ROM) and measure, via a strain gauge force transducer, the force applied. The subject works maximally against a crank that is moving at a constant angular velocity over a range of angles. Active machines allow torques to be measured under eccentric-concentric conditions. The angular velocity may be set to zero so that isometric trials can be performed. The resistance of the device equals the applied muscular torque throughout the ROM. The advantage of this method over isoinertial testing (variable speed with a fixed resistance) is that the effect of angular acceleration on the torque produced does not need to be accounted for (King, 1998).

The disadvantages are that the machine will not operate at very high angular velocities (typically no higher than 500 deg/s) and this may require the researcher to extrapolate the torque-angular velocity data (e.g. King & Yeadon, 2002). Additionally, the data collection procedure assumes that the participant is able to reach maximum activation throughout the central eccentric-concentric phases of each trial. In a review of isovelocity dynamometry, Herzog (1988) states that (a) gravitational effects, (b) inertial effects, and (c) the non-rigidity of the limb / crank arm system must be accounted for if the isovelocity torque data is to accurately represent the movement in question.

2.5.4 Wobbling masses

To date, most biomechanists have made the significant modelling assumption that the human body is composed of a set of rigid bodies. Hatze (1988) argues that the rigid-body approximation for segments is justifiable since during the course of a motion, the muscles will change their contractive state, and hence their consistency from very soft in the relaxed state to almost rigid in the completely contracted state. However, it has been shown that wobbling masses play an important role in

dissipating energy during an impact (Pain & Challis, 2001a) and upper-body vibration (Yue & Mester, 2001).

As many of the parameters in a wobbling mass model are unknown, attempts to separate the rigid and wobbling components in whole-body simulation models have been simple (e.g. Kong, 2005; Mills, 2005). Here, the bone has been separated from all other components and the relative mass components of each were calculated. This gives two rigid bodies that are connected to each other via non-linear spring-dampers in such a way that the visco-elastic properties of the soft tissue can be modelled. Data from the literature (e.g. Clarys & Marfell-Jones, 1986) can be used to determine the ratios of bone to soft tissue mass in a subject-specific model. However, care must be taken when applying the ratios to athletes with considerably less body fat than those in the literature.

2.5.5 Spring parameters

In a mathematical simulation model of a tennis ball-racket impact, it is anticipated that springs will be needed in the modelling of the ball-racket system, the grip, and any wobbling masses that are incorporated.

Equipment parameters

Previous models of tennis equipment (e.g. Brody, 1979; Cross, 2000a; Leigh & Lu, 1992) have included spring-damper systems. In a simple one-dimensional analysis, Leigh and Lu (1992) modelled the ball, strings and racket separately and then assembled the whole system.

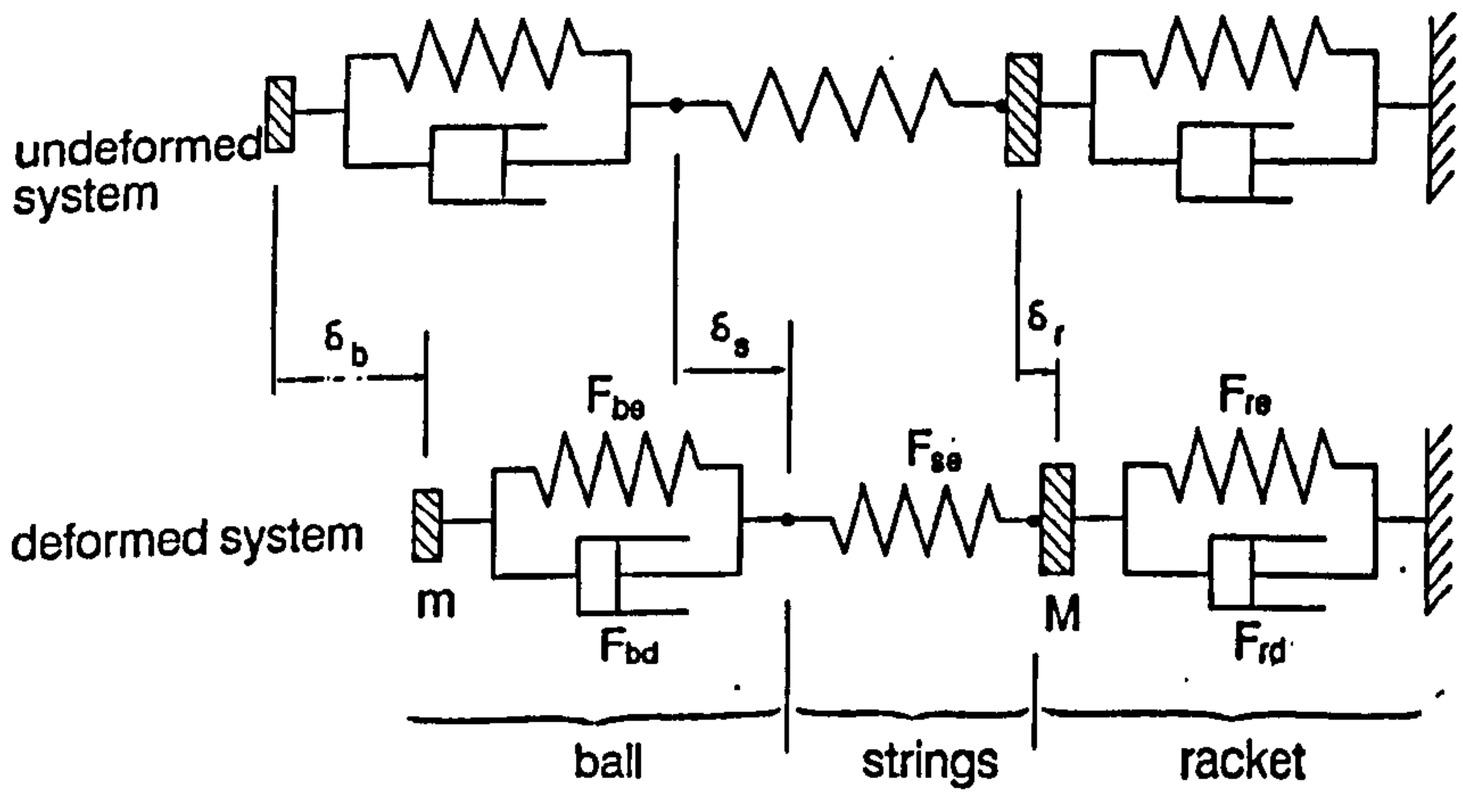

Figure 2.20. Model of ball-strings-racket system
(adapted from Leigh & Lu, 1992, pg. 193)

Simple experiments were carried out to determine the elastic and damping properties of the system. A quasi-static test was performed on a tennis ball to determine the elastic force F_{be} as a function of the deformation δ_b of the ball. The non-linear relationship observed was Equation 2.4:

$$F_{be} = k_b\delta_b + n_b\delta_b^3 \qquad (2.4)$$

where k_b and n_b are the spring constants that were found to be $k_b = 18.44$ kN/m and $n_b = 23860$ kN/m^3. A limitation of a quasi-static test is that the ball is subjected to surface forces on both sides. Brody (1979) performed a force-deformation test on a tennis ball that was placed in a rigid cup so that only one side deformed. His results indicated a value for k_b of about 12.26 kN/m. Neither test can account for the inertia forces distributed throughout the ball during an impact (Leigh & Lu, 1992). Additionally, the behaviour of a ball during a rapid compression (a ball hitting a hard surface) is not the same as that for a slow compression during testing (Brody et al., 2002). Dignall and Haake (2000) found that tennis ball stiffness and damping coefficients show a linear relationship with incoming velocity (Figure 2.21).

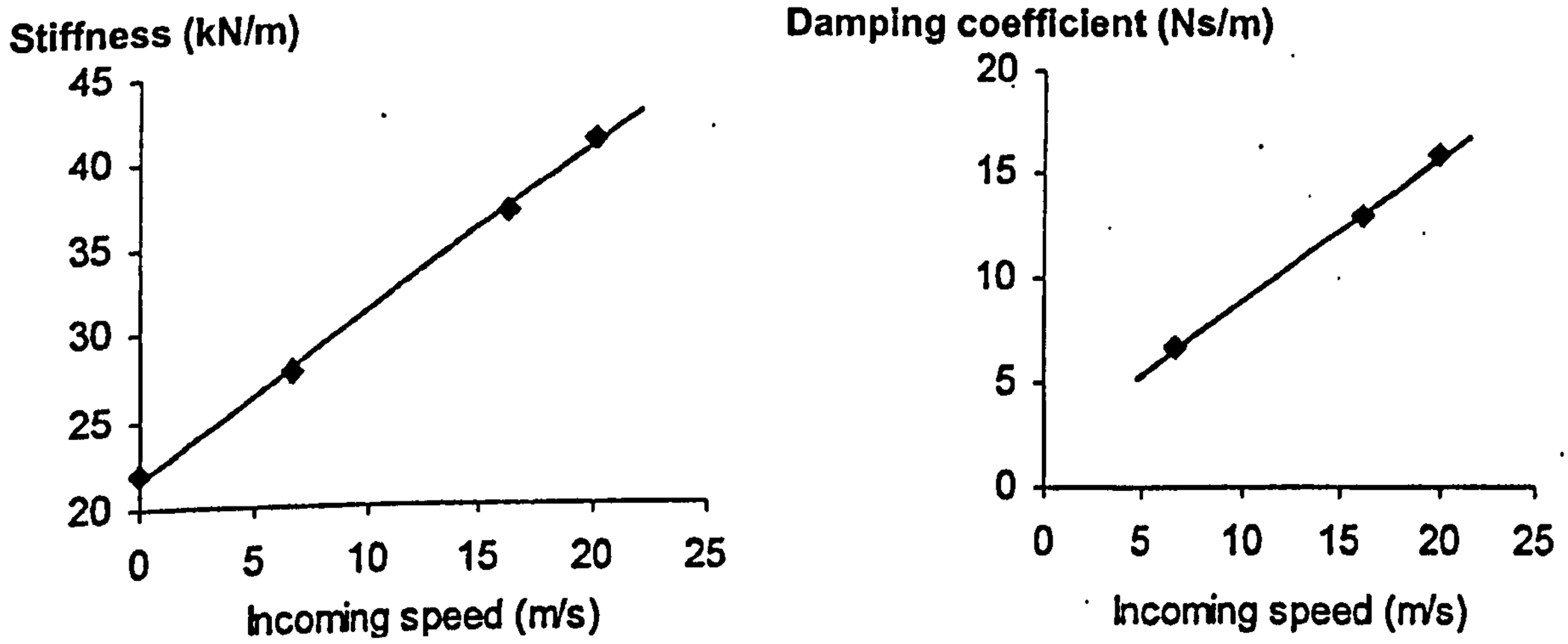

A B

Figure 2.21. The variation of (A) tennis ball stiffness and (B) tennis ball damping coefficient against incoming speed (adapted from Dignall & Haake, 2000, pg. 158)

Cross (2000a) used separate spring stiffness values for the compression and expansion phases to account for the hysteresis in the ball although the spring stiffness

values did not vary as a function of ball deformation or relative ball velocity. The hysteresis loss in the ball was determined by finding the area enclosed by a force-compression curve for a complete compression and expansion cycle. Reasoning that the ball parameters (k_b and c_b) are not constant throughout the impact phase, Goodwill and Haake (2003) determined them empirically using the coefficient of restitution and contact time data from an experiment in which a ball was propelled towards a force platform, perpendicular to the surface. It was assumed that the values of k_b and c_b were dependent only on the maximum displacement value of the centre of mass of the ball and not on the stiffness of the force plate surface.

The stringbed stiffness has been determined by dropping an incompressible sphere onto the strings of a clamped racket (Leigh & Lu, 1992) and by a quasi-static compression test (Goodwill & Haake, 2003). In the later experiment, loads of up to 700 N were applied over a circular area of varying diameter, perpendicular to the stringbed of a racket. For the range of contact areas and stringbed deflections tested, the string-bed stiffness was found to lie between 40 and 60 kN/m. The damping coefficient has been considered negligible (e.g. Leigh & Lu, 1992) or in the case of Goodwill and Haake (2003), has been assigned a constant value which equates to a 5% loss of energy in the stringbed, equal to that found experimentally by Cross (2000b).

Wobbling mass parameters

Springs that are heavily damped have been used in the past as a way of connecting wobbling masses to each skeletal part. These approaches have been both linear (Cole et al., 1996) and non-linear (Pain & Challis, 2001b). Pain and Challis (2001b) determined the spring and damping parameter values using an optimisation technique. The magnitude and frequencies of the movement of the wobbling masses in the simulation model were matched as closely as possible to the movements of wobbling masses, determined experimentally.

2.5.6 Summary of parameter determination

The above sections have described some of the techniques that have been used to evaluate the subject and equipment-specific parameters needed to develop a computer simulation model. The next section will focus upon the techniques that will

be needed to record and analyse performances of one-handed tennis backhand groundstrokes.

2.6 IMAGE ANALYSIS

2.6.1 Overview of image analysis

A 3D image analysis of one-handed backhand performances is required so that realistic inputs can be obtained for the simulation model. Data must be collected and then processed accordingly.

2.6.2 Data collection techniques

One of the earliest methods used to acquire the time histories of various body landmarks was cinematography. However, analysing the film is a slow, pedestrian task, and subject to human error whilst the cost of purchasing and processing cine film is high (Atha, 1984). For the analysis of impacts where the duration of contact can be very short, Atha (1984) suggests that high-speed cinematography (a minimum framing rate of 300 Hz) should be used. High-speed digital cameras can offer high sensor pixel counts, high speed framing rates and excellent image quality. Unlike cine techniques, they offer immediate playback direct from the camera memory or archived image files. If the performance is recorded using at least two cameras and the body landmarks are digitised manually, then the direct linear transformation (DLT) technique (Abdel-Aziz & Karara, 1971) or modifications thereof (e.g. Hatze, 1988) can be used to reconstruct the 3D locations of body landmarks.

The most recent technique for the quantitative analysis of movement is based around systems where markers are automatically tracked. The markers can be active (e.g. light emitting diodes (LEDs) with SELSPOT), or passive (e.g. reflective markers with VICON). The advantages of passive markers are that they require no power source or connecting wires, are lightweight and inexpensive to replace. The disadvantages of such systems are the limited image resolution at sample rates higher than 50 or 60 Hz, the interference caused by sunlight and the difficulty in automatically identifying markers (Yeadon & Challis, 1994). In contrast, LED-based systems generally have higher spatial and temporal resolution and have automatic marker identification.

The system will digitise the locations of these markers, a significant advantage over cinematography and video that require much manual digitisation for quantitative analysis (Bartlett, 1997). However, only the locations of the surface placed markers are given and unlike the aforementioned systems that rely on manual digitisation, the operator cannot estimate the joint centre locations of obscured points (Yeadon & Challis, 1994). Displacements (relative to the joint centre) of the individual skin-mounted markers of up to 20 mm have been observed due to soft tissue movement (Fuller et al., 1997).

2.6.3 Data processing: filtering and curve fitting techniques

Having reconstructed the coordinates of important body landmarks, this data needs additional processing before it is in a suitable form for interpretative analysis. The recorded coordinates may contain systematic errors due to lens distortion or incorrect marker placement and random errors (noise). These must be reduced before further calculations and differentiation (Bartlett, 1997). Data smoothing is also needed for the determination of interpolated values (Yeadon, 1990b). The most popular techniques for the removal of random noise are: digital filters, truncated Fourier series, and splines. Tennis impacts are complicated by the large accelerations at impact and the data smoothing necessary to model the lower-frequency movements (Knudson, 2001).

All three methods produce good fits to displacement data but the digital filter does not provide a smooth analytical function for future computations whilst the Fourier series requires equispaced data (Wood, 1982). A comparison of the techniques described, all with optimum filtering applied, was performed by Challis and Kerwin (1987) for the analysis of film data. They showed that the quintic spline (Wood & Jennings, 1979) was superior to other techniques in terms of smoothing and evaluating the second differentials, whilst the Reinsch cubic spline proved to be superior for interpolating data.

2.6.4 Summary of image analysis

This section has reviewed the techniques required to collect and analyse data on sports performances. The nature of a tennis ball-racket impact means that a high-speed data collection system will be needed to obtain sufficient information. The techniques required to obtain an accurate 3D reconstruction and then process the data

have been discussed with reference to the literature. The method used to smooth the data before analysis depends on the individual application. Yeadon and Challis (1994) warn of errors incurred by over smoothing the data at points of impact, especially when the sampling frequency is low.

2.7 CHAPTER SUMMARY

This chapter has reviewed the literature that has implications for creating a computer simulation model of one-handed tennis backhand groundstrokes. There are two main sections as issues concerning the tennis stroke and simulation modelling in general are addressed. The next chapter will focus on the development of the simulation model using a software package.

CHAPTER 3

MODEL DEVELOPMENT AND FEATURES

3.1 CHAPTER OVERVIEW

A computer simulation model of one-handed tennis backhand groundstrokes was developed. The model comprised a tennis ball-racket system linked to an upper-limb and torso. This chapter describes how the model was formulated using Autolev^{TM} 3.4 Professional software package and details the specific features of the model.

3.2 MODEL DEVELOPMENT USING AUTOLEV

3.2.1 Overview of model development

As a multi-body 3D model was required, it was necessary to have a complete understanding of the software package used and to test ideas for modelling aspects of the dynamic system. Initially, a simple 2D model was formulated based on first principles that consisted of a rigid beam tennis racket and point-mass ball system fixed to an upper-limb segment. An Autolev model of the same system was then coded and the results of simulations with this code were compared with the output from the model coded from first principles. Once satisfied that output from the model generated by Autolev code was correct, more segments and features were systematically added until a tennis ball-racket and upper-limb system were represented in 3D.

At each stage error checks were performed, for example, ensuring that angular momentum about the mass centre of the system was constant when no external forces were acting on the system. In addition, a Matlab code enabled stick figure representations of the simulations to be animated and viewed from three different positions. Figure 3.1 is an example of a simulation where the ball is viewed from above, directly behind and to the side of the human. The torso, upper-limb segments, the racket and the ball are shown for an instant in time when peak ball-stringbed deformation occurred.

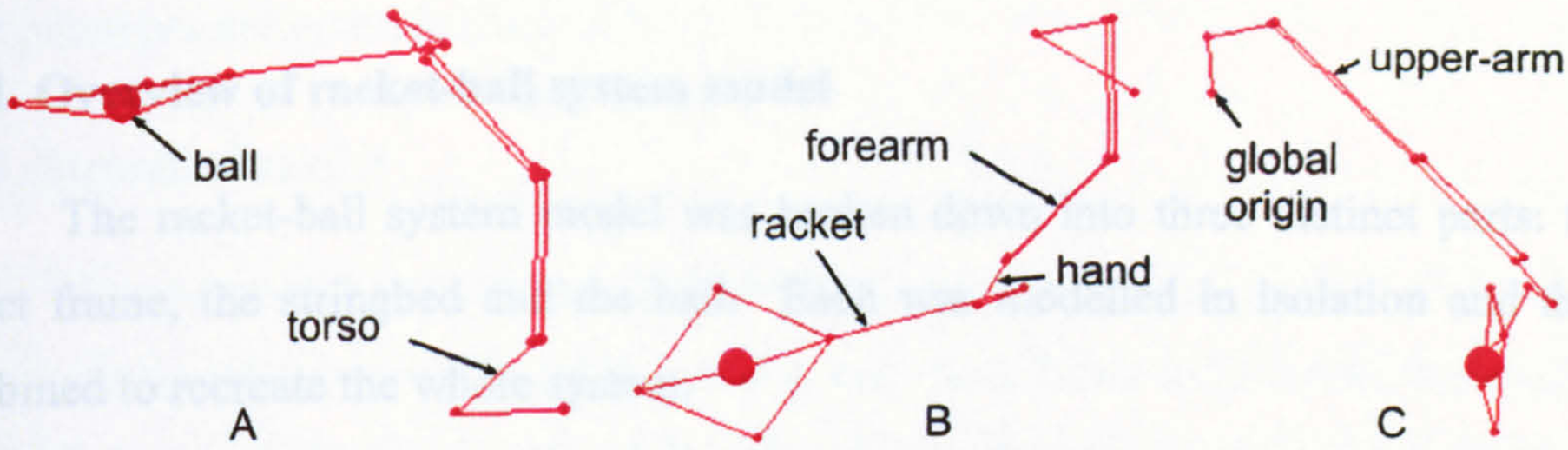

Figure 3.1. Matlab stick figure animations to observe simulations from directly above (A), behind (B) and to the side of the human (C)

3.2.2 Formulating equations of motion

Autolev™ 3.4 Professional software package (Kane & Levinson, 1996) was used to formulate the equations of motion for the model. Expressions relating to constrained generalised inertia forces and constrained generalised active forces were determined resulting in the equations of motion being formulated. Autolev utilises a Kutta-Merson numerical integration algorithm, with a variable step size Runge-Kutta integration method to advance the solutions of the equations of motion. The Autolev command file *backhand* (Appendix 1) describes the structure of the model. Here, commands defining the positions and orientations of each body and the internal and external forces acting on the system were expressed. Three files were produced when the Autolev command file was run: a Fortran program, an input file for the simulation model, and a directory of output files generated when the model was executed.

3.2.3 Customisation of Fortran code

The Fortran code had to be compiled although customisation was first required for the model to meet the needs of the study. The equations of motion remained untouched but alterations were necessary to allow both single simulations and multiple simulations as part of optimisations to be run. It was also necessary to evaluate the model by comparing performances and simulation output by minimising differences in kinematic variables. The Fortran programme generated by the Autolev code was converted into a subroutine of a main programme. By calling further subroutines and selecting certain options, the joint angle time histories used to drive the simulation were specified.

3.3 RACKET-BALL SYSTEM MODEL

3.3.1 Overview of racket-ball system model

The racket-ball system model was broken down into three distinct parts: the racket frame, the stringbed and the ball. Each was modelled in isolation and then combined to recreate the whole system.

3.3.2 Racket frame model

The racket frame was modelled as two rigid bodies connected by a frictionless pin joint located at the antinode of the fundamental modes of vibration in and out of the plane of the racket face (Figure 3.2). Vibration of the racket frame was modelled using two torsional spring-dampers to allow motion in and out of the racket plane. The passive torque between the two bodies E and F about an axis was given by Equation 3.1:

$$T = -k_f\theta - c_f\dot{\theta} \qquad (3.1)$$

where T = the torque between the two bodies E and F

k_f = the stiffness coefficient

c_f = the damping coefficient

θ = the angle between the two bodies E and F

$\dot{\theta}$ = the angular velocity of body E relative to F

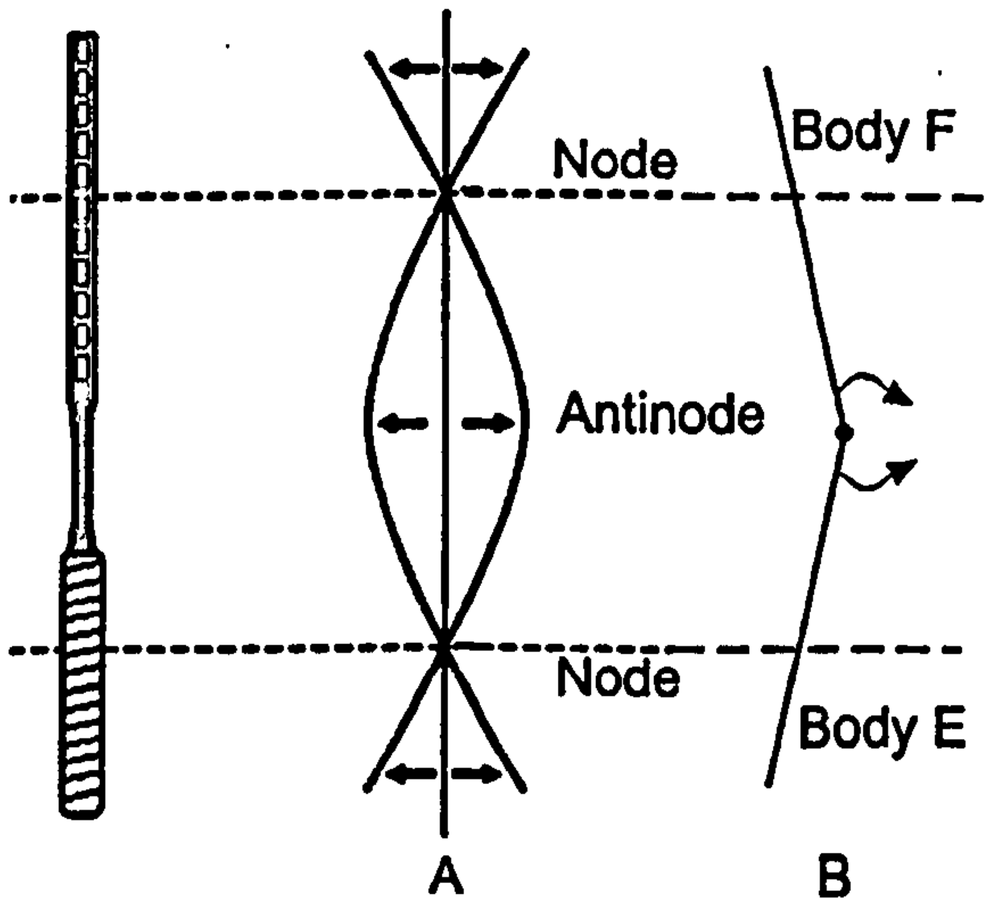

Figure 3.2. Location of nodes and antinode for a fundamental mode shape (A) and the rigid body approximation of the tennis racket (B)

Details of the determination of the stiffness and damping coefficient for each torsional spring-damper are given in Section 5.4.2.

3.3.3 Stringbed model

It was important to design a model that would incorporate impacts away from the geometric stringbed centre (GSC) as this may be a factor influencing the loading at the elbow joint (Hennig et al., 1992). The stringbed model (Figure 3.3) comprised a point of impact at the GSC and then an additional eight points were positioned around it so that each was the diameter of a tennis ball away from the adjoining contact point. In this way, almost the entire stringbed surface could be covered and a variety of impacts could be modelled. Each point of contact was considered a particle with its mass being that of the synthetic gut used to string the racket divided by nine (the number of points of contact).

Point masses were connected to additional points of contact and / or a point(s) on the racket frame by a linear spring. When the springs were of natural length at the start of a simulation, the force in them was due to a constant term representing initial string tension. Stringbed stiffness varied as four spring constants were defined around the GSC (ks1:ks4). An additional six constants (k5:k10) were defined to give the stiffness of the springs near the racket frame as a multiple of the four spring constants (Figure 3.3). In this way, the determination of the spring constants by optimisation (Section 5.6.2) was made easier. A damping term was not included since the strings absorb the incoming ball energy by deforming and returning 95% of that energy back to the ball (Brody, 1995).

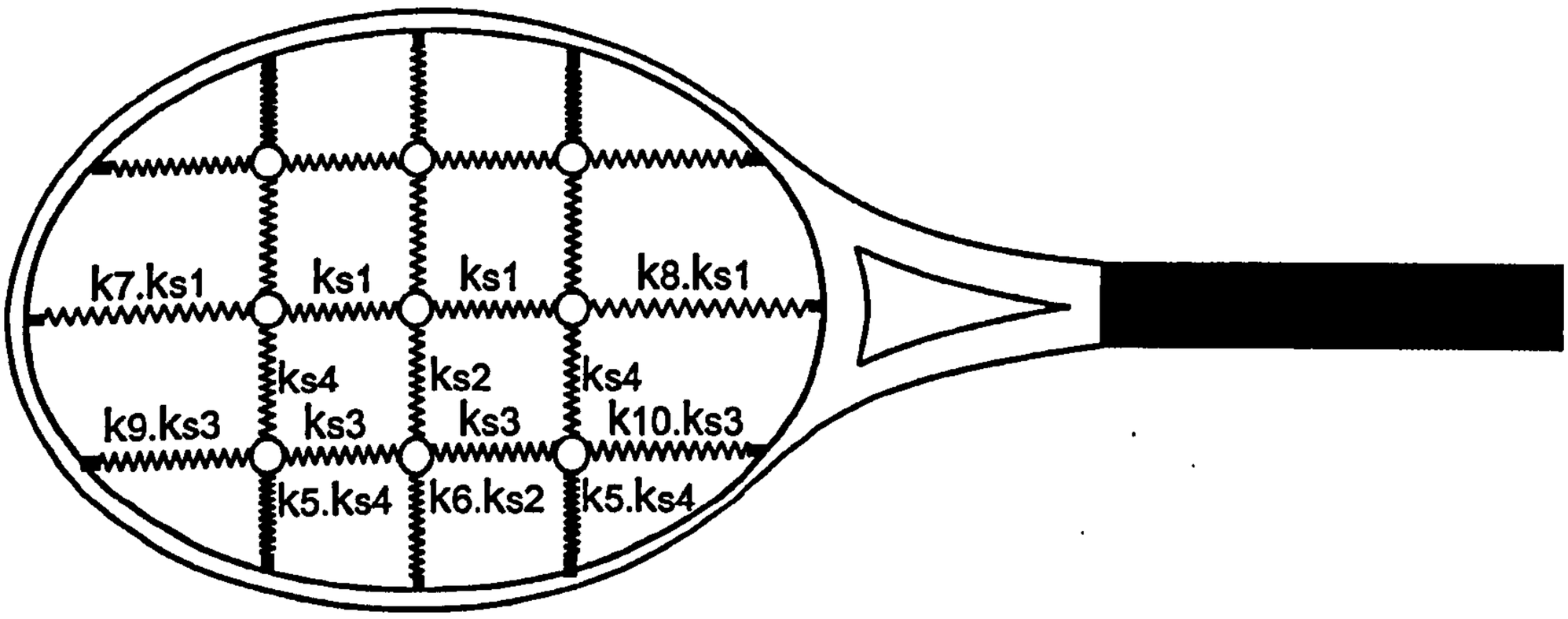

Figure 3.3. Points of ball contact and spring constants for the stringbed model

Each contact point had a single degree of freedom (DOF) to allow deformation of the contact point perpendicular to the plane of the racket in its resting state. High-speed video data (Section 4.2.1) showed that for the impacts observed on the stringbeds tested, movement of the point on the stringbed in the plane of the racket was small. The extra 2 DOF per point mass (an extra 18 DOF for the simulation model) would have caused high computational requirements and were therefore assumed to be zero. Any movement of the ball relative to the contact point on the stringbed was incorporated in the 3 DOF ball model (Section 3.3.4).

The force in each spring in the stringbed was defined using Equation 3.2 with Ls_i equal initially to Lo_i so that the force in all springs at the start of a simulation was equal to the initial force within each spring, ST0:

$$ST_i = -ks_i\left(Ls_i - Lo_i + \left(ST0/ks_i\right)\right) \tag{3.2}$$

where: ST_i = the restoring force in the spring

ks_i = the stiffness of the spring

Ls_i = the length of the spring during the simulation

Lo_i = the initial length of the spring

ST0 = the initial force within the spring

3.3.4 Tennis ball-stringbed impact model

For a typical one-handed backhand groundstroke, the tennis ball is struck at or near the top of its bounce. Analysis of high-speed video data of one-handed backhand groundstrokes (Section 4.2.2) showed that the major component of ball velocity was normal to the racket plane on impact. Vicon motion analysis of the same trials (Section 4.2.2) showed that the tennis racket had considerable components of velocity in the plane of the racket as well as the main component of velocity out of the plane of the racket. Since the relative velocity between the ball and the racket is important when considering the force between the ball and the stringbed, oblique impacts were incorporated when creating the ball model.

The ball was modelled in 1D as a point mass (m_b) connected to a point mass on the stringbed (m_s) by a spring and damper in parallel (Figure 3.4). The normal force (N) acting on the ball was given by Equation 3.3 where x was the displacement

and $\dot{x}$ was the velocity of the ball relative to the point on the stringbed, whilst k and c were the spring and damping coefficients respectively.

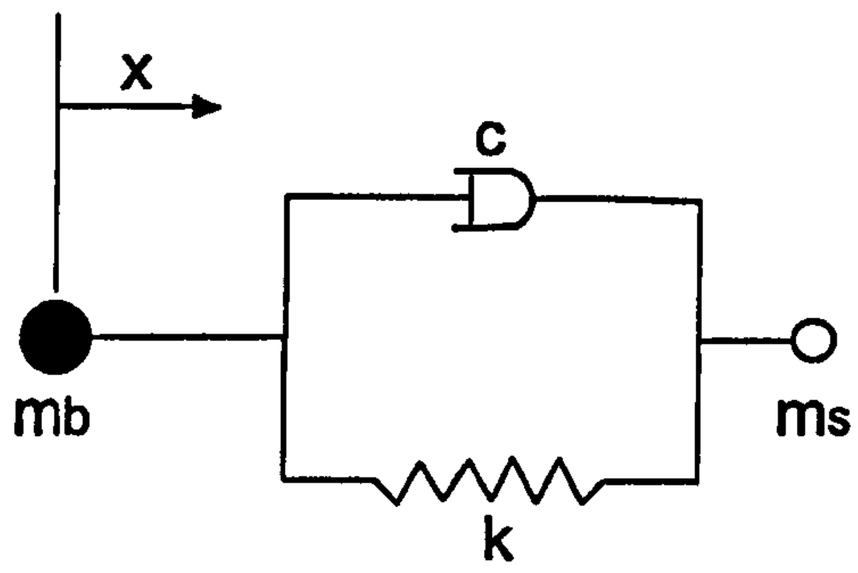

Figure 3.4. Spring-damper model of the normal component of ball-stringbed impact

$$N = -kx - c\dot{x} \tag{3.3}$$

The oblique component of the ball was represented by a friction force opposing its motion. A tennis ball will initially slide on contact with the stringbed. If the friction force and the angle at which the ball strikes is large enough, the ball may begin to roll (Brody, 1984). The interaction between the ball and the stringbed can be analysed in terms of the coefficients of sliding and rolling friction. For the purpose of this simplified model, a single coefficient of friction (μ_i) was used to define the friction force (F) acting perpendicular to the normal force and in the opposite direction to the horizontal component of the ball velocity (v_b). Weight (mg) is the other force acting on the ball (Figure 3.5).

$$F = \mu_i N \tag{3.4}$$

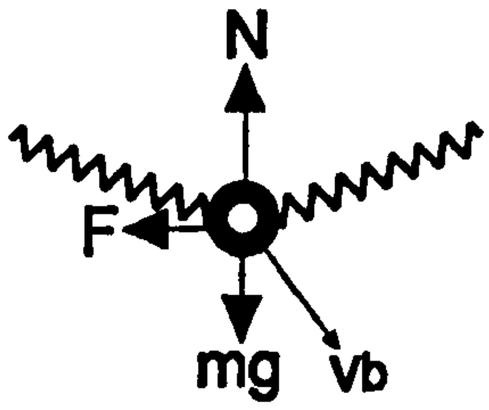

Figure 3.5. Forces acting on the ball during impact with the stringbed

Since tennis ball rebound velocity depends on the stringbed stiffness at the point of impact, three values for μ_i were included for the oblique component of the ball model (Figure 3.6).

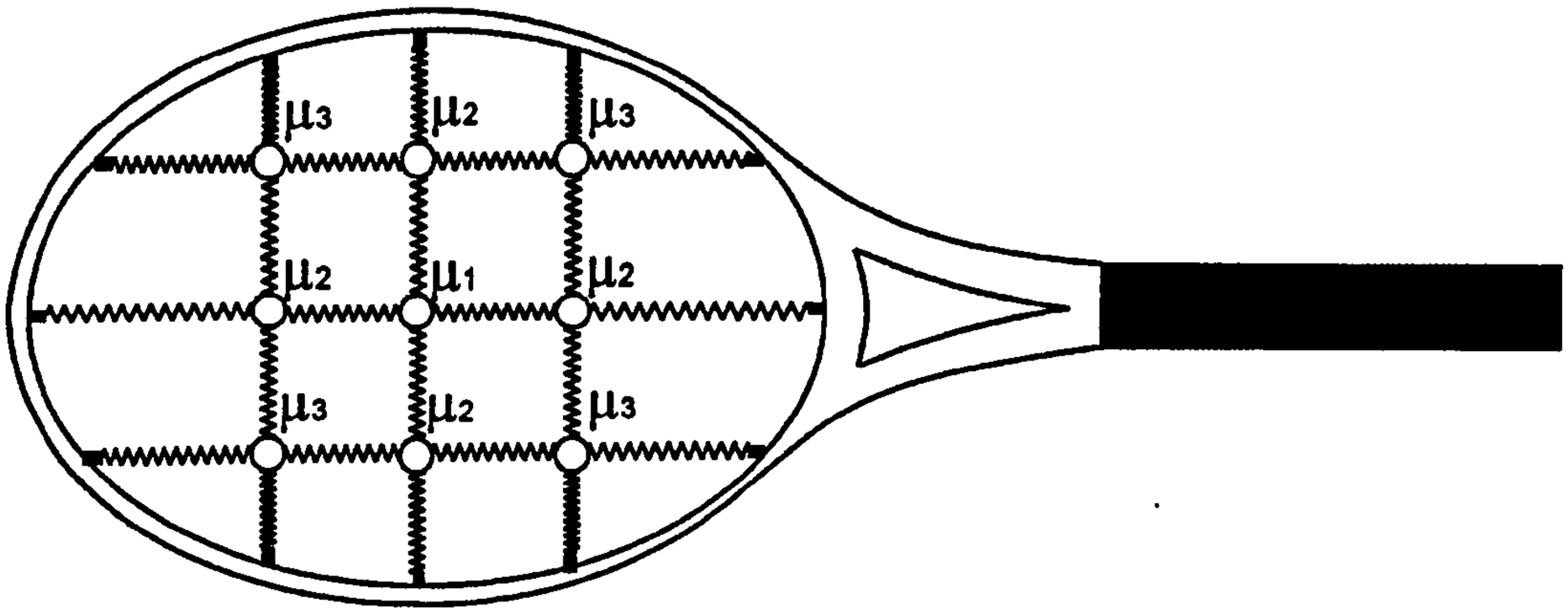

Figure 3.6. Coefficients of friction corresponding to points of impact on the stringbed

3.4 TENNIS PLAYER MODEL

3.4.1 Overview of tennis player model

Based on the kinematic analysis of the performance data collected, explained in Section 4.2.1, the need for a 3D model incorporating a torso, upper-arm, forearm and hand segment was evident. Wobbling masses were necessary to model the soft tissue motion relative to the bone and a method of gripping the racket at the handle was required that would result in realistic inputs to the human system.

3.4.2 Upper-limb model

The global origin of the system was coincident with the centre of the thorax segment at the start of a simulation. The displacement, velocity and acceleration of the thorax centre from the global origin were specified in the global x, y and z directions with respect to time for the course of the simulation. A rigid segment with three rotational DOF connected the thorax centre to the shoulder joint. Each joint was modelled as a simple pin joint and the centres were connected by rigid bodies of fixed length (Figure3.7). At the shoulder joint there were three rotational DOF to allow flexion / extension (θ_{sfe}), horizontal adduction / abduction (θ_{saa}) and internal / external rotation (θ_{sie}). At the elbow joint, there were three rotational DOF to allow flexion /

extension (θ_{efe}), pronation / supination (θ_{eps}) and the adduction / abduction (θ_{eaa}) which creates the carry angle. At the wrist joint there were also two rotational DOF to allow flexion / extension (θ_{wfe}) and radial / ulnar deviation (θ_{wru}).

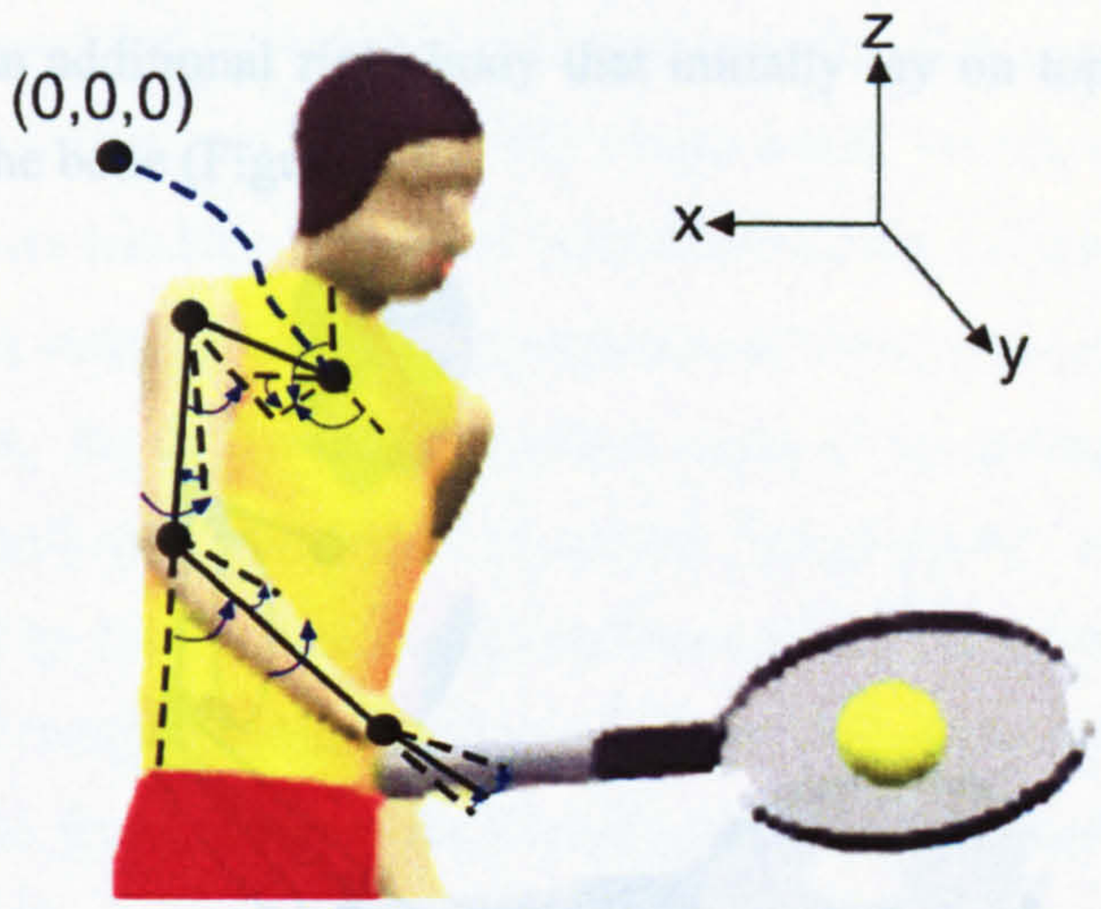

Figure 3.7. The human rigid-body model with 11 rotational and 3 translational DOF

Joint angles were based on the standard anatomical position (Figure 3.8). Shoulder flexion, shoulder abduction, shoulder internal rotation, elbow flexion, forearm pronation, wrist flexion and wrist radial deviation were defined as positive movements (an increase in joint angle).

Figure 3.8. Standard anatomical position

3.4.3 Wobbling masses

Wobbling masses were included within the upper-arm and forearm segments to represent the movement of soft tissue relative to the rigid bone. Both arm segments were divided into the fixed and wobbling component (Section 4.4.3). Each wobbling mass was modelled as an additional rigid body that initially lay on top of the fixed rigid body representing the bone (Figure 3.9).

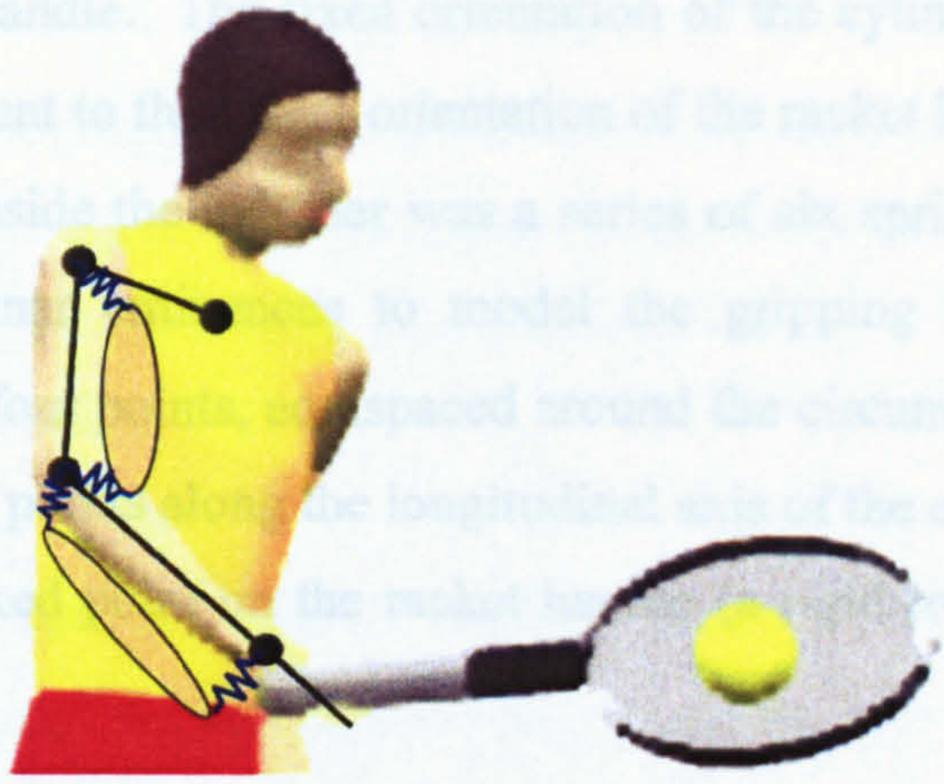

Figure 3.9. The wobbling mass attached to the rigid segment through two sets of non-linear damped springs

The wobbling masses were attached to the fixed rigid components by two identical 3D non-linear damped springs. The springs were near critically damped and the spring-damper force was given by the following equation (Pain & Challis, 2001a):

$$F = -kx^3 - cv \tag{3.5}$$

where F = spring force

k = stiffness

c = damping

x = displacement

v = velocity

3.4.4 Racket-hand interface

Research has shown that for the one-handed backhand topspin drive groundstroke, peak forces occur at the thenar and hypothenar eminences (Hatze, 1976; Knudson, 1991b; Knudson & White, 1989a) whilst the axis of rotation of the racket

handle is located almost exactly in the middle of the hand (Cross, 1998). In reality, the movement of the racket relative to the hand is influenced by muscular contractions modifying the grip forces. However, at impact and for a short time period after the racket recoils and behaves like a spring-damper relative to the hand.

The hand was represented by a rigid segment connecting the wrist joint centre to the proximal end of the metacarpal of the middle finger which in turn was fixed to a cylinder encasing the racket handle. The fixed orientation of the cylinder relative to the rigid segment was equivalent to the initial orientation of the racket handle relative to the same rigid segment. Inside the cylinder was a series of six spring-dampers at both the thenar and hypothenar eminences to model the gripping forces. Both eminences were modelled by four points, equispaced around the circumference of the cylinder and an additional two points along the longitudinal axis of the cylinder. Each point was connected to the fixed point on the racket handle (a rigid rod) by a linear spring-damper (Figure 3.10).

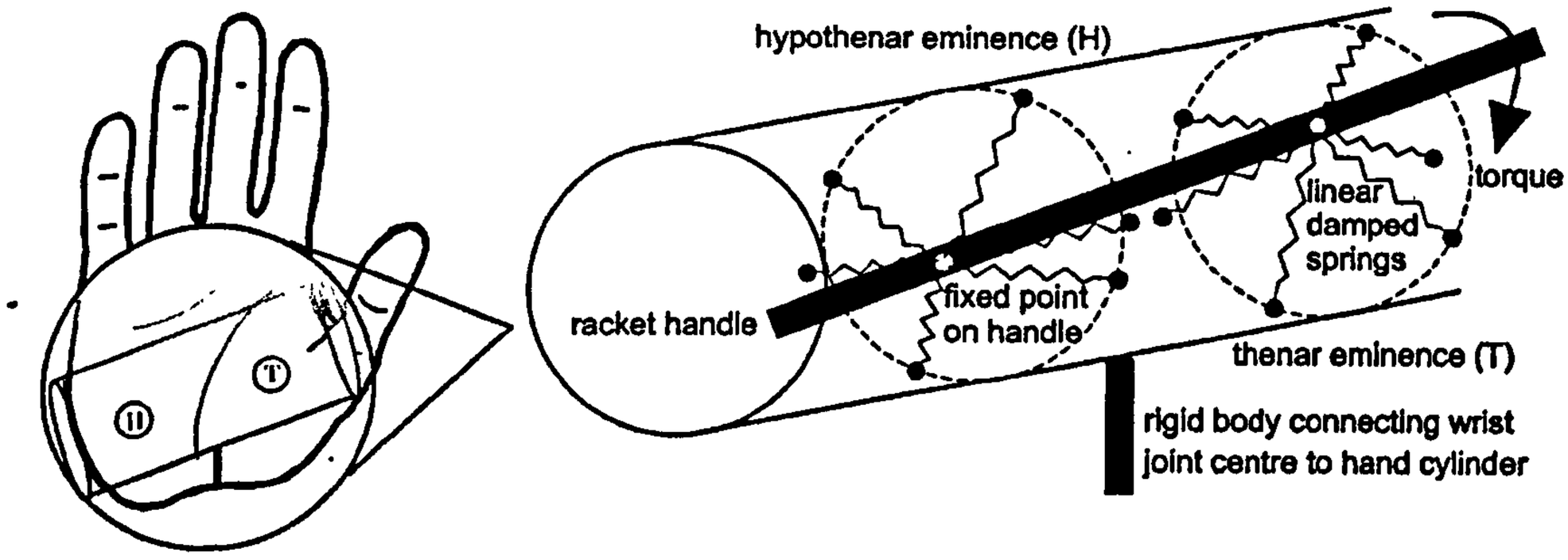

Figure 3.10. Racket-hand interface

The dimensions of the cylinder and the location of the eminences were determined from anthropometric measurements (Section 4.3.3). The initial lengths of the springs were all equal so that the tendency of the racket was always to revert back to this equilibrium position after ball impact. An initial force term at both eminences meant that the force in the springs was non-zero whilst in its initial position at impact. Motion analysis of the one-handed backhand groundstrokes showed that there was linear and angular acceleration of the mass centre of the racket at ball impact in the global reference frame. Additional forces at each eminence were therefore needed to generate non-zero net force at the two contact points on the racket handle. These

forces at each eminence were ramped down using a quintic function (Yeadon, 1984) over a time period of 10 ms. A sensitivity analysis was performed (Section 6.4.8) to show the effect of ramping down time on outputs at the arm. The gripping force acting on the point on the racket handle was given by Equation 3.7:

$$F = -k(L - L_0 + (F_0/k)) - c\dot{L}(L - L_0) + R_0 \qquad (3.7)$$

where F = force between the points on the racket handle and hand eminences

F_0 = the initial force acting on the fixed point on the racket handle

R_0 = initial force ramped down using a quintic function

k = the stiffness coefficient

c = the damping coefficient

L = the length of the spring during the simulation

$\dot{L}$ = the rate of change of the length of the spring with respect to time

L_0 = the initial length of the spring

Since gripping forces were applied to two single points on the racket handle, a mechanism for modelling resistance to the rotation of the racket handle about its longitudinal axis was needed (particularly for off-centre impacts). This was achieved by using a torsional spring-damper. The initial torque was ramped down using the same quintic function as for the gripping forces. The torque acting about the longitudinal axis of the racket handle was given by Equation 3.8:

$$T_E = -k_E(\theta - \theta_0) - c_E\dot{\theta}|\theta - \theta_0| + T_0 \qquad (3.8)$$

where T_E = the torque about the longitudinal axis of the racket handle

T_0 = initial torque ramped down using a quintic function

k_E = the stiffness coefficient

c_E = the damping coefficient

θ = angle of the racket handle about longitudinal axis relative to hand

θ_0 = initial angle of the racket handle about longitudinal axis relative to hand

$\dot{\theta}$ = angular velocity of the racket handle relative to hand

3.5 ANGLE-DRIVEN MODEL

3.5.1 Overview of angle-driven model

Movements of the tennis player segments were driven by joint angle time histories obtained from Vicon motion analysis (Section 4.2.2). Input parameters were specified and a series of output files produced after running a simulation.

3.5.2 Joint angle time histories

Joint angle time histories and their first two derivatives of the movements about the thorax centre and at the shoulder, elbow and wrist joints were obtained by fitting the original data with quintic splines (Wood & Jennings, 1979). Each trial was cropped and spline coefficients determined for when the wrist joint centre began moving forward towards the incoming ball to the point when the wrist joint centre was no longer moving forwards in the direction of the outbound ball in the follow through phase. With the correct initial conditions, a simulation could be run for any time period between these two events. However, many features of interest in terms of the subsequent loading at the elbow joint (ball impacting the stringbed and leaving, racket frame oscillation and decay, transmission of force through arm system) occur in the first 50 ms after ball impact (Brody, 1989). Therefore, simulations were run from ball impact to a point in time 50 ms afterwards.

3.5.3 Input parameters and model output

The input to the model included the initial position and velocity of the ball in the global reference frame along with the relative velocity between the ball and selected contact point on the stringbed. The position of the racket handle relative to the hand and the initial angles, angular and linear velocities between the racket handle and the hand were also required. Subject-specific inertia parameters for the tennis player (Section 4.3.3) and tennis rackets (Section 5.3.3) determined from experiments were used. Some of the model parameters such as the stiffness and damping coefficients at the racket-hand interface were difficult, if not impossible to measure directly from an experiment. These parameters were determined indirectly by driving the model with the known initial conditions and joint angle time histories and

optimising the uncertain parameters to minimise the difference between simulation and performance. Details of the optimisation procedures are in Section 4.5.2.

The model outputs of most interest were the resultant internal joint forces at the wrist and elbow joints and the net torques around the joints required to produce the movement. For the purpose of evaluating the model, the linear and angular displacements of the racket relative to the hand, the time of contact between the ball and the stringbed and the outbound ball velocities were required.

3.5.4 Joint torque limit

In reality the muscles around a joint create a torque that causes changes in joint angles. Section 4.6.2 outlines the procedures used to determine the subject-specific parameters of 3D surface functions which describe the joint torque / angle / angular velocity profiles for the movements of interest at a joint. The surface function calculates the maximum voluntary joint torque that the tennis player can produce for a given angle and angular velocity. An isovelocity dynamometer was used to collect data for a range of angles and angular velocities. The joint torques output from the simulation model are compared to the maximum voluntary joint torques determined from strength tests in Section 6.2.5.

3.6 CHAPTER SUMMARY

This chapter describes the development and features of the computer simulation model used to answer the research questions posed in Chapter 1. The model incorporates a ball-racket system linked to an upper-limb and torso segment. Details of the data collections and the procedures used to calculate the model parameters are given in the following chapters.

CHAPTER 4

PERFORMANCE DATA COLLECTION AND SUBJECT PARAMETER DETERMINATION

4.1 CHAPTER OVERVIEW

In this chapter an explanation of the equipment used and protocol for collecting kinematic, kinetic and electromyography (EMG) data of an elite male subject performing one-handed tennis backhand groundstrokes is given. This chapter also explains the experimental and theoretical procedures used to obtain inertia, wobbling mass and gripping parameters of the subject, required as input to the model. In addition, there is an overview of the methods used to calculate subject-specific maximum voluntary torque profiles which could be used to establish if theoretical maximum joint torque limits are violated for a given technique.

4.2 PERFORMANCE DATA COLLECTION

4.2.1 Overview of performance data collection

To have confidence that a computer simulation model can replicate real life movement, the simulation output must be compared to performances of the subject / equipment. A testing protocol was established to collect synchronised kinematic, kinetic and EMG data for this purpose.

4.2.2 Kinematic data collection

Vicon motion tracking system

A Vicon 624 motion tracking system, situated within the National Gymnastics Centre at Loughborough University, was utilised to collect kinematic data. Twelve M2 strobe cameras sampling at a frequency of 250 Hz were used to calibrate a volume of approximately 2.5 m^3 and then track the motion of markers attached to the subject as he performed one-handed backhand groundstrokes. Reflective markers 25 mm in diameter, were attached to body landmarks in accordance with the Gollum

generic marker set. Additional markers were placed on the right biceps brachii, the forearm and at six locations on the racket frame (Figure 4.1). Wand calibration of the performance volume yielded a mean reconstruction error of 2.2 mm. Within the Vicon Bodybuilder software a model code *tennisgollum.mod* (Appendix 2) was developed specifically for the analysis of the data collected. Markers were assigned labels and then joint centres and specified angles and displacements were calculated.

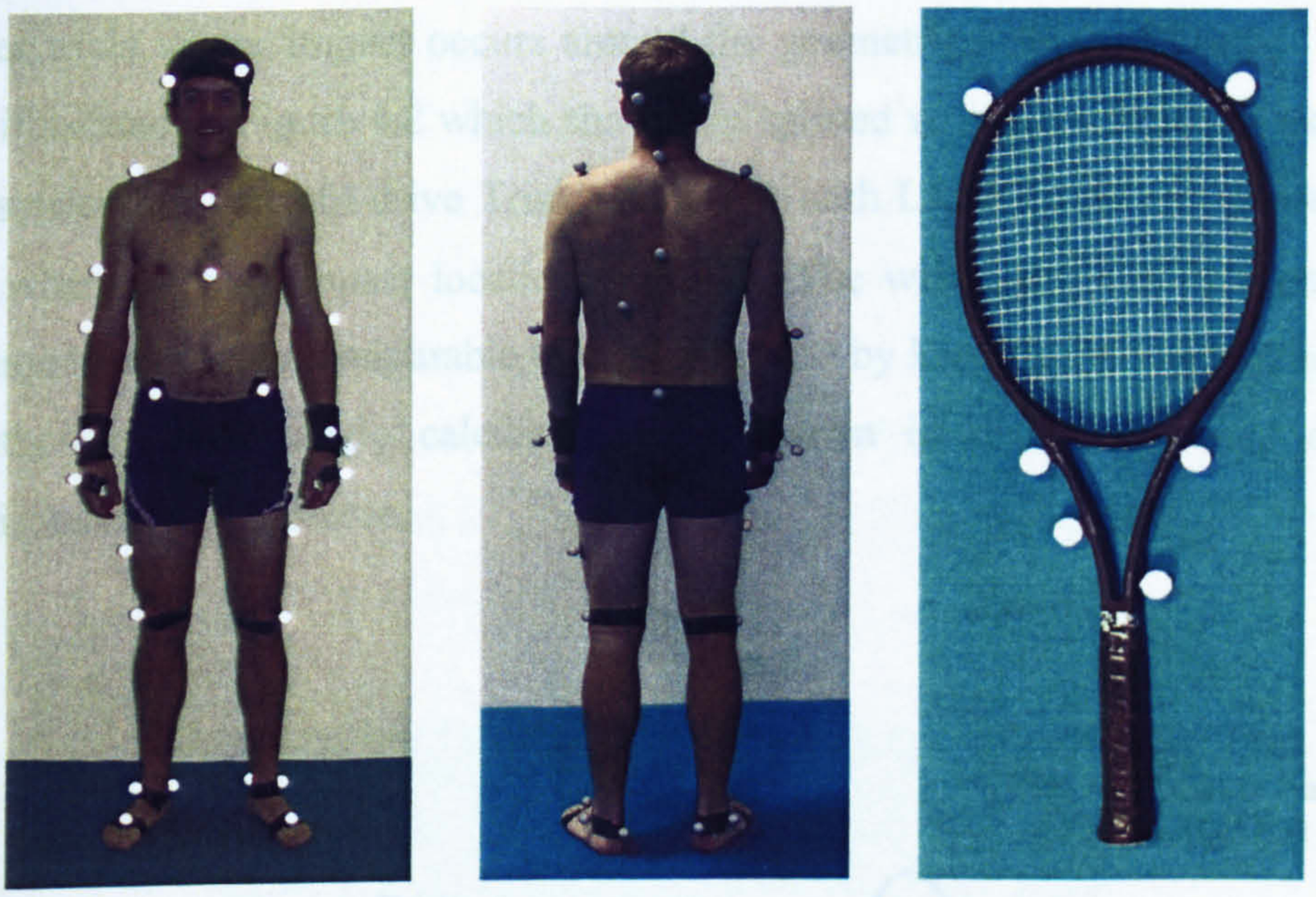

A B C

Figure 4.1. Marker placement for the front (A) and back (B) of the subject and a tennis racket (C)

Fitting splines to data

Raw kinematic data from the Vicon motion analysis was fitted using quintic splines (Wood & Jennings, 1979) to smooth errors in the data and to give time histories which could be used in the simulation model. The error in each data point was calculated by comparing each data point with an equivalent pseudo data value determined by averaging data values from adjacent frames (King, 1998).

Joint angle-time histories

Joint angles were defined as in Section 3.4.2 and joint angle-time histories for each selected trial can been seen in Appendix 3 for 50 ms before and after initial ball impact. The joint angles at impact observed in this study are comparable to those

reported by Wang et al. (1998). As expected for an elite performer, the angle-time histories for a particular joint movement are consistent across trials. On closer inspection, there was a noticeable difference in the shoulder flexion / extension angle for Trial 56 (slice groundstroke) when compared to the topspin drive groundstrokes as the subject 'chops' down on the ball by extending the shoulder joint to generate underspin. Additionally, for Trial 8 where the ball impacts the stringbed off-centre, the wrist appears to be forced into more flexion after ball impact when compared to the other trials where impact occurs around the geometric stringbed centre. This is clearly illusrated in Figure 4.2 which shows the splined wrist joint flexion / extension time histories for Topspin drive Trials 8 and 24 (both LM 8 racket frames strung at 57 lbs) when the ball impact location changes. The wrist joint flexion / extension angle-time histories are comparable to those reported by Riek et al. (1999) although as the method of joint angle calculation is unknown in that case, more detailed comparisons are not possible.

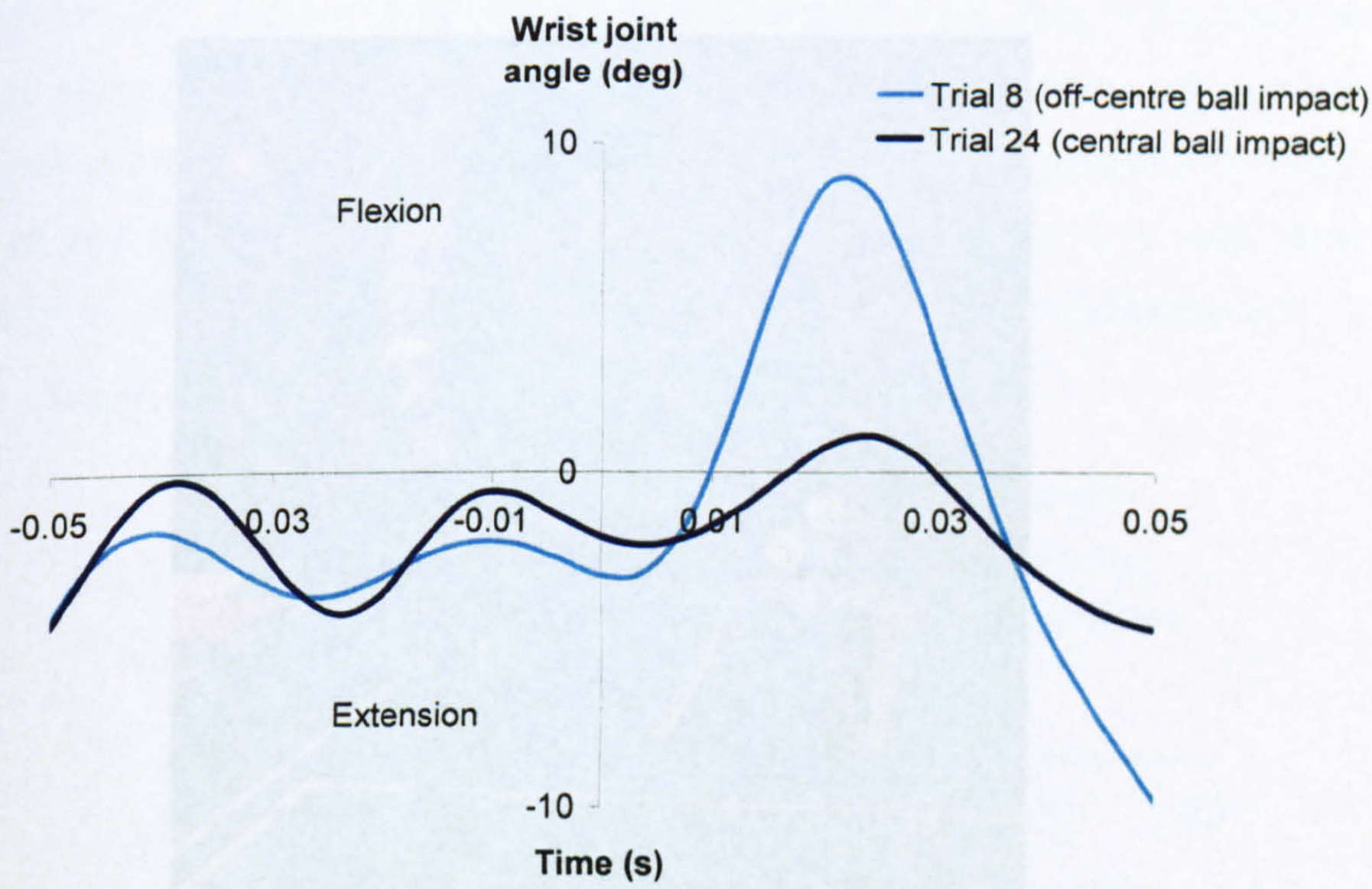

Figure 4.2. Splined wrist joint flexion / extension angle-time histories for a central and off-centre ball impact

High-speed cameras

Two Phantom v4.1 high-speed digital cameras (Vision Research Inc.) operating at 2500 Hz were used to calculate the inbound and outbound ball velocities by digitising the centre of the ball using the associated Phantom software. The impact location and the time of ball contact with the stringbed were also obtained. The cameras were genlocked with the master camera directly behind the tennis player (Figure 4.3) and the slave approximately in line with the longitudinal axis of the tennis racket at the point of impact. The exposure time was set to 390 μs whilst the trigger was chosen so that the ball impact occurred approximately in the middle of the data capture. For the selected trials, Table 4.1 shows the inbound and outbound ball velocities in the global y and z directions (indicated on Figure 4.3). The component of inbound and outbound ball velocity in the x direction was assumed to be close to zero for each trial as the ball cannon was fixed and only shots hit back into the target area were selected. The impact location (indicated on Figure 4.3) and the time of ball contact on the stringbed are also presented.

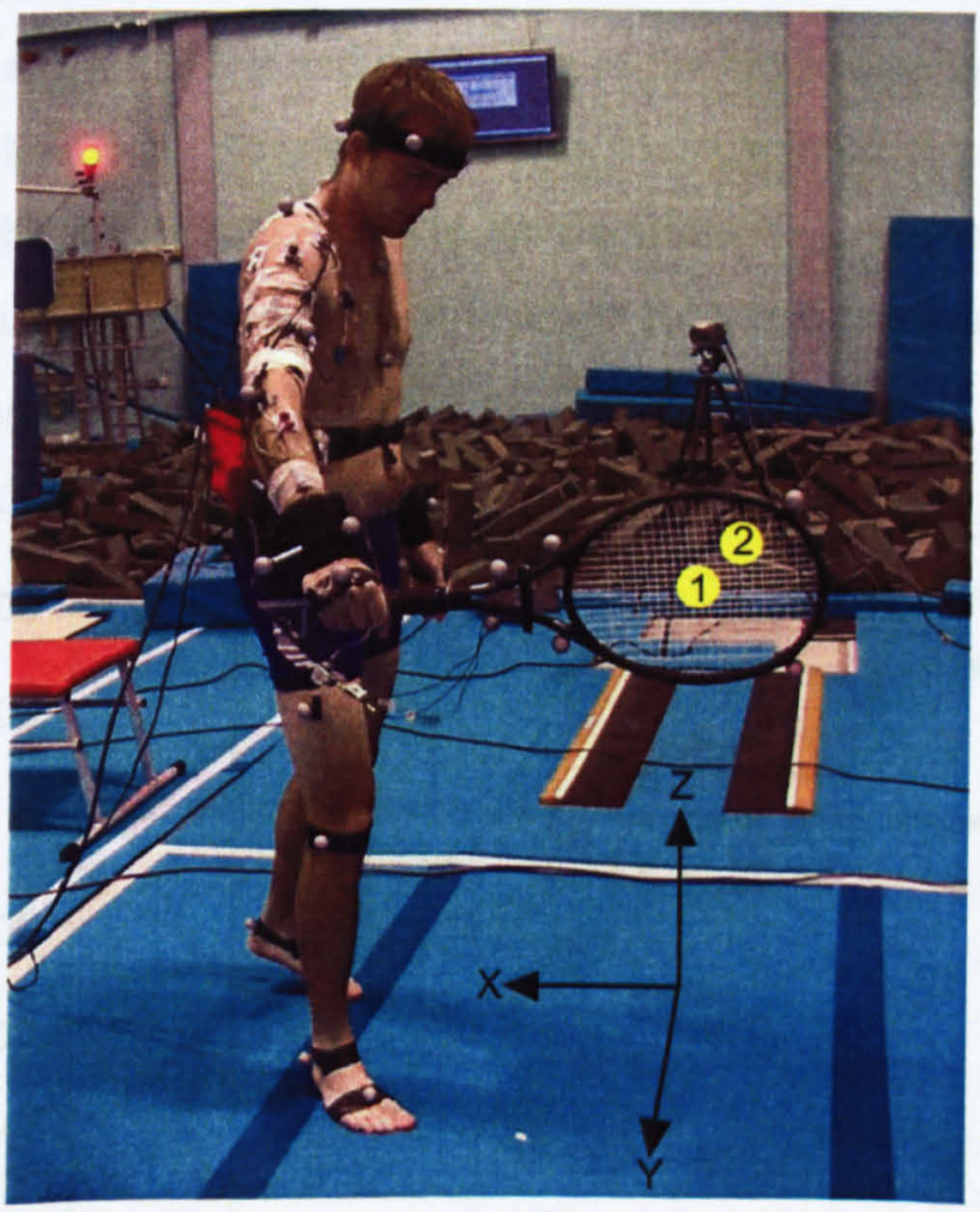

Figure 4.3. View of the subject with an instrumented racket standing in the hitting volume with a high-speed camera directly behind

Table 4.1. Inbound and outbound ball velocities for selected performance trials

Trial number	Inbound ball velocity (m/s)		Outbound ball velocity (m/s)		Contact time (ms)	Impact location
	y	z	y	z		
1	-10.04	-0.17	34.13	1.88	4.2	1
8	-8.68	-1.45	24.75	5.06	3.8	2
24	-8.80	-0.59	30.07	1.84	4.0	1
31	-9.98	-2.35	33.08	4.05	4.0	1
36	-9.00	-1.35	30.94	6.19	4.0	1
56	-10.01	-1.58	27.73	2.95	4.0	1

Uni-axial accelerometers

For certain trials, tennis rackets had three uni-axial, Brüel and Kjaer charge accelerometers mounted at the throat of the tennis racket using custom manufactured aluminium brackets clamped to the frame. Accelerometers were fixed in the centre to measure in plane and at the left and right sides of the bracket to measure out of plane racket frame accelerations. Accelerometer data were captured at a frequency of 2000 Hz to compare the actual racket frame accelerations (e.g. Figure 4.4) with those predicted by the simulation model. A comparison for a trial is made in Section 6.2.3.

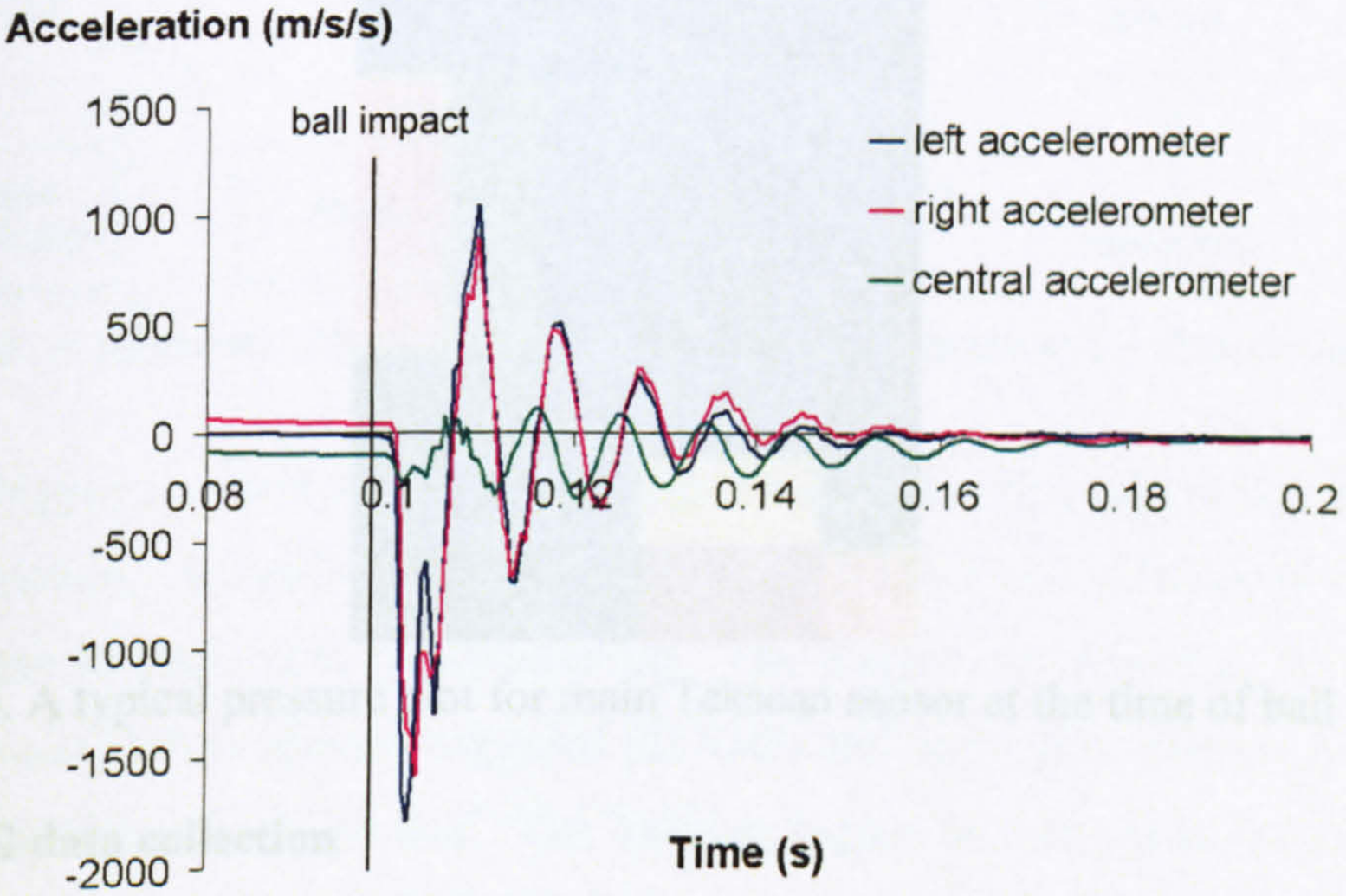

Figure 4.4. Examples of raw acceleration traces from uni-axial accelerometers mounted on a bracket attached to the racket frame

4.2.3 Kinetic data collection

Tekscan pressure sensors

To obtain information on how the tennis racket was interacting with the hand, one of each of the two racket models was instrumented with Tekscan pressure sensors under the grip. Two Tekscan sensors, sampling at 250 Hz allowed full grip pressure to be monitored. The main sensor allowed 6 of the 8 flats of the racket handle to be covered whilst an additional sensor monitored the pressure over the remaining two flats. Each sensor was mounted on plastic strips to cover the soft and uneven polyurethane foam surface. The Tekscan system was pre-calibrated in the laboratory and pressures were recorded in PSI over individual sensor areas of 0.25 square inches.

Figure 4.5 shows a section of a typical Tekscan trace from the main sensor at the time of ball impact for a topspin drive backhand groundstroke. The system accurately predicts the relative changes in grip pressure. The high pressures around the thenar (top left) and hypothenar (bottom right) eminences are clearly shown by the 'hot' colours. This supports the idea that the hand-racket complex can be modelled as suggested in Section 3.4.4. A comparison is made for a particular trial in the model evaluation (Section 6.2.4). The absolute pressure values predicted by the Tekscan system are limited due to the low sampling frequency at impact, and the inability to measure forces that are not perpendicular to the plane of the sensor.

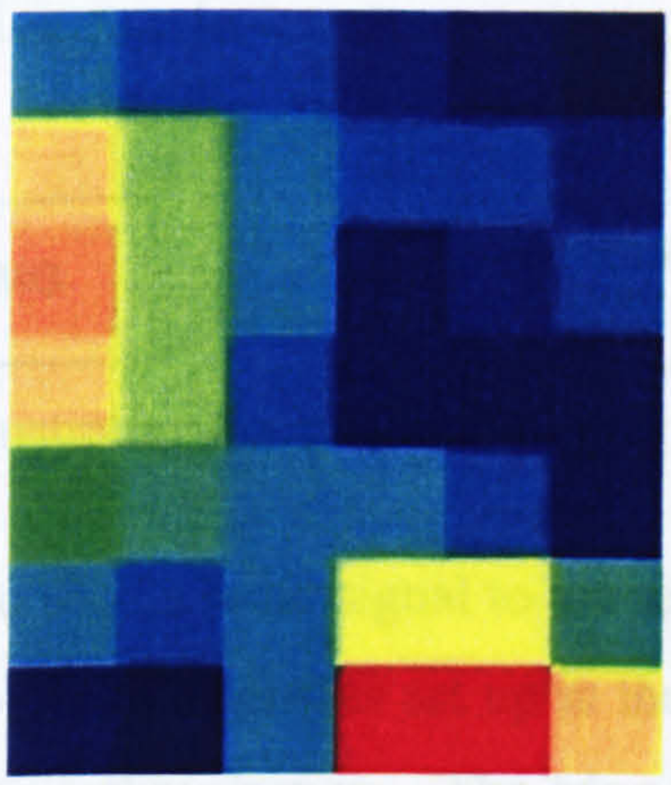

Figure 4.5. A typical pressure plot for main Tekscan sensor at the time of ball impact

4.2.4 EMG data collection

A Biovision electromyography (EMG) system was used for the analysis of muscle activity during each trial. The purpose of this was to obtain information that

would help to optimise muscle activation timings for any muscle-driven model developed in the future. Nine channels were utilised so that the muscle activation timings of the extensor carpi radialis brevis, flexor carpi radialis, biceps brachii, triceps brachii, pectoralis major, latissimus dorsi, anterior deltoid, medial deltoid and posterior deltoid muscles could be obtained. The associated wires and amplifiers were taped to the subject's skin to minimise any movement and hence reduce noise. The sampling frequency was set to 1000 Hz and an electrical gain of ± 5 V was used. The collection time for the data in each trial was 10 seconds.

4.2.5 Synchronisation

Synchronisation of all the equipment used during performance analysis was achieved using a trigger system (Figure 4.6).

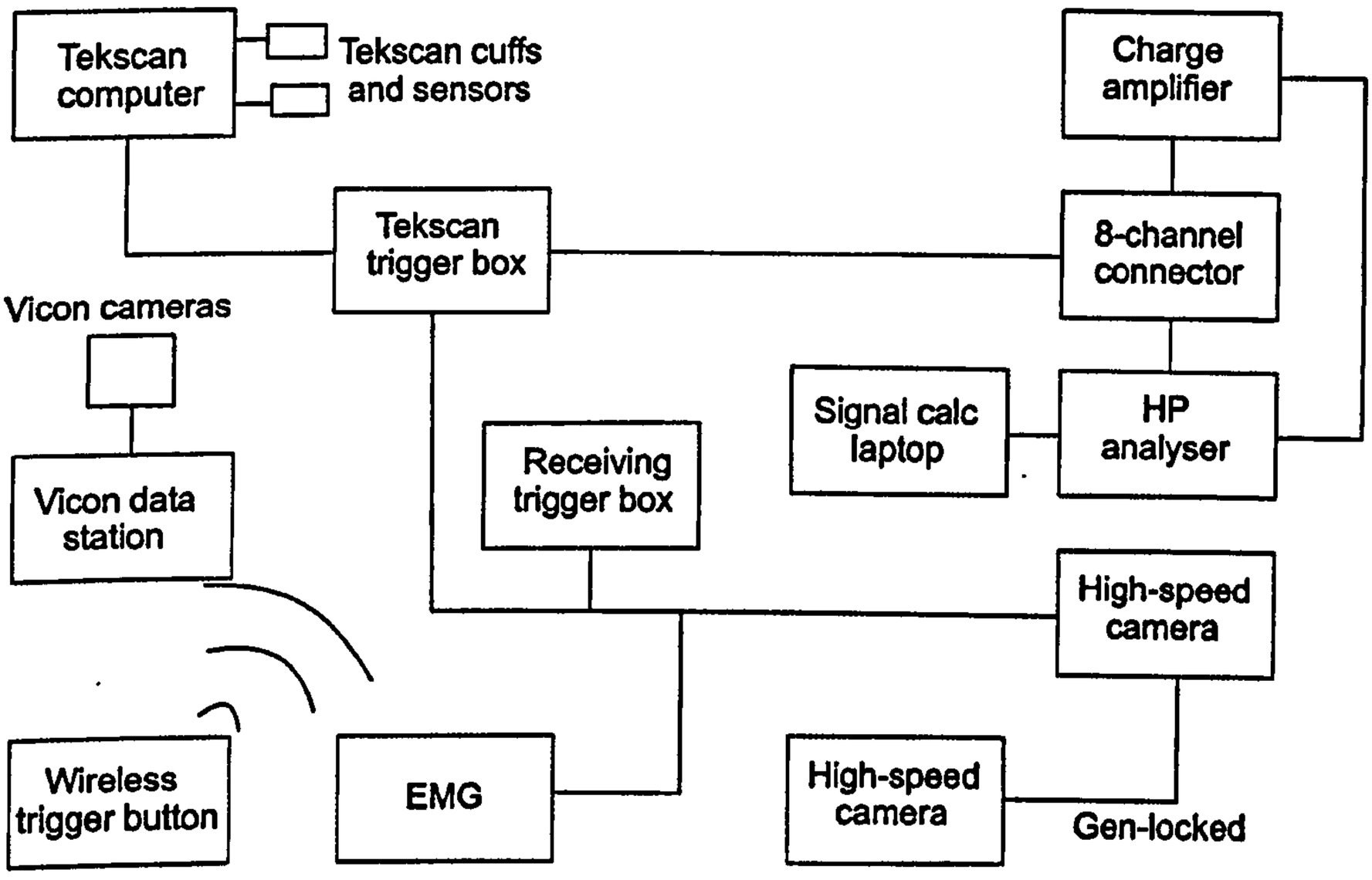

Figure 4.6. A schematic illustrating the synchronisation process for data collected

A wireless trigger was used to send a radio signal to the receiving trigger box and the Vicon data station. An analogue channel was set up in the Vicon software to receive a square pulse to allow post-synchronisation. The trigger box receiving the signal from the wireless button directly triggered the EMG and high-speed camera systems, along with the Tekscan trigger box. The Tekscan trigger box triggered the Tekscan system through a serial connection not present on the receiving trigger box. The Signal Calc system was triggered from the Tekscan trigger box through a standard BNC cable to reduce the number of connections to the receiving trigger box.

4.2.6 Testing Protocol

The testing procedures were explained to the subject in accordance with the Loughborough University ethical guidelines and an informed consent form was signed (Appendix 4). The subject was asked to warm up thoroughly and then hit one-handed topspin and slice backhand groundstrokes until he felt ready to start the data collection process. Reflective markers and surface EMG electrodes were placed on the subject in specified locations.

A tennis court section was created along the vaulting track using masking tape (Figure 4.7). A hitting area was established just behind the baseline. A pilot study established that a hitting volume of 2.5 m^3 was sufficient to enable a one-handed backhand groundstroke to be performed and an experienced tennis player believed the bounce of the ball on the runway surface to be consistent with that of a slow tennis court. The Vicon cameras were positioned and the focus and zoom of each were adjusted so that the entire hitting volume was covered.

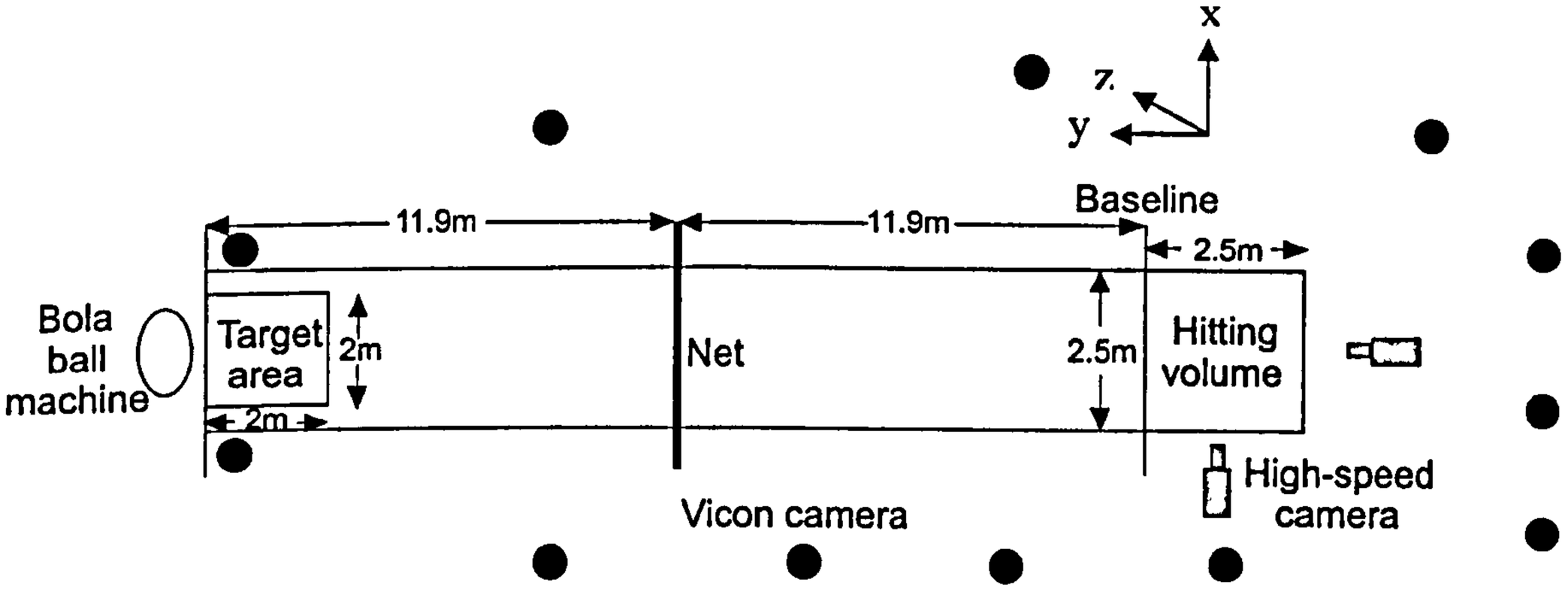

Figure 4.7. Experimental set-up for the performance data collection

New 'Penn Titanimum' tennis balls were launched from a Bola ball machine which was situated just behind the opposite baseline. The intention was to mimic a baseline rally and the trajectory and ball velocity were adjusted until the subject felt comfortable with the ball delivery. The subject aimed to return the ball so that it landed within a target area just inside the opposite baseline. Once a consistent ball path had been established the high-speed video cameras could be positioned so that the tennis racket head and impacting ball could be seen clearly from the side and from behind. Fifty-six trials were captured with Vicon and EMG data collected for each.

There were eight combinations of rackets with two frame types (Head LM Prestige and Head LM 8), two different string tensions (57 lbs and 70 lbs for the LM Prestige and 57 lbs and 75 lbs for the LM 8) for each racket and either no instrumentation, Tekscan pressure sensors under the grip, or uni-axial accelerometers mounted at the racket throat. A trial was considered to be successful if all the equipment had been triggered correctly / received a pulse for synchronisation purposes and the subject felt that he had hit the ball with good technique into or close to the target area. For each racket combination, data were collected for at least three successful slice groundstrokes and three successful topspin groundstrokes. In total, six successful trials were selected (Table 4.1) for further analysis as they provided all the information needed to compare actual and simulation model outputs for a variety of impact conditions.

4.3 SUBJECT INERTIA PARAMETERS

4.3.1 Overview of subject inertia parameters

The segmental inertia parameters of the subject were required as input to the model. A successful protocol in the past (King, 1998; Wilson, 2003) has been to use the geometric model of Yeadon (1990b). This method is practical and the researcher can determine the inertia parameters with little inconvenience to the subject.

4.3.2 Method

The geometric model of Yeadon (1990b) splits the body into 11 segments. To calculate the inertia parameters of each, 95 anthropometric measurements were taken on the subject by an experienced researcher (Figure 4.8). Lengths, widths, depths and perimeters from various parts along the body were recorded (Appendix 5). The inertia model used the segmental density values of Chandler et al. (1975) as initial estimates. These values were subsequently varied within a subroutine until there was a match between the whole body mass determined by the inertia model and the body mass of the subject measured using Seca Alpha digital scales.

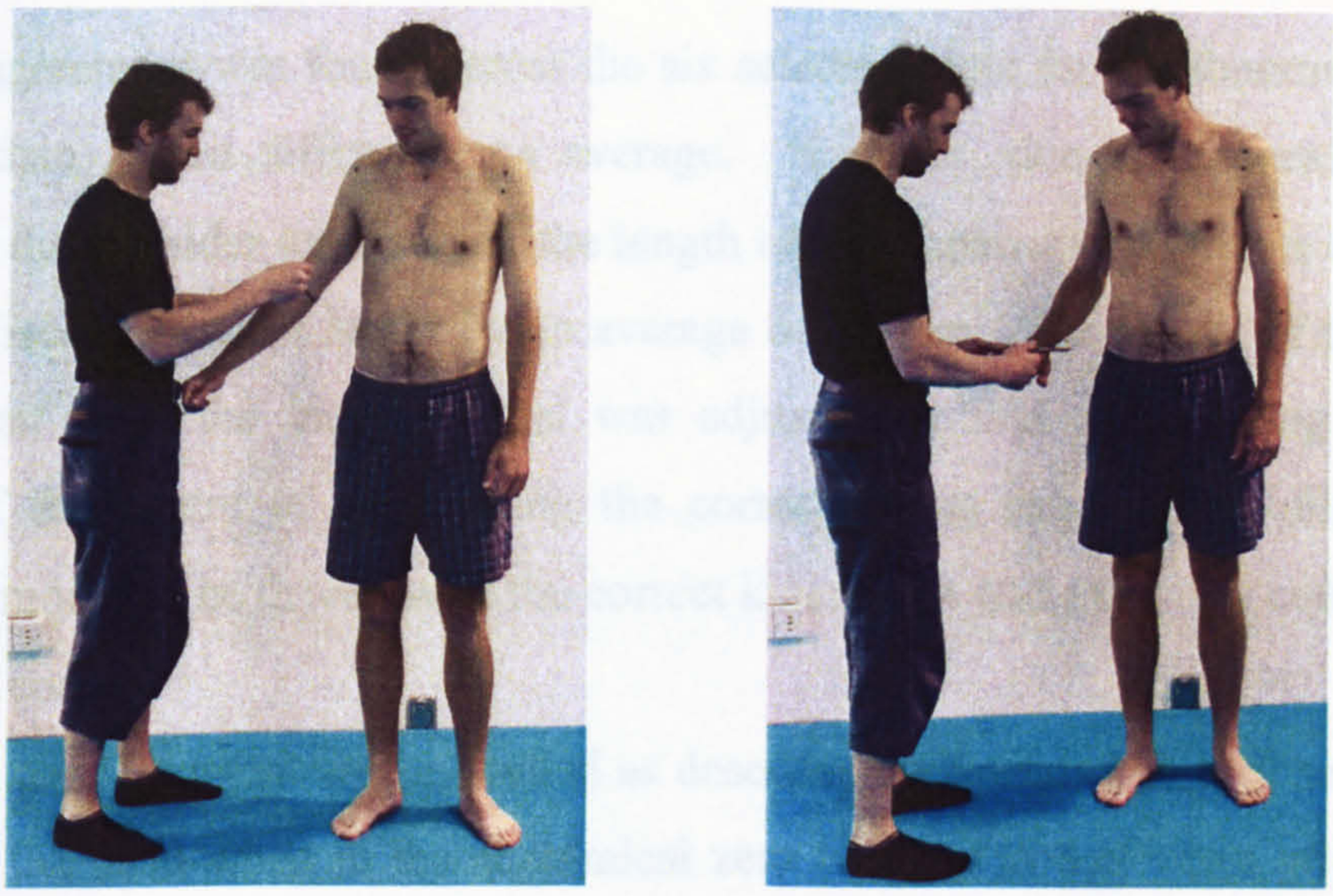

A B

Figure 4.8. Anthropometric measurements at the elbow (A) and wrist joints (B)

4.3.3 Results

Table 4.2 shows the segmental inertia parameters used as input to the geometric model. I_x, I_y, and I_z refer to the moments of inertia about the lateral, frontal and longitudinal axes respectively (Yeadon, 1990a).

Table 4.2. Segmental inertia parameters for the upper-arm, forearm and hand

segment	mass (kg)	distance of COM from proximal joint (m)	length of segment (m) depth[1] (m) width[2] (m)	moment of inertia (kgm^2) I_x	I_y	I_z
right upper-arm	2.1810	0.1470	0.3380	0.01694	0.01694	0.00258
right forearm	1.5170	0.1240	0.2960	0.01009	0.01017	0.00121
right hand	0.4010	0.0500	0.08 0.098[1] 0.05[2]	0.00045	0.00054	0.00054

The lengths of the upper-limb segments calculated from the inertia model were then compared with the lengths of the segments determined by the distance between joint centres established from the Vicon motion analysis (Section 4.2.2).

Excellent agreement was found across the six selected trials for the forearm segment with less than 2 mm difference on average. However, due to disparities in the location of the shoulder joint centre, the length of the upper-arm segments calculated from the Vicon data were larger by an average of 49 mm. The length of the upper-arm segment from the inertia model was adjusted by this offset along with the location of the centre of mass using the corresponding ratio. This allowed the simulation model to be driven with the correct kinematics and made the conditions at ball impact correct.

The hand segment was modelled as described in Section 3.4.4. The different position of the hand when in the anatomical zero position to that when gripping the racket was accounted for. The mass value of the hand from the geometric model was used along with anthropometric measurements to calculate the moments of inertia of the hand gripping the racket by using mathematical equations for specific shapes. The cylinder encasing the racket handle was taken to be hollow with an internal diameter equal to that of the tennis racket handles used (assuming the handle to be a cylinder).

4.4 WOBBLING MASS PARAMETERS

4.4.1 Overview of wobbling mass parameters

The wobbling mass parameters required include the spring stiffness and damping coefficients, the mass distribution, centre of mass (COM) location and the moments of inertia of the fixed and wobbling components.

4.4.2 Spring stiffness and damping

Both wobbling masses were attached to the fixed segments at each end by identical non-linear spring-dampers (Section 3.4.3). A Fast Fourier was performed on the Vicon positional data of markers on the upper-arm and forearm at locations where most wobbling mass movement would occur. By filtering out the low frequency vibration due to the motion of the upper-limb (approximately 2 Hz), the vibration frequencies of both upper-arm and forearm could be estimated. For the six selected trials, the vibration frequencies of the upper-arm and forearm displacements were 9 ± 0.5 Hz and 14 ± 0.5 Hz respectively. The stiffness coefficients were varied and simulations of selected trials run until the actual and simulated displacement frequencies of the wobbling masses matched during the performance. Near-critical

damping coefficients were selected (Pain & Challis, 2001a). Table 4.3 gives the stiffness and damping coefficients of the wobbling mass springs that gave the best match across all six selected trials. A sensitivity analysis was later performed and the results are shown in Section 6.4.7.

Table 4.3. Stiffness and damping coefficients of the wobbling mass spring-dampers

wobbling mass	stiffness coefficient (10^7N/m^3)	damping coefficient (Ns/m)
upper-arm	2	95
forearm	3	120

4.4.3 Mass distribution

Measuring body composition

Values for the masses and the percentage composition of fat and bone for the upper-arm and forearm were taken from Clarys and Marfell-Jones (1986) who performed anthropometry on 6 embalmed cadavers (3 male, 3 female). Values for the percentage composition of bone and fat and whole body mass of these 6 subjects were obtained from Clarys et al. (1984).

To relate this information to the subject in this study, an estimate of body fat as a percentage of whole body mass was calculated based on skinfold measurements. The principle behind this technique is that the amount of subcutaneous fat is proportional to the total amount of body fat. Based on a standardised description of skinfold sites and procedures (Balady et al., 2000), measurements were taken at seven sites on the body (chest, midaxillary, triceps, subscapular, abdomen, suprailiac, thigh). All measurements were taken on the right (dominant) side of the body and the folds were created in a location and at an angle specified by Balady, Berra et al. (2000). The calliper was placed 10 mm away from the thumb and finger, perpendicular to the skinfold, and halfway between the crest and the base of the fold. The measurement was taken for no longer than 2 seconds after initiating the pinch, which was maintained whilst reading the calliper (Figure 4.9). Duplicate measurements were taken at each site and a retest was performed if the measurements were not within 2 mm.

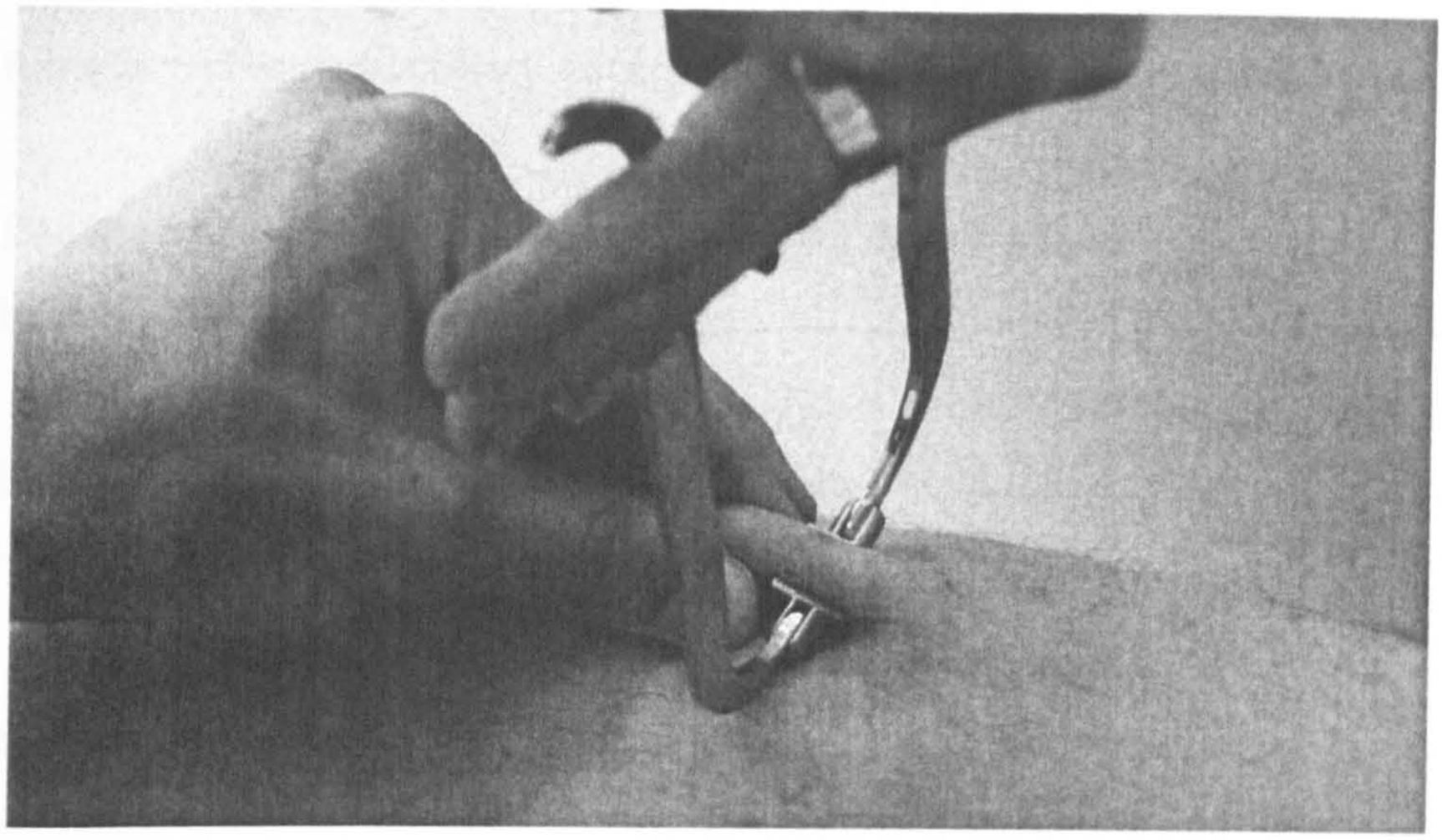

Figure 4.9. Skinfold measurement on the anterior midline of the right thigh

Regression equations for body density (Db) were used to convert the sum of the seven skinfolds to percent fat. As the first equation for Db is based on the population of males (Balady et al., 2000) and the other is based on a population of white male athletes (Withers et al., 1987), an average of the two values was obtained. This yielded an average body fat composition of 8.4%.

Table 4.4. Skinfold measurements (mm) to determine body composition

skinfold site	test 1	test 2	average
chest	8.5	8.5	8.5
midaxillary	6.0	6.0	6.0
triceps	6.5	6.5	6.5
subscapular	8.0	8.0	8.0
abdomen	12.5	11.5	12.0
suprailiac	6.0	6.0	6.0
thigh	9.0	8.0	8.5
total			55.5

7 site formulae (chest, midaxillary, triceps, subscapular, abdomen, suprailiac, thigh):

Body Density = 1.112 – 0.00043499 (sum of 7 skinfolds) +
(Balady et al., 2000) 0.00000055 (sum of 7 skinfolds)^2 – 0.00028826 (age)
= 1.083210473 (1)

Body Density = 1.0988 – 0.0004 (sum of 7 skinfolds)
(Withers et al., 1987) = 1.0766 (2)

Average body density (Db) = [(1) + (2)]/2
= 1.0799

Body fat % = [(4.95/Db) – 4.5] x 100
= **8.4%**

Scaling from the literature

For the cadavers in their study, Clarys et al. (1984) reported the average body mass and body fat percentage as 64.3 kg and 34.6% respectively. The corresponding values for the elite subject in this study were 75.5 kg and 8.4% respectively. The following procedure was applied to find an estimate of the fixed and wobbling mass within the upper-arm and forearm segments:

Mass subject	=	75.5 kg
% fat subject	=	8.4%
upper-arm mass	=	1.560 kg (Clarys & Marfell-Jones, 1986)
fat mass	=	0.587 kg (Clarys & Marfell-Jones, 1986)
fat-free mass	=	1.560 - 0.587 = 0.973 kg
% fat in upper-arm	=	$\frac{0.587}{1.560} = 37.63\%$
fat ratio	=	$\frac{\%\text{ fat in upper - arm}}{\text{whole body \% fat}} = \frac{37.63}{34.6} = 1.0876$
new % fat in upper-arm	=	1.0876 x 8.4% = 9.14%
new fat mass	=	1.560 x 9.14% = 0.142 kg

new upper-arm mass = fat-free mass + new fat mass

= 0.973 + 0.142

= 1.115 kg

bone mass = 0.218 kg (Clarys & Marfell-Jones, 1986)

fixed mass ratio = $\frac{\text{bone mass}}{\text{new upper - arm mass}} = \frac{0.218}{1.115} = \mathbf{19.55\%}$

wobbling mass ratio = (100 – 19.55)% = **80.45%**

forearm mass = 0.764 kg (Clarys & Marfell-Jones, 1986)

fat mass = 0.181 kg (Clarys & Marfell-Jones, 1986)

fat-free mass = 0.764 - 0.587 = 0.973 kg

% fat in forearm = $\frac{0.181}{0.764} = 23.69\%$

fat ratio = $\frac{\text{\% fat in forearm}}{\text{whole body \% fat}} = \frac{23.69}{34.6} = 0.6847$

new % fat in forearm = 0.6847 x 8.4% = 5.75%

new fat mass = 0.764 x 5.75% = 0.044 kg

new forearm mass = fat-free mass + new fat mass

= 0.583 + 0.044

= 0.627 kg

bone mass = 0.122 kg (Clarys & Marfell-Jones, 1986)

fixed mass ratio = $\frac{\text{bone mass}}{\text{new forearm mass}} = \frac{0.122}{0.627} = \mathbf{19.46\%}$

wobbling mass ratio = (100 – 19.55)% = **80.54%**

The mass of the fixed (m_f) and wobbling (m_w) components were calculated using the segmental masses obtained from Yeadon's (1990b) model and the above fixed to wobbling ratios.

Table 4.5. Masses of the fixed and wobbling components

inertia parameter	upper-arm	forearm
m_f (kg)	0.426	0.295
m_w (kg)	1.755	1.237

4.4.4 Centre of mass location and moment of inertia

The moment of inertia (MOI) of the whole segment (I_g) about an axis was determined from Yeadon's (1990b) model. I_g is the sum of the MOIs of the fixed (I_f) and wobbling (I_w) components. Using the Parallel Axis Theorem and considering the MOI about the x (lateral) axis:

$$I_g = I_f + m_f(x_f - x)^2 + I_w + m_w(x_w - x)^2 \qquad (4.1)$$

where x = distance of the whole segment COM to the proximal joint centre

x_f = distance of the fixed component COM to the proximal joint centre

x_w = distance of the wobbling component COM to the proximal joint centre

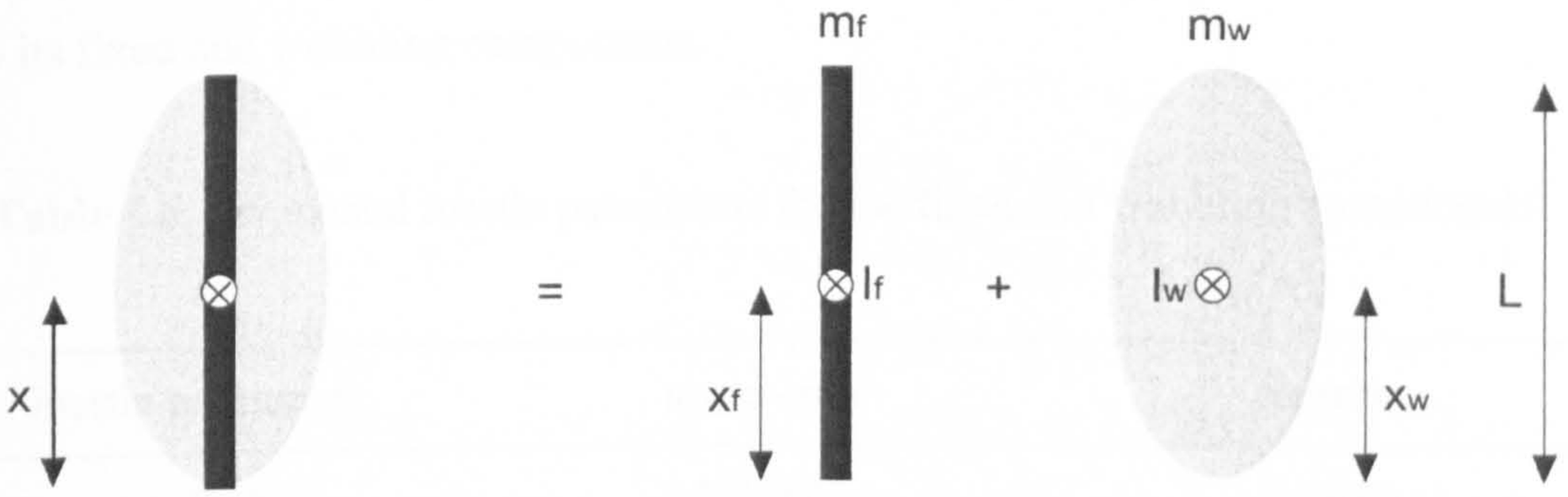

Figure 4.10. Modelling a segment as a fixed and wobbling component

It was assumed that the lengths of the fixed and wobbling components were the same as the length (L) of the whole segment. The fixed component was modelled as a uniform cylinder. The volume of the cylinder was calculated by dividing its mass (m_f) by its density (d). Density values from Clarys & Marfell-Jones (1986) for the upper-arm and forearm were 1224.0 and 1308.0 mg/m^3 respectively. The radius of the cylinder (r) was calculated using Equation 4.2:

$$\pi r^2 L = \frac{m_f}{d} \qquad (4.2)$$

I_f was determined using the equation defining MOI for a uniform cylinder:

$$I_f = \frac{1}{12} m_f L^2 + \frac{1}{4} m_f r^2 \qquad (4.3)$$

For the fixed component with uniform density, x_f was taken as:

$$x_f = \frac{1}{2}L \tag{4.4}$$

For the wobbling component, x_w was calculated using Equation (4.5):

$$m_f x_f + m_w x_w = (m_f + m_w)x \tag{4.5}$$

I_w was then calculated using Equation 4.1. Due to symmetry, the MOI values about the y (frontal) axes were equal to those about the x (lateral) axes. The ratio of I_f to I_w for these two axes was then used to separate the MOI about the z (longitudinal axis) into its fixed and wobbling components.

Table 4.6. Segmental inertia parameters for the fixed and wobbling components

inertia parameter	upper-arm	forearm
m_f (kg)	0.4260	0.2950
m_w (kg)	1.7550	1.2370
I_{fx}/I_{fy} (kgm^2)	0.0030	0.0020
I_{wx}/I_{wy} (kgm^2)	0.0140	0.0080
I_{fz} (kgm^2)	0.0005	0.0002
I_{wz} (kgm^2)	0.0025	0.0008
x_f/y_f (m)	0.1450	0.1480
x_w/y_w (m)	0.1210	0.1180
L (m)	0.2890	0.2960
r (m)	0.0196	0.0156

4.5 GRIP PARAMETERS

4.5.1 Overview of grip parameters

Section 3.4.3 describes the model for the hand-racket system which included six identical spring-dampers at the hypothenar and the thenar eminences and a torsional spring-damper to apply a passive torque about the longitudinal axis of the racket handle. These visco-elastic parameters for an individual trial were determined by a matching optimisation process which minimised the differences between simulation and performance. In Chapter 5 all the parameters for the tennis racket frames, stringbeds and ball were determined from independent experimental tests. These parameters were then fixed in the model for all matching optimisations.

4.5.2 Matching optimisation process

The output variables chosen for comparison were the three displacements of a point on the racket frame (in global x, y, z directions) relative to the wrist joint centre and the time histories of the three angles between the hand and the racket handle. In this way, the six degrees of freedom of the racket relative to the hand are represented. Comparisons were made from the time of ball impact and every ms thereafter for 50 ms. A simulation score S_{GRIP} (Figure 4.11) was calculated as the average root-mean-squared percentage difference between simulation and performance for the aforementioned variables.

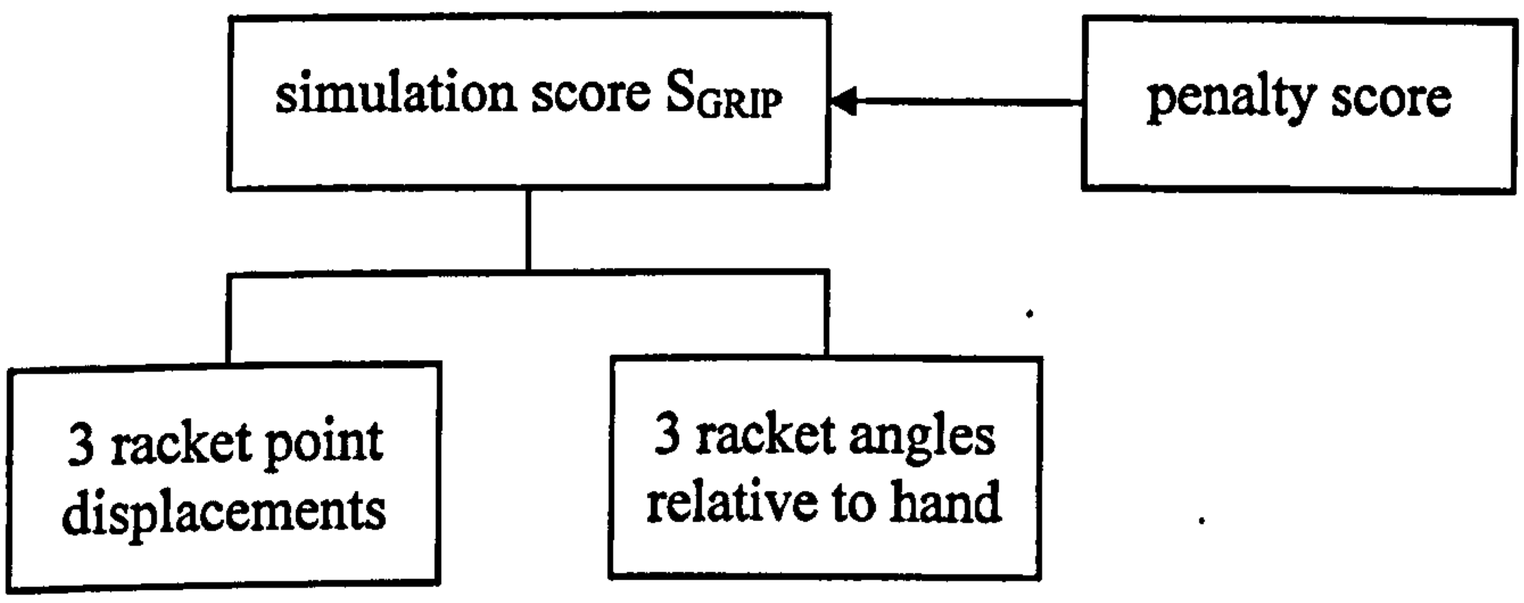

Figure 4.11. Summary of the components of the simulation score S_{GRIP}

To make comparisons between variables of different units, a 1 deg difference in racket angle was assumed to be equivalent to a 1 cm difference in racket point displacement (based on how a 1 deg change in an angle at the wrist could affect the

position of a point on the racket approximately 60 cm away). Each of the 3 racket point and 3 racket angle displacements were given a weighting of 1/6. Although the outbound ball velocity was not directly compared in this score function, an additional penalty score was used to encourage a solution that would allow the ball to land in or near to the target area. For each 1 m/s difference between the simulation velocity and the specified limit, 1 penalty point was added to the score.

4.5.3 Initial conditions for matching optimisations

The initial displacements and velocities of the three angular degrees of freedom of the racket relative to the hand were taken from the Vicon motion analysis data. However, unlike Section 4.2.2 where the whole data set was splined, the data set was cropped at the frame just before impact to avoid smoothing across the impact. Since the Vicon sampling frequency was 250 Hz, the instant of ball contact with the stringbed was often between two frames. The instant of ball contact was determined by the high-speed video images allowing the associated Vicon frames to be determined due to synchronisation of the data sets. The angular displacements and velocities at the instant of ball contact were obtained by linear extrapolation of the values from Vicon just prior to impact.

The linear displacements and velocities of the wrist joint centre in global coordinates were determined by splining the associated Vicon data that had been cropped just prior to ball impact. When compared with the model output, small differences were found in the linear displacements (maximum 3 mm) and velocities (0.12 m/s). These differences can be attributed to errors in segment lengths and joint angles propagated throughout the system. Small adjustments were made to the linear displacements and velocities of the thorax centre to match the model output with the raw data at ball impact. Once the model wrist joint was in the correct position and had the same linear velocities at ball impact, the racket was positioned within the hand to match the global coordinates of a marker on the racket frame of known location. Any differences in the linear velocities of the point on the racket frame were therefore due to linear velocities of the racket handle relative to the hand which could be input to the model.

4.5.4 Results of matching optimisations

The matching process for the 6 trials was achieved by varying the 8 gripping parameters until the best match between simulation and performance was found. The score S_{GRIP} was minimised using the Simulated Annealing optimisation algorithm (Corana et al., 1987). All S_{GRIP} values shown in Table 4.7 have no penalty score associated with them indicating that the direction of the simulation outbound ball velocity was agreeable with performance data.

Table 4.7. Parameters for hand-racket interface from matching optimisations

Parameter (units)	Optimised value					
Trial number	1	8	24	31	36	56
CH (Ns/m)	716500	778400	453000	116500	574000	553500
CT (Ns/m)	741800	837600	473000	441800	579000	82600
CTORE (Nms/rad)	9.0	2.3	0.8	16.9	10.8	30.1
KH (N/m)	65200	61800	101000	65300	74000	115300
KT (N/m)	64000	11900	94800	64100	76300	60400
KTORE (Nm/rad)	70.0	26.9	30.0	98.9	99.0	29.1
RH0 (N)	12.6	16.6	18.7	11.0	10.0	13.2
RT0 (N)	14.6	8.9	10.1	10.1	10.0	12.3
S_{GRIP} (%)	0.83	0.32	0.47	0.30	0.14	0.29

where CH = damping coefficient for hypothenar eminence
CT = damping coefficient for thenar eminence
CTORE = damping coefficient for torsional spring-damper
KH = stiffness coefficient for hypothenar eminence
KT = stiffness coefficient for thenar eminence
KTORE = stiffness coefficient for torsional spring-damper
RH0 = initial force at hypothenar eminence
RT0 = initial force at thenar eminence

Figures 4.12 and 4.13 give examples of performance and simulated racket angular displacements relative to the hand and racket point linear displacements respectively for a matched trial. The displacements are in global x, y, z directions whilst racket angle axes x, y, z correspond to rotations about the longitudinal, transverse and frontal axes of the tennis racket.

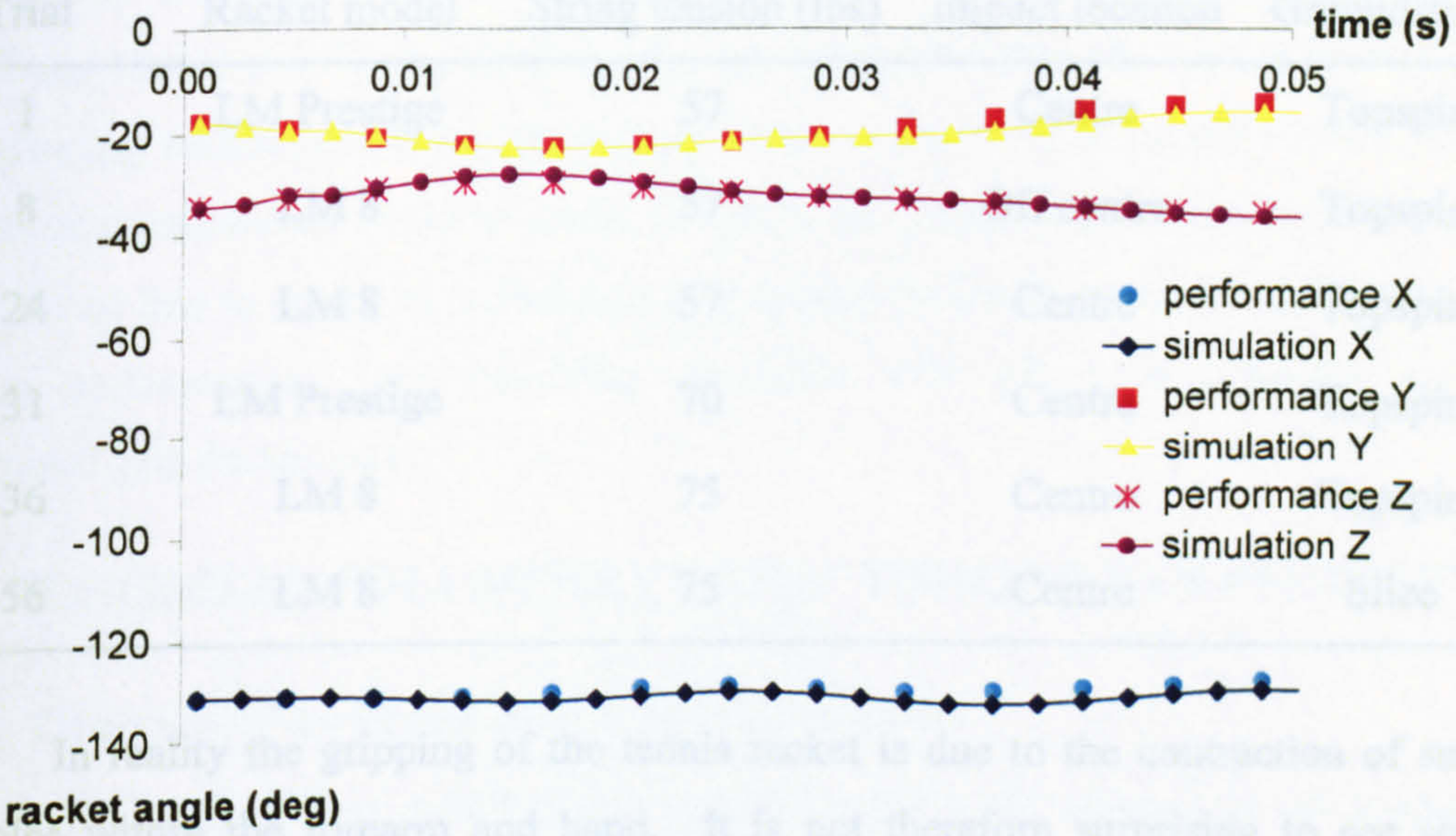

Figure 4.12. Comparison of simulation and performance racket angles

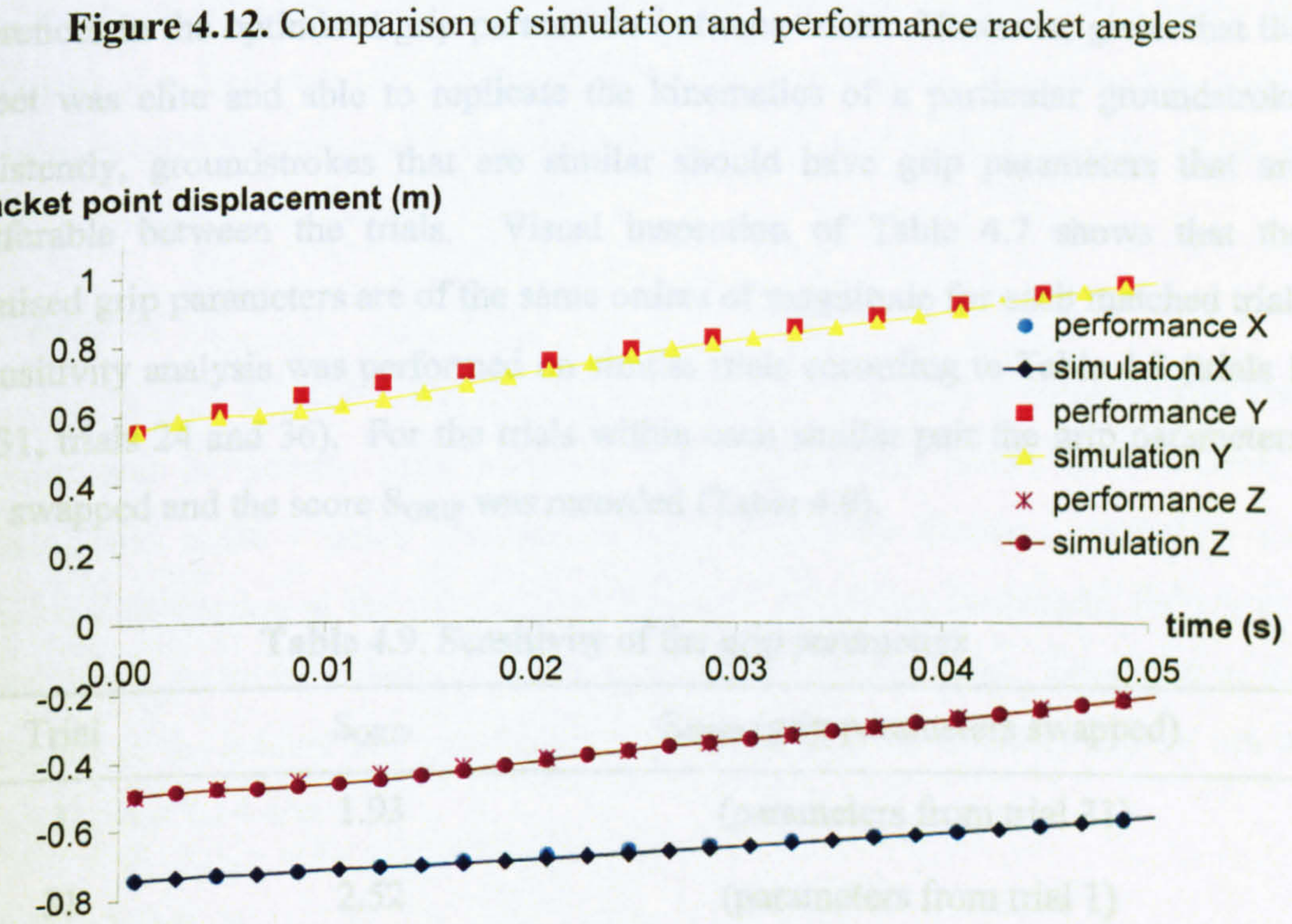

Figure 4.13. Comparison of simulation and performance racket point displacements

4.5.5 Sensitivity of grip parameters

Table 4.8 summarises the trials that were chosen and the variations between the trials to enable the research questions to be answered.

Table 4.8. Summary of the six trials chosen for further analysis

Trial	Racket model	String tension (lbs)	Impact location	Groundstroke
1	LM Prestige	57	Centre	Topspin
8	LM 8	57	Off centre	Topspin
24	LM 8	57	Centre	Topspin
31	LM Prestige	70	Centre	Topspin
36	LM 8	75	Centre	Topspin
56	LM 8	75	Centre	Slice

In reality the gripping of the tennis racket is due to the contraction of small muscles within the forearm and hand. It is not therefore surprising to see some differences in the optimised grip parameters between trials. However, given that the subject was elite and able to replicate the kinematics of a particular groundstroke consistently, groundstrokes that are similar should have grip parameters that are transferable between the trials. Visual inspection of Table 4.7 shows that the optimised grip parameters are of the same orders of magnitude for each matched trial. A sensitivity analysis was performed on similar trials according to Table 4.8 (trials 1 and 31, trials 24 and 36). For the trials within each similar pair the grip parameters were swapped and the score S_{GRIP} was recorded (Table 4.9).

Table 4.9. Sensitivity of the grip parameters

Trial	S_{GRIP}	S_{GRIP} (grip parameters swapped)
1	1.93	(parameters from trial 31)
31	2.52	(parameters from trial 1)
24	0.97	(parameters from trial 36)
36	0.82	(parameters from trial 24)

When the grip parameters from trials 24 and 36 were swapped, the score S_{GRIP} increased as expected in each case. The magnitude of the increase was 0.50 deg for trial 24 and 0.68 deg for trial 36. As a close match was achieved when the parameters were swapped, this suggests that the solutions are not 'knife-edge solutions' and that the model is not very sensitive to perturbations to the gripping parameters. The corresponding increases in S_{GRIP} for trials 1 and 31 are 1.10 and 2.22 deg respectively. The S_{GRIP} scores of 1.93 deg and 2.52 deg are agreeable but in this case it is clear that the gripping technique has varied slightly between trials. It is possible that a set of robust grip parameters could be found to match for similar trials. However, it would appear that due to subtle modifications of gripping technique made by the performer during performances, each matching simulation trial will have a unique set of optimised grip parameters.

4.6 MAXIMUM VOLUNTARY JOINT TORQUE PARAMETERS

4.6.1 Overview of maximum joint torque parameters

The angle-driven model of the human in this study allows the net torque at each joint to be calculated. The maximum voluntary torque generated by a particular movement at a joint can be represented by a 9-parameter surface function, which expresses maximum torque as a function of joint angle and angular velocity (King et al., 2006; Yeadon et al., 2006).

4.6.2 Method

A CYBEX NORM™ isovelocity dynamometer was used to measure maximal isometric and isovelocity joint torques. The movements tested were flexion / extension and radial / ulnar deviation at the right wrist; flexion / extension and pronation / supination at the right elbow; flexion / extension, horizontal abduction / adduction and internal / external rotation at the right shoulder joint. Examples of the positioning of the subject and dynamometer for different joints and movements can be seen in Figures 4.14 and 4.15.

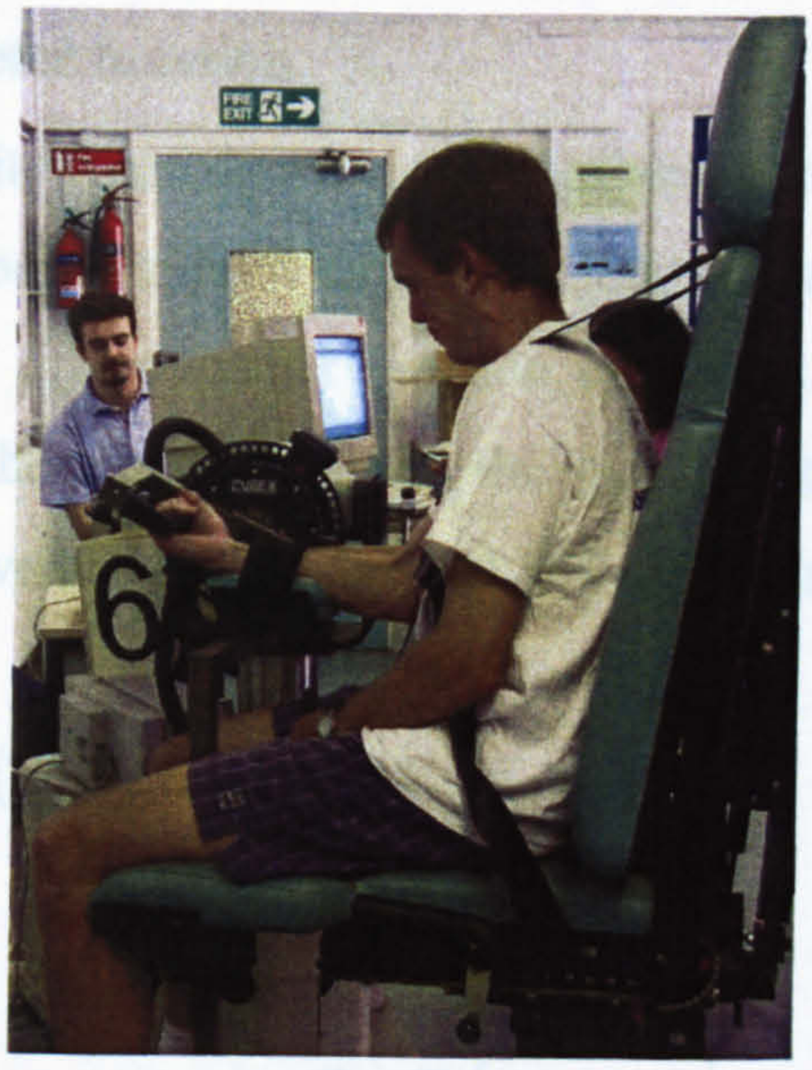

Figure 4.14. Positioning of subject and dynamometer for wrist flexion

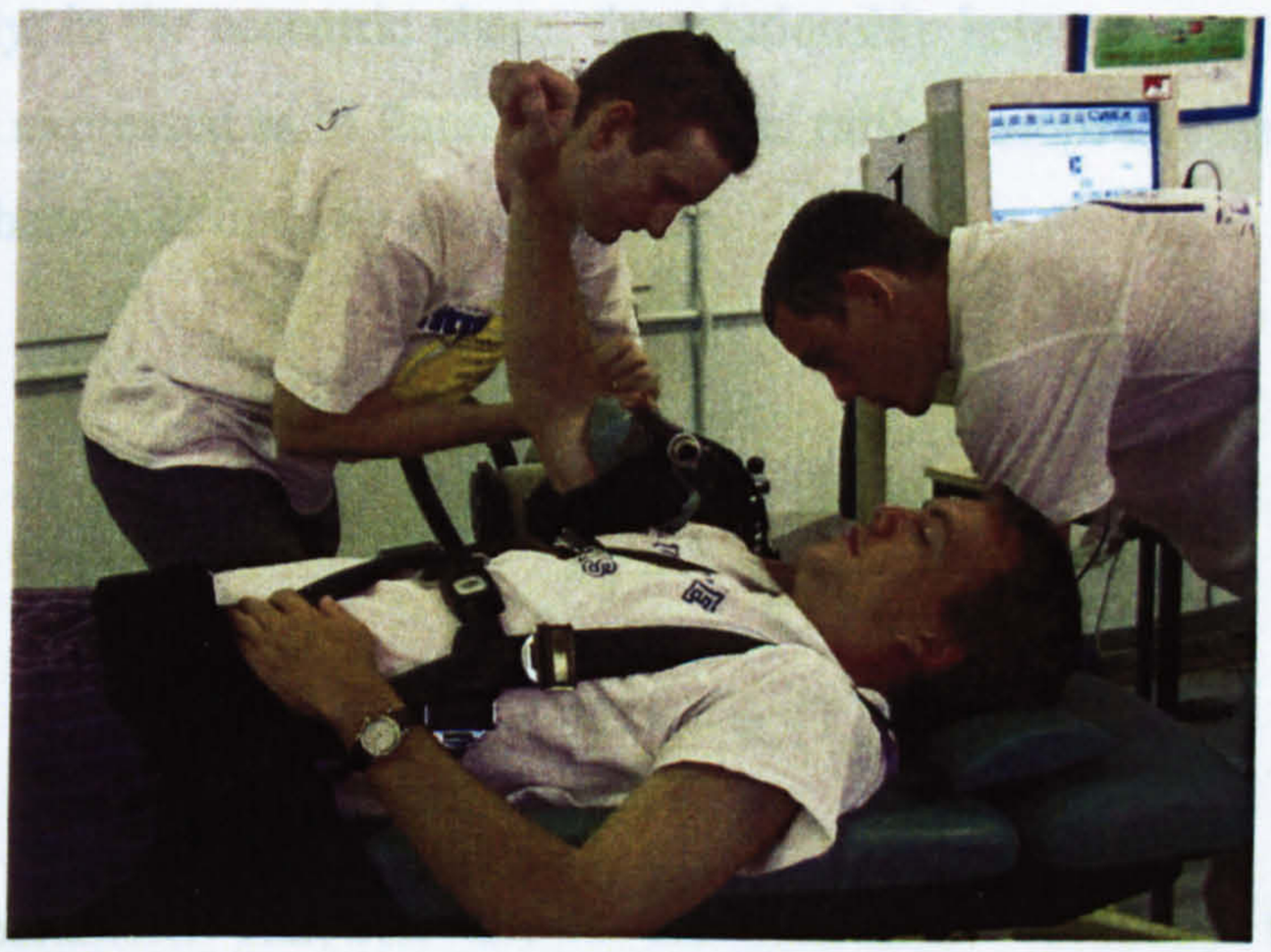

Figure 4.15. Positioning of subject and dynamometer for shoulder flexion

An established protocol (King et al., 2006) was used to calculate the 9 parameters needed to define the theoretical maximum voluntary torque profiles. The raw angle and torque data were converted from a voltage to radians and Newton-metres respectively, corrected for the combined weight of the limb and the crank arm and converted from crank angle / angular velocity / torque data to joint angle / angular velocity / torque data.

4.6.3 Fitting a 9-parameter function

From the isovelocity trials, data are only available at certain angular velocities. To obtain a relationship between joint torque and joint angular velocity which holds for any angular velocity, a 7-parameter function can be fit to the raw data (Kong, 2005; Wilson, 2003). In the concentric phase, the relationship between torque (T) and angular velocity (ω) is governed by the classical Hill (1938) hyperbola (Equation 4.6).

$$(T+T_c)(\omega+\omega_c)=C \tag{4.6}$$

where,

$$T_c=\frac{T_o\omega_c}{\omega_{max}}$$

$$C=T_c(\omega_{max}+\omega_c)$$

Similarly, in the eccentric phase, the relationship between torque and angular velocity can be expressed as in Equation 4.7. The ratio of slopes between concentric and eccentric phase is defined by a constant k.

$$(T_e-T)(\omega_e-\omega)=-E \tag{4.7}$$

where,

$$\omega_e=\frac{(T_{max}-T_o)}{kT_o}\cdot\frac{\omega_{max}\omega_c}{(\omega_{max}+\omega_c)}$$

$$E=-\omega_e(T_{max}-T_o)$$

The 7-parameter function allows the maximum voluntary torque to be calculated for a range of joint angular velocities. To incorporate angle dependence, two additional parameters were needed to define how the torque changes over an angle range (King et al., 2006).

4.6.4 Results

For each joint movement tested, a 9-parameter function as described above was used to fit the experimental data from the isovelocity dynamometer trials. Tables 4.10 to 4.12 give the optimised 9 parameters for the wrist, elbow and shoulder joints respectively. Figure 4.16 is an example of a 3D surface plot of the theoretical maximum voluntary torque that the subject can produce for a given joint angle and angular velocity during a specified movement.

Table 4.10. Optimised parameters for the wrist joint

Parameter	Flexion	Extension	Radial deviation	Ulnar deviation
T_o (Nm)	44.37	23.74	31.47	41.05
T_{max} (Nm)	62.12	33.23	44.06	57.47
ω_{max} (rad/s)	32.25	27.00	27.17	27.00
ω_c (rad/s)	16.13	8.10	10.25	8.10
a_{min}	0.97	0.99	0.81	0.97
m	0.95	3.00	0.17	3.00
ω_1 (rad/s)	0.88	0.74	-0.82	-1.19
q	0.26	0.27	0.65	0.47
theopt (rad)	0.68	0.07	0.04	0.06

Table 4.11. Optimised parameters for the elbow joint

Parameter	Flexion	Extension	Pronation	Supination
T_o (Nm)	81.31	53.15	16.88	23.25
T_{max} (Nm)	113.83	74.41	23.64	30.54
ω_{max} (rad/s)	29.17	27.03	28.96	33.11
ω_c (rad/s)	10.51	8.11	10.94	15.34
a_{min}	0.90	0.89	0.71	0.89
m	0.87	0.07	0.27	0.05
ω_1 (rad/s)	-1.59	-1.20	-0.23	-1.12
q	0.46	0.48	0.42	0.17
theopt (rad)	1.33	0.6	1.22	1.50

Table 4.12. Optimised parameters for the shoulder joint

Parameter	Flexion	Extension	Horizontal abduction	Horizontal adduction	Internal rotation	External rotation
T_o (Nm)	56.29	120.75	67.07	92.31	42.34	33.22
T_{max} (Nm)	78.81	169.04	93.90	129.24	59.27	46.50
ω_{max} (rad/s)	27.00	32.76	27.00	27.00	28.92	28.92
ω_c (rad/s)	8.10	13.83	8.10	8.13	9.83	9.83
a_{min}	0.99	0.91	0.92	0.92	0.92	0.92
m	3.00	2.47	0.04	0.01	0.84	0.84
ω_1 (rad/s)	-3.00	1.49	-1.27	-0.62	-0.13	-0.13
q	0.29	0.14	0.07	0.25	0.34	0.37
theopt (rad)	0.42	1.09	1.26	2.39	2.20	2.74

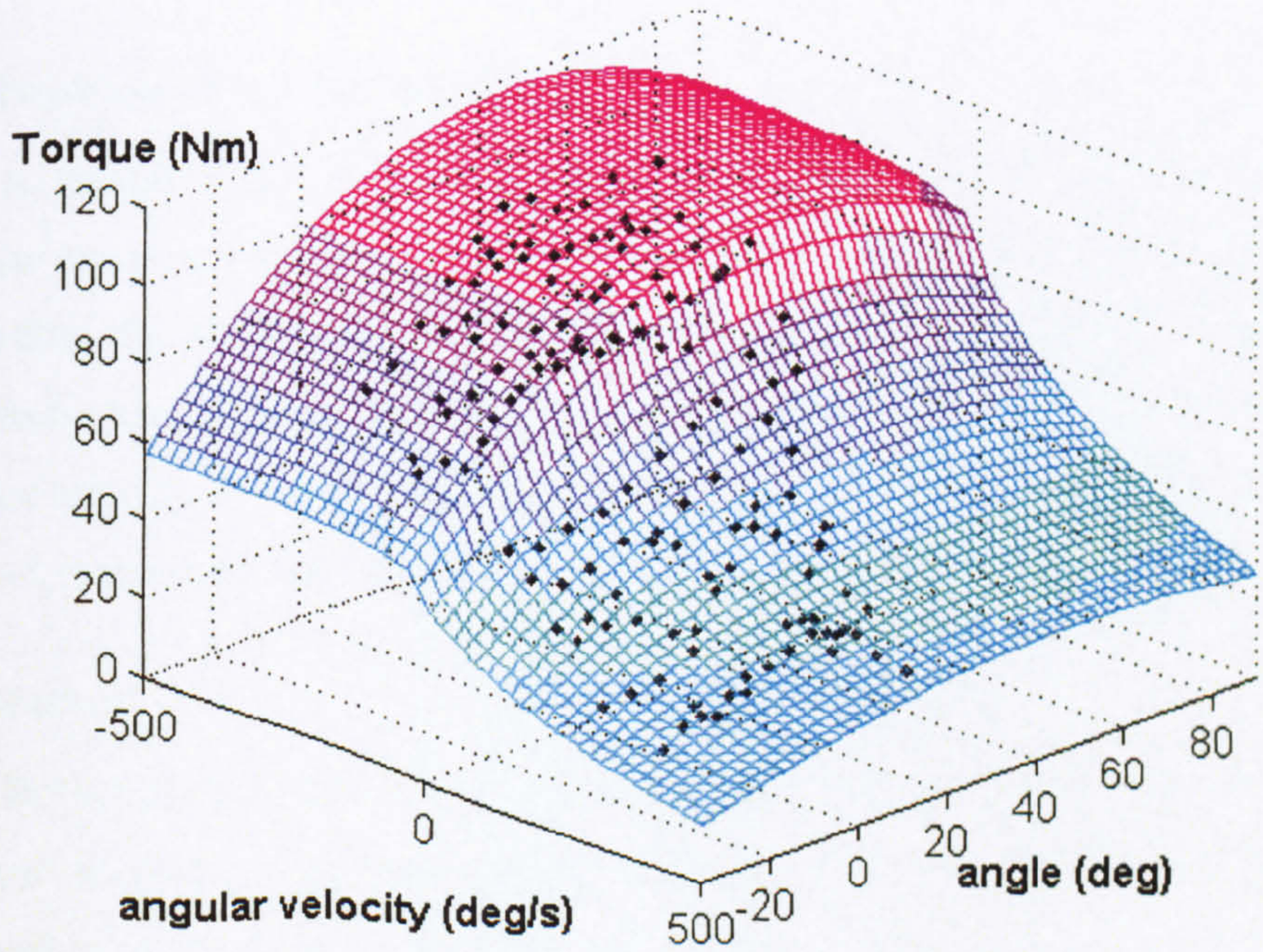

Figure 4.16. Nine parameter fit to raw data for shoulder horizontal adduction

4.7 CHAPTER SUMMARY

This chapter has described the methods that have been used to collect data of the subject performing one-handed backhand groundstrokes. This was necessary to compare simulation and performance. Subject-specific inertia, wobbling mass and gripping parameters were calculated to be used as input to the simulation model. The following chapter describes the methods used to determine parameters for the racket frame, stringbed and ball models.

CHAPTER 5

EQUIPMENT PARAMETER DETERMINATION

5.1 CHAPTER OVERVIEW

Section 3.3.1 describes a model of a tennis racket frame consisting of two rigid bodies connected by a frictionless pin joint. Two torsional spring-dampers were used to apply passive torques between the two bodies and allow motion in and out of the racket plane. A point mass model of the tennis ball and stringbed interaction incorporated visco-elastic and friction components to model both normal and oblique components of ball movement. The stringbed was represented by nine point masses connected using elastic springs. In this chapter the methods used to determine equipment-specific parameters for the models of the racket frames, tennis ball and stringbeds are presented along with the results.

5.2 MODAL ANALYSIS

5.2.1 Overview of modal analysis

A modal analysis of each tennis racket used during the performance data collection was carried out to identify its mode shapes and natural frequencies. To achieve this, the tennis rackets were stimulated by an electromagnetic exciter attached to the frame via a 'sting' (a thin longitudinally stiff wire with little lateral stiffness) and force transducer. The response of the racket in terms of force and velocity was measured at several locations using a Doppler laser vibrometer.

5.2.2 Method

Both racket models at a low and high string tension were analysed. The racket frame was excited in a direction normal to the plane of the racket stringbed and also in the direction of the plane of the stringbed. Reflective tape was placed at 31 locations along the racket frame and handle and at 9 points on the stringbed for the out of plane testing. For the in plane modal analysis, 16 reflective markers were used. Before each racket was analysed, an industry standard test was performed using a Babolat Racket Diagnostic Centre (BRDC) and the values obtained are presented in Table 5.1.

Figure 5.1 shows the location of the axes for the BRDC testing about which the moment of inertia (MOI) values were calculated and the positions of reflective markers for the modal analysis.

Table 5.1. Industry standard tennis racket parameters

Racket Property	LM Prestige (57 lbs)	LM Prestige (70 lbs)	LM 8 (57 lbs)	LM 8 (75 lbs)
Mass (kg)	0.323	0.318	0.266	0.270
String bed stiffness (%)	66.0	86.0	51.0	68.0
Frame stiffness (%)	57.0	57.0	61.0	61.0
MOI about X axis ($kgm^2 \times 10^{-1}$)	0.326	0.322	0.331	0.334
MOI about Y axis ($kgm^2 \times 10^{-1}$)	0.341	0.337	0.351	0.354
Balance point from butt cap (m)	0.325	0.331	0.380	0.380

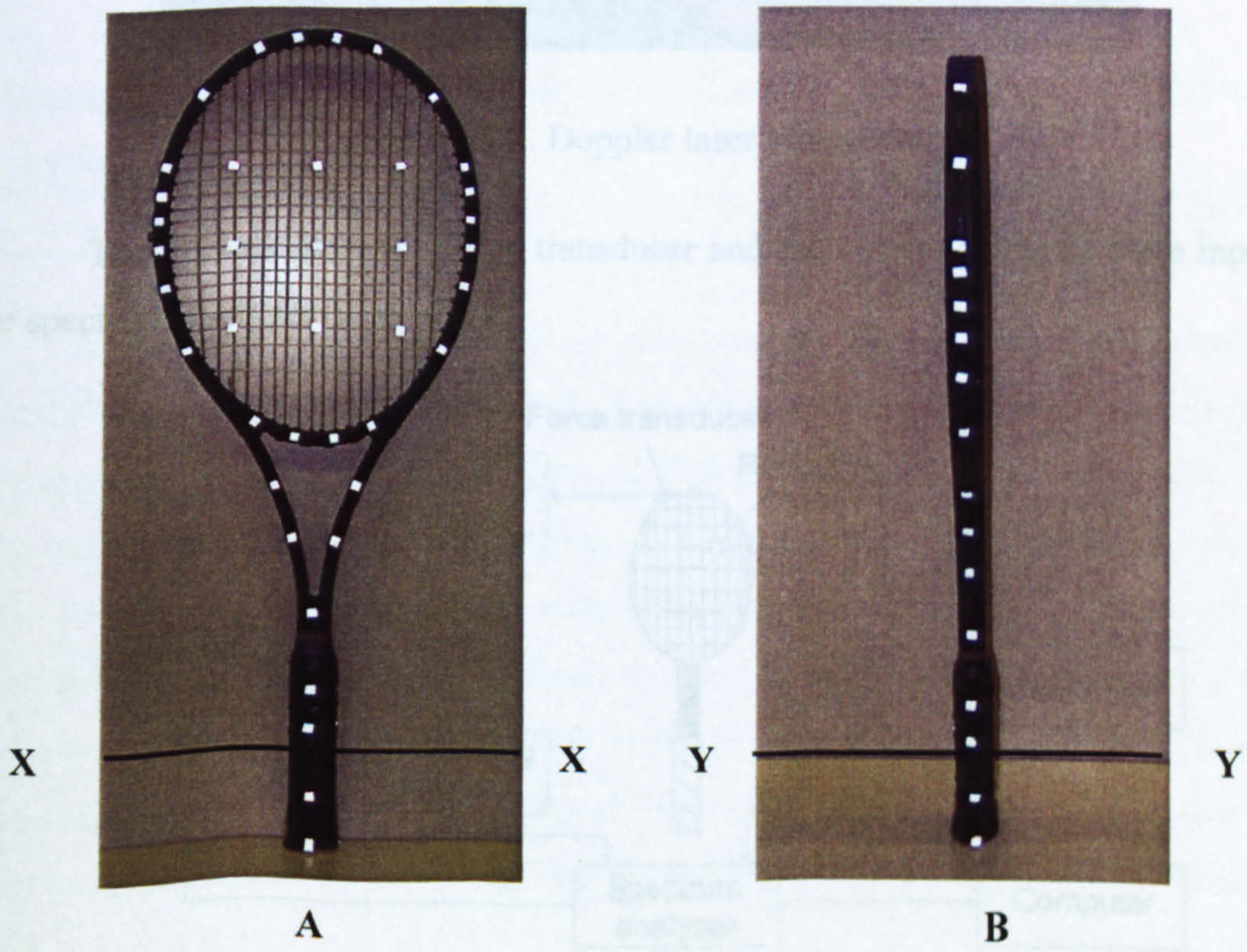

Figure 5.1. Locations of axes for MOI calculations and reflective markers for the (A) out of plane and (B) in plane modal analysis

A shaker was attached via a sting and a force transducer to the racket frame. The sting kept the force transmitted acting in a direction that was either out of or in the plane of the stringbed in its resting position. The method of attachment for the out of plane testing allowed both the transverse and torsional modes of vibration to be excited. The shaker was controlled by a spectrum analyser, which excited the racket with a selected frequency range of 0 - 1000 Hz. Measurements were taken at the selected points on the strings, frame and handle using a Polytec Doppler laser vibrometer (Figure 5.2). The velocity of these points was established by measuring the Doppler shift between the frequency of the transmitted and reflected light.

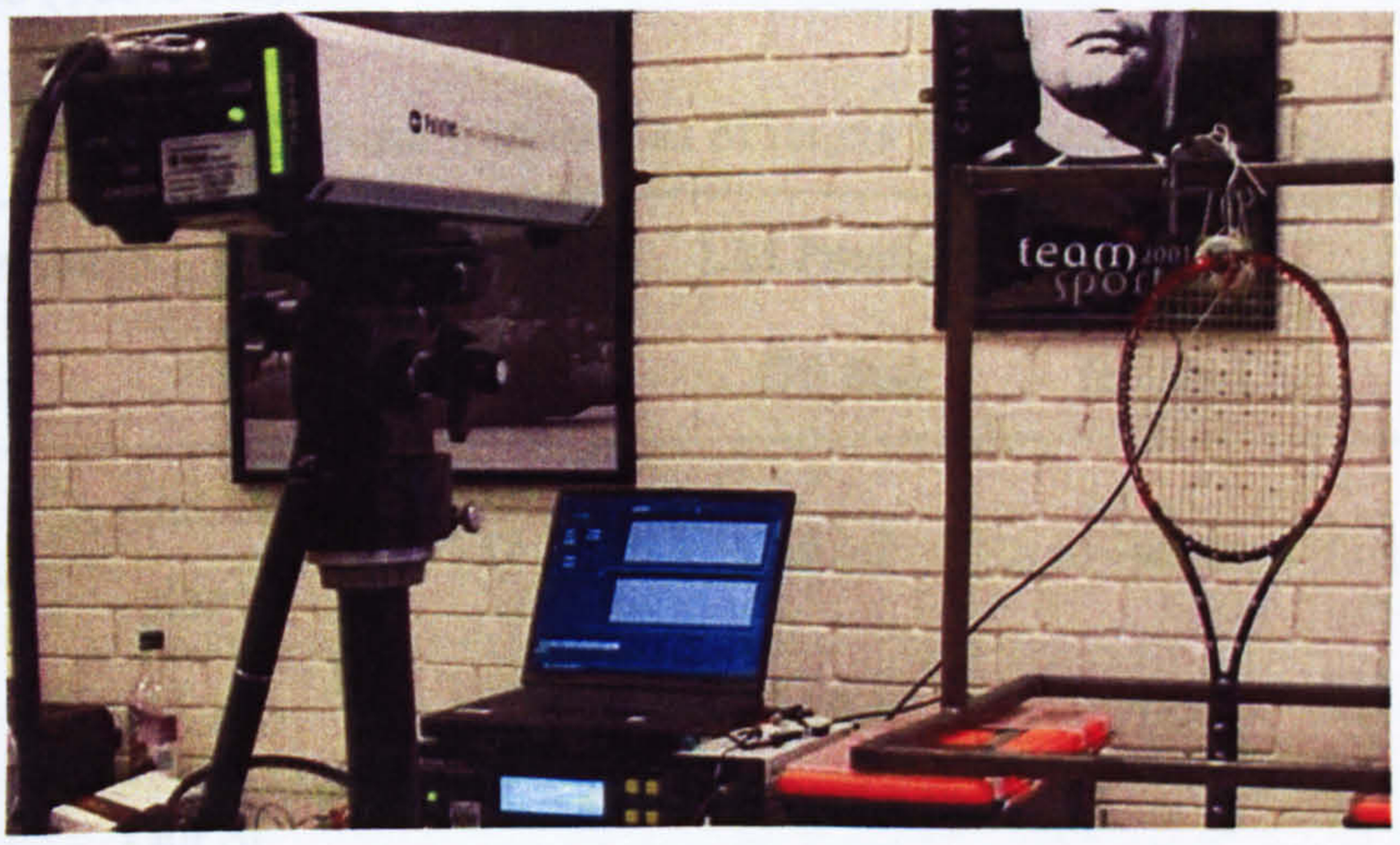

Figure 5.2. Doppler laser vibrometer

The outputs from the force transducer and the laser vibrometer were input to the spectrum analyser (Figure 5.3).

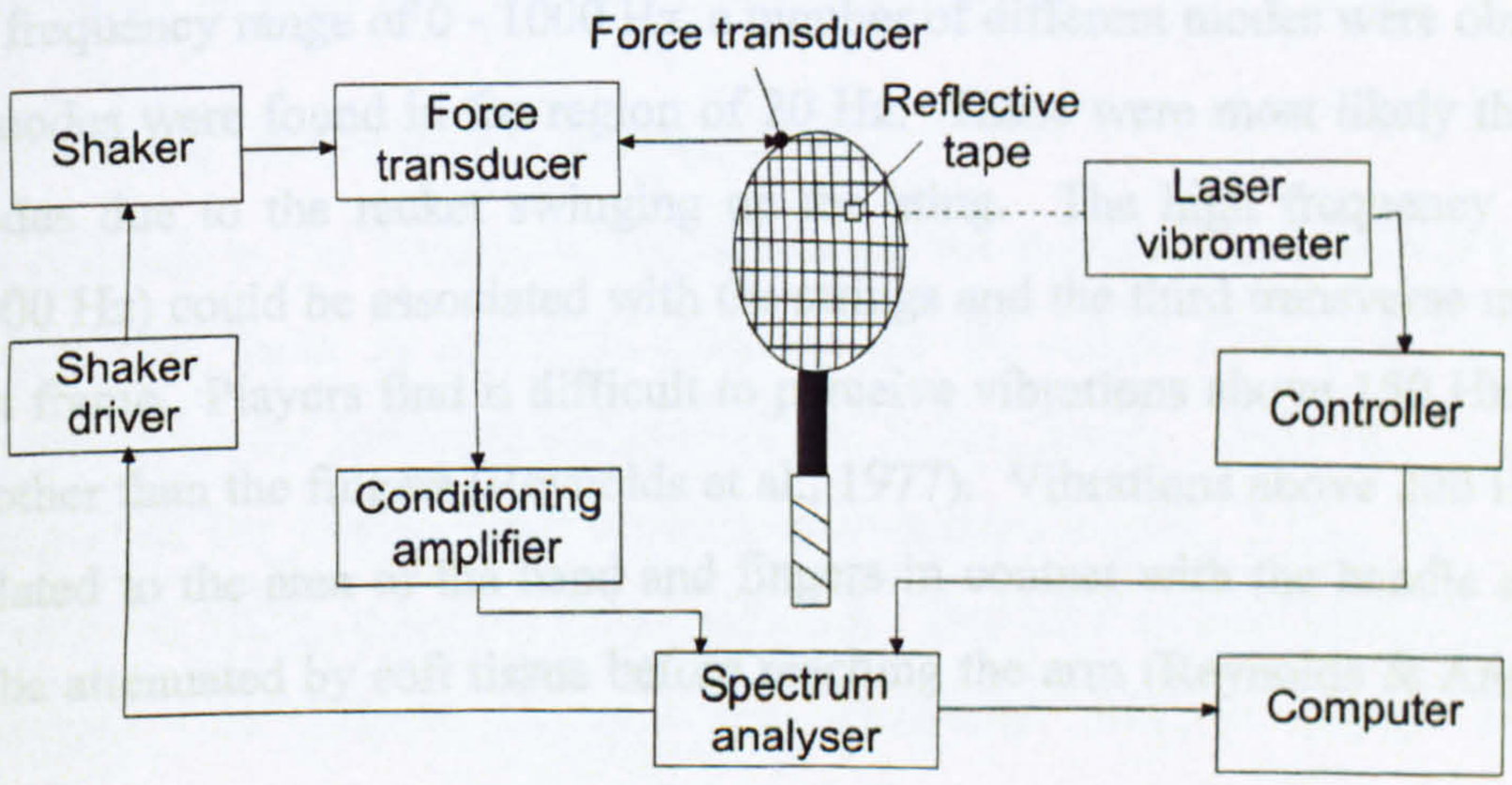

Figure 5.3. Experimental arrangement for the modal analysis of tennis rackets

Fifty trials were averaged to obtain a frequency response function (FRF). The FRF was the ratio between the harmonic displacement response and the harmonic force response, with both displacement and force being complex numbers. At resonance, the real part was zero and the imaginary part was at its maximum. Each FRF was acquired using software that performed a Fast Fourier Transform. The FRFs were exported in ASCII Universal File format for further analysis.

5.2.3 Results

A modal frequency was found by observing where the real component of the FRF was zero (Table 5.2).

Table 5.2. Natural frequencies of tennis racket frames (Hz)

Mode shape		LM Prestige (57 lbs)	LM Prestige (70 lbs)	LM 8 (57 lbs)	LM 8 (75 lbs)
Fundamental mode	Out of plane	132.2	132.2	149.8	149.3
	In plane	158.4	158.4	178.1	179.1
Second mode	Out of plane	353.4	360.0	358.1	359.4
	In plane	382.5	383.4	381.6	375.0

An impact will excite the tennis racket across the full frequency spectrum. Over the frequency range of 0 - 1000 Hz, a number of different modes were observed. Several modes were found in the region of 20 Hz. These were most likely the rigid body modes due to the racket swinging on the sting. The high frequency modes (600 - 1000 Hz) could be associated with the strings and the third transverse mode of the racket frame. Players find it difficult to perceive vibrations above 150 Hz at any location other than the fingers (Reynolds et al., 1977). Vibrations above 200 Hz tend to be isolated to the area of the hand and fingers in contact with the handle and are likely to be attenuated by soft tissue before reaching the arm (Reynolds & Angevine, 1977).

In this study the fundamental modes of the racket frame in and out of the plane of the racket were modelled. If significant levels of vibration are generated and transmitted to the elbow at these frequencies, an extension of the model in the future to approximate the higher frequency response of the racket would be necessary.

From its real and imaginary components, the amplitude of the FRF at each frequency of excitation and the phase difference was calculated. This enabled the mode shapes of each tennis racket to be animated using a Macro that was programmed in Visual Basic. Since the fundamental modal frequencies for both racket models were very similar for the two different string tensions, the mode shapes were assumed to be the same in each case. A quadratic equation was fitted through the amplitude data so that, with appropriate scaling, the position of the nodes and antinodes (Section 3.3.1) could be estimated (Table 5.3). The lengths of the LM Prestige and LM 8 rackets tested were 0.686 m and 0.695 m respectively from the butt end of the racket handle to the tip of the racket frame.

Table 5.3. Location of the antinodes for the fundamental modes of vibration of the racket frames (from butt end)

Mode feature	LM Prestige	LM 8
Antinode location out of plane (m)	0.349	0.350
Antinode location in plane (m)	0.366	0.375

5.3 RACKET INERTIA PARAMETERS

5.3.1 Overview of racket inertia parameters

In addition to the location of the antinodes, the moments of inertia (MOIs) of each tennis racket about its principal axes through the centre of mass (COM) were needed to calculate the torsional stiffness of the racket frame. Since the rigid body approximation of the tennis racket consists of two rigid bodies, it was necessary to find the principal MOIs about the COM for each. The MOI of each racket about the three principal axes (Figure 5.4) was first measured with the strings intact to determine their contribution. The same procedures were then applied when the strings were removed and then the racket was cut at the average position of the

antinodes in and out of the plane of the racket frame. Table 5.3 shows that the antinodes for the in and out of plane cases were within 25 mm of each other for both racket frames. Assuming that they were in the same location simplified the model code considerably. The MOI of the racket segment with the handle was calculated and therefore that of the other part of the racket could also be found. Where the measurement was not taken through the COM of the racket / racket part, the parallel axes theorem was used (Equation 5.1). This meant that at each stage, the location of the COM had to be determined.

$$I = I_{CG} + md^2 \tag{5.1}$$

I = the MOI of the racket about an axis

I_{CG} = the MOI of the racket about a parallel axis through its COM

m = the mass of the racket

d = the distance between the parallel axes

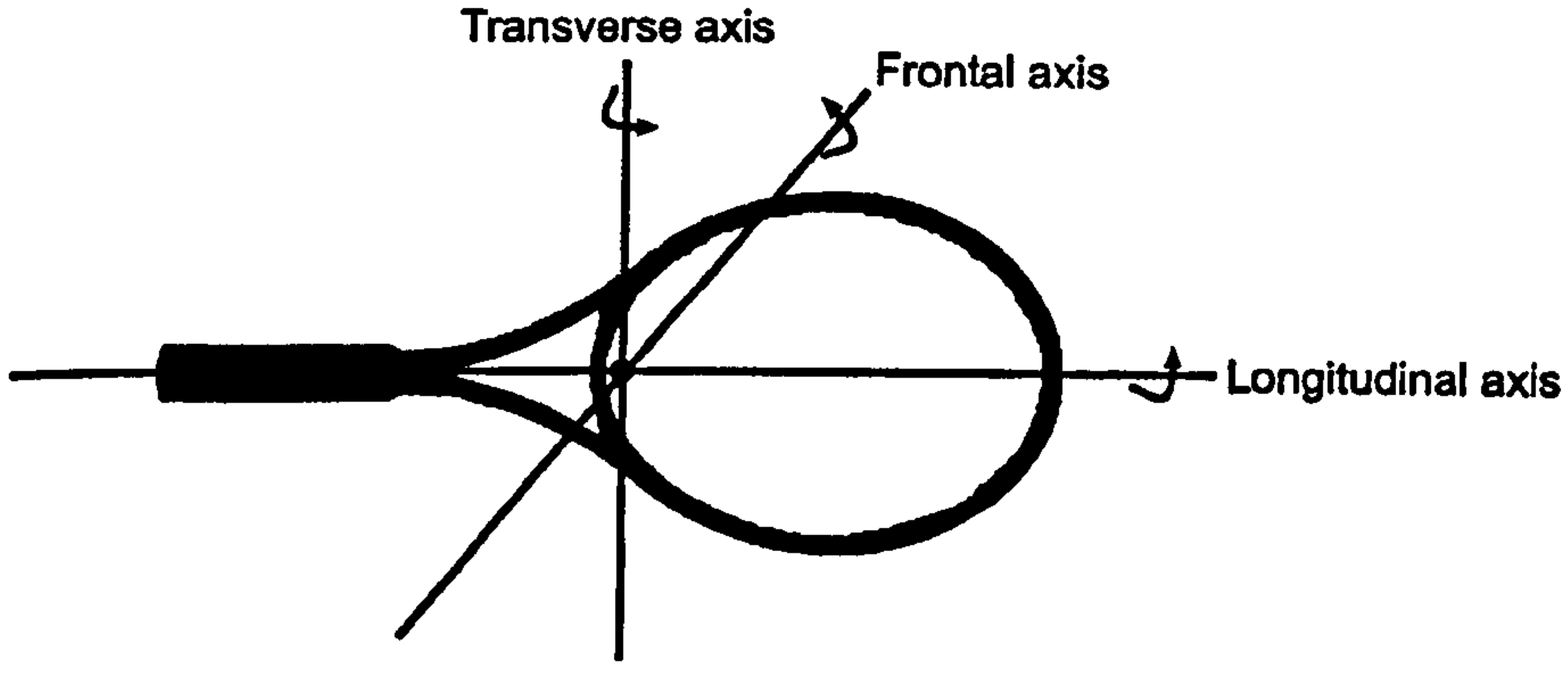

Figure 5.4. The three principle axes through the COM of the tennis racket

5.3.2 Method

MOI about longitudinal axis

The BRDC (Section 5.2.2) could not be used to calculate the MOI of the racket frame about its longitudinal axis. Additionally, the BRDC could not measure MOI values for parts of the racket frame directly. An industrial measuring device was used to calculate the MOI of the tennis racket about the longitudinal axis. A custom made attachment (Figure 5.5) allowed the racket to be securely mounted onto the device so that the longitudinal axis was directly above the centre of rotation.

Figure 5.5. Measuring the MOI about the longitudinal axis of the tennis racket

Once an initial measurement had been taken to zero the scale, MOI values could be determined by allowing the racket to oscillate and reading the digital scale. A custom built calibration device was built consisting of an aluminium stand and discs of known MOI. Tests showed that there was no difference between the theoretical and measured MOI values to four decimal places throughout a range within which the racket parts would lie. Therefore no adjustment was made to the values taken directly from the measuring device.

MOI about the transverse and frontal axes

Calculating the MOI of the racket about its transverse and frontal axes involved using a pendulum method to time the period of oscillation. The period of a pendulum (Brody, 1985) is:

$$T = 2\pi\sqrt{\frac{I}{mgh}} \qquad (5.2)$$

where T = the period of the pendulum

m = the mass of the racket and the attachment

g = acceleration due to gravity

h = the height of the pivot above the COM of the racket

Rearranging:

$$I = \frac{mghT^2}{4\pi^2} \tag{5.3}$$

Equation 5.3 gives the MOI of the racket plus the pendulum attachment. To find the MOI of the pendulum attachment to be subtracted, sample objects of known MOI similar to that of a tennis racket were tested. The known MOI values were then subtracted from the overall MOI values to leave the MOI of the attachment.

A custom built rig (Figure 5.6) was used to provide a flat, level surface for the pendulum to swing. A metal plate had a rectangular slot cut in the centre to accept a racket and a shallow groove of semi-circular profile was made. This allowed the needle point contacts of the pendulum to move back to the centre of the groove and not impart too much friction on the system. To find the period of the racket oscillation an oscilloscope was used in conjunction with a laser, light gate and receiver. The laser gate was cut twice for each racket oscillation allowing the period of oscillation to be determined by observing the difference between every second trigger. The light gate was positioned in the middle of the swing plane and the angle of the pendulum swing from the vertical did not exceed 15 degrees.

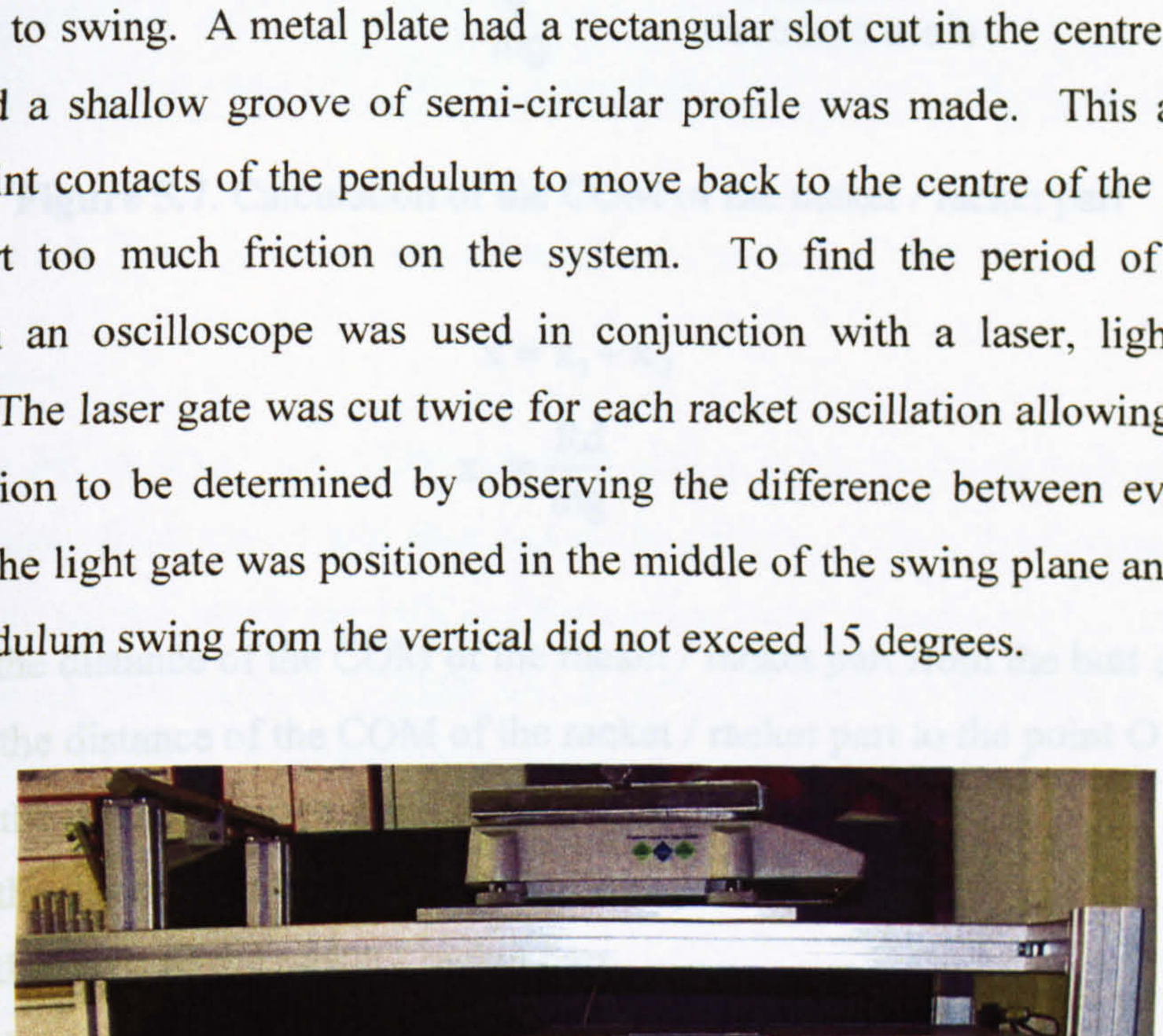

Figure 5.6. Experimental rig used to calculate the racket frame MOI values about the frontal and transverse axes

Centre of mass

A fixed knife edge and a knife edge on a set of electronic scales were used to balance the racket and calculate its COM location by taking moments about point O (Figure 5.7) and then applying Equation 5.4.

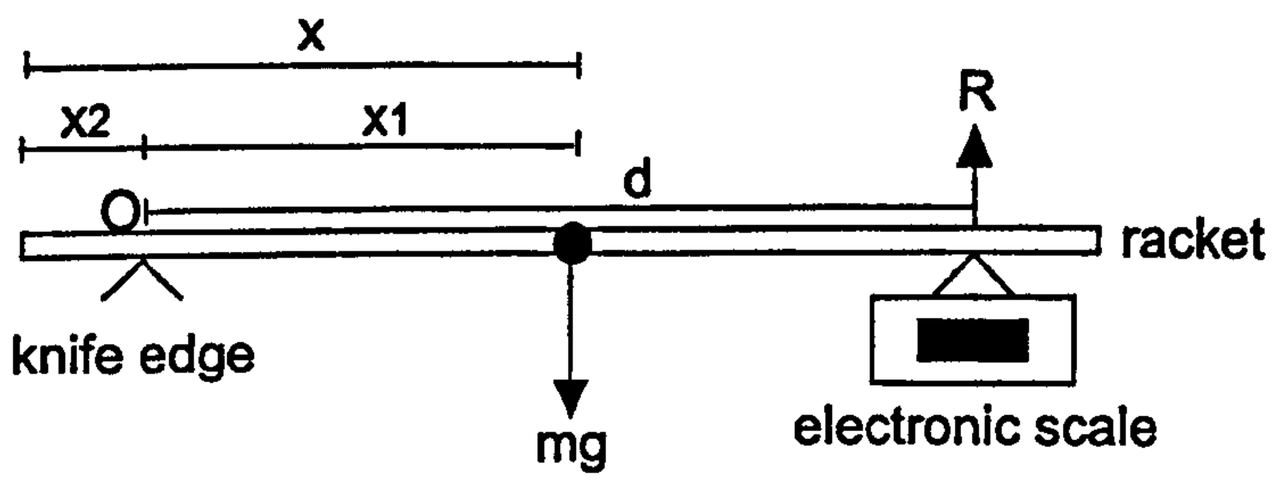

Figure 5.7. Calculation of the COM of the racket / racket part

$$x = x_1 + x_2$$

$$x_1 = \frac{Rd}{mg} \qquad (5.4)$$

where x = the distance of the COM of the racket / racket part from the butt end

x_1 = the distance of the COM of the racket / racket part to the point O

x_2 = the distance between the butt end and point O

d = the distance between the two knife edges

m = the mass of the racket / racket part

g = the acceleration due to gravity

R = reaction force at the knife on the electronic scale

Figure 5.8 overleaf shows the scales being supported by a sheet of machined aluminium which provided a flat, level surface. The knife edge on top of the scales sat on two supports and the two overhangs were butted up against the side of the scales. This allowed the apparatus to be accurately positioned but easily removed as well. The other fixed knife edge had a hinged datum attached which allowed the racket to be correctly positioned.

Figure 5.8. The rig, scales and knife edges used to calculate the racket COM

5.3.3 Results

The MOIs about the COM of each racket were calculated about the three principle axes. Each racket was then cut at the antinode of the fundamental mode of vibration and subsequently the MOIs of the separate racket parts were calculated. For the purpose of this analysis, racket part E refers to that component of the racket containing the handle. The COM of the racket part is measured from the butt end or the racket part that would be closest to the butt end of the racket.

Table 5.4. MOI values for the racket frame about three perpendicular axes through the COM for the LM Prestige

Racket part	Mass (kg)	Distance of COM from butt end (m)	MOI about longitudinal axis (kgm^2)	MOI about frontal axis (kgm^2)	MOI about transverse axis (kgm^2)
Whole (strings)	0.30890	0.33007	0.00146	0.01788	0.01606
Whole (no strings)	0.29400	0.32419	0.00141	0.01722	0.01586
Part E	0.13350	0.11365	0.00004	0.00173	0.00172
Part F	0.16050	0.15032	0.00137	0.00465	0.00331

Table 5.5. MOI values for the racket frame about three perpendicular axes through the COM for the LM 8

Racket part	Mass (kg)	Distance of COM from butt end (m)	MOI about longitudinal axis (kgm^2)	MOI about frontal axis (kgm^2)	MOI about transverse axis (kgm^2)
Whole (strings)	0.25540	0.39014	0.00166	0.01316	0.01252
Whole (no strings)	0.24050	0.38463	0.00161	0.01284	0.01200
Part E	0.10690	0.19543	0.00010	0.00203	0.00200
Part F	0.13360	0.18702	0.00151	0.00392	0.00311

Tables 5.4 and 5.5 suggest that the strings have a relatively small influence on the MOI values for both rackets. For the simulation model where the stringbed was represented using nine point masses, their inertia parameters were incorporated within racket frame part F.

Comparison of results from pendulum tests and BRDC

When comparisons were made with the results from Table 5.1 it could be seen that the position of the COM of the whole racket from the butt end was 5 mm less when calculated using the BRDC for the LM Prestige and 12 mm less for the LM 8 racket. Table 5.6 compares the MOI values about the frontal and transverse axes through the COM points of both whole rackets calculated by the pendulum oscillation technique described and by the BRDC.

Table 5.6. Comparison of MOI values using the pendulum oscillation technique and the BRDC

Axis through the COM of the whole racket about which the MOI was calculated	LM Prestige (kgm^2)		LM 8 (kgm^2)	
	BRDC	Pendulum	BRDC	Pendulum
Frontal	0.0173	0.0179	0.0152	0.0134
Transverse	0.0158	0.0161	0.0122	0.0125

A simple calculation using Equation 5.1 was performed to convert from the axis of the BRDC (10 cm from the butt end of the racket) to an axis through the COM of the whole racket. Table 5.6 shows the differences in the MOI values derived using the two different techniques for the whole rackets. Differences between the two values varied from 3.4 to 13.4%. The BRDC could not be used to calculate the MOI values for racket parts as well as the whole racket. An error analysis was performed for the methods used in this study.

5.3.4 Error analysis

Centre of mass

Since the measurements were repeated and differed slightly, it was necessary to look at the uncertainty in such variables. Error propagation was used with the approximate percentage error in the final result being calculated by using estimated measured values and their known ranges of random error. The constants π and g were assumed to have no error associated with them.

$m = 0.3 \pm 0.0001$ kg $\quad x_2 = 0.1 \pm 0.002$ m $\quad R = 0.2 \pm 0.0001$ kg $\quad d = 0.4 \pm 0.002$ m

$$\frac{\delta Rd/m}{Rd/m} = \sqrt{\left(\frac{\delta d}{d}\right)^2 + \left(\frac{\delta R}{R}\right)^2 + \left(\frac{\delta m}{m}\right)^2} \qquad (5.5)$$

$$\frac{\delta Rd/m}{Rd/m} = \sqrt{\left(\frac{0.002}{0.4}\right)^2 + \left(\frac{0.0001}{0.2}\right)^2 + \left(\frac{0.0001}{0.3}\right)^2} = 0.0050$$

Adding the uncertainty of x_2:

$$\delta\left[\left(\frac{Rd}{m}\right) + x_2\right] = \sqrt{0.0050^2 + 0.002^2} = 0.0054$$

A final estimated error of 0.54% for the value of the COM obtained using this rig was calculated.

MOI from pendulum tests

The same method as above was used to estimate the percentage error involved in calculating the MOI of the racket segment.

$m = 0.3 \pm 0.0001$ kg $\qquad$ $h = 0.35 \pm 0.002$ m $\qquad$ $T = 1.4 \pm 0.001$ s

$$\frac{\delta(mhT^2)}{mhT^2} = \sqrt{\left(\frac{\delta m}{m}\right)^2 + \left(\frac{\delta h}{h}\right)^2 + \left(2\left(\frac{\delta T}{T}\right)\right)^2} \qquad (5.6)$$

$$\Rightarrow \sqrt{\left(\frac{0.0001}{0.3}\right)^2 + \left(\frac{0.002}{0.35}\right)^2 + \left(2\left(\frac{0.001}{1.4}\right)\right)^2} = 0.0059$$

Therefore, the error associated with the MOI calculated using the pendulum was 0.59%. This value is an estimate of the error due to the measurable factors and not the error incurred by any friction in the pivot. Additionally, this value was associated with the MOI about an axis through the pivot point and therefore there was an additional error associated with using the parallel axes theorem (Equation 5.1).

$$\frac{\delta(mh^2)}{mh^2} = \sqrt{\left(\frac{\delta m}{m}\right)^2 + \left(2\left(\frac{\delta h}{h}\right)\right)^2} \qquad (5.7)$$

$$\Rightarrow \frac{\delta(mh^2)}{mh} = \sqrt{\left(\frac{0.0001}{0.3}\right)^2 + \left(2\left(\frac{0.002}{0.35}\right)\right)^2} = 0.011$$

This gives a value for the fractional uncertainty of mh^2 of 1.1%. Adding the uncertainty of the MOI about the pivot point gives:

$$\delta[mhT^2 + mh^2] = \sqrt{0.0059^2 + 0.011^2} \qquad (5.8)$$
$$= 0.0125$$

The final estimated error of the MOI of the racket about an axis through its COM calculated using the pendulum was 1.25%.

5.4 FRAME STIFFNESS AND DAMPING PARAMETERS

5.4.1 Overview of frame stiffness and damping coefficient determination

Stiffness and damping coefficients for the torsional spring-dampers applying passive torques around the frictionless pin joint connecting two racket frame bodies (Section 3.3.2) were determined. This enabled the vibration response and the associated energy loss of flexible racket frames to be approximated. The coefficients were established by matching the vibration response of the actual and simulated racket frames in terms of acceleration amplitudes and rates of decay.

5.4.2 Method

An experiment was performed whereby the racket frame was freely suspended from a rig by fishing wire and then struck by an impact hammer at a point on the handle that would be in the middle of the player's grip (away from the node located at the top of the handle). A small cross-section of the polyurethane foam handle was cut away to enable the racket to be struck and an accelerometer to be mounted opposite using beeswax on the metal frame. The direction of the strike was either directly in or out of the plane of the racket to excite both mode shapes with higher amplitudes. The impact hammer was connected to a charge amplifier to measure the magnitude and duration of the impact force. The decay trace was observed using Signal Calc software.

A simulation model of the two-part racket frame vibrating in space was created using Autolev with the inertia parameters from Section 5.3.3 as input. The stiffness and damping coefficients were perturbed manually and simulations run until the best match was found between the acceleration traces collected experimentally and those predicted by the simulation model. Values were compared every 1 ms over a simulation period of 100 ms. The score function was equal to the root-mean-square (RMS) difference between the experimental and model acceleration values. The same procedure was applied for both the out of plane and in plane cases.

5.4.3 Results

The optimised stiffness and damping coefficients for both racket models are displayed in Tables 5.7 and 5.8 along with the RMS score expressed as a percentage of maximum experimental acceleration. Figures 5.9 and 5.10 compare the

experimental and simulation model acceleration versus time traces for a point on the handle of the LM 8 racket frame when it was excited by a force out of plane and in plane respectively.

Table 5.7. Torsional stiffness and damping coefficients (out of plane)

Racket model	Torsional stiffness coefficient (Nm/rad)	Torsional damping coefficient (Nms/rad)	RMS (%)
LM Prestige	910	0.03	9.8
LM 8	1075	0.04	8.9

Table 5.8. Torsional stiffness and damping coefficients (in plane)

Racket model	Torsional stiffness coefficient (Nm/rad)	Torional damping coefficient (Nms/rad)	RMS (%)
LM Prestige	1650	0.09	8.7
LM 8	1800	0.10	9.6

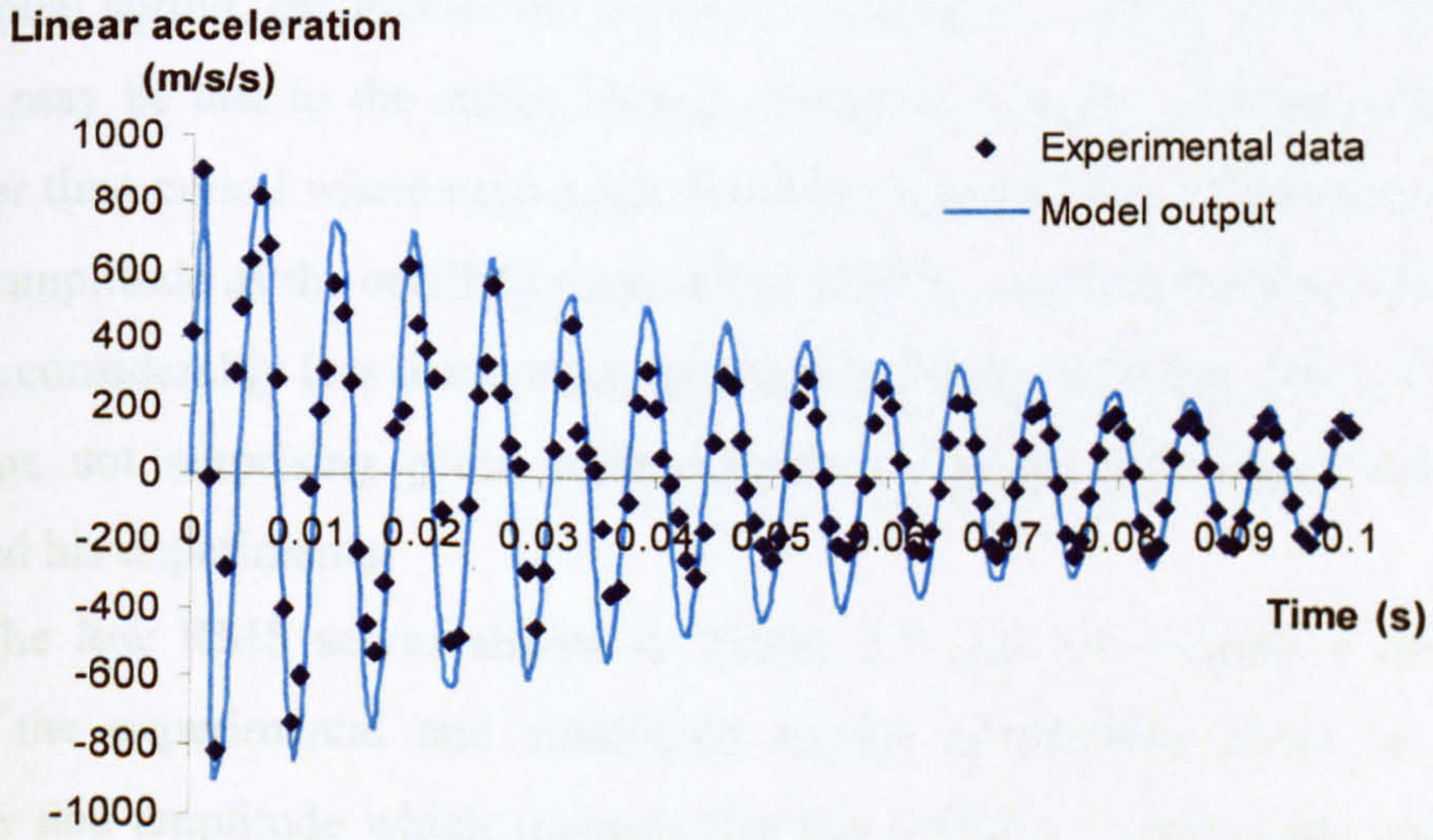

Figure 5.9. Comparison of experimental and model acceleration (out of plane)

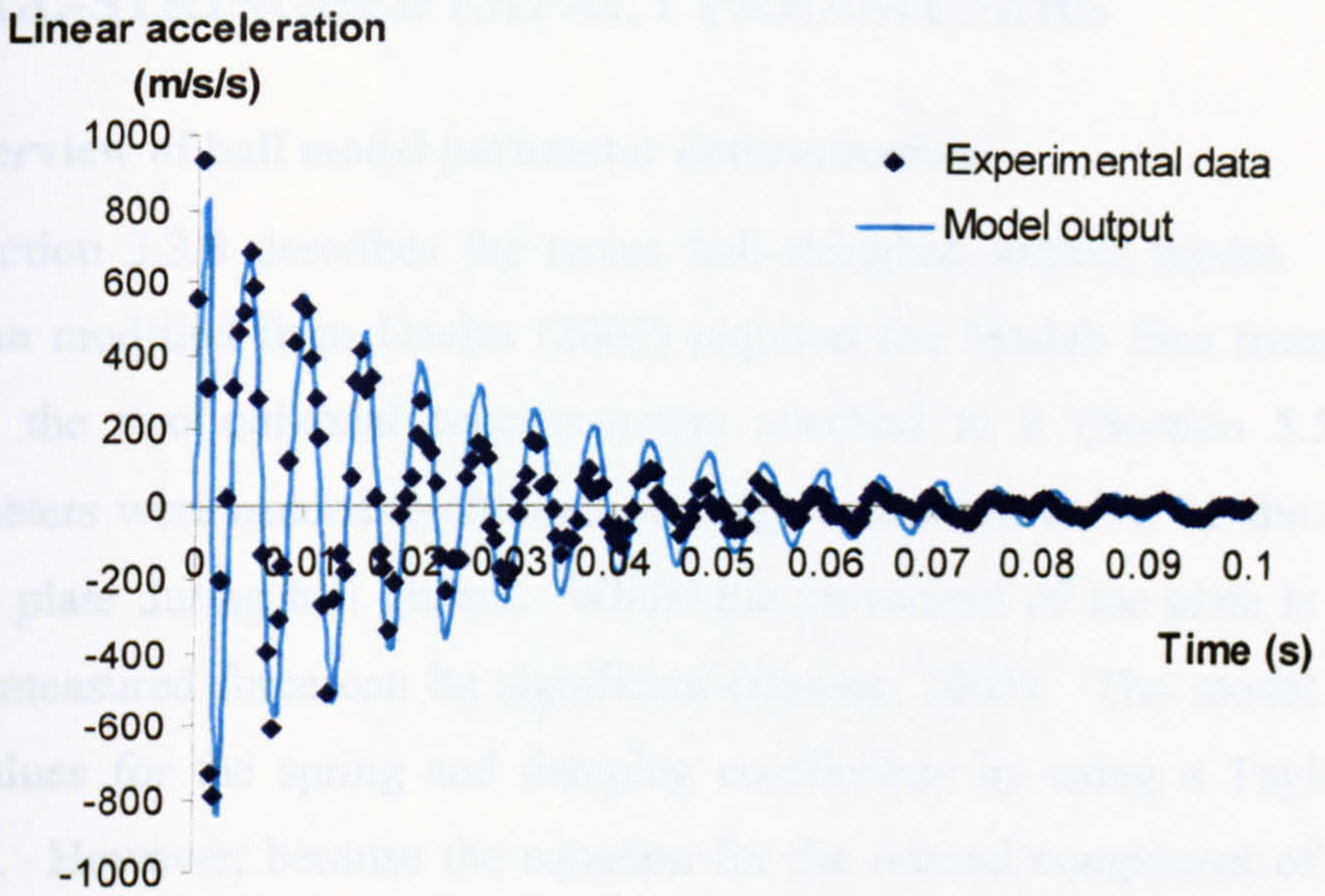

Figure 5.10. Comparison of experimental and model acceleration (in plane)

Figures 5.9 and 5.10 show that the LM 8 racket frame vibrates at a higher resonant frequency when excited in the plane of the racket when compared to the out of plane case. The same trend was observed for the LM Prestige racket frame although the resonant vibration frequencies were lower than the corresponding values for the LM 8 for both the in and out of plane cases This was expected from the aforementioned modal analysis results as the fundamental modal frequency was higher for the out of plane and in plane cases. The results also show that the stiffer the torsional spring, the greater the damping coefficient. Brody et al. (2002) stated that this may be due to the stiffer frames storing less energy and there being more cycles per time period where each cycle dissipates some of the vibration energy. The time for amplitude of the oscillations to fall to half its value ranged from 20 to 59 ms. This was considerably less than values reported by Brody (1989) of 180 to 750 ms but is perhaps not surprising given advancements in racket technology since Brody performed his experiments.

The low RMS scores shown in Tables 5.7 and 5.8 indicate a close match between the experimental and simulation model acceleration traces in terms of frequency and amplitude which suggests that the stiffness to mass ratio and also the damping coefficient are sensible.

5.5 BALL-STRINGBED IMPACT PARAMETERS

5.5.1 Overview of ball model parameter determination

Section 3.3.3 describes the tennis ball-stringbed impact model. A Matlab programme modified from Davies (2005) required the Matlab files from the force plate and the two uni-axial accelerometers attached to it (Section 5.5.2). The accelerometers were needed to obtain an average correction factor for the movement of the top plate during ball impact. Whilst the movement of the plate is small, the effect on measured force can be significant (Davies, 2005). The model calculates best-fit values for the spring and damping coefficients by using a Taylor's series expansion. However, because the equation for the normal component of ball force gives a high force at initial contact with the stringbed, an adjustment had to be made for use within the simulation model. The force was ramped up from zero to the value calculated by Equation 3.3 over an interval of 0.5 ms. This was achieved using a quintic function.

To model the oblique component of the impact between the ball and the point on the stringbed further ball cannon testing was needed so that the rebound angle data could be used within optimisation routines to calculate the friction coefficients for each stringbed.

5.5.2 Method

Normal component of ball-stringbed impact model

To obtain the required force traces, several pieces of equipment were needed. A piezoelectric Kistler Type 9067 force plate was attached securely to the rig within the impact chamber and positioned such that the ball would impact normally and into the centre of the force plate. This was achieved using a digital goniometer and an infrared laser respectively. Two uni-axial Brüel and Kjaer charge accelerometers were mounted at the rear of the force plate either side using beeswax (Figure 5.11).

Figure 5.11. Piezoelectric force plate and uni-axial accelerometers

Balls were fired at the force plate using a custom built pneumatic ball cannon. Air was supplied from the main compressor to a reservoir at 80 PSI which was connected to an amplifier allowing pressures up to 160 PSI to be generated. By adjusting the air pressure in the reservoir, the velocity at which the ball left the horizontal barrel was moderated. Analysis of high-speed video from the performance data collection (Section 4.2.2) allowed the relative velocities between the ball and tennis racket at impact to be calculated. Successive images of the tennis ball and racket frame were digitised using Phantom v5.0 software. The tennis ball (average diameter of 67.5 mm) was used as the calibration object for each trial as the ball was in a slightly different plane for each trial. The average relative impact velocities between the ball and stringbed were found to be 28.90 and 25.95 m/s for the topspin drive and slice one-handed backhand groundstrokes respectively. A range of inbound ball velocities of between 18 and 33 m/s were therefore used. For each of the six target inbound velocities (18, 21, 24, 27, 30 and 33 m/s), five impacts were measured so that experimental fluctuations were averaged and extremes filtered. Trials were accepted if the inbound velocity was within ± 0.5 m/s of the target velocity.

The ball passed through a set of ballistic light gates to record its velocity. As the ball went through the first light gate it partially blocked the light received by the sensor causing an electronic counter to be triggered. As the ball passed through the second light gate the counter was stopped. The gates remained a fixed distance apart allowing the calibrated counter to calculate the ball velocity. The light gates triggered

a pulse generator that in turn triggered a high-speed camera which operated at 10,000 Hz. Simultaneously, a pulse was sent to the HP analyser so that the force plate and accelerometer data could be synchronised with the high-speed data. The high-speed camera software allowed a series of bitmap images to be saved onto the laptop computer so that contact time between ball and force plate could be obtained (Figure 5.12).

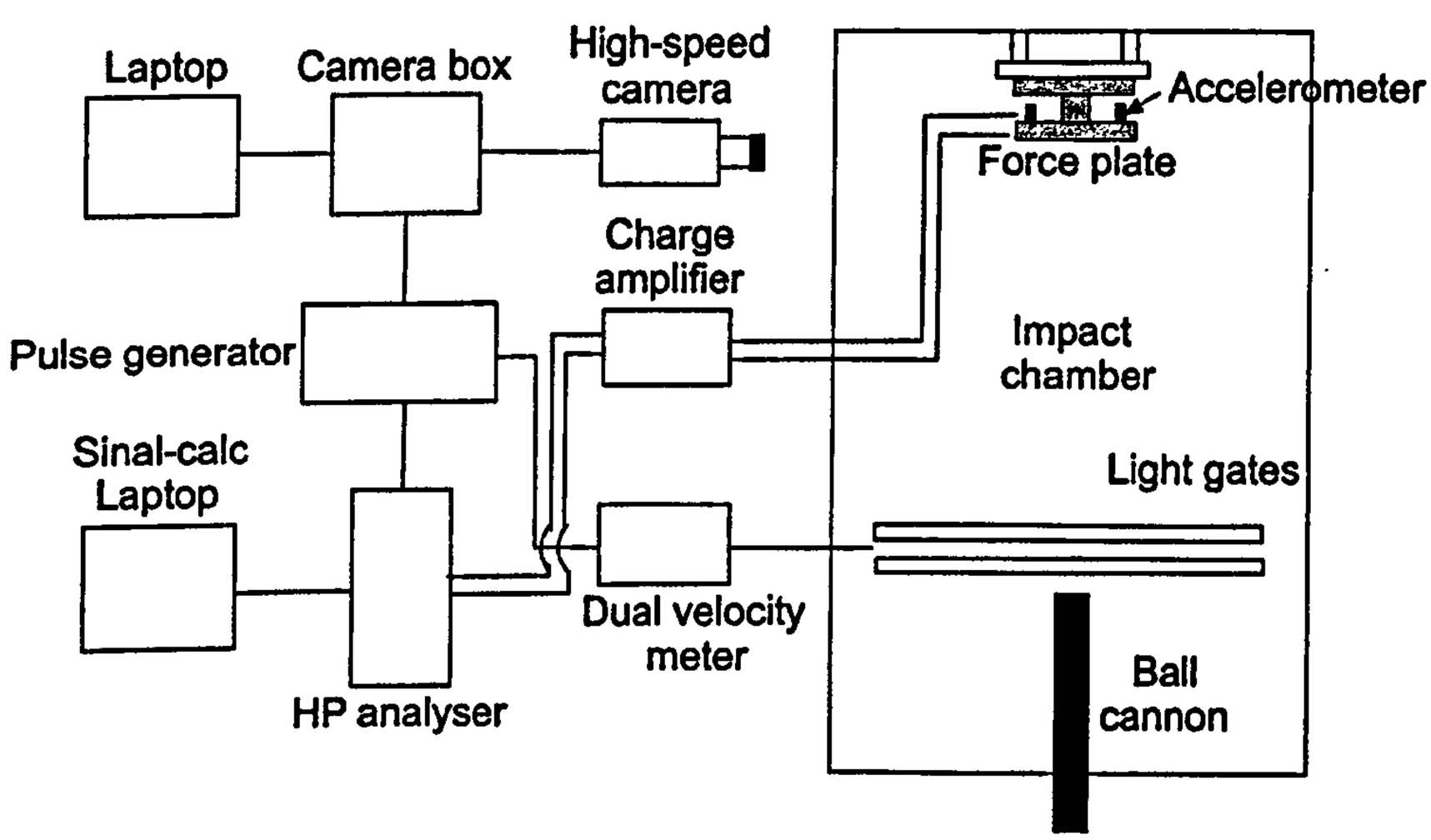

Figure 5.12. Equipment set-up to record force traces from tennis ball impacts

Oblique component of ball-stringbed impact model

In addition to the normal impacts described in Section 5.5.2, a series of oblique impacts were studied. The relative angles and velocities for the topspin and slice one-handed backhand groundstrokes were calculated from the high-speed video recordings. However, instead of impacting with a force plate, balls were propelled from the ball cannon at points on a racket stringbed. Balls were fired at two angles and velocities at all nine points on the racket stringbed (Figure 5.13).

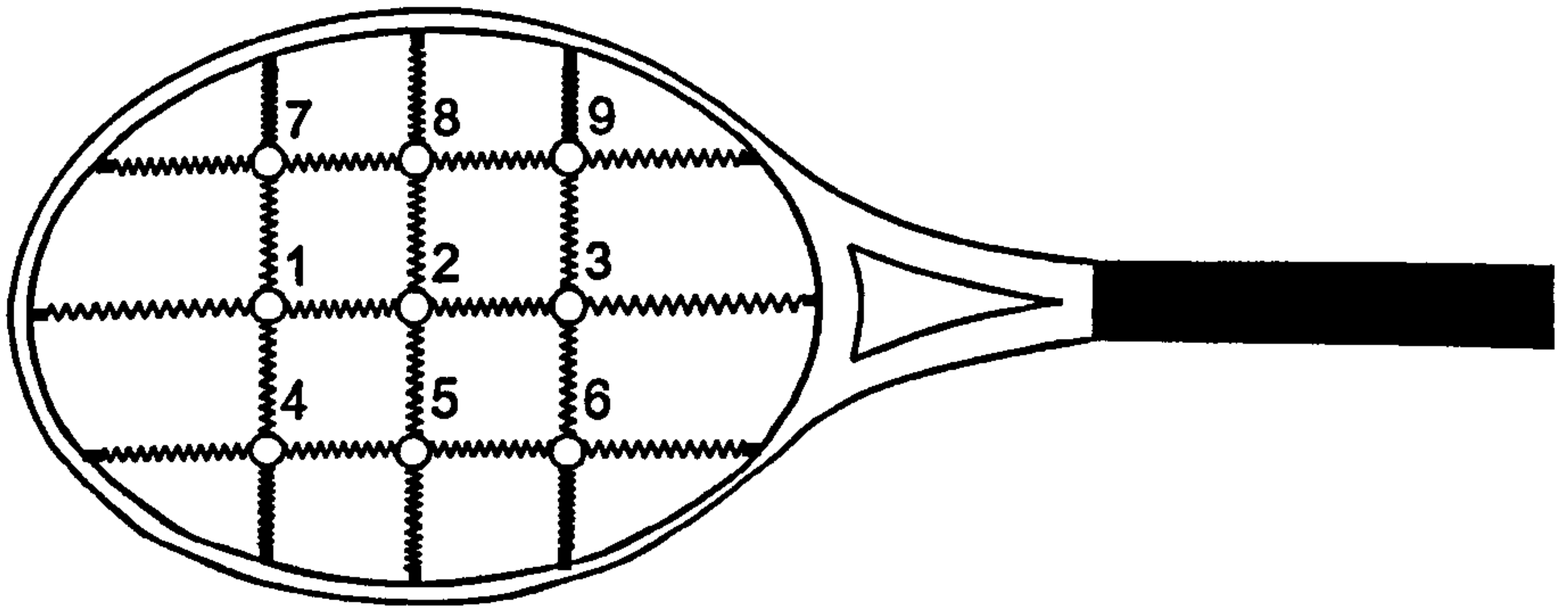

Figure 5.13. Ball impact locations on the stringbed

Figure 5.14 shows the two average relative angles and linear velocities between the ball and stringbed for the topspin drive and slice one-handed backhand groundstrokes.

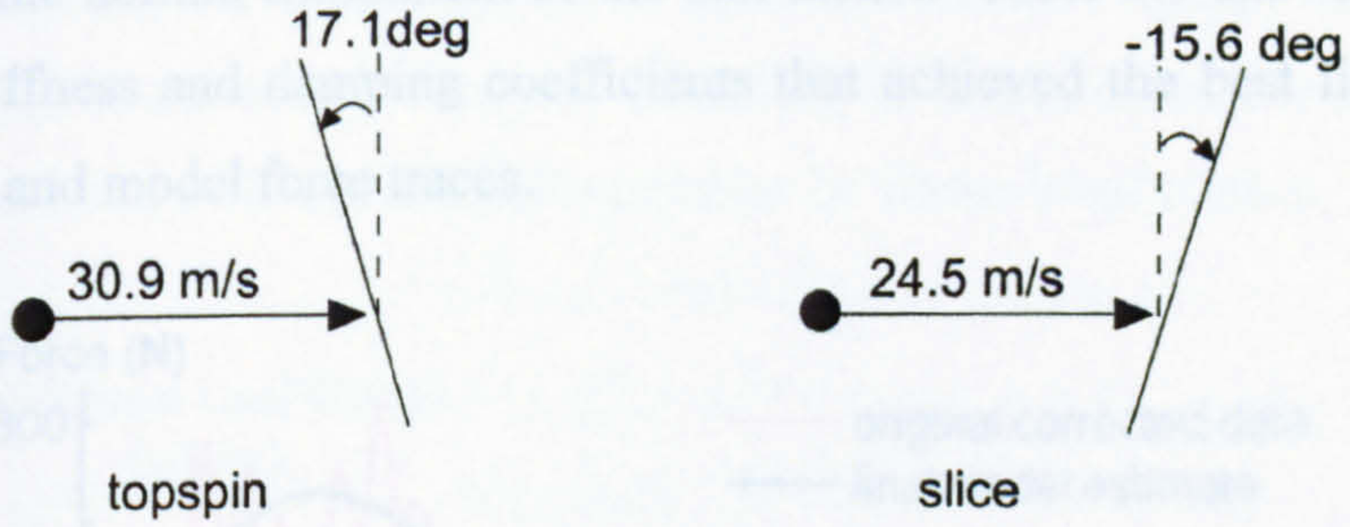

Figure 5.14. Ball cannon impact conditions to replicate topspin drive and slice groundstrokes

Sequential post-impact ball images were digitised to calculate the rebound angle relative to a line perpendicular to the stringbed plane (Figure 5.15).

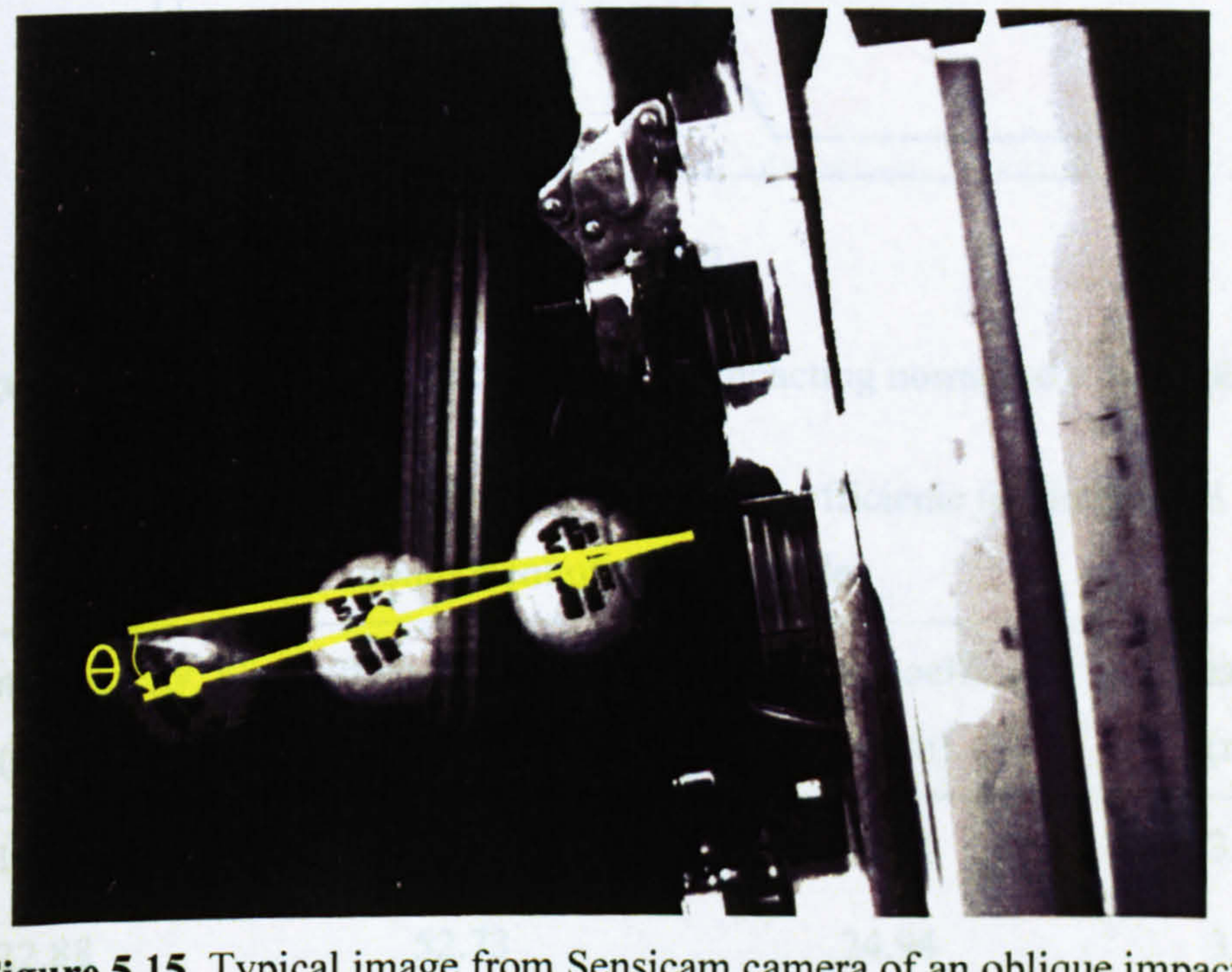

Figure 5.15. Typical image from Sensicam camera of an oblique impact

An Autolev programme was written to simulate the impact conditions using the stringbed model described in Section 3.3.2. The Fortran code became part of an optimisation routine where only the friction coefficients were varied until the best match was found between the measured and simulation rebound angles.

5.5.3 Results

Normal component of ball-stringbed impact model

Figure 5.16 shows an experimental force trace along with the force trace predicted by the normal component of the ball model. Table 5.9 shows the values of the spring stiffness and damping coefficients that achieved the best fit between the experimental and model force traces.

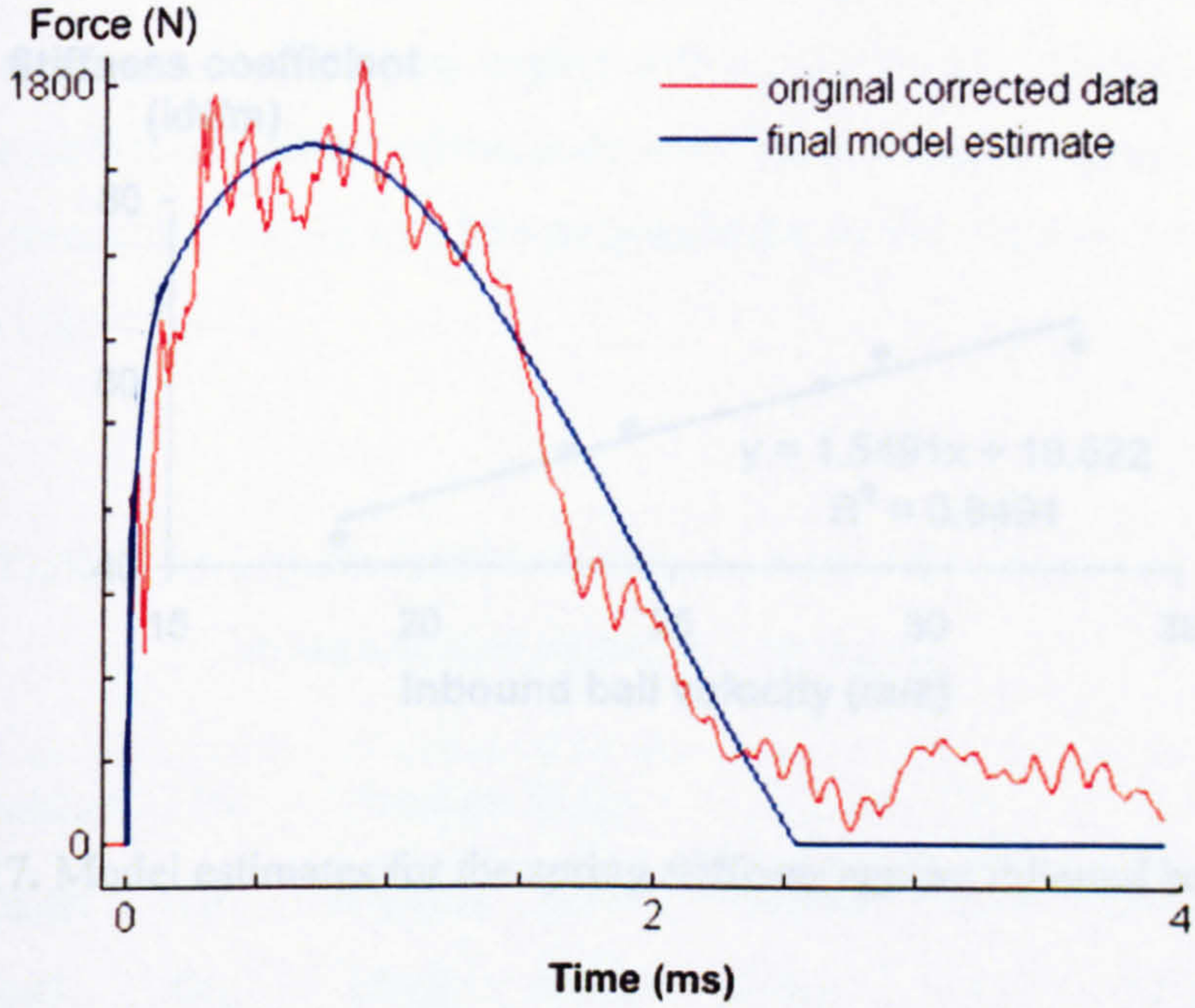

Figure 5.16. Typical force traces for a ball impacting normal to a force plate

Table 5.9. Stiffness and damping coefficients for the normal component of the ball model

Inbound velocity (m/s)	Stiffness coefficient (kN/m)	Damping coefficient (Ns/m)	Contact time (ms)
18.37	43.04	18.61	3.50
22.88	52.73	24.94	3.30
24.14	55.08	25.19	3.20
27.93	60.20	30.54	3.10
29.07	63.70	31.63	3.00
32.93	64.99	36.05	2.90

For each of the six inbound ball velocities a spring stiffness and damping coefficient were determined by optimisation as described in Section 5.5.1. The spring stiffness (Figure 5.17) and damping coefficients (Figure 5.18) were plotted against inbound ball velocity. The coefficients of determination (R^2 values) were close to 1 indicating strong linear correlations and this allowed values to be determined within the experimental range of inbound ball velocities by linear interpolation.

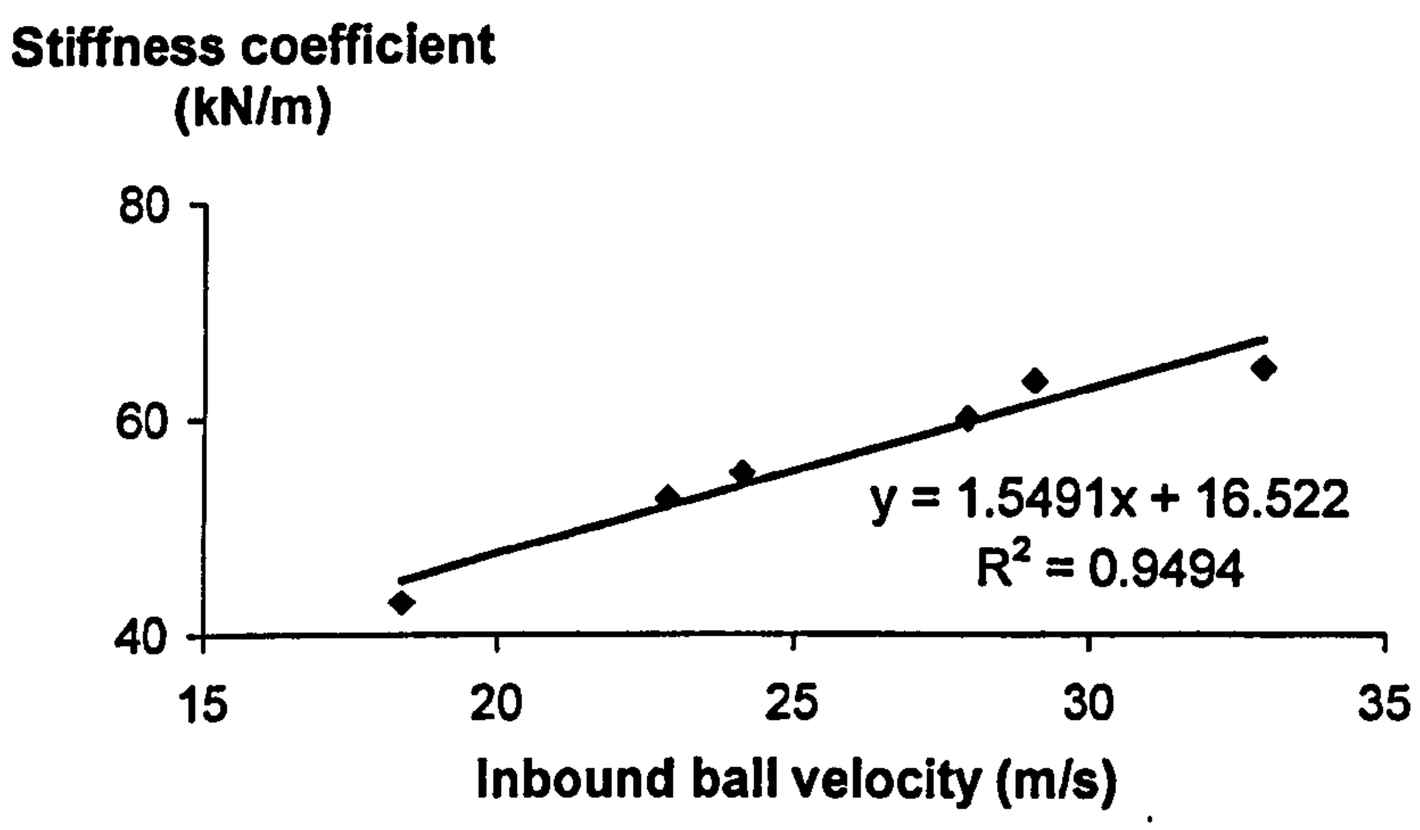

Figure 5.17. Model estimates for the spring stiffness against inbound ball velocity

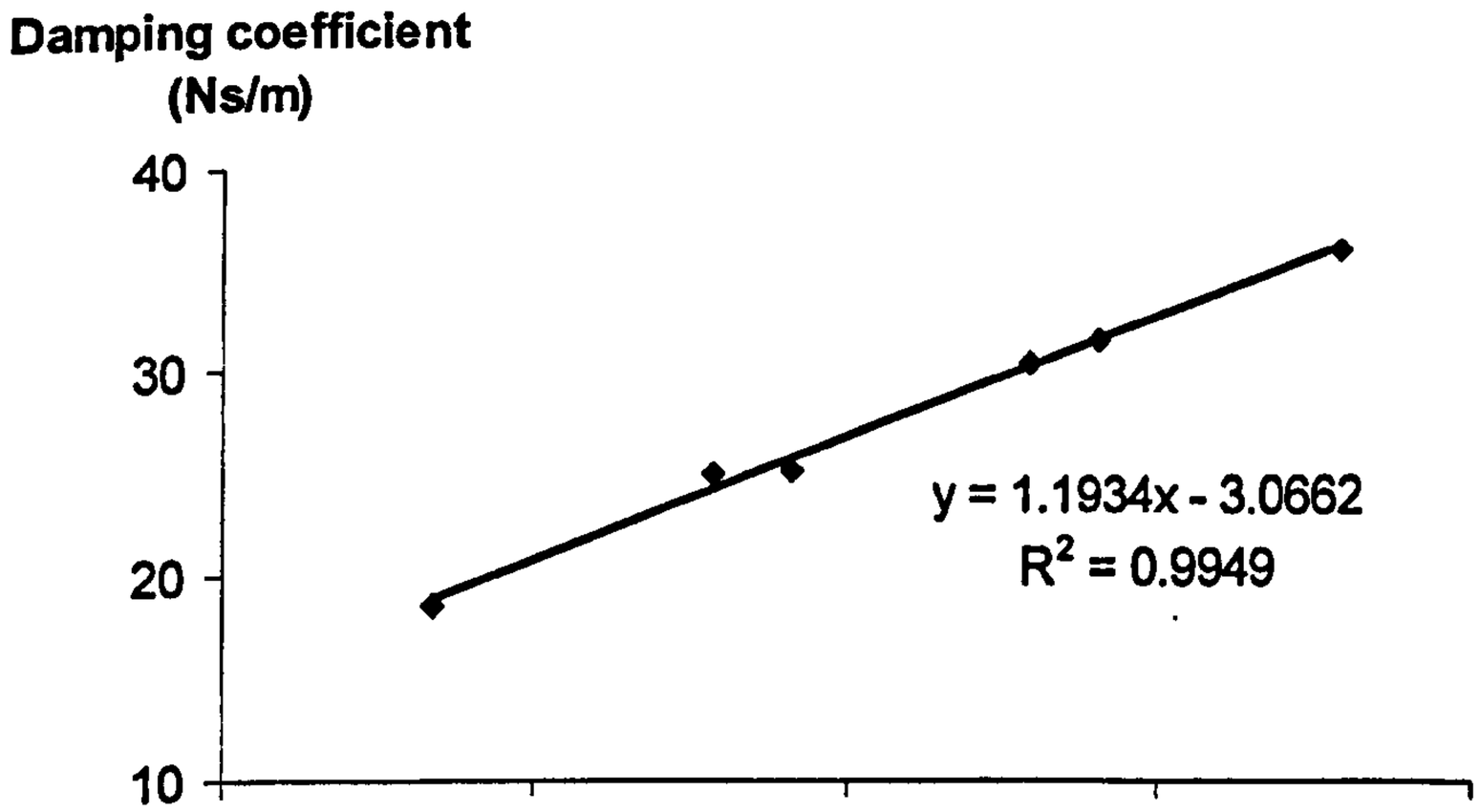

Figure 5.18. Model estimates for the spring damping against inbound ball velocity

The results from determining the ball spring parameters were consistent with the findings of other studies (e.g. Dignall et al., 2000) that tennis ball stiffness and damping coefficients show a positive linear relationship with incoming velocity for the range of impact velocities tested.

Oblique component of ball-stringbed impact model

Table 5.10 shows the experimental rebound angles obtained by digitising high speed video images of the ball post impact with a point on the stringbed. The target initial ball velocities and racket orientations were those shown in Figure 5.14 and the angles were measured relative to a line perpendicular to the plane of the stringbed as illustrated in Figure 5.15.

Table 5.10. Experimental ball rebound angles for oblique ball impacts at nine points on a stringbed

Point of impact	Prestige 57 lbs Topspin (deg)	Prestige 57 lbs Slice (deg)	Prestige 70 lbs Topspin (deg)	Prestige 70 lbs Slice (deg)	LM8 57 lbs Topspin (deg)	LM8 57 lbs Slice (deg)	LM8 75 lbs Topspin (deg)	LM8 75 lbs Slice (deg)
1	13.0	-11.7	12.7	-11.6	13.9	-11.1	14.2	-11.9
2	11.5	-10.8	11.3	-10.8	12.6	-10.3	13.6	-10.8
3	12.9	-11.7	12.6	-11.8	12.8	-11.4	14.3	-12.0
4	14.5	-11.1	14.2	-11.2	14.2	-10.8	14.6	-11.1
5	13.1	-10.6	12.7	-10.7	13.0	-10.7	13.9	-10.8
6	14.1	-11.0	13.8	-11.2	14.3	-10.9	14.7	-11.2
7	15.1	-10.6	14.8	-10.3	15.7	-9.5	15.8	-10.1
8	14.0	-9.7	13.7	-9.2	14.3	-9.7	14.6	-9.8
9	15.0	-10.7	14.7	-10.4	15.8	-9.7	15.9	-10.2

Table 5.11 shows the optimised coefficients of friction for each racket stringbed. The score refers to the average percentage difference between the experimental and simulation model rebound angles.

Table 5.11. Optimised coefficients of friction for each racket stringbed

Racket stringbed	Coefficients of friction			Score	Standard
	μ_1	μ_2	μ_3	(%)	deviation
LM Prestige (57lbs)	0.35	0.36	0.37	6.11	0.31
LM Prestige (70lbs)	0.35	0.36	0.38	6.89	0.45
LM 8 (57lbs)	0.26	0.29	0.32	7.24	0.39
LM 8 (75lbs)	0.26	0.30	0.35	7.71	0.43

Each score value is less than 8%, which is encouraging given the level of complexity with which the interaction between the ball and a point on the stringbed is modelled. Also presented is the average standard deviation of the percentage differences between the experimental and model rebound angles for the 18 trials (9 points of impact, 2 inbound velocities). The average standard deviation values are low in each case which indicates that the data is not widely dispersed and that the optimised values produce sensible results for each impact condition.

Digitising errors

The results for the outbound velocity of the ball and its angle of rebound were obtained by digitisation within customised ball tracking software. Errors may have occurred when digitising due to a lack of ball sphericity. Having hit the stringbed, the balls took a certain amount of time to reform back to their original shape but when the software calculated the centre box of the 'mapped out' ball, it assumed the ball was spherical. Figure 5.14 illustrates that there was some distortion in the images obtained. The user could not be certain that the outline of the ball was marked out correctly. Selected images were digitised three times to check for fluctuations in results. The magnitudes of the differences were calculated and suggested that an error of 2% was possible in the results for outbound velocity and rebound angle.

5.6 STRINGBED PARAMETERS

5.6.1 Overview of stringbed parameter determination

To determine the spring parameters for the model of the stringbed described in Section 3.3.2, information regarding the coefficient of restitution (COR) as well as the amount of deflection of the stringbed was collected. Once this data had been obtained for a range of impact conditions, the spring coefficients could be determined by computer optimisation.

5.6.2 Method

Ball cannon tests

To project balls onto the stringbed, the pneumatic ball cannon was used. The ball was projected through ballistic light gates to obtain inbound ball velocity. For each of the six target inbound velocities (18, 21, 24, 27, 30 and 33 m/s), five impacts were measured so that experimental fluctuations were averaged and extremes filtered. The light gates triggered a pulse generator that in turn triggered the Sensicam 2000 flash and camera units to record the post impact conditions (Figure 5.19). The camera unit consisted of a high-resolution multiple exposure digital camera which operated at 250 Hz. Three images of the ball were captured. By placing a calibration chart image in the plane of the ball path (10 x 10 cm) and using a customised ball tracking software package to digitise these images, an estimate of outbound ball velocity and associated ball features such as rebound angle (for oblique impacts) were obtained.

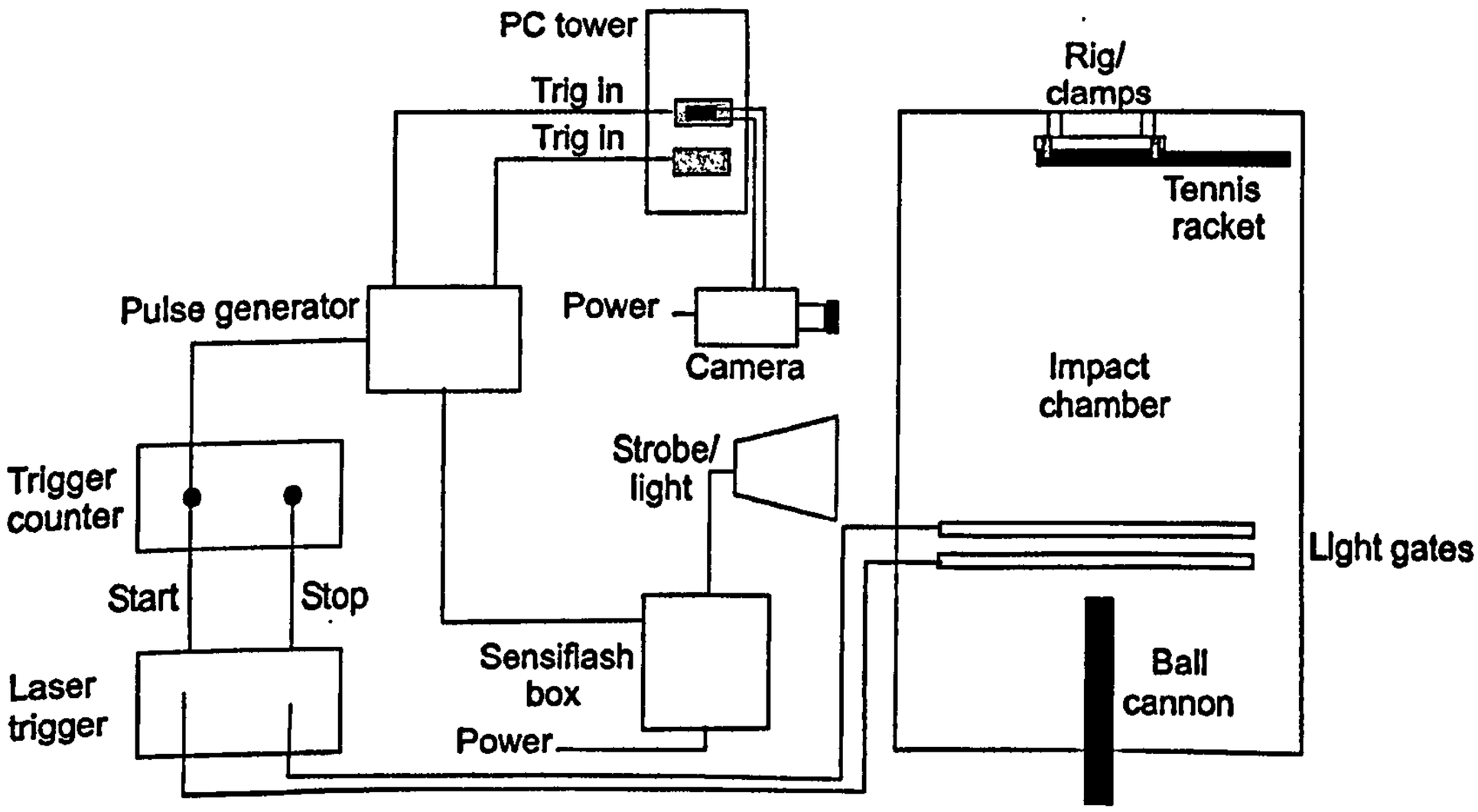

Figure 5.19. Equipment set-up to record ball velocity for impacts onto the stringbed

The testing was carried out for each of the two types of racket used at both string tensions. Since the model incorporated nine points of impact on the stringbed, the point of impact was systematically varied. Due to the symmetry of the stringbed, only six points of impact were tested for each of the four racket combinations during the normal impacts. These impact locations were marked on the stringbed using small pieces of reflective tape. An infrared laser, lodged within the cylinder of the ball cannon, allowed the point of impact to be determined (Figure 5.20). The rig and associated clamps were adjusted accordingly and then tightened to prevent them moving significantly during impact. The rig was set in place so that the ball impacted normally onto the surface of the stringbed. This was achieved with the aid of a digital goniometer.

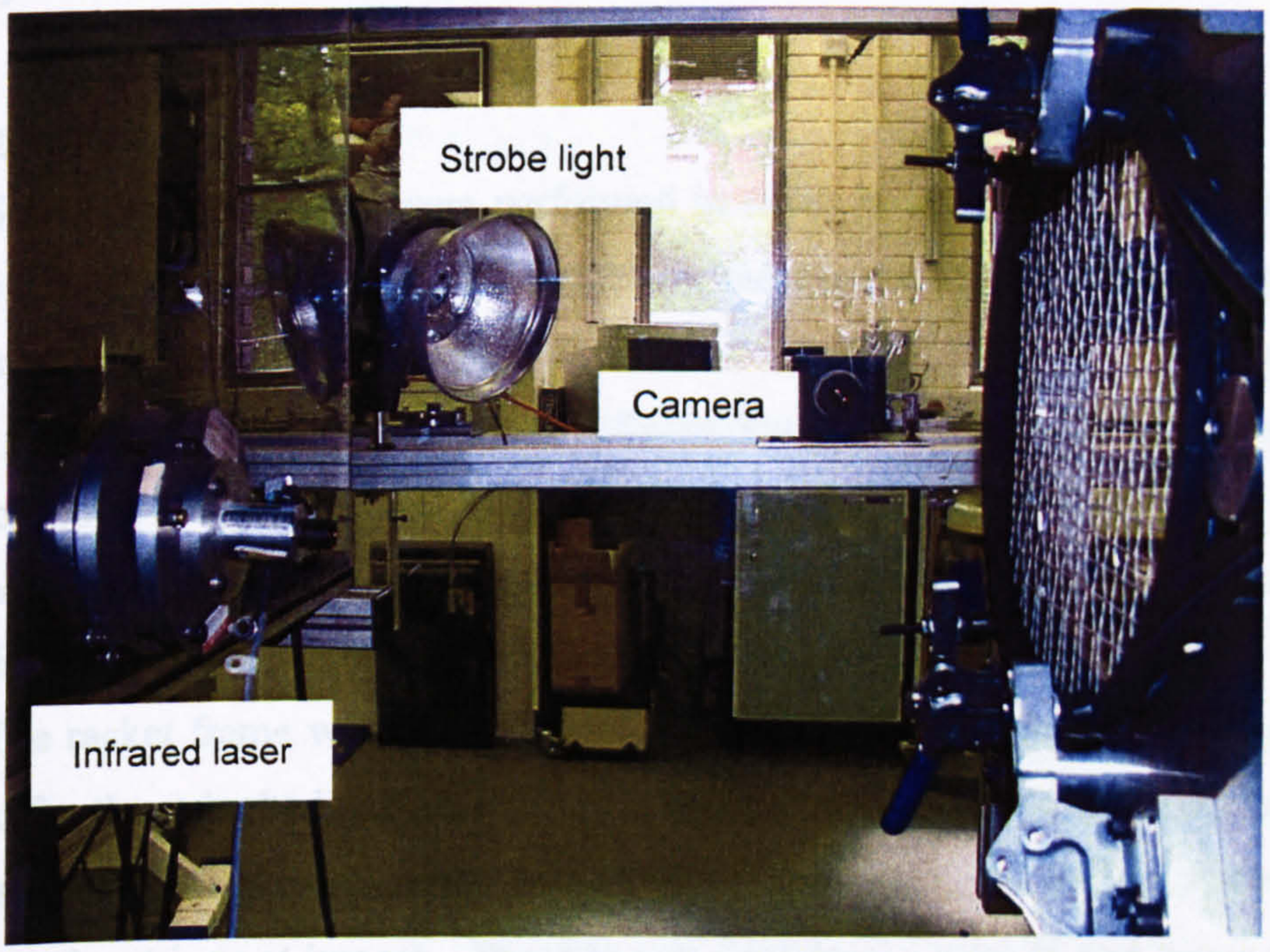

Figure 5.20. The impact chamber and Sensicam 2000 set-up

Experimental controls

To ensure the consistency of the experimentation and to optimise the accuracy of the results, a number of controls were necessary. The Pro Penn Titanium tennis balls were taken out of their pressurised tubes 24 hours prior to testing and left to acclimatise in the laboratory to minimise the effects of environmental conditions. The temperature in the laboratory was noted and found to be consistently around 21 degrees centigrade. The tennis balls were then placed in a ball clamp device and

compressed by approximately an inch in several directions by applying force using the lever handle. Further to these controls the ball masses, diameters and deformation characteristics were noted prior to ball cannon testing to achieve a level of consistency. Ball deformation was read from the scale of a Stevens Machine which allowed a known force to be applied to the ball placed between two plates. After each stringbed had been tested (approximately 30 impacts), the 3 balls used were discarded and an additional 3 balls were used for the next stringbed.

The BRDC was used to check that stringbed stiffness had not changed within an extended testing period. When a certain inbound ball velocity was required, the images were only taken forward to digitisation if the inbound velocity was within 0.5 m/s of the nominal velocity. The stringbed pattern was checked and repositioned if necessary to ensure consistent impact conditions.

Static deflection tests

Static deflection tests were performed in order to see if the results from the dynamic (COR) tests yielded sensible results for the amount of deflection of that point on the stringbed normal to the stringbed plane. For each of the four rackets, and for each six points of impact a series of five different loads (10.74 to 30.22 kg) were hung from each point (Figure 5.21A). Preliminary tests suggested that these loads would cover the range of deflection expected during a typical impact of the ball on the strings during a typical groundstroke in tennis (Brody et al., 2002).

The racket frame was secured to a rig using a series of clamps. The circular disc used for the stringbed stiffness test on a BRDC was used to hang the loads from. This was to simulate how an actual tennis ball would recruit and distribute the force throughout the strings at impact. The disc was 50 mm in diameter and it has shown using high-speed video data that an area of between 35 and 65 mm on the stringbed (depending on the inbound velocity) will be covered by the ball (Goodwill & Haake, 2000a). The BRDC disc was modified so that it had a flat surface on top. This enabled the needle of a Dial Test Indicator (DTI) to touch the surface (Figure 5.21B). As the stringbed depressed when more weight was added, the DTI could measure the amount of depression normal to the plane of the racket to an accuracy of ± 0.01 mm.

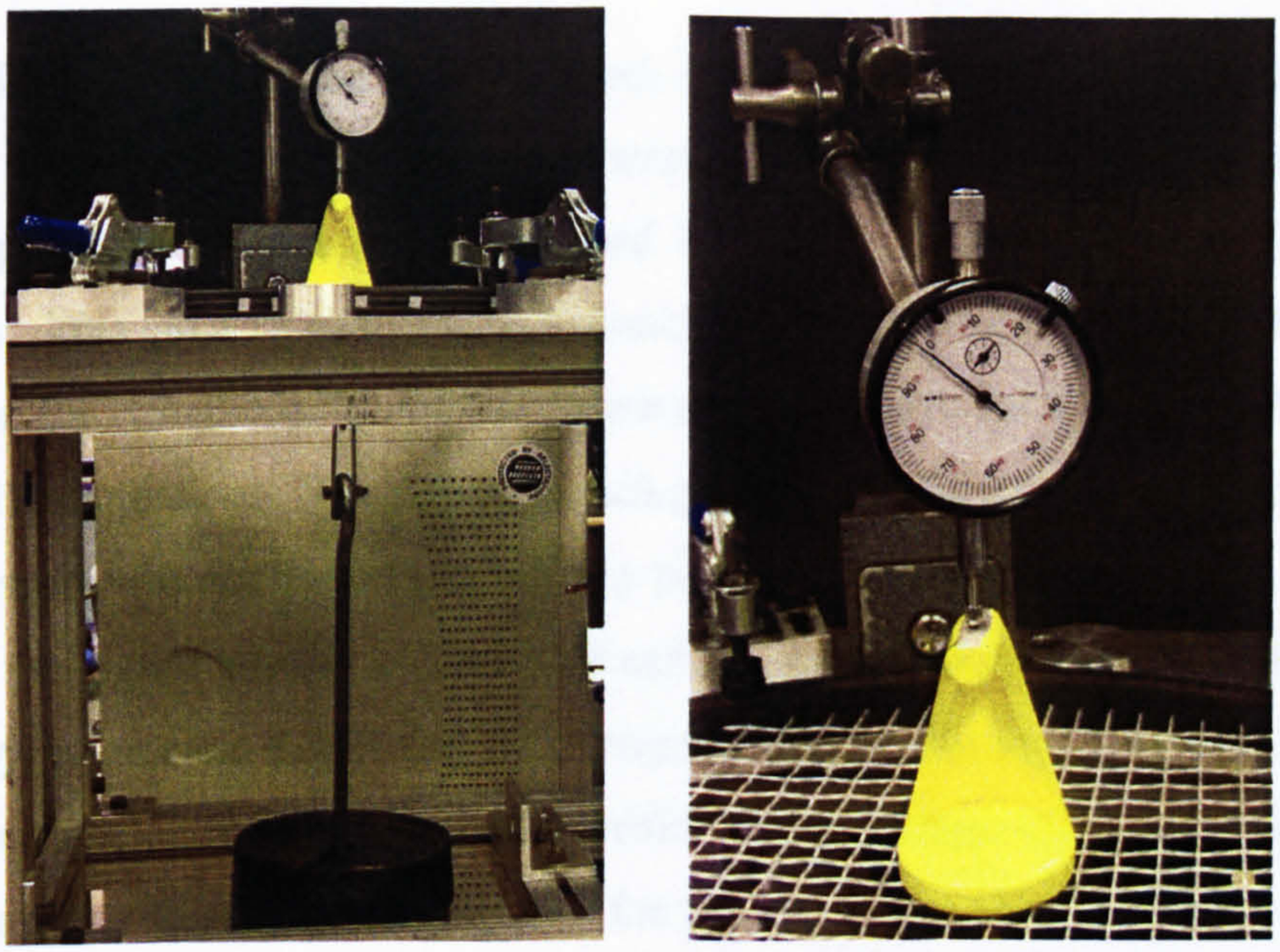

A B

Figure 5.21. Set-up for measuring the static deflection of points on the stringbed (A) and the digital gauge used to take the measurements (B)

Measurements were taken as more weights were added. Readings were also taken as the weights were unloaded to check for any hysteresis in the strings. The difference in the amount of deflection seen was considered negligible (0 - 0.02 mm) and could equally have been attributed to experimental error.

Optimisations

Two programmes were generated using Autolev to simulate a ball impacting normally onto a point on the stringbed and also a fixed load being hung from a point on the stringbed. The dynamic programme then became a subroutine of a separate optimisation routine. After establishing sensible starting values and bounds by running single simulations, the Simulated Annealing Algorithm (Corana et al., 1987) was used to systematically vary the 11 stringbed parameters (ST0,KS1:4,K5:10) until a best match was found between the experimental results and the simulation output (see Section 3.3.3 for an explanation of the stringbed parameters).

For the range of inbound ball velocities used (approximately 18 to 33 m/s) a linear relationship (R^2 greater than 0.86) was observed between the inbound ball velocity and the COR for each dynamic case. A strong linear relationship (R^2 greater than 0.99) was also found between the applied load and the amount of deflection

perpendicular to the stringbed plane for each static case. Using this information and to simplify the optimisation process, the lowest and highest velocities were used in the dynamic optimisations and the lowest and highest loads were used in the static simulations. This gave 12 simulations to match in each case (2 velocities and 6 points of impact on the stringbed). The score function was the average percentage difference across the 12 simulations. The scores at each point were also monitored to ensure that the overall score was not biased towards any point or points in particular.

For the higher tension LM Prestige and LM 8 models, optimisations were then run whereby parameters KS1:4 and K5:10 remained the same as the optimised values for the lower tension racket. The initial tension in the springs, ST0, was then varied. The intention was to see if changing ST0 for a particular racket stringbed could then accurately model the behaviour of the same stringbed with a higher initial tension.

Once parameters had been established which yielded a close match to the COR values determined experimentally, it was desirable to know if the same parameters would yield sensible results in terms of the amount of deflection of the point on the stringbed in a direction perpendicular to the stringbed plane. The optimised values from the dynamic simulations were input to the static model and a single simulation was run. The score function was again the average percentage difference across the 12 simulations. A comparison was then made between the scores when all 11 parameters had been optimised using the dynamic model and when only ST0 had been optimised in the case of the higher tension rackets.

5.6.3 Results

Ball cannon tests

Figure 5.22 shows how the mean COR varied for different rackets at a certain point of impact on the stringbed. A linear function was fitted through the data points and the coefficients of determination (R^2) values were noted. Based on these results, the highest and lowest inbound ball velocities were used in the optimisation process. Tables 5.12 to 5.15 show the mean COR results for each racket type at low and high string tensions. Each table presents the results for the 6 points of impact at a low and high inbound ball velocity. The number in brackets is the standard deviation for the 5 trials at each data point.

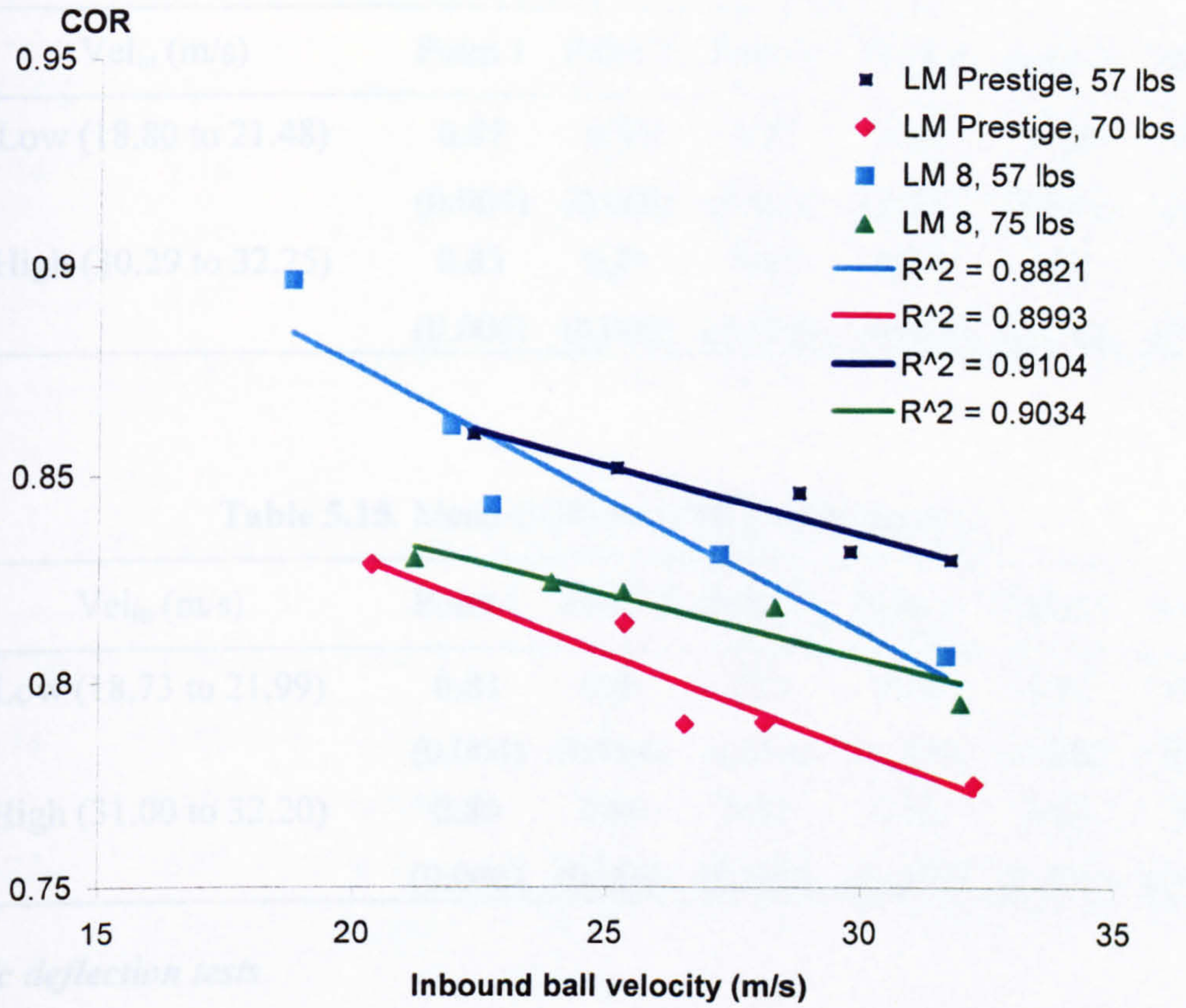

Figure 5.22. Variation in mean COR for different rackets over a range of inbound ball velocities at point 2 on the stringbed

Table 5.12. Mean COR for LM Prestige (57 lbs tension)

Vel_{in} (m/s)	Point 1	Point 2	Point 3	Point 4	Point 5	Point 6
Low (21.26 to 22.36)	0.84	0.86	0.81	0.80	0.83	0.79
	(0.006)	(0.006)	(0.004)	(0.002)	(0.006)	(0.004)
High (30.85 to 33.13)	0.78	0.83	0.81	0.74	0.77	0.75
	(0.004)	(0.004)	(0.004)	(0.002)	(0.006)	(0.004)

Table 5.13. Mean COR for LM Prestige (70 lbs tension)

Vel_{in} (m/s)	Point 1	Point 2	Point 3	Point 4	Point 5	Point 6
Low (19.90 to 20.89)	0.80	0.83	0.80	0.77	0.80	0.77
	(0.002)	(0.004)	(0.006)	(0.002)	(0.002)	(0.004)
High (30.02 to 33.13)	0.76	0.78	0.76	0.74	0.76	0.73
	(0.004)	(0.002)	(0.004)	(0.002)	(0.004)	(0.004)

Table 5.14. Mean COR for LM8 (57 lbs tension)

Vel_{in} (m/s)	Point 1	Point 2	Point 3	Point 4	Point 5	Point 6
Low (18.80 to 21.48)	0.85	0.90	0.87	0.83	0.86	0.86
	(0.004)	(0.002)	(0.004)	(0.002)	(0.004)	(0.004)
High (30.29 to 32.25)	0.83	0.81	0.83	0.74	0.83	0.78
	(0.006)	(0.004)	(0.004)	(0.002)	(0.004)	(0.004)

Table 5.15. Mean COR for LM8 (75 lbs tension)

Vel_{in} (m/s)	Point 1	Point 2	Point 3	Point 4	Point 5	Point 6
Low (18.73 to 21.99)	0.81	0.83	0.81	0.77	0.82	0.77
	(0.004)	(0.004)	(0.004)	(0.002)	(0.006)	(0.004)
High (31.00 to 32.20)	0.80	0.80	0.81	0.73	0.80	0.73
	(0.006)	(0.004)	(0.002)	(0.002)	(0.004)	(0.004)

Static deflection tests

Figure 5.23 shows the deflection normal to the stringbed plane at the 6 points of impact for a particular racket. Tables 5.16 to 5.19 show the deflection at the lowest and highest applied loads at each point on the stringbed and for each racket type. The number in brackets refers to the difference in deflection recording when the weight was loaded and then unloaded.

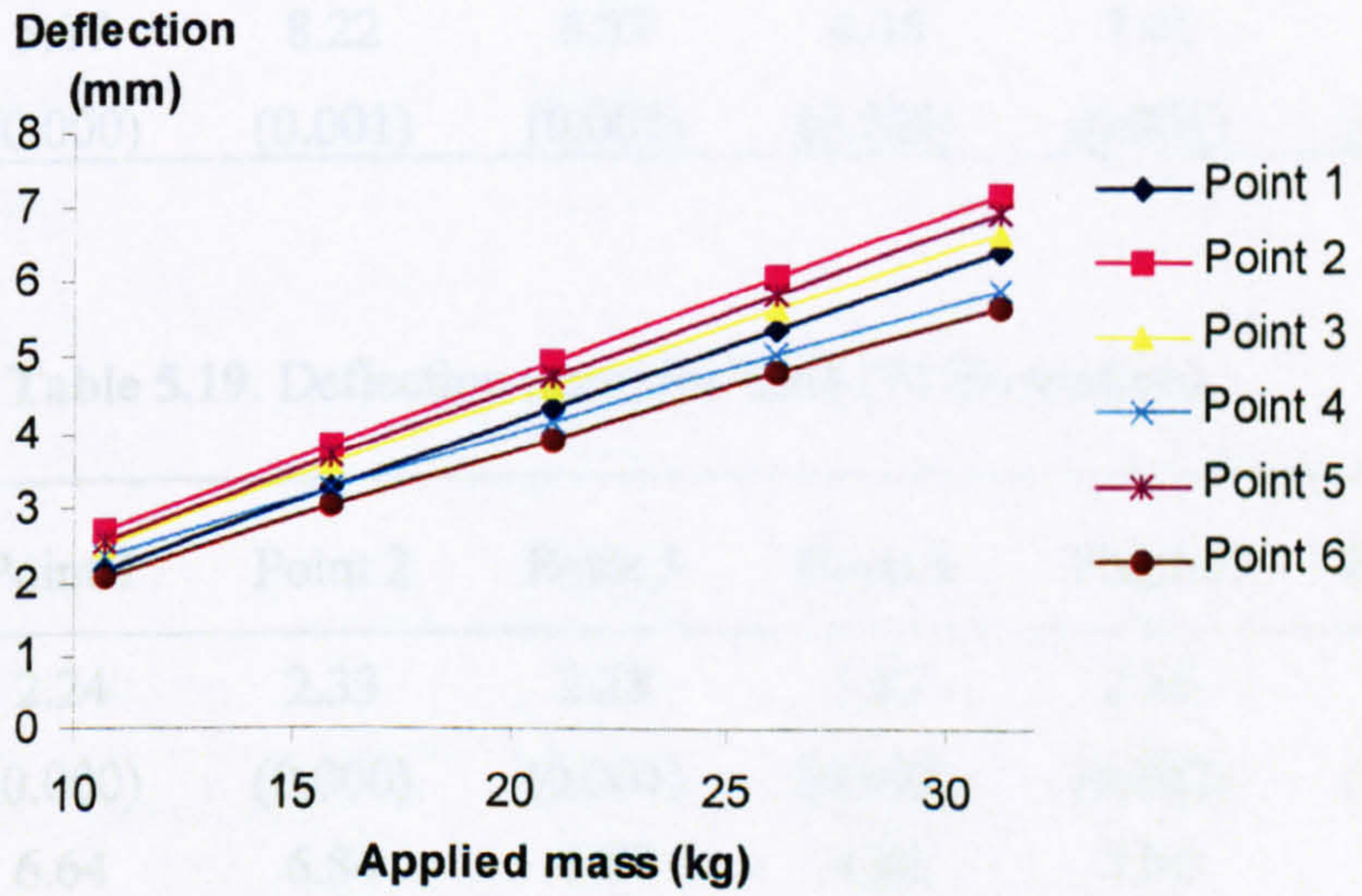

Figure 5.23. Variation in deflection normal to the stringbed at different points on the stringbed for the LM Prestige (57lbs tension)

Table 5.16. Deflection (mm) for LM Prestige (57 lbs tension)

Mass (kg)	Point 1	Point 2	Point 3	Point 4	Point 5	Point 6
10.74	2.16	2.69	2.53	2.35	2.55	2.10
	(0.001)	(0.000)	(0.001)	(0.001)	(0.002)	(0.001)
31.22	6.40	7.16	6.65	5.89	6.91	5.65
	(0.000)	(0.001)	(0.001)	(0.001)	(0.002)	(0.002)

Table 5.17. Deflection (mm) for LM Prestige (70lbs tension)

Mass (kg)	Point 1	Point 2	Point 3	Point 4	Point 5	Point 6
10.74	1.80	2.10	2.00	1.64	1.82	1.59
	(0.001)	(0.000)	(0.001)	(0.001)	(0.002)	(0.001)
31.22	6.02	6.21	5.90	4.69	5.60	4.44
	(0.001)	(0.000)	(0.001)	(0.002)	(0.002)	(0.002)

Table 5.18. Deflection (mm) for LM8 (57lbs tension)

Mass (kg)	Point 1	Point 2	Point 3	Point 4	Point 5	Point 6
10.74	2.09	2.93	2.54	1.56	2.72	2.56
	(0.000)	(0.000)	(0.001)	(0.001)	(0.002)	(0.001)
31.22	5.87	8.22	6.37	4.38	7.05	5.54
	(0.000)	(0.001)	(0.001)	(0.001)	(0.001)	(0.001)

Table 5.19. Deflection (mm) for LM8 (75 lbs tension)

Mass (kg)	Point 1	Point 2	Point 3	Point 4	Point 5	Point 6
10.74	2.24	2.33	2.28	1.87	2.16	1.97
	(0.000)	(0.000)	(0.001)	(0.001)	(0.002)	(0.001)
31.22	6.64	6.84	6.57	4.86	5.96	5.16
	(0.000)	(0.001)	(0.001)	(0.001)	(0.002)	(0.002)

Optimisations

Table 5.20 summarises the results from the optimisations. Initially the values when all 11 parameters were optimised for a particular racket and string tension are presented. The results for the two rackets with high initial string tension when only ST0 was varied (stiffness values from the lower tension racket) are then shown. Table 5.21 shows how well these optimised parameters matched the amount of deflection normal to the stringbed plane for an applied load. The score in each case was the average percentage difference between the experimental and simulation output across the 12 trials.

Table 5.20. Stringbed parameters optimised from dynamic results

Parameter	LM Prestige (57 lbs)	LM Prestige (70 lbs)	LM 8 (57 lbs)	LM 8 (75 lbs)
KS1 (N/m x 10^5)	1.77	9.44	1.02	0.98
KS2 (N/m x 10^5)	2.00	1.38	1.03	1.16
KS3 (N/m x 10^5)	5.97	6.82	1.20	4.25
KS4 (N/m x 10^5)	7.91	4.30	1.13	7.13
K5	0.53	0.69	0.44	0.45
K6	0.77	1.90	0.38	0.34
K7	1.00	3.03	0.95	0.69
K8	0.83	0.51	0.32	0.57
K9	0.74	0.88	0.40	1.03
K10	1.40	0.43	1.58	1.04
ST0 (N)	648.2	821.3	735.8	1067.7
SCORE (%)	0.84	1.09	2.13	1.19
standard deviation	0.11	0.13	0.15	1.00
ST0 (only ST0 varied) (%)	-	772.9	-	967.7
SCORE (only ST0 varied) (%)		1.5		1.4

Table 5.21. Score when the parameters from the dynamic optimisation are input to the static model

	LM Prestige (57 lbs)	LM Prestige (70 lbs)	LM 8 (57 lbs)	LM 8 (75 lbs)
11 parameters optimised (%)	6.5	10.7	6.0	9.1
Only ST0 optimised (%)	-	8.0	-	8.7

Table 5.20 shows that the optimisation routine could vary the 11 parameters and achieve values resulting in less than an average of 2.2% difference between the experimental results and simulation output. The standard deviation of the 12 simulations for each stringbed is also small indicating that the parameters are not biased towards certain impact conditions. When ST0 only was varied in the case of the higher tension rackets, an increase in the score of less than 0.5% was found.

When single simulations were run using the static model to observe the amount of deflection of the point on the stringbed, scores of between 6 and 11% were obtained (Table 5.21). In the case of the higher tension rackets, the score when the static model was run with eleven parameters that had been optimised was higher than that when only ST0 had been varied and the stiffness values were the same as for the lower tension racket of that type. This strengthens the argument that to model the same tennis racket with a different string tension, only ST0 needs perturbing.

5.7 CHAPTER SUMMARY

This chapter describes the methods that have been used to determine the parameters for the racket frame, tennis ball and stringbed. Where possible parameters have been determined directly from experiments. Alternatively, experimental results have been input to optimisation routines to determine parameters by a matching optimisation process. In Chapter 6, these parameters have been inputted to the computer model of one-handed backhand groundstrokes and simulations have been run to determine the effects of perturbing selected parameters.

CHAPTER 6

MODEL EVALUATION AND RESULTS

6.1 CHAPTER OVERVIEW

Before the simulation model could be used with confidence, it was necessary to show how simulations compared with the subject's performances. This chapter describes how the simulation model was evaluated based on differences in the racket kinematics, ball-stringbed contact time and outbound ball velocity between performances and matching simulations. Comparisons of racket frame acceleration, grip force and net torques around the wrist and elbow joints for matched trials are also presented. Results from simulations using the model are then shown. Initially, direct comparisons were made between matching simulations. A sensitivity analysis was then performed as simulation parameters were perturbed for two matched trials.

6.2 MODEL EVALUATION

6.2.1 Overview of model evaluation

In addition to comparing the displacements of the racket handle relative to the hand, comparisons of ball-stringbed contact time and outbound ball velocity for the performance and matching simulation were made. Whilst not used directly in the simulation score since not all trials had the same racket instrumentation, comparisons of racket frame accelerations and net torques about perpendicular axes through the centre of the racket handle were made for matched trials. The net joint torques around the wrist and elbow joints predicted by the simulation model were then compared to the theoretical maximum voluntary torques achievable, determined from strength tests on the subject.

6.2.2 Simulation score

A score function based on the kinematics of the racket relative to the hand was developed to optimise the grip parameters for the matching trials (Section 4.5.2). All trials resulted in an average root-mean-squared (RMS) percentage difference score

between simulation and performance of less than 1%. To give an overall score for a simulation, the ball-stringbed contact time and the outbound ball velocities were also compared. An objective score S_{MOD} (Figure 6.1) was calculated as the average RMS percentage difference between a simulation and a performance for the aforementioned variables.

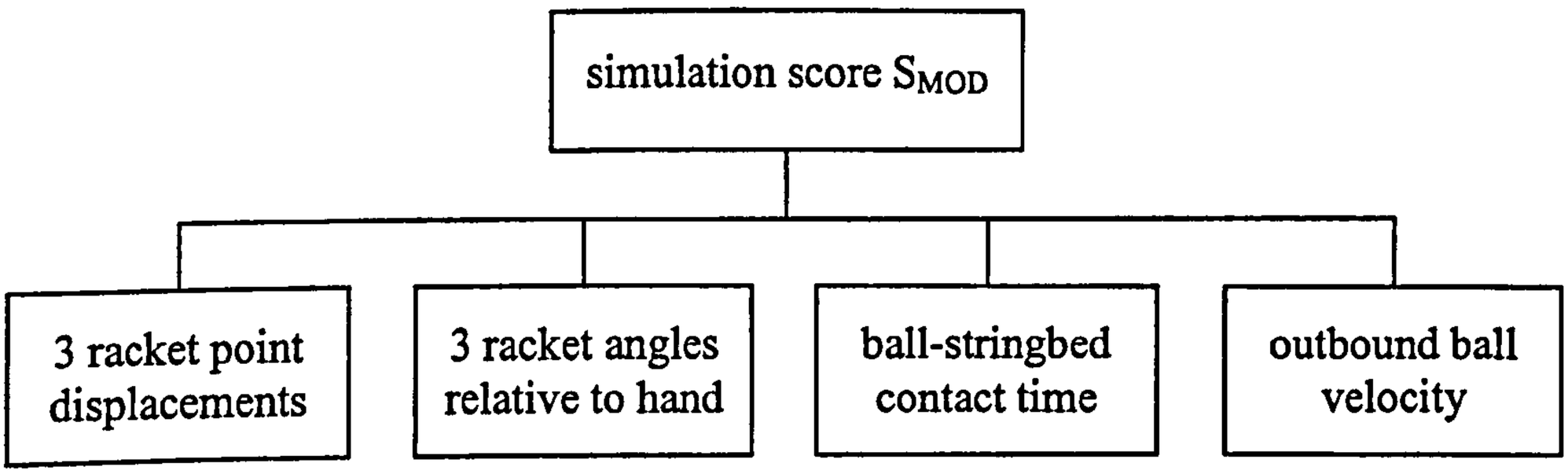

Figure 6.1. Summary of the components of the simulation score S_{MOD}

For the displacement of the racket relative to the hand, comparisons were made from the time of ball impact and every ms thereafter for 50 ms (Section 4.5.2). Since S_{MOD} consisted of variables with different units, a 1 deg difference in racket angle and a 1 cm difference in racket point displacement were assumed to be equivalent to a 1% difference in the other variables. Each of the 3 racket point and 3 racket angle displacements were given a weighting of 1/9 whilst the ball contact time and outbound velocity were given weightings of 1/6 each. The combined racket point displacements, the combined racket angles and the combined ball-stringbed contact time and outbound ball velocity therefore had a weighting of 1/3 each.

Table 6.1. Simulation results and model evaluation score S_{MOD}

Trial	Resultant ball velocity (m/s)		Ball-stringbed contact time (ms)		S_{MOD}
number	Performance	Simulation	Performance	Simulation	(%)
1	34.13	33.92	4.2	4.2	0.81
8	26.26	27.30	3.8	3.7	1.09
24	30.13	34.13	4.0	4.0	2.62
31	33.33	33.24	4.0	4.1	0.63
36	31.55	29.19	4.0	4.0	1.67
56	27.89	28.16	4.0	4.0	0.66

6.2.3 Comparison of racket frame accelerations

Racket frame accelerations were measured using uni-axial accelerometers mounted on an aluminium bracket attached to the racket frame (Section 4.2.2) and then compared to the matched simulation output. Racket frame accelerations out of the plane of the racket and in the plane of the racket were plotted every 0.5 ms from ball impact until 50 ms afterwards (Figure 6.2). Since the measured acceleration was from a trial where the ball hit the stringbed close to its geometric centre, the two accelerometers measuring out of plane accelerations showed very similar traces and therefore only one has been plotted.

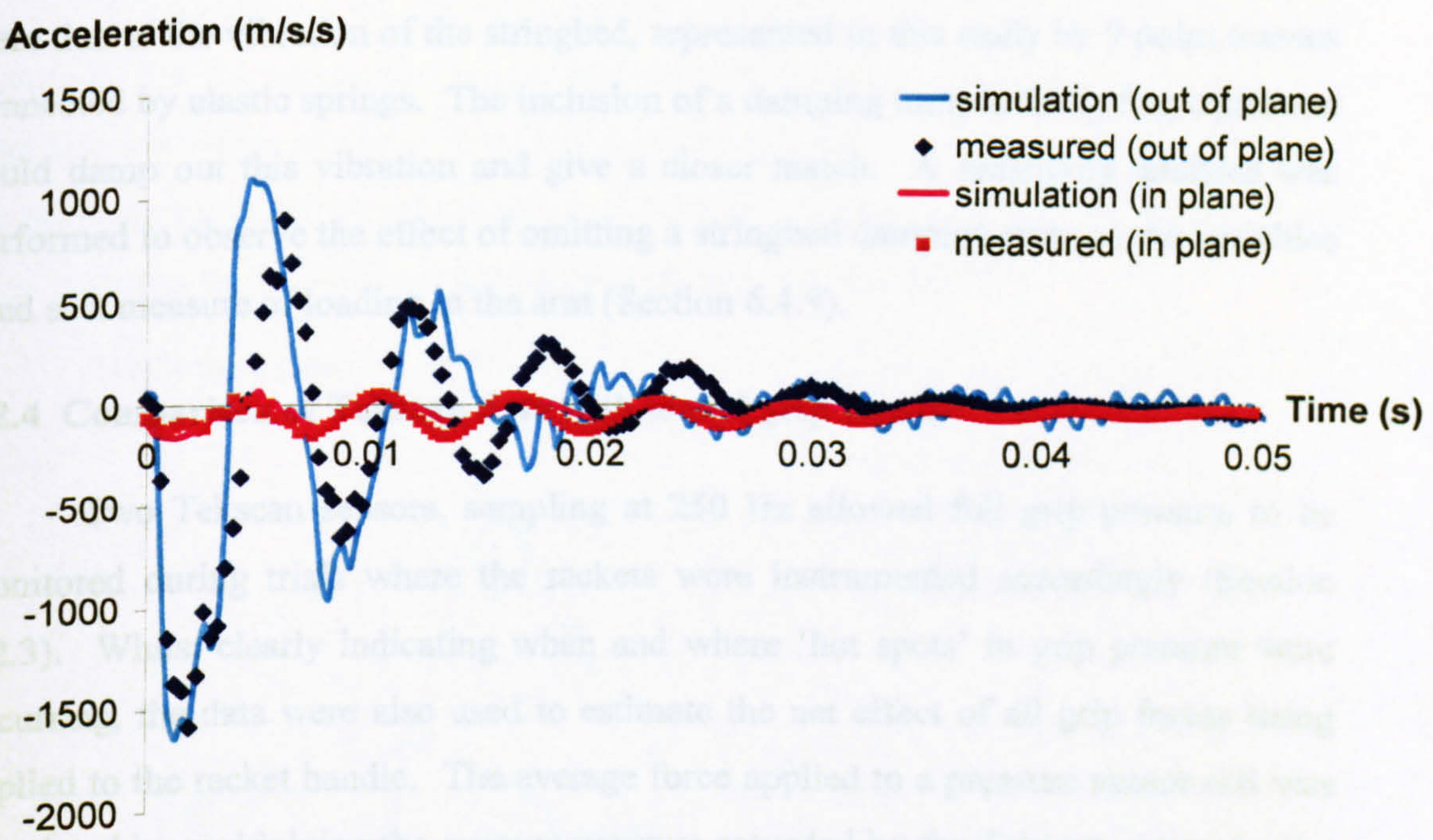

Figure 6.2. Comparison of measured and simulation racket frame accelerations

Figure 6.2 illustrates that in terms of acceleration amplitude and rate of decay, the simulation model compared well with measured acceleration for both the in plane and out of plane cases. Overall the comparisons are good with RMS difference scores, expressed as a percentage of maximum measured acceleration, of 10.2 and 12.1% for the in and out of plane cases respectively. The frequencies of oscillation matched well initially although at around 15 ms after ball impact, the simulation acceleration lagged slightly behind that of the measured acceleration. Whilst the selection of appropriate frame stiffness and damping coefficients resulted in good agreement between simulation racket frame accelerations and those measured from

simple impact hammer tests (Section 5.4.2), it would appear that the inclusion of a ball-stringbed system and a hand gripping the handle also influence the model acceleration value. This match could have been improved by including non-constant visco-elastic parameters for the grip, but this was deemed an unnecessary level of complexity for this study.

The simulation and measured in plane acceleration traces were appreciably smaller in amplitude than for the out of plane cases since the ball impacted almost perpendicular to the plane of the stringbed. Whilst not present for motion in the plane of the racket, high frequency components of racket frame acceleration out of the plane of the racket were predicted by the simulation model in the order of 600 Hz. These were due to the vibration of the stringbed, represented in this study by 9 point masses connected by elastic springs. The inclusion of a damping term in the spring equations could damp out this vibration and give a closer match. A sensitivity analysis was performed to observe the effect of omitting a stringbed damping term on the variables used as a measure of loading in the arm (Section 6.4.9).

6.2.4 Comparison of Tekscan data with model grip forces

Two Tekscan sensors, sampling at 250 Hz allowed full grip pressure to be monitored during trials where the rackets were instrumented accordingly (Section 4.2.3). Whilst clearly indicating when and where 'hot spots' in grip pressure were occurring, the data were also used to estimate the net effect of all grip forces being applied to the racket handle. The average force applied to a pressure sensor cell was calculated by multiplying the average pressure recorded by the Tekscan sensor by the area of the cell (0.25 square inches). The moments of force about axes x and y through the centre of the grip (Figure 6.3B) were then calculated by multiplying the corresponding resultant forces by the distance (d) to the centre of the grip for each cross-section (Figure 6.3A). The net torques Tx and Ty about the x and y axes respectively were equal to the sum of the individual moments. The net torques about the z axis (Tz) measured from performances were due to the couple of the forces from opposite flats of the handle where the lines of action of the forces did not always pass through the centre of the octagon since flats were of different lengths.

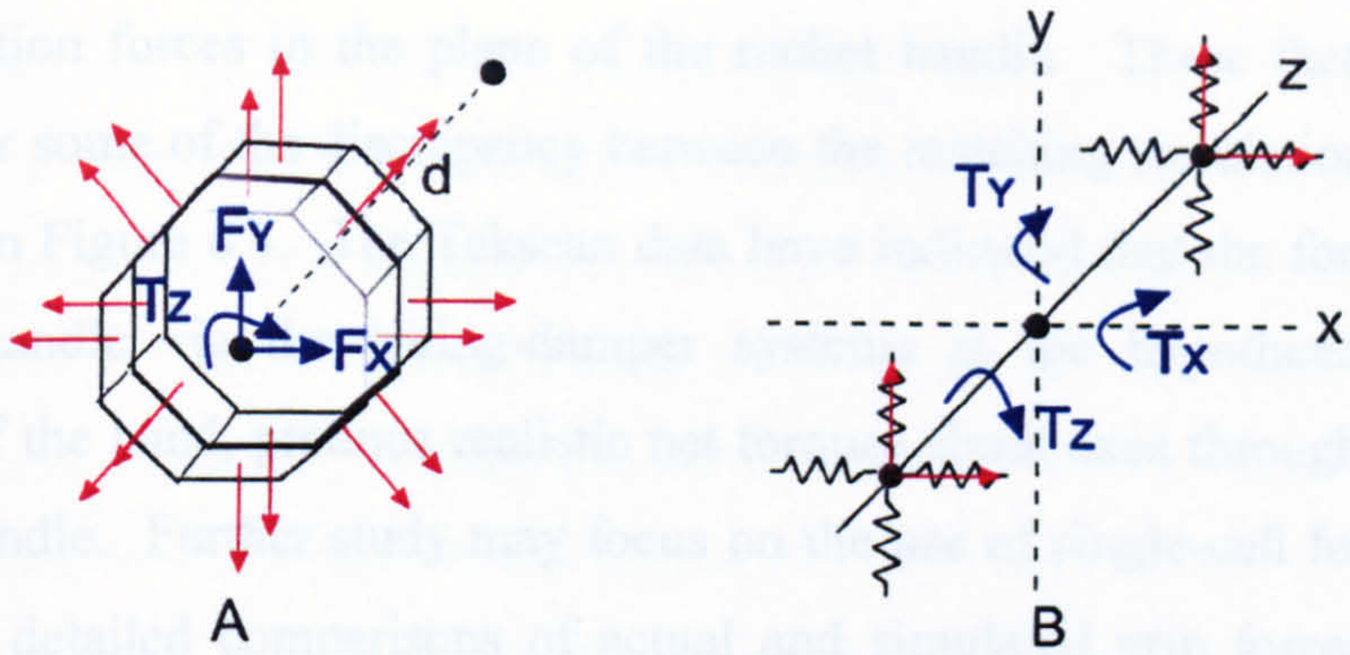

Figure 6.3. A cross-section through the octagonal racket handle (A) and the resultant forces and net torques for the simulation grip model (B)

A comparison of the net torques calculated from Tekscan data and those predicted by the simulation model was performed for a matched trial (Figure 6.4). Net torques were calculated from ball impact and every 4 ms until 50 ms afterwards about three mutually perpendicular axes through the centre of the racket handle, half way between the hypothenar and thenar eminences of the hand.

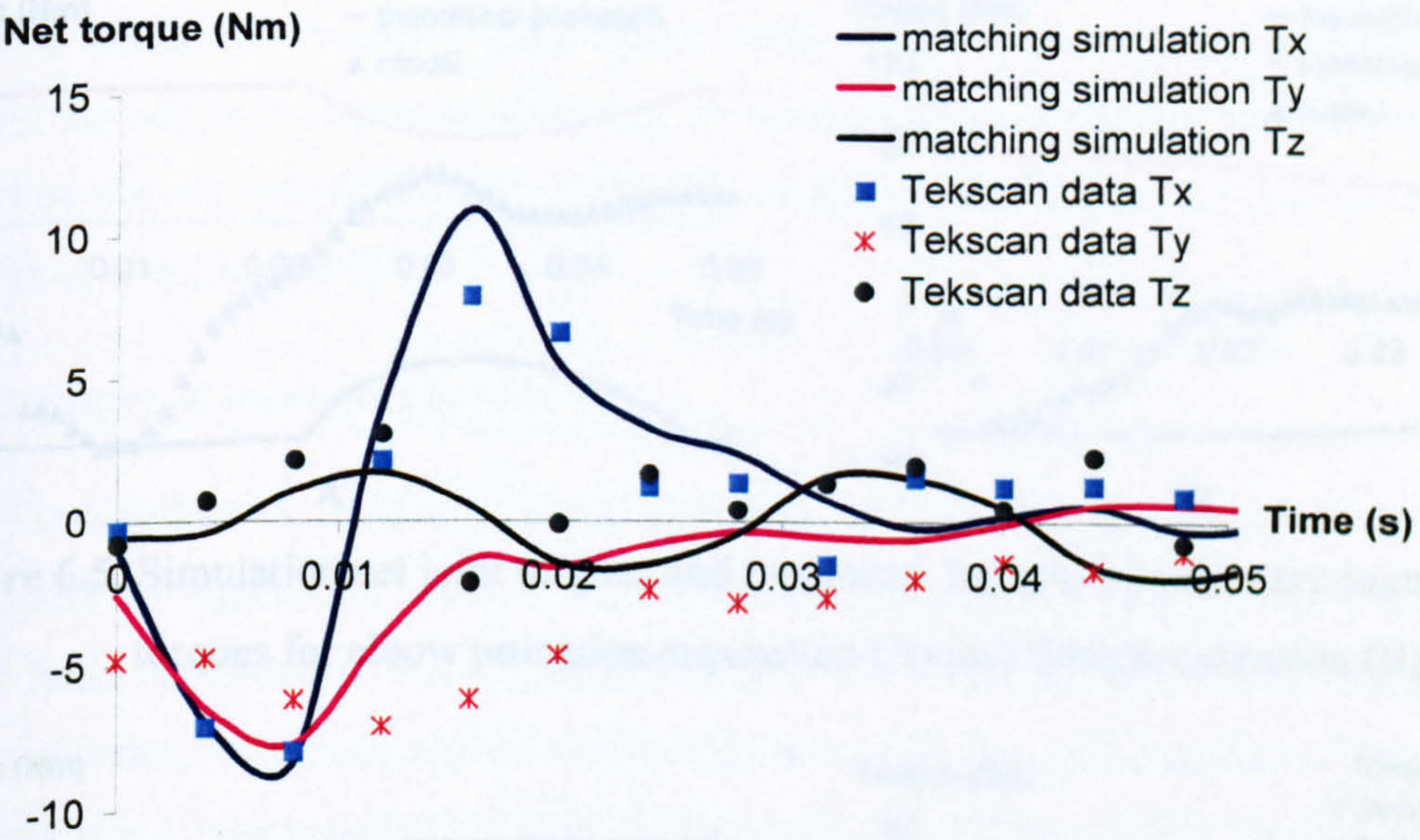

Figure 6.4. A comparison of the net torques about the centre of the handle from Tekscan data and the simulation model for a matched trial

Figure 6.4 suggests that in terms of the net torques about axes through the centre of the racket handle, the simulation model produces magnitudes comparable to those calculated from experimental Tekscan data. Limitations of using the Tekscan system in this study were the low sampling frequency of 250 Hz and the inability to

measure friction forces in the plane of the racket handle. These factors may have accounted for some of the discrepancy between the matching simulation and Tekscan data shown in Figure 6.4. The Tekscan data have indicated that the forces applied to the racket handle via the spring-damper systems at the hypothenar and thenar eminences of the hand, produce realistic net torques about axes through the centre of the racket handle. Further study may focus on the use of single-cell force sensors to enable more detailed comparisons of actual and simulated grip forces during one-handed backhand groundstrokes.

6.2.5 Comparison of joint torques

For the movements of most interest at the wrist and elbow joints, the net joint torques calculated for a matching simulation were compared with the theoretical maximum voluntary torques for a particular joint movement, determined from strength tests on the subject (Section 4.6.2). Initial ball impact is at time zero.

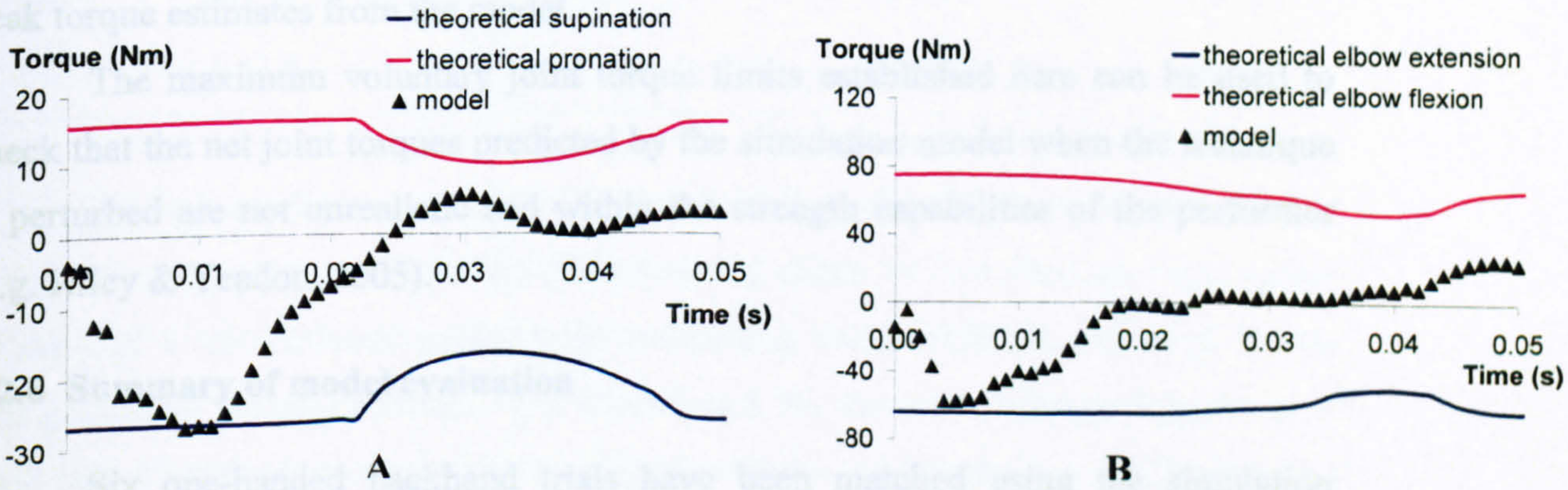

Figure 6.5. Simulation net joint torques and maximum theoretical voluntary joint torques for elbow pronation-supination (A) and flexion-extension (B)

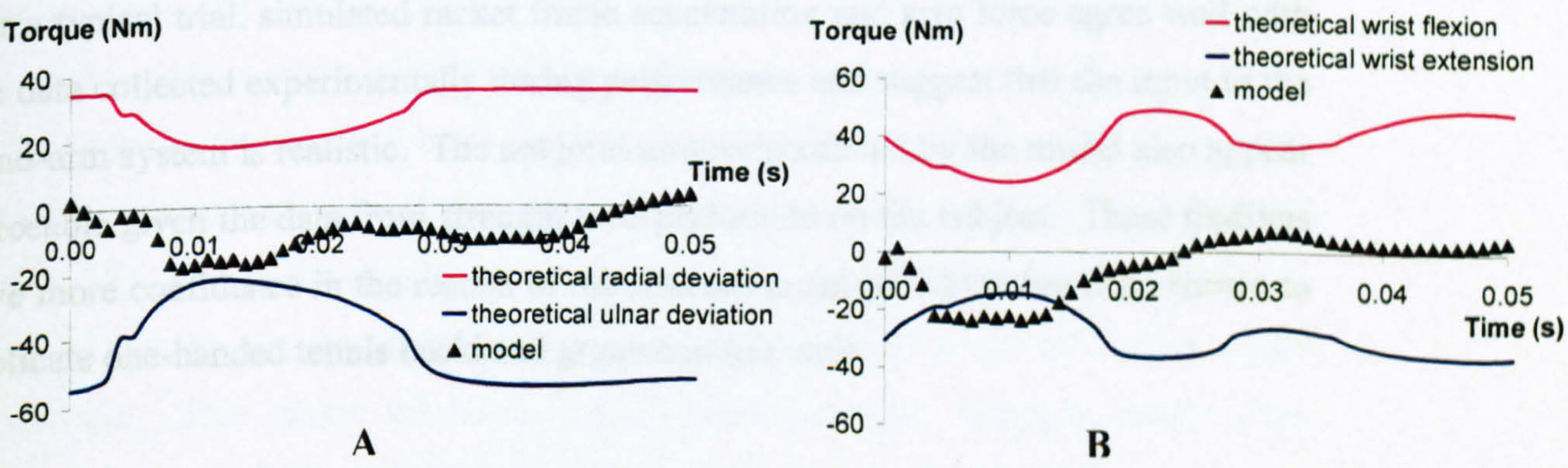

Figure 6.6. Simulation net joint torques and maximum theoretical voluntary joint torques for wrist radial-ulnar deviation (A) and flexion-extension (B)

For each of the movements presented, net joint torque ramps up to its maximum value approximately 7 ms after ball impact and then decreases in a similar fashion from this point. This suggests that the muscles are working almost maximally for a short period of time to maintain control of the racket after ball impact. Running a simulation from 10 ms before impact to the point of ball impact confirmed that net joint torques were low just prior to ball impact and were not artefacts of initialisation of the simulation model. With the exception of small maximum voluntary joint torque violations for elbow supination (Figure 6.5A) and wrist extension (Figure 6.6B), the net joint torques predicted by the model would appear to be well within the capabilities of the subject. The likely explanation for the violations is that the subject was not sufficiently familiarised with the isovelocity dynamometer and therefore unable to produce maximum torques, especially for high velocity trials (Kong, 2005). Additionally, the effect of the muscle-tendon complex and errors in the angular acceleration values obtained from the motion analysis may also have influenced the peak torque estimates from the model.

The maximum voluntary joint torque limits established here can be used to check that the net joint torques predicted by the simulation model when the technique is perturbed are not unrealistic and within the strength capabilities of the performer (e.g. Hiley & Yeadon, 2005).

6.2.6 Summary of model evaluation

Six one-handed backhand trials have been matched using the simulation model. Excellent agreement has been found between performance and simulations in terms of racket kinematics, ball-stringbed contact time and outbound ball velocity. For a typical trial, simulated racket frame acceleration and grip force agree well with the data collected experimentally during performance and suggest that the input to the hand-arm system is realistic. The net joint torques predicted by the model also appear agreeable given the data from strength tests performed on the subject. These findings give more confidence in the results of the simulation model which has been shown to replicate one-handed tennis backhand groundstrokes well.

6.3 SIMULATION RESULTS

6.3.1 Overview of simulation results

Six trials from the performance data collection (Section 4.2.6) were selected for further analysis (Table 6.2).

Table 6.2. Summary of the six trials chosen for further analysis

Trial	Racket model	String tension (lbs)	Ball impact location	Groundstroke
1	LM Prestige	57	Centre	Topspin
8	LM 8	57	Off centre	Topspin
24	LM 8	57	Centre	Topspin
31	LM Prestige	70	Centre	Topspin
36	LM 8	75	Centre	Topspin
56	LM 8	75	Centre	Slice

Trials 8 and 24 were used to compare the effect of ball impact location. Trials 1 and 36 were used to compare the effect of using either the LM Prestige 'tour' racket or the LM 8 'recreational' racket with contrasting frame stiffness, damping, inertia and geometric frame properties. For trials 1 and 36, the initial stringbed tensions of each racket resulted in comparable stringbed stiffness values (Section 5.2.2) allowing a direct comparison of the contrasting racket frame parameters to be performed. Trials 36 and 56 were used to compare the effect of performing a slice as oppose to topspin drive one-handed backhand groundstroke. Trials 1 and 31 were used to examine the effect of the initial stringbed tension on loading at the elbow.

For the six matched trials used in this analysis the relative ball-racket linear velocities and the racket angles relative to global x, y and z axes were calculated (Table 6.3). Due to the consistent kinematics of the subject and inbound ball velocity from the ball cannon, the pairs of trials used for direct comparisons had similar impact conditions. This meant that comparisons could be made between certain trials without the results being greatly influenced by the initial impact conditions.

Table 6.3. Comparison of global relative ball-racket linear velocities and racket angles at impact

Trial number	Linear relative ball-racket velocities (m/s)			Racket angles (deg)		
	x	y	z	x	y	z
1	-0.15	32.16	2.03	-199.5	0.2	-101.4
8	-2.32	30.45	3.90	-187.1	-24.9	-100.2
24	-1.69	31.27	5.15	-201.0	-1.1	-99.0
31	-2.65	32.67	3.74	-213.3	-2.3	-95.3
36	-0.52	30.96	3.21	-202.7	-9.4	-89.8
56	4.07	28.63	-9.11	-188.0	-15.5	-91.1

6.3.2 Loading at the elbow

The loading at the elbow joint is a combination of the internal forces and torques due to the muscles generating the joint motion and external forces and torques applied to the system through the ground and tennis racket (Elliott, 2006). Whilst the model developed cannot predict the loading within the muscle tendons where micro-tears may occur, the net joint torques, internal joint forces and forces within the wobbling mass springs can be used as representative measures. For the following trial comparisons, maximum flexion-extension (MFET) and maximum pronation-supination (MPST) net torques, maximum resultant internal joint forces (MIJF) and maximum force in the forearm wobbling mass spring-damper (MWMF) at the elbow were noted. Each variable was calculated every 0.5 ms from ball impact until 50 ms afterwards. Figure 6.7 shows Matlab stick figures for a typical one-handed topspin drive backhand groundstroke, looking from directly above the performer.

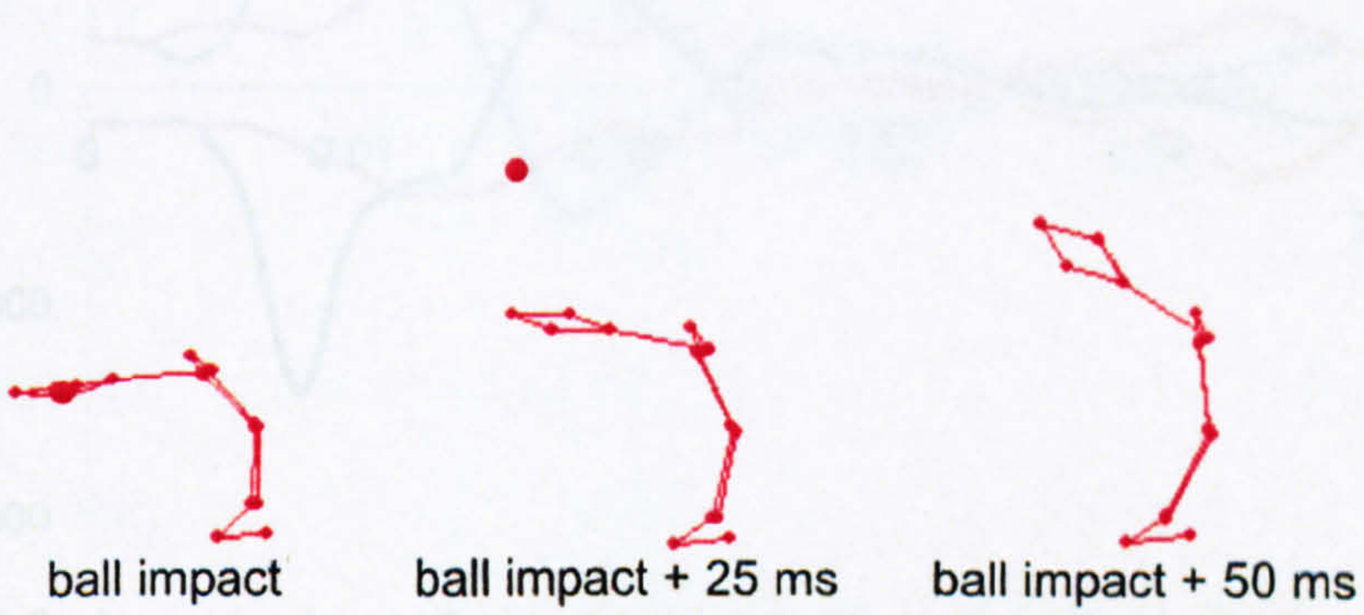

Figure 6.7. Matlab stick figure representations of a typical one-handed topspin drive backhand groundstroke from ball impact until 50 ms afterwards

6.3.3 Impact location: trial 8 versus trial 24

The loading at the elbow joint for trials 8 (off-centre) and 24 (centre) was collated by running single simulations using the model (Table 6.4).

Table 6.4. A comparison of peak loading at the elbow for trials 8 and 24

Trial	MFET (Nm)	MPST (Nm)	MIJF (N)	MWMF (N)
8 (off-centre)	-80.2	-39.0	212.6	-88.9
24 (centre)	-74.1	-35.8	180.0	-75.4

For each variable used to represent elbow loading as described in Section 6.3.2, the values were higher for trial 8 where the ball impacted away from the geometric stringbed centre (GSC). The greatest increases in loading were observed in MIJF and MWMF as both increased by 18%. The difference in the wrist joint flexion-extension angles was commented on in Section 4.2.2 with the wrist being forced approximately 8 deg more into flexion after ball impact for trial 8. In terms of the model kinetics, perhaps the most noticeable difference between the trials was the magnitude and timing of the peak grip forces. Figure 6.8 shows the net forces due to the spring-damper systems at the hypothenar and thenar eminences of the hand in a direction approximately equal to that of the inbound ball at impact with the stringbed.

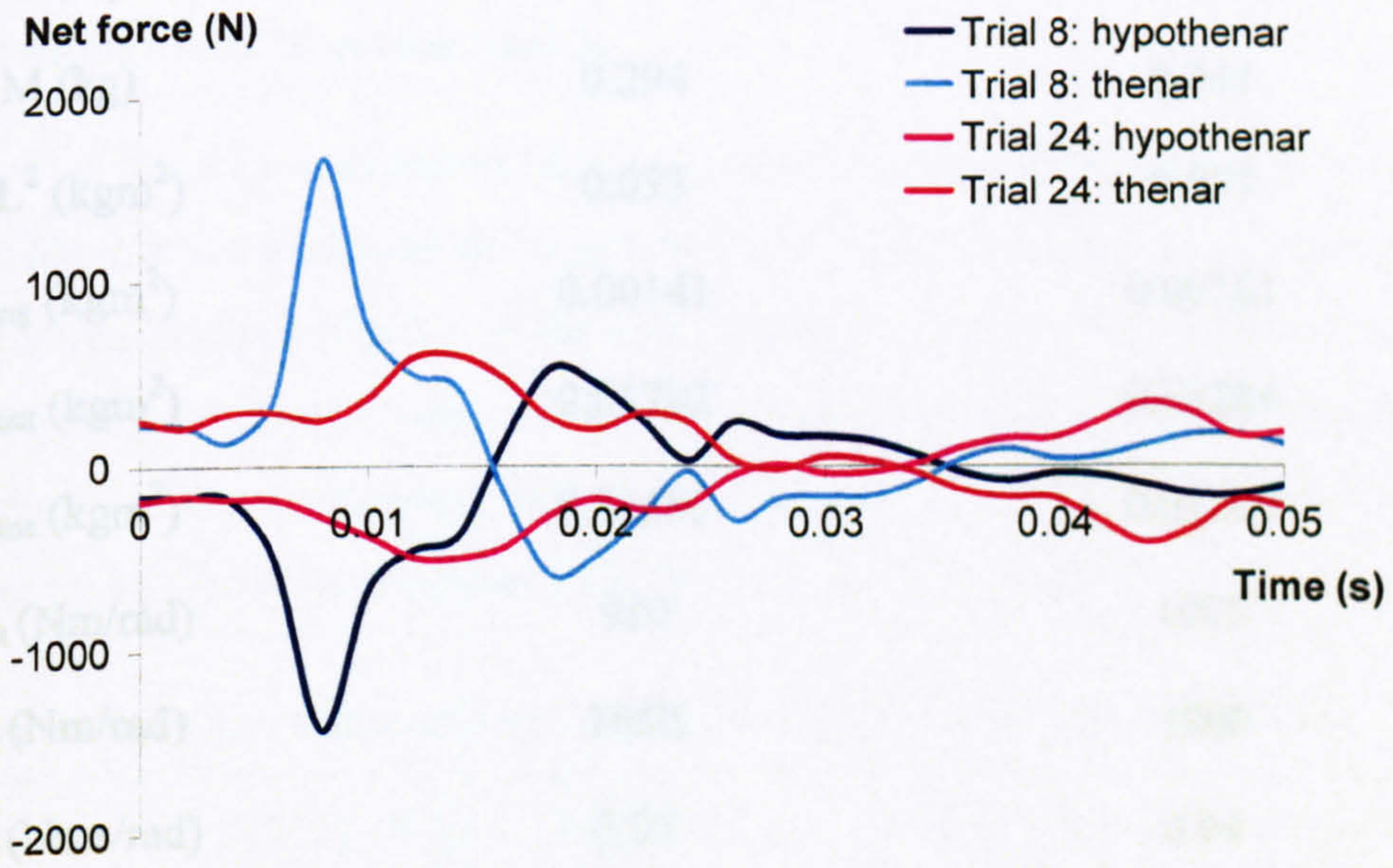

Figure 6.8. A comparison of net grip forces due to the spring-damper systems at the hypothenar and thenar eminences for trials 8 and 24

The peaks in the grip force components are clearly of greater magnitude and occur sooner after ball impact for trial 8. For both trials, the forces in opposite spring-dampers at the thenar and hypothenar eminences of the hand were almost equal and opposite due to the rotation of the racket handle about the centre of the hand.

6.3.4 Racket frame: trial 1 versus trial 36

Table 6.5 summarises some of the model racket frame parameters for the LM Prestige (trial 1) and LM 8 (trial 36) racket frames that were determined experimentally. L is the distance of the centre of mass of the racket from the butt end, M is the mass of the racket whilst I_{long}, I_{front} and I_{trans} refer to the moments of inertia about the frontal, transverse and longitudinal axes respectively through the centre of mass of each racket. The parameters k and c are the stiffness and damping coefficients for the torsional spring-dampers in and out of the plane of the racket. Whilst making a direct comparison between trials 1 and 36 (Table 6.6), differences can only be attributed to the combined effects of the interrelated racket frame parameters.

Table 6.5. Parameters for racket frames used in trials 1 and 36

Parameter	Trial 1	Trial 36
L (m)	0.333	0.392
M (kg)	0.294	0.241
ML^2 (kgm^2)	0.033	0.037
I_{long} (kgm^2)	0.00141	0.00161
I_{front} (kgm^2)	0.01722	0.01284
I_{trans} (kgm^2)	0.01586	0.01200
k_{out} (Nm/rad)	910	1075
k_{in} (Nm/rad)	1650	1800
c_{out} (Nms/rad)	0.03	0.04
c_{in} (Nms/rad)	0.09	0.10

Table 6.6. A comparison of peak loading at the elbow for trials 1 and 36

Trial	MFET (Nm)	MPST (Nm)	MIJF (N)	MWMF (N)
1 (tour)	-71.1	-40.6	173.0	-80.9
36 (recreational)	-75.2	-44.9	186.4	-77.8

MFET for trial 1 is 4.1 Nm lower in magnitude than the corresponding value for trial 36. It has been proposed that there is a positive linear relationship between MFET and the difference in moments of inertia (ML^2) between values about axes through the centre of mass and the grip (Nesbit et al., 2006). Since ML^2 is slightly higher for trial 36, the results of this comparison would appear to support this hypothesis. MPST is 4.3 Nm greater for trial 1 than the corresponding value for trial 36. The longitudinal axes of the racket and forearm are almost in line with each other just after ball impact when peak pronation-supination torques are predicted to occur. I_{long} may therefore have the greatest influence on resisting the motion of the racket generated by the pronator-supinator muscle groups. A higher value for I_{long} for trial 36 adds support to this argument. MIJF was 13.4 N greater although MWMF was 3.1 N less in magnitude respectively for trial 36 compared to trial 1. A sensitivity analysis may shed more light on the relative effects of the racket frame parameters (Section 6.4.3).

6.3.5 Technique: trial 36 versus trial 56

Trial 36 was a topspin one-handed backhand drive groundstroke whilst trial 56 was a slice one-handed backhand drive groundstroke. Shoulder, elbow and wrist joint angles are given in Appendix 3. Wrist and elbow joint angle time histories would appear to be similar between trials. However, the shoulder joint angle-time histories and the shoulder flexion-extension angles in particular, showed distinct differences. The loading at the elbow was compared for the two trials (Table 6.7).

Table 6.7. A comparison of peak loading at the elbow for trials 36 and 56

Trial	MFET (Nm)	MPST (Nm)	MIJF (N)	MWMF (N)
36 (topspin)	-75.2	-44.9	186.4	-77.8
56 (slice)	-78.2	-42.2	188.9	-70.3

Simulation results suggest that performing a slice as opposed to a topspin drive groundstroke gives no notable change in the elbow loading. Whilst for trial 56 small increases in the magnitudes of MFET and MIJF were seen, MPST and MWMF were smaller in magnitude than for trial 36. Since the wrist and elbow joint angle-time histories are similar for both trials, this would suggest that they are more important than movements at the shoulder in terms of the loading observed at the elbow. Whilst speculative at this point in time, further research may be able to advance knowledge on the effect of player technique on elbow loading.

6.3.6 Initial stringbed tension: trial 1 versus trial 31

The net torques about the elbow were not notably different for trials 1 and 31 (Table 6.8). Trial 1, where the racket was strung at initial (low) tension of 57 lbs, resulted in a smaller MFET value but a larger MPST when compared to trial 31 where the racket was strung at a (high) tension of 70 lbs. Predicted MIJF and MWMF were 5.0 and 7.4 N higher respectively for trial 31, possibly due to the higher predicted force between the ball and point on the stringbed when in contact (Figure 6.9).

Table 6.8. A comparison of peak loading at the elbow for trials 1 and 31

Trial	MFET (Nm)	MPST (Nm)	MIJF (N)	MWMF (N)
1 (low tension)	-71.1	-40.6	173.0	-80.9
31 (high tension)	-81.6	-34.8	178.0	-98.3

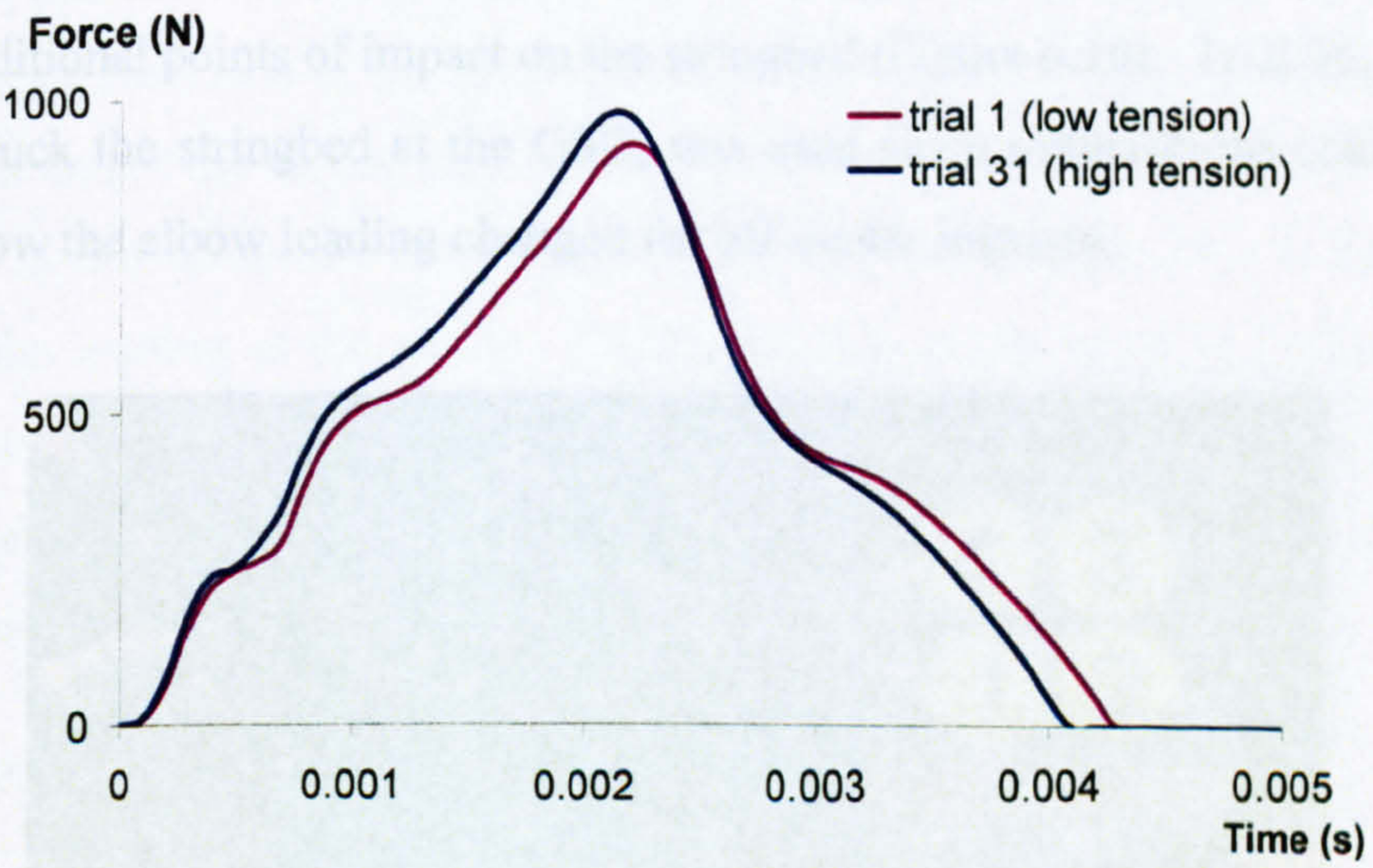

Figure 6.9. Ball-stringbed contact forces for rackets with low and high initial string tensions

The ball-stringbed force-time histories were similar in appearance although the peak force for trial 31 was greater and occurred just earlier. In addition, the time of contact of the ball on the stringbed was predicted to be lower. Estimates of the total impulse for ball-stringbed contact time suggested a slightly higher value for trial 31 of 1.96 Ns as opposed to 1.92 Ns for trial 1.

When considering the effect of the stringbed properties on loading at the elbow, the dynamic stiffness of the strings must be taken into account along with the initial string tension as the two combined determine stringbed stiffness. This will be investigated, as part of a sensitivity analysis.

6.4 SENSITIVITY ANALYSIS

6.4.1 Overview of sensitivity analysis

Whilst direct comparisons have been made between the simulation output of the six matched trials, small variations in the kinematics of the arm and ball-racket relative velocity may account for some of the differences in elbow loading. To address this issue and investigate any uncertainty in other input parameters, a sensitivity analysis was performed on individual matched simulations as model output could then be attributed to the perturbation of a single parameter.

6.4.2 Ball impact location

Ball impact location was perturbed from the geometric stringbed centre (GSC) to three additional points of impact on the stringbed (Figure 6.10). Trial 36, for which the ball struck the stringbed at the GSC, was used since observations could then be made on how the elbow loading changed for off-centre impacts.

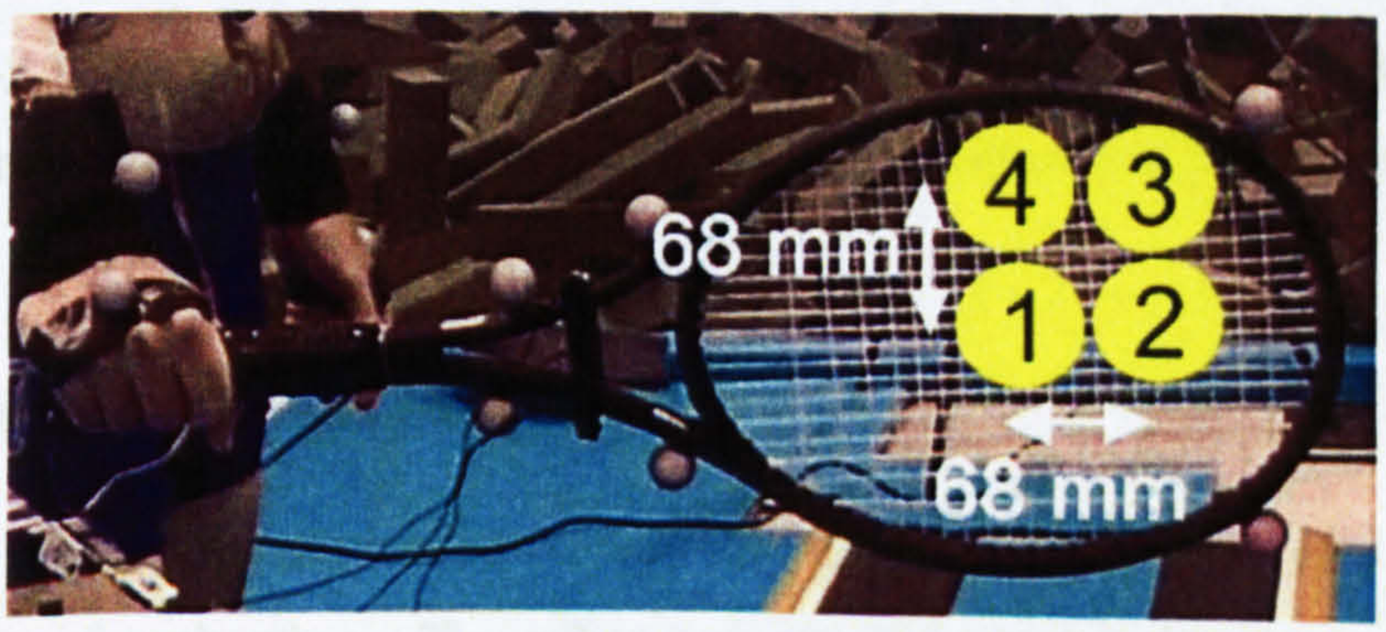

Figure 6.10. Ball impact locations for simulation perturbations

The effect of varying the impact location from the GSC at point 1 to points 2, 3 and 4 on peak loading at the elbow was recorded (Table 6.9). Small adjustments were made to the initial relative linear velocity between the ball and point on the stringbed for each simulation perturbation to account for varying points on the stringbed having slightly different linear velocities.

Table 6.9. The effect of ball impact location on peak loading at the elbow

Point of ball impact on the stringbed	MFET (Nm)	MPST (Nm)	MIJF (N)	MWMF (N)
1	-75.2	-44.9	186.4	-77.8
2	-89.6	-45.4	207.0	-77.8
3	-85.2	-54.7	203.0	-77.8
4	-77.4	-53.9	199.0	-77.8

The most striking observation from Table 6.9 was that MWMF did not change as the ball impact location varied. This finding was investigated further in Section 6.4.7. In line with previous observations when trials 8 and 24 were compared, a simulated ball impact at point 3 yielded higher values in MFET, MPST and MIJF when compared with an impact at point 1. MPST were higher for impacts displaced from the longitudinal axis of the racket as the arm was forced to resist the recoil of the racket about this axis. The highest absolute value for MFET of -94.6 N was for point 2 on the longitudinal axis of the racket nearer to its tip. An impact at point 3, further from the butt end of the racket, also increased MFET.

The results presented in this section indicate that the location of ball impact influences the loading at the elbow. Loading has been found to be higher for ball impacts away from the GSC. The following sections will therefore investigate the effects of parameter perturbations for trial 8 where the location of ball impact was off-centre (point 3 on Figure 6.10).

6.4.3 Racket frame stiffness and damping

The racket frame stiffness and damping coefficients were perturbed independently of each other. The effects of twofold increases in each variable on

loading at the elbow, for the torsional spring-dampers in and out of the racket plane, were observed for each simulation perturbation (Table 6.10). Simulation results suggest that the damping of the racket frame had a small effect on peak loading at the elbow in terms of forces and net torques when compared to changing the ball impact location. The visco-elastic properties of the torsional spring-damper allowing movement out of the plane of the racket, had more effect on the loading at the elbow than the in plane parameters. This would appear sensible given the lower frequency and higher amplitude of vibration for the fundamental mode shape out of the plane of the racket, measured experimentally and also predicted by the model (Section 6.2.3).

Table 6.10. The effect of racket frame stiffness and damping on peak loading at the elbow

Point of ball impact on the stringbed	MFET (Nm)	MPST (Nm)	MIJF (N)
No perturbation	-80.2	-39.0	212.6
In plane frame stiffness x 2	-81.1	-38.8	215.0
Out of plane frame stiffness x 2	-85.3	-36.8	227.5
In plane frame damping x 2	-78.8	-38.9	212.6
Out of plane frame damping x 2	-79.4	-39.1	190.6

The most noticeable change in the initial peak loading at the elbow was a 7% increase in MIJF for a twofold increase in the out of plane racket frame stiffness. As well as observing the peak loading values, the time histories for loading variables were also examined since cyclic loading has been suggested as a possible mechanism for injury to the elbow (Knudson, 2004).

The resultant internal joint reaction force at the elbow was plotted from ball impact and every 0.5 ms thereafter for 50 ms. When no racket was present the resultant internal joint force-time history at the elbow lay below the corresponding trace when the ball-racket system was present. The greatest difference between the two traces occurred in the first 15 ms. This corresponds with previously presented racket frame acceleration, net joint torque, grip force and ball-stringbed force data which have all peaked in this period after the ball has impacted the stringbed.

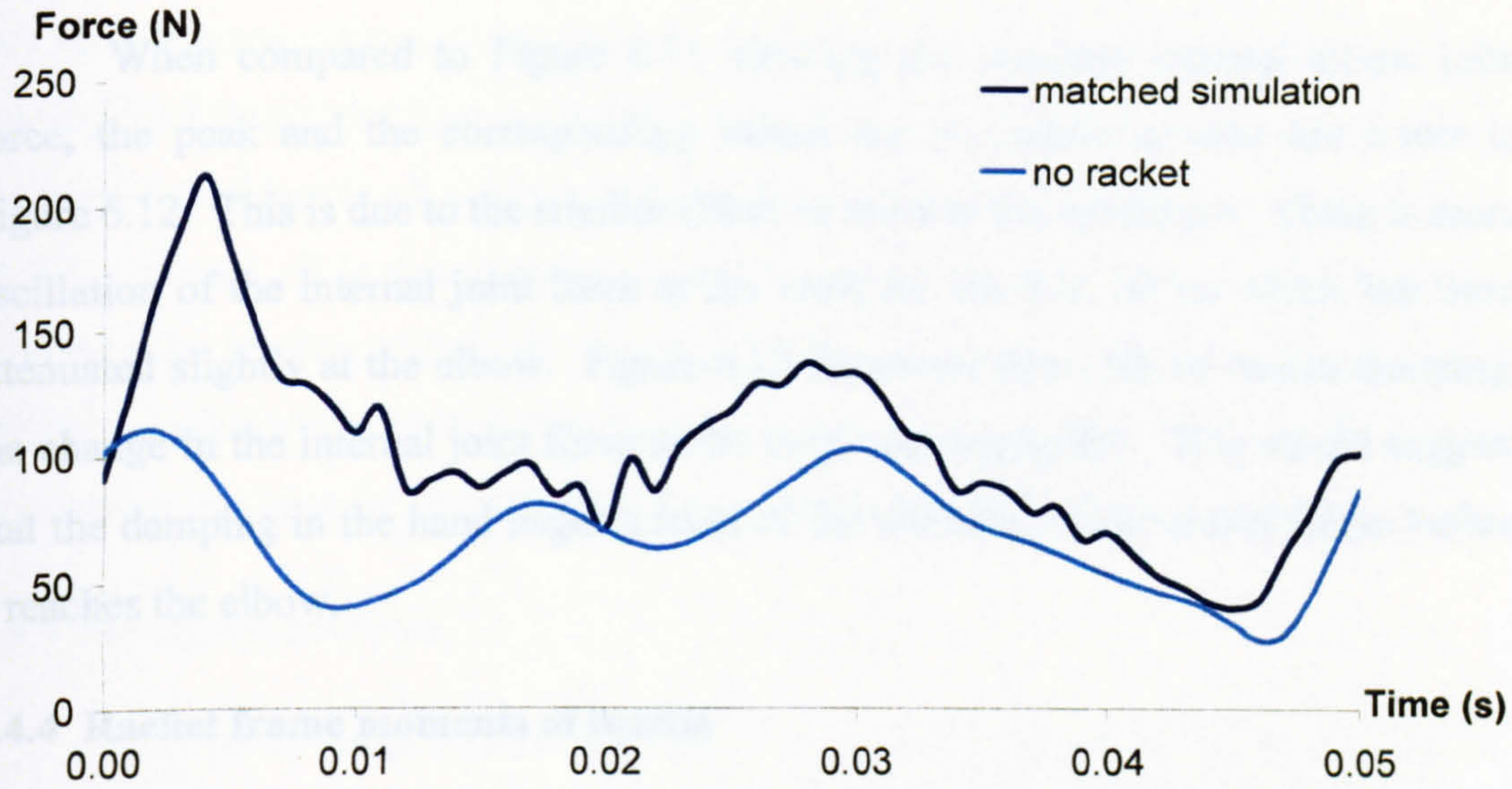

Figure 6.11. Comparison of resultant internal elbow joint force for trial 8 for the matched simulation and a simulation where no racket is present

Figure 6.11 shows that there was no frequency component of around 178 Hz (the frequency of the fundamental mode of vibration out of the plane of the racket from Section 5.2.3) on the internal joint force-time histories which suggests that the racket frame vibration is significantly damped out by the hand after the initial peak, before reaching the elbow. Figure 6.12 shows the resultant internal joint force at the wrist for the matched simulation of trial 8 and also when there was no racket frame damping in the system.

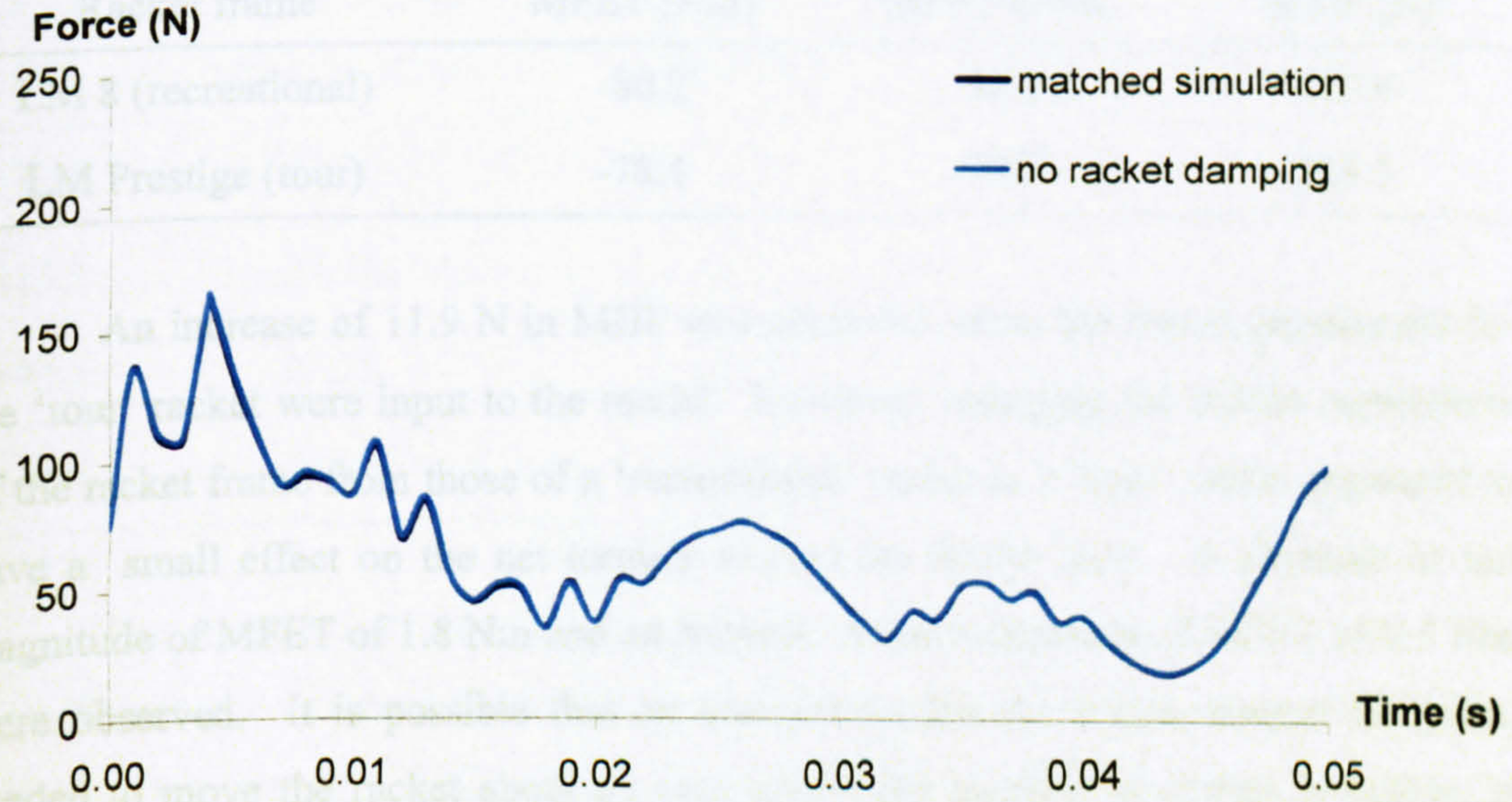

Figure 6.12. Comparison of resultant internal wrist joint force for trial 8 for the matched simulation and a simulation with no racket damping

When compared to Figure 6.11 showing the resultant internal elbow joint force, the peak and the corresponding values for an instant in time are lower in Figure 6.12. This is due to the smaller effective mass at the wrist joint. There is more oscillation of the internal joint force at the wrist for the first 10 ms which has been attenuated slightly at the elbow. Figure 6.12 illustrates that with no racket damping, the change in the internal joint force at the wrist was negligible. This would suggest that the damping in the hand negates most of the vibration of the racket frame before it reaches the elbow.

6.4.4 Racket frame moments of inertia

The peak loading at the elbow was investigated when the inertia parameters for the racket frame were swapped from the 'recreational' LM 8 to the 'tour' LM Prestige model. The inertia parameters have been summarised in Table 6.5 (Section 6.3.4). Essentially, the LM 8 was a lighter, longer racket of wide-body construction with a greater moment of inertia about the longitudinal axis but a smaller moment of inertia about the frontal and transverse axes when compared to the LM Prestige. The results are summarised in Table 6.11.

Table 6.11. The effect of racket frame inertia parameters on peak loading at the elbow

Racket frame	MFET (Nm)	MPST (Nm)	MIJF (N)
LM 8 (recreational)	-80.2	-39.0	212.6
LM Prestige (tour)	-78.4	-39.5	224.5

An increase of 11.9 N in MIJF was observed when the inertia parameters for the 'tour' racket were input to the model. However, changing the inertia parameters of the racket frame from those of a 'recreational' racket to a 'tour' racket appeared to have a small effect on the net torques around the elbow joint. A decrease in the magnitude of MFET of 1.8 Nm and an increase in the magnitude of MPST of 0.5 Nm were observed. It is possible that an increase in the net torque around the joint, needed to move the racket about an axis where the moment of inertia is higher, is balanced by the extra cushioning the racket provides in resisting the recoil due to ball impact. However, it would appear that the differences in the inertia properties of the

two rackets used were not sufficient to observe a positive effect on reducing elbow loading for either racket frame. When a simulation was run with a twofold increase in the moment of inertia of the racket about the longitudinal axis, a 6 Nm reduction in MPST occurred. It is possible that perturbing the inertia parameters of the racket can influence the loading at the elbow. Further research may be able to optimise racket design to reduce the potential for injury. However, the design of the racket would also have to account for performance outcomes and governing body regulations.

6.4.5 Stringbed stiffness

The initial string tension for trial 8 was 57 lbs corresponding to a value for ST0 of 735.8 N in the model (Section 3.3.3). Three simulations were run where the value of ST0 was increased in increments of 77.3 N with the fourth and highest value for ST0 being equal to the initial stringbed tension for the racket strung at 75 lbs. The effects of varying ST0 on the variables used as indicators of elbow loading as well as the resultant outbound ball velocity and the time of contact of the ball on the stringbed were noted (Table 6.12).

Table 6.12. The effect of ST0 on the outbound ball velocity, time of contact with the stringbed and the peak loading at the elbow

ST0 (N)	Outbound ball velocity (m/s)	Ball-stringbed contact time (ms)	MFET (Nm)	MPST (Nm)	MIJF (N)
735.8	27.30	3.8	-80.2	-39.0	212.6
813.1	27.28	3.7	-80.9	-39.9	221.5
890.4	27.22	3.6	-81.9	-40.1	229.1
967.7	27.21	3.5	-83.2	-41.9	232.4

The predicted effect of a change in the initial string tension of the racket on the ball-stringbed contact time would appear comparable to the results of previous research (e.g. Brody, 1988). Whilst increasing the string tension resulted in an decrease in outbound ball velocity, the change is only small, bringing the simulation results in line with the experimental findings of Elliott (1982) and Goodwill and

Haake (2004). An increase in MFET, MPST and MIJF was seen for each incremental increase in ST0. The largest increase between the two extremes of 9% was in MIJF.

In reality, stringbed stiffness is determined by the dynamic stiffness of the springs as well as the initial string tension. Each spring stiffness in the model was increased by 10% to examine the effect on the loading at the elbow. Small increases were observed in MFET, MPST and MIJF. An increase in the dynamic string stiffness of approximately 70% was needed to see a comparable increase in loading variables as for a 32% increase in initial string tension.

6.4.7 Wobbling mass parameters

The results from this sensitivity analysis suggest that MWMF is insensitive to other parameter changes. The visco-elastic parameters of the non-linear spring-dampers used to attach the wobbling mass segments to the rigid bone segments were perturbed by ± 10% to observe the effect on the net torques and resultant internal joint forces at the elbow joint. For a 10% increase, the maximum displacement of the wobbling mass from the rigid component decreased by 2% with less than a 1% increase in the peak force in the spring-damper. There was no observable effect for either a decrease or increase in the visco-elastic parameters on the net torques around the elbow joint or in the magnitude of the resultant internal forces at the elbow joint. The loading at the elbow joint was relatively insensitive to the wobbling mass visco-elastic parameters when the kinematics used to drive the simulation were unchanged. Hence, the kinematics of the arm would appear to be the overriding factor governing the interaction between the rigid and wobbling components of the arm.

6.4.8 Generating initial racket acceleration

The equation for the forces acting between a point on the racket handle and the hypothenar / thenar eminences (F) incorporated an initial force term (R_0) which was ramped down over a 10 ms time period using a quintic function (Equation 6.1).

$$F = -k(L - L_0 + (F_0/k)) - c\dot{L}(L - L_0) + R_0 \qquad (6.1)$$

The purpose of these additional terms was to generate the correct linear and angular accelerations of the racket handle for the instant of ball impact with the stringbed at the start of the simulation. A sensitivity analysis was needed to ensure that the grip

forces were predominantly due to the visco-elastic parameters of the spring-dampers and not too sensitive to the ramping down time of the additional grip force terms. The maximum and average resultant net force in the spring-dampers at the thenar and hypothenar eminences of the hand were compared for simulations from ball impact until 50 ms afterwards. A simulation with no additional force terms and two further simulations where the additional force terms were ramped down to zero in 10 and 20 ms respectively were run (Table 6.13).

Table 6.13. The effect of additional force terms on the maximum and average resultant net forces at the hypothenar and thenar eminences of the hand

Simulation	Hypothenar eminence		Thenar eminence	
	Max (N)	Average (N)	Max (N)	Average (N)
No additional force term	1022.4	232.8	907.3	223.1
Ramp time = 10 ms	968.5	232.1	868.0	221.2
Ramp time = 20 ms	974.6	235.2	868.0	223.2

The additional force terms reduced the maximum resultant net forces due to the spring-dampers at the hypothenar and thenar eminences by approximately 5%. Whilst indicating that modelling the non-zero linear and angular accelerations of the racket at ball impact influences the net grip forces, the additional forces needed to achieve this are small compared to the forces in the spring-dampers. As a consequence, increasing the ramp-down time for the additional force terms from 10 to 20 ms resulted in small increases in the maximum and average resultant net forces due to the spring-dampers. A selected ramp-down time of 10 ms would not appear to have a large effect on the net grip forces and therefore the input to the hand-arm system. In future, a more elegant way of generating the initial accelerations of the racket could be achieved by calculating the required offsets between the hand and racket to generate initial forces within the spring-dampers. However, for the purpose of this study, such a level of complexity has been shown unnecessary.

6.4.9 Stringbed damping

To observe its effect on the loading at the elbow joint, a damping term was included in the equations for the springs connecting the point masses representing the stringbed, so that the energy returned to the ball was 95% of the value when no damping was present (Brody, 1995). The damping term was ramped up from zero to this calculated value over a period of 8 ms (approximately double ball-stringbed contact time) so that the interaction of the ball with the stringbed was still governed predominantly by the stiffness of the stringbed as in reality. Whilst reducing the amplitude of the high frequency component of the racket frame vibration due to the stringbed oscillating, the addition of the stringbed damping parameter did not influence the maximum net resultant torques or the resultant internal joint force at the elbow to any noticeable extent. A 1% reduction in each case was seen due to a reduction in the impact force between the ball and the point on the stringbed. The omission of a stringbed damping term would therefore appear to have little influence on the predicted relative effects of the simulation model.

6.5 CHAPTER SUMMARY

This chapter has described the methods used to evaluate the model. The simulation results from making direct comparisons between six matched trials are presented. A sensitivity analysis was subsequently performed to observe the effects of perturbing model parameters on the observed model outputs. Direct comparisons between trials suggested that for one-handed backhand groundstrokes with similar kinematics of the arm, small differences in elbow loading are observed if the racket properties are perturbed. A sensitivity analysis confirmed that the location of ball impact produced greater net changes in the loading at the elbow. The following chapter concludes with an application of the results obtained to answering the specific research questions posed in Chapter 1. A general discussion of the study is also given with comments on its limitations and implications for future research.

CHAPTER 7

SUMMARY AND DISCUSSION

7.1 CHAPTER OVERVIEW

This chapter gives an overview of the present study by discussing the main topics covered in each chapter. A discussion of the limitations of this investigation along with suggestions for future research is also included. Finally, the model has been applied to answering the research questions raised in Chapter 1 by discussing the simulation results presented in Chapter 6.

7.2 DISCUSSION

7.2.1 Kinematic and kinetic data collection

One-handed backhand groundstrokes were recorded using an automatic motion analysis system. Camera frame rate was limited to 250 Hz to ensure that the hitting volume of approximately 2.5 m^3 was in the field of view of all cameras. A recent study at Loughborough University on triple jumping using a fully portable, upgraded motion analysis system enabled data to be captured at a higher camera frame rate of 480 Hz and for a larger performance volume. Such a set-up would result in more detailed kinematic data for future studies.

Tekscan pressure sensors were attached to the grip of certain rackets and monitored grip pressures at a sampling frequency of 250 Hz. The results showed where peak grip pressures occurred over the entire grip surface at discrete time intervals during a groundstroke. This allowed comparisons of the net effect of gripping forces on net torques, about perpendicular axes through the centre of the racket handle, to be made (Section 6.2.4). It is anticipated that for future studies a custom built wireless device will be available, with tri-axial accelerometers within the grip and single-cell force sensing resistors on the grip surface. This would enable more detailed observations of grip force and racket motion relative to the hand to be made for each trial.

7.2.2 Parameter determination

Equipment-specific parameters for the ball, stringbeds and racket frames were determined from independent experimental tests. In isolation, the ball, stringbed and racket frame models gave excellent agreement with experimental results. The equipment parameters were fixed before the ball-racket system was combined with an upper-limb and torso system to model one-handed tennis backhand groundstrokes. By fixing these parameters, it is harder to match performances using the model and this strengthens the evaluation of the model.

In the present study, body segmental inertia parameters for the subject were calculated using the geometric model of Yeadon (1990b). Previous rigid body simulation models using segmental inertia parameters calculated using this method, have shown to produce realistic human motion (e.g. Yeadon & King, 2002). Splitting the segmental inertia parameters into rigid and wobbling components is more problematic as direct measurements cannot be taken. In this study, components were based on body composition estimates and bone to non-bone mass ratios reported in the literature. In the future, more accurate subject-specific inertia parameters could be obtained using alternative methods such as magnetic resonance imaging (MRI).

Encouragingly, evaluation of the model showed that matched simulation trials agreed well with a variety one-handed backhand performances. It would appear that for the level of complexity of the simulation model, the methods of equipment parameter determination have been appropriate.

7.2.3 Optimisation and model evaluation

The Simulated Annealing optimisation algorithm (Corana et al., 1987) was used in this study to determine certain model parameters. Although costly in terms of the number of function evaluations needed, it has been shown to be very robust and capable of finding a global as opposed to a local optimum (Goffe et al., 1994). Since computer processors are becoming faster all the time, more simulations can be run in a given time period. The optimisation score is perhaps the most important part of the optimisation process as the weightings of each component of the score and any penalties introduced may have a large influence on the solutions found. In the future, the optimisation score may incorporate kinetic variables directly.

Once determined, simulation model parameters were fixed for the six performance trials. For the function used to determine the visco-elastic parameters of the grip, an average root-mean-squared (RMS) difference score between simulation and performance of less than 1% was obtained. When a single simulation was run with the gripping parameters fixed, the model evaluation scores representing the average RMS difference between a simulation and a performance for the six degrees of freedom of the racket relative to the hand, the ball-stringbed contact time and the outbound ball velocity, ranged from 0.63 to 2.62%. This excellent agreement between matched simulations and performances shows that an accurate subject-specific simulation model has been developed which can be used to investigate loading in one-handed backhand groundstrokes with confidence. Comparisons of racket frame acceleration and grip pressure data have been made for selected trials and showed good agreement. Improved tennis racket instrumentation in the future may permit higher sampling frequencies and a kinetic comparison of variables for each matching simulation and performance.

7.2.4 Model limitations

The model in this study predicts the internal joint forces and the net torques about a joint. Ideally, knowledge of the individual muscle forces should be investigated. However, current muscle models (e.g. Alexander, 1990; Soest et al., 1993) assume the contractile components to be elements with no mass and the soft tissue is treated as a passive rigid component. To observe the transmission of force through the arm, a Finite Element model of the arm (e.g. Ng-Thow-Hing & Fiume, 1999) and the ball-racket system would be needed, increasing the complexity of the system considerably. In time, this level of complexity may be possible, but it is beyond the scope of the present study.

The upper-limb model is driven by joint-angle time histories and therefore technique is restricted to that of the subject in this study and it can be problematic to vary the technique substantially from that recorded. The model could be developed in the future to look at other players so that the effect of technique on the loading at the elbow can be quantified.

7.3 FUTURE RESEARCH

7.3.1 Application to other tennis player groups

In this study an elite male tennis player was selected since the subject was able to perform one-handed tennis backhand groundstrokes to a consistent and high standard. In addition, due to a high level of physical fitness, maximum voluntary strength tests were possible. Having established a series of protocols for processing data collected for the subject, repeating the process for more subjects would be less time consuming.

As a natural progression, different groups could be analysed including females, juniors and senior players of varying abilities. The latter may be most important since the prevalence of tennis elbow in recreational players is well reported (Priest et al., 1980; Roetert et al., 1995). Since most young tennis players today will choose to hit a topspin drive with two hands on the racket, this is a feature which could be incorporated into the model in the future. Additional parameters and modification of the gripping mechanism may be needed to achieve this. At present, the model could be used to investigate loading in the arm during forehand and service motions by making alterations to the model input files and optimising for new gripping parameters.

7.3.2 Technique optimisation

The upper-limb model was driven by quintic splines of joint angle-time histories. Joint motion was fixed for a given trial and therefore limited conclusions can be drawn as to the effect of technique on loading in the arm. The next level of model complexity would be to generate joint motion using quintic functions (e.g. Hiley and Yeadon, 2005). This type of model allows manipulation of joint angle changes and is suitable for analysis of movement for which maximum muscle force is not being generated. The measured maximum voluntary joint torques that can be used to limit joint angle changes to those that are possible for the subject to achieve.

A further progression would be to drive the simulation model with joint torques (e.g. King & Yeadon, 2002). The 9-parameter functions have already been calculated, which represent the maximum voluntary torques achievable by the subject, can be combined with torque activation timings to generate joint motion. The EMG data obtained from the performance data collection (Section 4.2.4) could be used in

the optimisation process for the torque activation timings. Developing this model further so that individual muscles instead of net joint torques drive the simulation model could provide the best insight yet as to why damage might occur to extensor muscle tendons in the forearm when performing one-handed backhand groundstrokes. In principle, the effects of net muscular strength and muscle activation timings could be investigated.

In this study the gripping technique of the performer for a given trial has not been perturbed. Hatze (1976) suggested that grip force could have an influence on the development of tennis elbow. Using a quintic function to vary the initial grip force could be used to investigate this in the future.

7.3.3 Implications for performance

This study has focussed on the possible effects of tennis racket parameters on the loading at the elbow experienced during one-handed tennis backhand groundstrokes. In theory, an optimal set of racket parameters could be found to achieve the lowest level of loading at the elbow. However, this optimal racket would have to conform to governing body regulations to be used in competitive play. Previous research has shown that perturbing properties of the racket frame and stringbed can have a large effect on the outbound ball performance. Whilst certain aspects of this model, for example the tennis ball representation as a point mass, are perhaps too simplistic to fully investigate performance factors, any conclusions on improved racket design must take into account the possible effect on performance.

7.4 RESEARCH QUESTIONS

Q1. How do the inertia and the stiffness and damping properties of the tennis racket frame affect elbow loading in one-handed tennis backhand groundstrokes?

Changing the inertia parameters of the racket frame from those of a 'recreational' racket to a 'tour' racket appeared to have a small effect on the net torques around the elbow joint. It is possible that an increase in the net torque around the joint needed to move the racket about an axis where the moment of inertia is higher, was balanced by the extra cushioning the racket provided in resisting the recoil due to ball impact. However, it would appear that the differences in the inertia

properties of the two rackets used in this study were not sufficient to observe a positive effect on reducing elbow loading for either racket frame. When a simulation was run with a twofold increase in the moment of inertia of the racket about the longitudinal axis, a 6 Nm reduction in MPST occurred. It is therefore possible that perturbing the inertia parameters of the racket can influence the loading at the elbow to some extent. Further research may be able to optimise racket design to reduce the potential for injury.

The stiffness and damping parameters of the racket frame primarily determine its modal response. The model was able to match the modal response of the racket well when freely suspended (Section 5.4.3) and hand-held (Section 6.2.3). When hand-held, the time for the magnitude of the out of plane racket frame acceleration had decreased to half its value at ball impact in approximately 10 ms. This was due to high levels of damping at the hand-racket interface. The in plane racket frame accelerations, measured experimentally and predicted by the model, were of small amplitude and were also damped out quickly by the hand. Therefore, perturbing the parameters for the in plane torsional spring-damper had little effect on the loading at the elbow. A twofold increase in the out of plane racket frame stiffness resulted in a 7% increase in the maximum internal reaction force at the elbow occurring just after ball impact. A twofold increase in racket frame damping reduced the maximum internal reaction force at the elbow by only 2%. However, these parameters are not representative of the rackets tested and in reality the stiffness and damping of the frame are interrelated (Brody et al., 2002).

The stiffness and damping properties of the racket frame are likely to affect the 'feel' of the tennis racket at the grip where racket frame vibrations are damped out by the soft tissue of the hand. Additionally, an increase in racket power for stiffer racket frames has been shown (Cross, 2000a). However, it is unlikely that the stiffness and damping properties of the racket frame within current design ranges will affect the loading at the elbow considerably.

Q2. How does the location of the ball impact on the stringbed and the stringbed stiffness affect elbow loading in one-handed tennis backhand groundstrokes?

Of all simulation perturbations, the location of ball impact on the stringbed had the most influence on the loading at the elbow. Simulated off-centre ball impacts

increased the peak internal joint force by 11.1%, increased the peak pronation-supination net torque by 21.8% and increased peak elbow-flexion extension net torque about the elbow by 19.1% when compared to peak loading for an impact at the geometric stringbed centre.

Whilst having well documented effects on outbound ball velocity and ball-stringbed contact time, an increase in stringbed stiffness also resulted in increased loading at the elbow. Net torques around the elbow were higher for a simulation with a 'high' initial string tension although the largest increase proportional of 9% was for the internal joint force. The dynamic string stiffness was found to have less influence on loading at the elbow than the initial string tension as a 70% increase in its value was needed to see a comparable effect on increasing elbow loading as for a 32% increase in initial string tension. The simulation model suggests that there may be some trade-off when increasing stringbed stiffness between desired performance outcomes such as improved hitting accuracy and reducing the loading at the elbow.

Q3. Does the rigid body recoil of the racket or its modal response have the greater influence on the loading components at the elbow?

In Section 6.4.3, time histories of resultant internal joint forces were shown. Whilst the simulation racket frame accelerations exhibited the fundamental modal frequencies obtained from experimental modal analysis, these vibrations were attenuated as they progressed to the grip. It would appear that the hand then damped almost all of the vibration of the racket frame before it reached the elbow leaving a prominent force peak at around 5 ms after ball impact. When no racket frame damping was simulated, the effect on the resultant internal joint force downstream at the wrist was negligible. The simulation results would suggest that it is the rigid body recoil of the racket producing a large initial impulse that has the greatest effect on loading components at the elbow.

Whilst the initial impact peak may be the overriding factor for the loading at the elbow, it is not clear at this point if the peak load from a 'worst case bad hit' is high enough to cause micro-tears in the tendons of the extensor muscles. This would in part depend on the physical attributes of the tennis player. It would seem logical that physically fit elite performers are better able to cope with such loading. In addition, by virtue of being elite performers, they are subject to less off centre 'bad

hits'. Although speculative at this point in time, a plausible explanation is that an accumulation of these high loads, especially from off-centre hits, may lead to micro-tears within the tendons of the extensor muscles.

7.5 CONCLUSION

The simulation model developed in this study has been successfully evaluated and applied to investigating the loading at the elbow joint in one-handed backhand groundstrokes. A discussion of the methods used to develop the model and determine its parameters, along with the limitations of the model, has been presented. This research provides a basis for further work to answer questions that are not possible by experimental study alone. Future work has been suggested. Results from model simulations show that the inertia and stiffness parameters of the racket frame and the initial stringbed tension have a relatively small influence on elbow loading within current design ranges. In contrast, the location of ball-impact would appear to be an important factor in determining the loading at the elbow. This research suggests that cyclic loading due the modal response of the racket is an unlikely mechanism for tennis elbow and that an accumulation of high loading from off-centre hits is more likely to be a causative factor.

REFERENCES

Abdel-Aziz, Y. I., & Karara, H. M. (1971). Direct linear transformation from comparator coordinates into object space coordinates in close-range photogrammetry. Paper presented at the ASP Symposium on Close-Range Photogrammetry, Falls Church, VA: American Society of Photogrammetry.

Akuthota, V. (2004). Sports and performing arts medicine 2. Shoulder and elbow overuse injuries in sports. Archives of Physical Medicine and Rehabilitation, 85, 52-58.

Alexander, R. M. (1990). Optimum take-off techniques for high jumps and long jumps. Philosophical Transactions of the Royal Society of London B, 329, 3-10.

Alexander, R. M. (1992). Simple models of walking and jumping. Human Movement Science, 11, 3-9.

Alexander, R. M. (1995). Simple models of human movement. Applied Mechanics Review, 48(8), 461-469.

Andrews, J. G., & Youm, Y. (1979). A biomechanical investigation of wrist kinematics. Journal of Biomechanics, 12, 83-93.

Atha, J. (1984). Current techniques for measuring motion. Applied Ergonomics, 15(4), 245-257.

Bahamonde, R. E., & Knudson, D. (2003). Kinetics of the upper extremity in the open and square stance tennis forehand. Journal of Science and Medicine in Sport, 6(1), 88-101.

Balady, G. J., Berra, K. A., Golding, L. A., Gordon, N. F., Mahler, D. A., Myers, J. N., et al. (2000). ACSM'S Guidelines for exercise testing and prescription (Sixth Edition ed.). Philadelphia, USA: Lippincott, Williams & Wilkins.

Bartlett, R. M. (1997). Biomechanical analysis of movement in sport and exercise. Leeds: British Association of Sport and Exercise Sciences.

Bartlett, R. M. (1999). Sports Biomechanics. Reducing injury and improving performance. London: E & F.N.Spon.

Bauer, J. (1997, September 24-27, 1997). Racket arm muscle activation patterns in healthy and injured tennis players. Paper presented at the Twenty-First Annual

Meeting of the American Society of Biomechanics, Clemson University, South Carolina, USA.

Bernhang, A. M., Dehner, W., & Fogarty, C. (1974). Tennis elbow: a biomechanical approach. Journal of Sports Medicine, 2(5), 235-260.

Blackwell, J. R., & Cole, K. J. (1994). Wrist kinematics differ in expert and novice tennis players performing the backhand stroke: implications for tennis elbow. Journal of Biomechanics, 27(5), 509-516.

Brannigan, M., & Adali, S. (1981). Mathematical modelling and simulation of a tennis racket. Medicine and Science in Sports and Exercise, 13(1), 44-53.

Brody, H. (1979). Physics of the tennis racket. American Journal of Physics, 47(6), 482-487.

Brody, H. (1981). Physics of the tennis racket II: The sweet spot. American Journal of Physics, 49, 816-819.

Brody, H. (1984). That's how the ball bounces. The Physics Teacher, 22, 494-497.

Brody, H. (1985). The moment of inertia of a tennis racket. The Physics Teacher, 23(4), 213-216.

Brody, H. (1988). Tennis science for tennis players (4 ed.). Philadelphia: University of Pennsylvania Press.

Brody, H. (1989). Vibration damping of tennis rackets. International Journal of Sports Biomechanics, 5, 451-456.

Brody, H. (1995). How would a physicist design a tennis racket? Physics Today, 48, 26-31.

Brody, H. (1997). The physics of tennis III. American Journal of Physics, 65(10), 981-987.

Brody, H., Cross, R., & Lindsay, C. (2002). The Physics and Technology of tennis. Solana Beach, California USA: Racquet Tech Publishing.

Buchanan, T. S., Moniz, M. J., Dewald, J. P. A., & Rymer, W. Z. (1993). Estimation of muscle forces about the wrist joint during isometric tasks using an EMG coefficient method. Journal of Biomechanics, 26(4/5), 547-560.

Casolo, F., & Lorenzi, V. (2000). On tennis equipment, impact simulation and stroke precision. Paper presented at the Tennis, science & technology.

Casolo, F., Lorenzi, V., & Lucchini, S. (1999). Dynamic simulation of tennis stroke. Paper presented at the Proceedings of the VIIth International Symposium on Computer Simulation in Biomechanics, University of Calgary, Canada.

Casolo, F., Lorenzi, V., & Sasahara, H. (2000). On tennis equipment, impact simulation and stroke precision. Paper presented at the Tennis Science & Technology, University of Roehampton, Surrey.

Casolo, F., & Ruggieri, G. (1991). Dynamic analysis of the ball-racket impact in the game of tennis. Meccanica, 26, 67-73.

Challis, J. H. (1991). Estimating individual muscle forces in human movement. Unpublished Doctoral Thesis, Loughborough University.

Challis, J. H., & Kerwin, D. G. (1987). Numerical data management using quintic spline functions. International journal of sports biomechanics, 4, 180-196.

Challis, J. H., & Kerwin, D. G. (1992). Calculating upper limb inertial parameters. Journal of Sports Sciences, 10, 275-284.

Clarys, J. P., & Marfell-Jones, M. J. (1986). Anthropometric prediction of component tissue masses in the minor limb segments of the human body. Human Biology, 58(5), 761-769.

Clarys, J. P., Martin, A. D., & Drinkwater, D. T. (1984). Gross tissue weights in the human body by cadaver dissection. Human Biology, 56(3), 459-473.

Clauser, C. E., McConville, J. T., & Young, J. W. (1969). Weight, volume and center of mass of segments of the human body (AMRL TR 69-70). Dayton, OH:: Wright-Patterson Air Force Base.

Cole, G. K., Bogert, A. J. v. d., Herzog, W., & Gerritsen, K. G. (1996). Modelling of force production in skeletal muscle undergoing stretch. Journal of Biomechanics, 29(8), 1091-1104.

Cooke, A. J., Roussopoulous, K., Pallis, J. M., & Haake, S. J. (2002). Correlation between racquet design and arm injuries. The Engineering of Sport, 4.

Corana, A., Marchesi, M., Martini, C., & Ridella, S. (1987). Minimizing multimodal functions of continuous variables with the "Simulated Annealing" algorithm. ACM Transactions on Mathematical Software, 13, 262-280.

Cross, R. (1997). The dead spot of a tennis racket. American Journal of Physics, 65(8), 754-764.

Cross, R. (1998). The sweet spots of a tennis racquet. Sports Engineering, 1(2), 63-78.

Cross, R. (2000a). Flexible beam analysis of the effects of string tension and frame stiffness on racket performance. Sports Engineering (Tennis Special Issue), 3, 111-122.

Cross, R. (2000b). Physical properties of tennis strings. In A. J. Subic & S. J. Haake (Eds.), The Engineering of Sport (pp. 213-220). Oxford: Blackwell Science.

Cross, R. (2000c). Dynamics of the collision between a tennis ball and a tennis racket. Paper presented at the Tennis Science & Technology, University of Roehampton, Surrey.

Cross, R. (2001). Customising a tennis racket by adding weights. Sports Engineering, 4(1), 1-14.

Cybex Norm™ Testing & Rehabilitation System – User's Guide.(1996). New York.

Davies, G. T. (2005). Determination and analysis of dimensions of 'feel' in tennis ball impacts. Unpublished Doctoral Thesis, Loughborough University.

Dempster, W. T. (1955). Space requirements of the seated operator (WADC TR 55-159). Dayton, OH: Wright-Patterson Air Force Base.

Dignall, R. J., & Haake, S. J. (2000). Analytical modelling of the impact of tennis balls on court surfaces. Paper presented at the Tennis Science & Technology, University of Roehampton, Surrey.

Dignall, R. J., Haake, S. J., & Chadwick, S. G. (2000). Modelling of an oblique tennis ball impact on a court surface. In A. J. Subic & S. J. Haake (Eds.), The Engineering of Sport (pp. 185-192). Oxford: Blackwell Sciences.

Dong, R. G., Schopper, A. W., McDowell, T. W., Welcome, D. E., Wu, J. Z., Smutz, W. P., et al. (2004). Vibration energy absorption (VEA) in human fingers-hand-arm system. Medical Engineering & Physics, 26, 483-492.

Drillis, R., Contini, R., & Bleustein, M. (1964). Body segment parameters. Artificial Limbs, 8, 44-66.

Ellenbecker, T. S. (1995). Rehabilitation of shoulder and elbow injuries in tennis players. Clinics in Sports Medicine, 14(1), 87-108.

Elliott, B. C. (1982). Tennis: the influence of grip tightness on reaction impulse and rebound velocity. *Medicine and Science in Sports and Exercise, 14*(5), 348-352.

Elliott, B. C. (2006). Biomechanics and tennis. British Journal of Sports Medicine, 40, 392-396.

Elliott, B. C., & Christmass, M. (1995). A comparison of the high and low backspin backhand drives in tennis using different grips. Journal of Sports Science, 13(2), 141-151.

Elliott, B. C., Marsh, T., & Blanksby, B. (1986). A three-dimensional cinematographic analysis of the tennis serve. International Journal of Sports Biomechanics, 2(4), 260-271.

Elliott, B. C., Marsh, A. P., & Overheu, P. R. (1989). The topspin backhand drive in tennis: a biomechanical analysis. Journal of Human Movement Studies, 16, 1-16.

Enoka, R. M. (1996). Eccentric contractions require unique activation strategies by he nervous system. Journal of Applied Physiology, 81(6), 2339-2345.

Fairley, T. E. (1985). Some measurements of tennis racket vibration and its transmission to the hand. Paper presented at the Human Response to Vibration, Derby, UK.

Fuller, J., Liu, L. J., Murphy, M. C., & Mann, R. W. (1997). A comparison of lower-extremity skeletal kinematics measured using skin- and pin-mounted markers. Human Movement Science, 16, 219-242.

Giangarra, C. E., Conroy, B., Jobe, F. W., Pink, M., & Perry, J. (1993). Electromyographic and cinematographic analysis of elbow function in tennis players using single- and double-handed backhand strokes. American Journal of Sports Medicine, 21(3), 394-399.

Glitsch, U., Schlarb, H., & Baumann, W. (1999, August 6th, 1999). Embedding of flexible bodies into a dynamic simulation of the tennis stroke. Paper presented at the Proceedings of the VIIth International Symposium on Computer Simulation in Biomechanics, University of Calgary, Canada.

Goffe, W. L., Ferrier, G. D., & Rogers, J. (1994). Global optimisation of statistical functions with simulated annealing. Journal of Econometrics, 60, 65-99.

Gohner, U., Schiebl, F., Dengler, J., & Subke, J. (1998). Forward dynamics for the evaluation of practical problems in sports. Paper presented at the XVI Symposium of the ISBS, University of Konstanz, Germany.

Goodwill, S., & Haake, S. (2000a). Comparison of standard and oversize tennis balls for normal impacts on a racket. In A. J. Subic & S. J. Haake (Eds.), The Engineering of Sport (pp. 221-228). Oxford: Blackwell Science.

Goodwill, S., & Haake, S. (2000b). Modelling the impact between a tennis ball and racket using rigid body dynamics. Tennis, science & technology, 49-56.

Goodwill, S., & Haake, S. (2003). Modelling of an impact between a tennis ball and a racket. Paper presented at the Tennis Science & Technology 2, University of Roehampton, Surrey.

Goodwill, S., & Haake, S. (2004). Effect of string tension on the impact between a tennis ball and racket. The Engineering of Sport, 2(5), 3-9.

Groppel, J. L. (1984). Tennis for Advanced Players (and those who would like to be). Champaign, Illinois: Human Kinetics Publishers Inc.

Groppel, J. L., Shin, I., Thomas, J. A., & Welk, G. J. (1987). The effects of string type and tension on impact in midsized and oversized tennis rackets. International Journal of Sports Biomechanics, 3, 40-46.

Haake, S., Carre, M., & Goodwill, S. (2003). Modelling of oblique tennis ball impacts on tennis surfaces. Paper presented at the Tennis Science & Technology 2, University of Roehampton, Surrey.

Hatze, H. (1975). A new method for the simultaneous measurement of the moment of inertia, the damping coefficient and the location of the centre of mass of a body segment in situ. European Journal of Applied Physiology, 34, 217-226.

Hatze, H. (1976). Forces and duration of impact, and grip tightness during the tennis stroke. Medicine and Science in Sports, 8(2), 88-95.

Hatze, H. (1980). A mathematical model for the computational determination of parameter values of anthropomorphic segments. Journal of Biomechanics, 13, 833-843.

Hatze, H. (1981). A comprehensive model for human motion simulation and its application to the take-off phase of the long jump. Journal of Biomechanics, 14, 135-142.

Hatze, H. (1988). High-precision three-dimensional photogrammetric calibration and object space reconstruction using a modified DLT-approach. Journal of Biomechanics, 21, 533-538.

Helm, F. C. T. V. d. (1994). A finite element musculoskeletal model of the shoulder mechanism. Journal of Biomechanics, 27(5), 551-569.

Hennig, E. M., Rosenbaum, D., & Milani, T. L. (1992). Transfer of tennis racket vibrations onto the human forearm. Medicine and Science in Sports and Exercise, 24(10), 1134-1140.

Herzog, W. (1988). The relation between the resultant moments at a joint and the moments measured by an isokinetic dynamometer. Journal of Biomechanics, 21(1), 5-12.

Hiley, M. J., & Yeadon, M. R. (2005). Maximal dismounts from high bar. Journal of Biomechanics, 38, 2221-2227.

Hinrichs, R. N. (1985). Regression equations to predict segmental moments of inertia from anthropometric measurements: an extension of the data of Chandler et al. (1975). Journal of Biomechanics, 18(8), 621-624.

Hubbard, M. (1993). Computer simulation in sport and industry. Journal of Biomechanics, 26, Supplement 1, 53-61.

Hummel, S. A., & Hubbard, M. (2001). A musculoskeletal model for backhand frisbee throws. Paper presented at the VIII International Symposium on Computer Simulations in Biomechanics, University of California, Davis.

Jobe, F. W., & Nuber, G. (1986). Throwing injuries of the elbow. Clinics in Sports Medicine, 5(4), 621-636.

Jozsa, L. G., & Kannus, P. (1997). Human tendons: anatomy, physiology, and pathology (1 ed.). Champaign, IL: Human Kinetics.

Kamien, M. (1990). A rational management of tennis elbow. Sports Medicine, 9(3), 173-191.

Kamien, M. (1992). A rationale management of tennis elbow. Sports Medicine, 9, 173-191.

Kane, T. R., & Levinson, D. A. (1996). Dynamics online: Theory and implementations with AUTOLEV. Sunnyvale: Online Dynamics Inc.

Kawazoe, Y. (1997). Experimental identification of a hand-held tennis racket and prediction of rebound ball velocity in an impact. Theoretical and Applied Mechanics, 46, 177-188.

Kawazoe, Y., Tanahashi, R., & Casolo, F. (2003). Experimental and theoretical criticism of the effectiveness of looser strings for the reduction of tennis elbow. Paper presented at the Tennis Science & Technology 2, University of Roehampton, Surrey.

Kibler, W. B., & Chandler, T. J. (1994). Racquet sports. In F. Fu (Ed.), Sports Injuries, Mechanisms, Prevention, and Treatments. Baltimore: Williams & Wilkins.

King, M. A. (1998). Contributions to performance in dynamic jumps. Unpublished Doctoral Thesis, Loughborough University.

King, M. A., & Yeadon, M. R. (2002). Determining subject-specific torque parameters for use in a torque-driven simulation model of dynamic jumping. Journal of Applied Biomechanics, 18, 207-217.

Kneib, B., Schlarb, H., & Glitsch, U. (1998). Influence of racket length on tennis stroke. Paper presented at the XVI Symposium of the International Society of Biomechanics in Sports, Konstanz, Germany.

Knudson, D. V. (1988). An analysis of grip forces and three-dimensional accelerations in the tennis forehand drive. University of Wisconsin, Madison.

Knudson, D. V. (1989). Hand forces and impact effectiveness in the tennis backhand. Journal of Human Movement Studies, 17, 1-7.

Knudson, D. V. (1991a). Forces on the hand in the tennis one-handed backhand. International Journal of Sports Biomechanics, 7, 282-292.

Knudson, D. V. (1991b). Factors affecting force loading on the hand in the tennis forehand. The Journal of Sports Medicine and Physical Fitness, 31(4), 527-531.

Knudson, D. V. (2004). Biomechanical studies on the mechanism of tennis elbow. The Engineering of Sport, 1(5), 135-141.

Knudson, D. V., & Blackwell, J. (1997). Upper extremity angular kinematics of the one-handed backhand drive in tennis players with and without tennis elbow. International Journal of Sports Medicine, 18(2), 79-82.

Knudson, D. V., & White, S. C. (1989). Forces on the hand in the tennis forehand drive: application of force sensing resistors. International Journal of Sports Biomechanics, 5, 324-331.

Kong, P. W. (2005). Computer simulation of the takeoff in springboard diving. Unpublished Doctoral Thesis, Loughborough University.

Leigh, D. C., & Lu, W. (1992). Dynamics of the interactions between ball, strings, and racket in tennis. International Journal of Sports Biomechanics, 8, 181-206.

Lemay, M. A., & Crago, P. E. (1996). A dynamic model for simulating movements of the elbow, forearm, and wrist. Journal of Biomechanics, 29(10), 1319-1330.

Li, F. X., Fewtrell, D., & Jenkins, M. (2004). String vibration dampers do not reduce racket frame vibration transfer to the forearm. Journal of Sports Sciences, 22, 1041-1052.

Lieber, R. L., Woodburn, T. M., & Friden, J. (1991). Muscle damage induced by eccentric contractions of 25% strain. Journal of Applied Physiology, 70, 2498-2507.

Ljung, B. O., Lieber, R. L., & Friden, J. (1999). Wrist extensor muscle pathology in lateral epicondylitis. Journal of Hand Surgery, 24(2), 177-183.

Luca, C. J. d., & Forrest, W. J. (1973). Force analysis of individual muscles acting simultaneously on the shoulder joint during isometric abduction. Journal of Biomechanics, 6, 385-393.

Maeda, H., & Okauchi, M. (2002). The transmission of impact and vibration from tennis racket to hand. Paper presented at the 4th International Conference of Sports Engineering, Kyoto, Japan.

Matsuhisa, H., Sonoda, M., Park, J. G., & Utsuno, H. (2004). Energy analysis of tennis ball-racket collision. The Engineering of Sport, 1(5), 17-23.

McCann, P. D., & Bigliani, L. U. (1994). Shoulder pain in tennis players. Sports Medecine, 1994(1), 53-64.

McCue, F. C. (1982). The elbow, wrist, and hand, in Kuland D (ed): The injured athlete. In (pp. 295-329). Philadelphia: JB Lippincott.

McLaughlin, T. M., & Miller, N. R. (1980). Techniques for the evaluation of loads on the forearm prior to impact in tennis strokes. Journal of Mechanical Design, 102, 701-710.

Miller, S. (2006). Modern tennis rackets, balls, and surfaces. British Journal of Sports Medicine, 40, 401-405.

Mills, C. (2005). Computer simulation of gymnastic vault landings. Unpublished Doctoral Thesis, Loughborough University.

Missavage, R. J., & Baker, J. A. W. (1984). Theoretical modelling of grip firmness during ball-racket impact. Research Quarterly for Exercise and Sport, 55(3), 254-260.

Mitchell, S. R., Jones, R., & King, M. (2000). Head speed vs. racket inertia in the tennis serve. Sports Engineering, 3, 99-110.

Mungiole, M. (1990). Estimating segment inertial properties: comparison of magnetic resonance imaging with existing methods. Journal of Biomechanics, 23(10), 1039-1046.

Nab, D., Hennig, E. M., & Schnabel, G. (1998). Ball impact location on a tennis racket head and its influence on ball speed, arm shock, and vibration. Paper presented at the XVI International Symposium on Biomechanics in Sports, Konstanz, Germany.

Nelder, J. A., & Mead, R. (1965). A simplex method for function minimisation. Computer Journal, 7, 308-313.

Nesbit, S. N., Elzinga, M., Herchenroder, C., & Serrano, M. (2006). The effects of racket inertia tensor on elbow loadings and racket behaviour for central and eccentric impacts. Journal of Sports Science and Medicine, 5, 304-317.

Ng-Thow-Hing, V., & Fiume, E. (1999). B-spline solids as physical and geometric muscle models for musculoskeletal systems. Paper presented at the VIIth International Symposium on Computer Simulation in Biomechanics, Calgary, Canada.

Nigg, B. M., & Herzog, W. (1999). Biomechanics of the Musculo-skeletal System (Second Edition). Chichester: John Wiley and Sons Ltd.

Nirschl, R. P. (1974). The etiology and treatment of tennis elbow. Journal of Sports Medicine, 2, 308-319.

Osterman, A. L., Moskow, L., & Low, D. W. (1988). Soft-tissue injuries of the hand and wrist in racquet sports. Clinics in Sports Medicine, 7(2), 329-348.

Pain, M. T. G., & Challis, J. H. (2001a). The role of the heel pad and shank soft tissue during impacts: a further resolution of a paradox. Journal of Biomechanics, 34, 327-333.

Pain, M. T. G., & Challis, J. H. (2001b). High resolution determination of body segment inertial parameters and their variation due to soft tissue motion. Journal of Applied Biomechanics, 17, 326-334.

Pandy, M. G. (2003). Simple and complex models for studying muscle function in walking. Philosophical Transactions of the Royal Society of London B, 358, 1501-1509.

Priest, J. D., Braden, V., & Gererich, S. G. (1980). An analysis of players with and without pain. The Physician and Sports Medicine, 8(4), 81-91.

Renstrom, P. A. F. H. (1994). Elbow injuries in tennis. In T. Reilly, M. Hugues & A. Lees (Eds.), Science and Racket Sports. London: E&FN Spon.

Reynolds, D. D., & Angevine, E. N. (1977). Hand-arm vibration, Part2: Vibration transmition characteristics of the hand and arm. Journal of Sound and Vibration, 51(2), 255-265.

Reynolds, D. D., Standlee, K. G., Angevine, E. N. (1977). Hand-arm vibration, Part 3: Subjective response characteristics of individuals to hand-induced vibration. Journal of Sound and Vibration, 51(2), 267-282.

Riek, S., Chapman, A. E., & Milner, T. (1999). A simulation of muscle force and internal kinematics of extensor carpi radialis brevis during backhand tennis stroke: implications for injury. Clinical Biomechanics, 14, 477-483.

Roetert, E. P., Brody, H., Dillman, C. J., Groppel, J. L., & Schultheis, J. M. (1995). The biomechanics of tennis elbow. An integrated approach. Clinics in Sports Medicine, 14(1), 47-57.

Roetert, E. P., & Groppel, J. L. (2001). World-Class Tennis Technique. Leeds: Human Kinetics Publishers, Inc.

Roussopoulos, K., & Cooke, A. J. (2000). Correlation between racket design and arm injuries. A feasibility study report (Technical report prepared for the International Tennis Federation, 2000).

Ryu, R. K., McCormick, J., Jobe, F. W., Moynes, D. R., & Antonelli, D. J. (1988). An electromyographic analysis of shoulder function in tennis players. American Journal of Sports Medicine, 16(5), 481-485.

Savelberg, H. H. C. M., Otten, J. D. M., Kooloos, J. G. M., Huiskes, R., & Kauer, J. M. G. (1993). Carpal bone kinematics and ligament lengthening studies for the full range of joint movement. Journal of Biomechanics, 26(12), 1389-1402.

Schlarb, H., Kneib, B., & Glitsch, U. (1998). Modelling of the elastic racket properties in the dynamic computer simulation of tennis. Paper presented at the Proceedings of the 16th ISBS Conference, Konstanz, Germany.

Segesser, B. (1985). Sportverletzungen und Sportschaden im Ellbogenbereich (Sports injuries and sports damage in the elbow region). Deutsche Zeitschrift fur Sportmedizin, 3, 80-83.

Soest, A. J. V., Schwab, A. L., Bobbert, M. F., & Schenau, G. J. V. I. (1993). The influence of the biarticularity of the gastrocnemius muscle on vertical-jumping achievement. Journal of Biomechanics, 26, 1-8.

Sorensson, A., & Burstrom, L. (1997). Transmission of vibration energy to different parts of the human hand-arm system. Int Arch Occup Environ Health, 70, 199-204.

Stone, R. J., & Stone, J. A. (2003). Atlas of skeletal muscles (4 ed.). New York: McGraw-Hill.

Tilmanis, G. A. (1975). Advanced tennis for coaches, teachers and players. Philadelphia, Pennsylvania: Lea and Febiger.

Tomosue, R., Mutoh, Y., Yoshinari, K., & Kawazoe, Y. (1991). Measuring the vibrations of a racket handle and the wrist joint in the tennis forearm drive. Paper presented at the Abstracts from International Society of Biomechanics XIII, Perth, Australia.

Wang, L. (1998). Kinematics of upper limb and trunk in tennis players using single handed backhand strokes. Paper presented at the International Society of Biomechanics in Sport - Proceedings I.

Wang, L. H., Wu, H. W., Lo, K. C., & Su, F. C. (1998). Kinematics of upper limb and trunk in tennis players using single handed backhand strokes. Paper presented at the XVI Symposium of the ISBS, University of Konstanz, Germany.

Widing, M. A. B., & Moeinzadeh, M. H. (1990). Finite element modelling of a tennis racket with variable string patterns and tensions. International Journal of Sports Biomechanics, 6, 78-91.

Wilson, C. (2003). Optimisation of performance in running jumps. Unpublished Doctoral Thesis, Loughborough University.

Withers, R. T., Craig, N. P., Bourdon, P. C., & Norton, K. I. (1987). Relative body fat and anthropometric prediction of body density of male athletes. European Journal of Applied Physiology, 56, 191-200.

Wood, G. A. (1982). Data smoothing and differentiation procedures in biomechanics. Exercise and Sport Science, 10, 308-362.

Wood, G. A., & Jennings, L. S. (1979). On the use of spline functions for data smoothing. Journal of Biomechanics, 12, 477-479.

Wu, S. K., Gross, M. T., Prentice, W. E., & Yu, B. (2001). Comparison of ball-and-racket impact force between two tennis backhand stroke techniques. Journal of Orthopaedic & Sports Physical Therapy, 31(5), 247-254.

Yeadon, M. R. (1984). The mechanics of twisting somersaults. Unpublished Doctoral Thesis, Loughborough University.

Yeadon, M. R. (1990a). The simulation of aerial movement - I. The determination of orientation angles from film data. Journal of Biomechanics, 23(1), 59-66.

Yeadon, M. R. (1990b). The simulation of aerial movement - II: A mathematical inertia model of the human body. Journal of Biomechanics, 23, 67-74.

Yeadon, M. R., Atha, J., & Hales, F. D. (1990c). The simulation of aerial movement - IV. A computer simulation model. Journal of Biomechanics, 23(1), 85-89.

Yeadon, M. R., & Challis, J. H. (1994). The future of performance-related sports biomechanics research. Journal of Sports Sciences, 12, 3-32.

Yeadon, M. R., & King, M. A. (2002). Evaluation of a torque-driven simulation model of tumbling. Journal of Applied Biomechanics, 18, 195-206.

Yeadon, M. R., & Morlock, M. (1989). The appropriate use of regression equations for the estimation of segmental inertia parameters. Journal of Biomechanics, 22(6), 683-689.

Yue, Z., & Mester, J. (2001). A model analysis of internal loads, energetics, and effects of wobbling mass during the whole-body vibration. Journal of Biomechanics, 35, 639-647.

APPENDIX 1

AUTOLEV CODE FOR BACKHAND MODEL

```
% BACKHAND.AL
%
% THIS IS THE AUTOLEV CODE WHICH GENERATES A FORTRAN AND INPUT FILE
% NEEDED FOR THE COMPUTER SIMULATION MODEL
%--------------------------------------------------------------------
% physical declarations

NEWTONIAN N
BODIES A,B,C,D,WB,WC,E,F
FRAMES INTNA,GRIP
PARTICLES P{41:50}
POINTS O,PO,PW,PE,P{1:7},P{9:20},P{25:40},P50S,PRDO,PVM,PU,CM,RO

%--------------------------------------------------------------------
% mathematical declarations

MASS A=MA,B=MB,C=MC,D=MD,WB=MWB,WC=MWC,E=ME,F=MF, &
   P41=MP41,P42=MP42,P43=MP43,P44=MP44,P45=MP45, &
   P46=MP46,P47=MP47,P48=MP48,P49=MP49,P50=MP50
INERTIA A, IA1,IA2,IA3
INERTIA B, IB1,IB2,IB3
INERTIA C, IC1,IC2,IC3
INERTIA D, ID1,ID2,ID3
INERTIA WB, IWB1,IWB2,IWB3
INERTIA WC, IWC1,IWC2,IWC3
INERTIA E, IE1,IE2,IE3
INERTIA F, IF1,IF2,IF3
SPECIFIED ANA1",ANA2",ANA3",AAB1",AAB2", AAB3",ABC1",ABC2", &
      ABC3",ACD2",ACD3",FIXX",FIXY",FIXZ"
VARIABLES POCMX,POCMY,POCMZ,VOCMX,VOCMY,VOCMZ, &
      AOCMX,AOCMY,AOCMZ, RB{1:2},RC{1:2},FEX,FEY,FEZ,FWX,FWY,FWZ,FE,FW, &
      TORA1,TORA2,TORA3,TORB1,TORB2,TORB3,TORC1,TORC2,TORC3,TORD2,TORD3, &
      Q{36}',U{44}', &
      POPOX,POPOY,POPOZ,POP{1:7}X,POP{1:7}Y,POP{1:7}Z, &
      POP{9:20}X,POP{9:20}Y,POP{9:20}Z,POP{25:40}X,POP{25:40}Y,POP{25:40}Z, &
      POPEX,POPEY,POPEZ,POPWX,POPWY,POPWZ,POPRDOX,POPRDOY,POPRDOZ, &
      POPVMX,POPVMY,POPVMZ,VPVMX,VPVMY,VPVMZ,APVMX,APVMY,APVMZ, &
      LP1P3,LP2P4,LP2P6,LP5P7,VP1P3,VP2P4,VP2P6,VP5P7,LOPO,VOPO, &
      YB45,YB45D,YB49,YB49D,YB46,YB46D,YB48,YB48D, &
      L4041,L4139,L4144,L4241,L2942,L4245,L4342,L3043, &
      L4346,L3143,L4438,L4447,L4544,L4548,L4645,L4649, &
      L3246,L4737,L4736,L4847,L4835,L4948,L4934,L3349, &
      ST4041,ST4139,ST4144,ST4241,ST2942,ST4245,ST4342,ST3043, &
      ST4346,ST3143,ST4438,ST4447,ST4544,ST4548,ST4645,ST4649, &
      ST3246,ST4737,ST4736,ST4847,ST4835,ST4948,ST4934,ST3349, &
      R45N,R49N,R46N,R48N,TOREF1,TOREF2,TORE3, &
      R9H,R10H,R11H,R12H,R13H,R14H,R15T,R16T,R17T,R18T,R19T,R20T, &
      L9H,L10H,L11H,L12H,L13H,L14H,L15T,L16T,L17T,L18T,L19T,L20T, &
      L9HD,L10HD,L11HD,L12HD,L13HD,L14HD,L15TD,L16TD,L17TD,L18TD, &
      L19TD,L20TD, B11,B12,B13,B21,B22,B23,B31,B32,B33 , &
      C11,C12,C13,C21,C22,C23,C31,C32,C33, &
```

```
        D11,D12,D13,D21,D22,D23,D31,D32,D33, &
        VP50,VP50X,VP50Y,VP50Z,W1,W2, &
        VELPWX,VELPWY,VELPWZ,VELPEX,VELPEY,VELPEZ,VELP1X,VELP1Y,VELP1Z, &
        APRDOE1,APRDOE2,APRDOE3,APU,AP26X,AP26Y,AP26Z,AP27X,AP27Y,AP27Z, &
        GALFENX,GALFENY,GALFENZ,LALFENX,LALFENY,LALFENZ, &
        LAROX,LAROY,LAROY,FHX,FHY,FHZ,FTX,FTY,FTZ, RHX,RHY,RHZ,RTX,RTY,RTZ
CONSTANTS L{1:35},G,KB,CB,KC,CC,KS{1:4},K{5:10},R9H0,R11H0,R13H0,R15T0, &
        R17T0,R19T0,TORE30,KH,KT,CH,CT,KF{1:3},KTOREF1,CTOREF1, &
        KTOREF2,CTOREF2,KTORE ,CTORE,VINY, &
        RACKANG0,RACKANGVEL0,RH0,RT0,ST0,T0,T1,T2,RSC,CONST20,
        CONST21,CONST22, L9H0,L10H0,L11H0,L12H0,L13H0, &
        L14H0,L15T0,L16T0,L17T0,L18T0,L19T0,L20T0

%-----------------------------------------------------------------
% simplify

AUTOZ ON
ZEE_NOT =
[FEX,FEY,FEZ,FWX,FWY,FWZ,TORB1,TORB2,TORB3,TORC1,TORC2,TORC3,TORD2,TORD3]

%-----------------------------------------------------------------
% geometry relating unit vectors

DIRCOS(N,INTNA,BODY321,ANA3,ANA2,ANA1)
DIRCOS(INTNA,A,BODY321,-PI/2,-PI/2,0)
DIRCOS(A,B,BODY321,AAB3,AAB2,AAB1)
DIRCOS(B,C,BODY321,ABC3,ABC2,ABC1)
DIRCOS(B,WB,BODY321,Q3,Q5,0)
DIRCOS(C,D,BODY321,ACD3,ACD2,0)
DIRCOS(C,WC,BODY321,Q8,Q10,0)
DIRCOS(D,E,BODY321,Q20,Q21,Q22)
DIRCOS(D,GRIP,BODY321,CONST20,CONST21,CONST22)
DIRCOS(E,F,BODY321,0,Q23,Q24)

%-----------------------------------------------------------------
% AL angles for simple rotations

ANA1 = T^3
ANA2 = T^3
ANA3 = T^3
AAB1 = T^3
AAB2 = T^3
AAB3 = T^3
ABC1 = T^3
ABC2 = T^3
ABC3 = T^3
ACD2 = T^3
ACD3 = T^3

%-----------------------------------------------------------------
% position vectors

P_O_PO> = FIXX*N1> + FIXY*N2> + FIXZ*N3>

FIXX = T^3
FIXY = T^3
FIXZ = T^3

P_PO_AO> = (L1/L2)*A1>
P_PO_P1> = L2*A1>
```

P_P1_BO> = L3*B1>
P_P1_P2> = L4*B1>

P_P1_P3> = Q1*B1> + Q2*B2> + Q4*B3>
P_P3_WBO> = L5*WB1>
P_P3_P4> = L4*WB1>

P_P2_PE> = Q11*C1> + Q12*C2> + Q13*C3>
P_PE_CO> = L6*C1>
P_PE_P5> = L7*C1>

P_PE_P6> = Q6*C1> + Q7*C2> + Q9*C3>
P_P6_WCO> = L8*WC1>
P_P6_P7> = L7*WC1>

P_P5_PW> = Q14*D1> + Q15*D2> + Q16*D3>
P_PW_DO> = L9*D1> + L35*D2>

P_DO_P9> = L10*GRIP1> + L11*GRIP2> + L12*GRIP3>
P_P9_PRDO> = Q17*E1> + Q18*E2> + Q19*E3>
P_P25_PRDO> = L13*E3>
P_P26_PRDO> = L14*E3>
P_PRDO_P27> = L14*E3>
P_P9_P10> = -2*L10*GRIP1>
P_P10_P16> = 2*L14*GRIP3>
P_P16_P15> = 2*L10*GRIP1>
P_P9_P11> = -L10*GRIP1> - L10*GRIP2>
P_P11_P12> = 2*L10*GRIP2>
P_P12_P18> = 2*L14*GRIP3>
P_P18_P17> = -2*L10*GRIP2>

P_P17_P19> = L10*GRIP2> - L10*GRIP3>
P_P19_P20> = 2*L10*GRIP3>
P_P11_P13> = L10*GRIP2> - L10*GRIP3>
P_P13_P14> = 2*L10*GRIP3>

P_P25_EO> = L15*E3>
P_P25_P28> = L16*E3>
P_P28_P29> = L17*F3>
P_P28_FO> = L18*F3>
P_P28_RO> = L34*F3>
P_P29_P30> = L19*F3> + L21*F1>
P_P30_P31> = L20*F3> + L22*F1>
P_P31_P32> = L24*F3> + L23*F1>
P_P32_P33> = L25*F3> - L26*F1>
P_P33_P34> = L28*F3> - L27*F1>

P_P25_PU> = L32*E3> + L33*E1>

P_P33_PVM> = L30*F1> + L31*F3>

P_P34_P35> = L29*F3> - L21*F1>
P_P35_P36> = -L29*F3> - L21*F1>
P_P36_P37> = -L28*F3> - L27*F1>
P_P37_P38> = -L25*F3> - L26*F1>
P_P38_P39> = -L24*F3> + L23*F1>
P_P39_P40> = -L20*F3> + L22*F1>
P_P29_P41> = -L21*F1> + Q25*F2> + (L19+L20)*F3>
P_P29_P42> = Q26*F2> + (L19+L20)*F3>

```
P_P29_P43> = L21*F1> + Q27*F2> + (L19+L20)*F3>
P_P29_P44> = -L21*F1> + Q28*F2> + (L19+L20+L24)*F3>
P_P29_P45> = Q29*F2> + (L19+L20+L24)*F3>
P_P29_P46> = L21*F1> + Q30*F2> + (L19+L20+L24)*F3>
P_P29_P47> = -L21*F1> + Q31*F2> + (L19+L20+L24+L25)*F3>
P_P29_P48> = Q32*F2> + (L19+L20+L24+L25)*F3>
P_P29_P49> = L21*F1> + Q33*F2> + (L19+L20+L24+L25)*F3>
P_O_P50> = Q34*N1> + Q35*N2> + Q36*N3>

P_P45_P50S> = P_P45_P50> - RSC*YB45*F2>
P_P49_P50S> = P_P49_P50> - RSC*YB49*F2>
P_P46_P50S> = P_P46_P50> - RSC*YB46*F2>
P_P48_P50S> = P_P48_P50> - RSC*YB48*F2>

%-----------------------------------------------------------------
% X,Y,Z co-ordinates of points

POPOX = DOT(P_O_PO>, N1>)
POPOY = DOT(P_O_PO>, N2>)
POPOZ = DOT(P_O_PO>, N3>)
POP1X = DOT(P_O_P1>, N1>)
POP1Y = DOT(P_O_P1>, N2>)
POP1Z = DOT(P_O_P1>, N3>)
POP2X = DOT(P_O_P2>, N1>)
POP2Y = DOT(P_O_P2>, N2>)
POP2Z = DOT(P_O_P2>, N3>)
POP3X = DOT(P_O_P3>, N1>)
POP3Y = DOT(P_O_P3>, N2>)
POP3Z = DOT(P_O_P3>, N3>)
POP4X = DOT(P_O_P4>, N1>)
POP4Y = DOT(P_O_P4>, N2>)
POP4Z = DOT(P_O_P4>, N3>)
POP5X = DOT(P_O_P5>, N1>)
POP5Y = DOT(P_O_P5>, N2>)
POP5Z = DOT(P_O_P5>, N3>)
POP6X = DOT(P_O_P6>, N1>)
POP6Y = DOT(P_O_P6>, N2>)
POP6Z = DOT(P_O_P6>, N3>)
POP7X = DOT(P_O_P7>, N1>)
POP7Y = DOT(P_O_P7>, N2>)
POP7Z = DOT(P_O_P7>, N3>)
POP9X = DOT(P_O_P9>, N1>)
POP9Y = DOT(P_O_P9>, N2>)
POP9Z = DOT(P_O_P9>, N3>)
POP10X = DOT(P_O_P10>, N1>)
POP10Y = DOT(P_O_P10>, N2>)
POP10Z = DOT(P_O_P10>, N3>)
POP11X = DOT(P_O_P11>, N1>)
POP11Y = DOT(P_O_P11>, N2>)
POP11Z = DOT(P_O_P11>, N3>)
POP12X = DOT(P_O_P12>, N1>)
POP12Y = DOT(P_O_P12>, N2>)
POP12Z = DOT(P_O_P12>, N3>)
POP13X = DOT(P_O_P13>, N1>)
POP13Y = DOT(P_O_P13>, N2>)
POP13Z = DOT(P_O_P13>, N3>)
POP14X = DOT(P_O_P14>, N1>)
POP14Y = DOT(P_O_P14>, N2>)
POP14Z = DOT(P_O_P14>, N3>)
POP15X = DOT(P_O_P15>, N1>)
```

POP15Y = DOT(P_O_P15>, N2>)
POP15Z = DOT(P_O_P15>, N3>)
POP16X = DOT(P_O_P16>, N1>)
POP16Y = DOT(P_O_P16>, N2>)
POP16Z = DOT(P_O_P16>, N3>)
POP17X = DOT(P_O_P17>, N1>)
POP17Y = DOT(P_O_P17>, N2>)
POP17Z = DOT(P_O_P17>, N3>)
POP18X = DOT(P_O_P18>, N1>)
POP18Y = DOT(P_O_P18>, N2>)
POP18Z = DOT(P_O_P18>, N3>)
POP19X = DOT(P_O_P19>, N1>)
POP19Y = DOT(P_O_P19>, N2>)
POP19Z = DOT(P_O_P19>, N3>)
POP20X = DOT(P_O_P20>, N1>)
POP20Y = DOT(P_O_P20>, N2>)
POP20Z = DOT(P_O_P20>, N3>)
POP25X = DOT(P_O_P25>, N1>)
POP25Y = DOT(P_O_P25>, N2>)
POP25Z = DOT(P_O_P25>, N3>)
POP26X = DOT(P_O_P26>, N1>)
POP26Y = DOT(P_O_P26>, N2>)
POP26Z = DOT(P_O_P26>, N3>)
POP27X = DOT(P_O_P27>, N1>)
POP27Y = DOT(P_O_P27>, N2>)
POP27Z = DOT(P_O_P27>, N3>)
POP28X = DOT(P_O_P28>, N1>)
POP28Y = DOT(P_O_P28>, N2>)
POP28Z = DOT(P_O_P28>, N3>)
POP29X = DOT(P_O_P29>, N1>)
POP29Y = DOT(P_O_P29>, N2>)
POP29Z = DOT(P_O_P29>, N3>)
POP30X = DOT(P_O_P30>, N1>)
POP30Y = DOT(P_O_P30>, N2>)
POP30Z = DOT(P_O_P30>, N3>)
POP31X = DOT(P_O_P31>, N1>)
POP31Y = DOT(P_O_P31>, N2>)
POP31Z = DOT(P_O_P31>, N3>)
POP32X = DOT(P_O_P32>, N1>)
POP32Y = DOT(P_O_P32>, N2>)
POP32Z = DOT(P_O_P32>, N3>)
POP33X = DOT(P_O_P33>, N1>)
POP33Y = DOT(P_O_P33>, N2>)
POP33Z = DOT(P_O_P33>, N3>)
POP34X = DOT(P_O_P34>, N1>)
POP34Y = DOT(P_O_P34>, N2>)
POP34Z = DOT(P_O_P34>, N3>)
POP35X = DOT(P_O_P35>, N1>)
POP35Y = DOT(P_O_P35>, N2>)
POP35Z = DOT(P_O_P35>, N3>)
POP36X = DOT(P_O_P36>, N1>)
POP36Y = DOT(P_O_P36>, N2>)
POP36Z = DOT(P_O_P36>, N3>)
POP37X = DOT(P_O_P37>, N1>)
POP37Y = DOT(P_O_P37>, N2>)
POP37Z = DOT(P_O_P37>, N3>)
POP38X = DOT(P_O_P38>, N1>)
POP38Y = DOT(P_O_P38>, N2>)
POP38Z = DOT(P_O_P38>, N3>)
POP39X = DOT(P_O_P39>, N1>)

```
POP39Y = DOT(P_O_P39>, N2>)
POP39Z = DOT(P_O_P39>, N3>)
POP40X = DOT(P_O_P40>, N1>)
POP40Y = DOT(P_O_P40>, N2>)
POP40Z = DOT(P_O_P40>, N3>)
POP41X = DOT(P_O_P41>, N1>)
POP41Y = DOT(P_O_P41>, N2>)
POP41Z = DOT(P_O_P41>, N3>)
POP42X = DOT(P_O_P42>, N1>)
POP42Y = DOT(P_O_P42>, N2>)
POP42Z = DOT(P_O_P42>, N3>)
POP43X = DOT(P_O_P43>, N1>)
POP43Y = DOT(P_O_P43>, N2>)
POP43Z = DOT(P_O_P43>, N3>)
POP44X = DOT(P_O_P44>, N1>)
POP44Y = DOT(P_O_P44>, N2>)
POP44Z = DOT(P_O_P44>, N3>)
POP45X = DOT(P_O_P45>, N1>)
POP45Y = DOT(P_O_P45>, N2>)
POP45Z = DOT(P_O_P45>, N3>)
POP46X = DOT(P_O_P46>, N1>)
POP46Y = DOT(P_O_P46>, N2>)
POP46Z = DOT(P_O_P46>, N3>)
POP47X = DOT(P_O_P47>, N1>)
POP47Y = DOT(P_O_P47>, N2>)
POP47Z = DOT(P_O_P47>, N3>)
POP48X = DOT(P_O_P48>, N1>)
POP48Y = DOT(P_O_P48>, N2>)
POP48Z = DOT(P_O_P48>, N3>)
POP49X = DOT(P_O_P49>, N1>)
POP49Y = DOT(P_O_P49>, N2>)
POP49Z = DOT(P_O_P49>, N3>)
POPVMX = DOT(P_O_PVM>, N1>)
POPVMY = DOT(P_O_PVM>, N2>)
POPVMZ = DOT(P_O_PVM>, N3>)
POPEX = DOT(P_O_PE>, N1>)
POPEY = DOT(P_O_PE>, N2>)
POPEZ = DOT(P_O_PE>, N3>)
POPWX = DOT(P_O_PW>, N1>)
POPWY = DOT(P_O_PW>, N2>)
POPWZ = DOT(P_O_PW>, N3>)
POPRDOX = DOT(P_O_PRDO>, N1>)
POPRDOY = DOT(P_O_PRDO>, N2>)
POPRDOZ = DOT(P_O_PRDO>, N3>)

%-----------------------------------------------------------------
% centre of mass of the system

P_O_CM> = CM(O)
POCMX = DOT(P_O_CM>,N1>)
POCMY = DOT(P_O_CM>,N2>)
POCMZ = DOT(P_O_CM>,N3>)

%-----------------------------------------------------------------
% wobbling mass displacements and velocities

LP1P3 = MAG(P_P1_P3>)
LP2P4 = MAG(P_P2_P4>)
LP2P6 = MAG(P_P2_P6>)
LP5P7 = MAG(P_P5_P7>)
```

```
VP1P3 = DT(LP1P3)
VP2P4 = DT(LP2P4)
VP2P6 = DT(LP2P6)
VP5P7 = DT(LP5P7)

%--------------------------------------------------------------------
% kinematical differential equations

Q1' = U1
Q2' = U2
Q3' = U3
Q4' = U4
Q5' = U5
Q6' = U6
Q7' = U7
Q8' = U8
Q9' = U9
Q10' = U10
Q11' = U11
Q12' = U12
Q13' = U13
Q14' = U14
Q15' = U15
Q16' = U16
Q17' = U17
Q18' = U18
Q19' = U19
Q20' = U20
Q21' = U21
Q22' = U22
Q23' = U23
Q24' = U24
Q25' = U25
Q26' = U26
Q27' = U27
Q28' = U28
Q29' = U29
Q30' = U30
Q31' = U31
Q32' = U32
Q33' = U33
Q34' = U34
Q35' = U35
Q36' = U36

%--------------------------------------------------------------------
% displacements and velocities of ball COM perpendicular to stringbed

YB45 = Q35 - POP45Y
YB49 = Q35 - POP49Y
YB46 = Q35 - POP46Y
YB48 = Q35 - POP48Y

YB45D = DT(YB45)
YB49D = DT(YB49)
YB46D = DT(YB46)
YB48D = DT(YB48)
```

```
%-----------------------------------------------------------------
% lengths of 'strings'

L4041 = MAG(P_P40_P41>)
L4139 = MAG(P_P41_P39>)
L4144 = MAG(P_P41_P44>)
L4241 = MAG(P_P42_P41>)
L2942 = MAG(P_P29_P42>)
L4245 = MAG(P_P42_P45>)
L4342 = MAG(P_P43_P42>)
L3043 = MAG(P_P30_P43>)
L4346 = MAG(P_P43_P46>)
L3143 = MAG(P_P31_P43>)
L4438 = MAG(P_P44_P38>)
L4447 = MAG(P_P44_P47>)
L4544 = MAG(P_P45_P44>)
L4548 = MAG(P_P45_P48>)
L4645 = MAG(P_P46_P45>)
L4649 = MAG(P_P46_P49>)
L3246 = MAG(P_P32_P46>)
L4737 = MAG(P_P47_P37>)
L4736 = MAG(P_P47_P36>)
L4847 = MAG(P_P48_P47>)
L4835 = MAG(P_P48_P35>)
L4948 = MAG(P_P49_P48>)
L4934 = MAG(P_P49_P34>)
L3349 = MAG(P_P33_P49>)

%-----------------------------------------------------------------
% distances between racket handle and thenar eminences

L9H = MAG(P_P9_P26>)
L10H = MAG(P_P10_P26>)
L11H = MAG(P_P11_P26>)
L12H = MAG(P_P12_P26>)
L13H = MAG(P_P13_P26>)
L14H = MAG(P_P14_P26>)
L15T = MAG(P_P15_P27>)
L16T = MAG(P_P16_P27>)
L17T = MAG(P_P17_P27>)
L18T = MAG(P_P18_P27>)
L19T = MAG(P_P19_P27>)
L20T = MAG(P_P20_P27>)

L9HD = DT(L9H)
L10HD = DT(L10H)
L11HD = DT(L11H)
L12HD = DT(L12H)
L13HD = DT(L13H)
L14HD = DT(L14H)
L15TD = DT(L15T)
L16TD = DT(L16T)
L17TD = DT(L17T)
L18TD = DT(L18T)
L19TD = DT(L19T)
L20TD = DT(L20T)
```

```
%----------------------------------------------------------------------
% matrix coefficients for angvel calculations

B11 = DOT(A1>,B1>)
B12 = DOT(A1>,B2>)
B13 = DOT(A1>,B3>)
B21 = DOT(A2>,B1>)
B22 = DOT(A2>,B2>)
B23 = DOT(A2>,B3>)
B31 = DOT(A3>,B1>)
B32 = DOT(A3>,B2>)
B33 = DOT(A3>,B3>)

C11 = DOT(B1>,C1>)
C12 = DOT(B1>,C2>)
C13 = DOT(B1>,C3>)
C21 = DOT(B2>,C1>)
C22 = DOT(B2>,C2>)
C23 = DOT(B2>,C3>)
C31 = DOT(B3>,C1>)
C32 = DOT(B3>,C2>)
C33 = DOT(B3>,C3>)

D11 = DOT(C1>,D1>)
D12 = DOT(C1>,D2>)
D13 = DOT(C1>,D3>)
D21 = DOT(C2>,D1>)
D22 = DOT(C2>,D2>)
D23 = DOT(C2>,D3>)
D31 = DOT(C3>,D1>)
D32 = DOT(C3>,D2>)
D33 = DOT(C3>,D3>)

%----------------------------------------------------------------------
% rotation - angular velocities and accelerations

ANGVEL(N,INTNA,BODY321,ANA3,ANA2,ANA1)
ALF_INTNA_N> = DT(W_INTNA_N>,INTNA)

W_A_INTNA> = 0>
W_A_N> = W_A_INTNA> + W_INTNA_N>
ALF_A_N> = DT(W_A_N>,N)

W_B_A> = (B13*DT(B12) + B23*DT(B22) + B33*DT(B32) + U37)*B1> + (B11*DT(B13) + &
B21*DT(B23) + B31*DT(B33) + U38)*B2> + (B12*DT(B11) + B22*DT(B21) + B32*DT(B31) + &
U39)*B3>
W_B_N> = W_B_A> + W_A_N>
ALF_B_N> = DT(W_B_N>,N)

W_C_B> = (C13*DT(C12) + C23*DT(C22) + C33*DT(C32) + U40)*C1> + (C11*DT(C13) +
C21*DT(C23) + C31*DT(C33) + U41)*C2> + (C12*DT(C11) + C22*DT(C21) + C32*DT(C31) +
U42)*C3>
W_C_N> = W_C_B> + W_B_N>
ALF_C_N> = DT(W_C_N>,N)

ANGVEL(B,WB,BODY321,Q3,Q5,0)
W_WB_N> = W_WB_B> + W_B_N>
ALF_WB_N> = DT(W_WB_N>,N)
```

```
W_D_C> = (D13*DT(D12) + D23*DT(D22) + D33*DT(D32))*D1> + (D11*DT(D13) +
D21*DT(D23) + D31*DT(D33) + U43)*D2> + (D12*DT(D11) + D22*DT(D21) + D32*DT(D31) +
U44)*D3>
W_D_N> = W_D_C> + W_C_N>
ALF_D_N> = DT(W_D_N>,N)

ANGVEL(C,WC,BODY321,Q8,Q10,0)
W_WC_N> = W_WC_C> + W_C_N>
ALF_WC_N> = DT(W_WC_N>,N)

ANGVEL(D,E,BODY321,Q20,Q21,Q22)
W_E_N> = W_E_D> + W_D_N>
ALF_E_N> = DT(W_E_N>,N)

W_GRIP_D> = 0>
W_GRIP_N> = W_GRIP_D> + W_D_N>
ALF_GRIP_N> = DT(W_GRIP_N>,N)

ANGVEL(E,F,BODY321,0,Q23,Q24)
W_F_N> = W_F_E> + W_E_N>
ALF_F_N> = DT(W_F_N>,N)

GALFENX = DOT(ALF_E_N>,N1>)
GALFENY = DOT(ALF_E_N>,N2>)
GALFENZ = DOT(ALF_E_N>,N3>)
LALFENX = DOT(ALF_E_N>,E1>)
LALFENY = DOT(ALF_E_N>,E2>)
LALFENZ = DOT(ALF_E_N>,E3>)

%----------------------------------------------------------------------
% translation - linear velocities and accelerations

V_O_N> = 0>
V_PO_N> = DT(P_O_PO>,N)
EXPRESS(V_PO_N>,A)
V2PTS(N,A,PO,AO)
EXPRESS(V_AO_N>,A)
V2PTS(N,A,PO,P1)

VELP1X = DOT(V_P1_N>, N1>)
VELP1Y = DOT(V_P1_N>, N2>)
VELP1Z = DOT(V_P1_N>, N3>)

V2PTS(N,B,P1,BO)
EXPRESS(V_BO_N>,B)
V2PTS(N,B,P1,P2)
EXPRESS(V_P2_N>,B)

V_P3_N> = DT(P_O_P3>,N)
EXPRESS(V_P3_N>,WB)
V2PTS(N,WB,P3,WBO)
EXPRESS(V_WBO_N>,WB)
V2PTS(N,WB,P3,P4)
EXPRESS(V_P4_N>,WB)

V_PE_N> = DT(P_O_PE>,N)
V2PTS(N,C,PE,CO)
EXPRESS(V_CO_N>,C)
V2PTS(N,C,PE,P5)
EXPRESS(V_P5_N>,C)
```

```
VELPEX = DOT(V_PE_N>, N1>)
VELPEY = DOT(V_PE_N>, N2>)
VELPEZ = DOT(V_PE_N>, N3>)

V_P6_N> = DT(P_O_P6>,N)
EXPRESS(V_P6_N>,WC)
V2PTS(N,WC,P6,WCO)
EXPRESS(V_WCO_N>,WC)
V2PTS(N,WC,P6,P7)
EXPRESS(V_P7_N>,WC)

V_PW_N> = DT(P_O_PW>,N)

VELPWX = DOT(V_PW_N>, N1>)
VELPWY = DOT(V_PW_N>, N2>)
VELPWZ = DOT(V_PW_N>, N3>)

V2PTS(N,D,PW,DO)
EXPRESS(V_DO_N>,D)
V2PTS(N,D,PW,P9)
EXPRESS(V_P9_N>,D)
V2PTS(N,D,PW,P10)
EXPRESS(V_P10_N>,D)
V2PTS(N,D,PW,P11)
EXPRESS(V_P11_N>,D)
V2PTS(N,D,PW,P12)
EXPRESS(V_P12_N>,D)
V2PTS(N,D,PW,P13)
EXPRESS(V_P13_N>,D)
V2PTS(N,D,PW,P14)
EXPRESS(V_P14_N>,D)
V2PTS(N,D,PW,P15)
EXPRESS(V_P15_N>,D)
V2PTS(N,D,PW,P16)
EXPRESS(V_P16_N>,D)
V2PTS(N,D,PW,P17)
EXPRESS(V_P17_N>,D)
V2PTS(N,D,PW,P18)
EXPRESS(V_P18_N>,D)
V2PTS(N,D,PW,P19)
EXPRESS(V_P19_N>,D)
V2PTS(N,D,PW,P20)
EXPRESS(V_P20_N>,D)

V_PRDO_N> = DT(P_O_PRDO>,N)
EXPRESS(V_PRDO_N>,E)
V2PTS(N,E,PRDO,P25)
EXPRESS(V_P25_N>,E)
V2PTS(N,E,PRDO,P26)
EXPRESS(V_P26_N>,E)
V2PTS(N,E,PRDO,P27)
EXPRESS(V_P27_N>,E)
V2PTS(N,E,PRDO,EO)
EXPRESS(V_EO_N>,E)
V2PTS(N,E,PRDO,P28)
EXPRESS(V_P28_N>,E)
V2PTS(N,E,PRDO,PU)
EXPRESS(V_PU_N>,E)
```

```
V2PTS(N,F,P28,FO)
EXPRESS(V_FO_N>,F)
V2PTS(N,F,P28,RO)
EXPRESS(V_RO_N>,F)
V2PTS(N,F,P28,P29)
EXPRESS(V_P29_N>,F)
V2PTS(N,F,P28,P30)
EXPRESS(V_P30_N>,F)
V2PTS(N,F,P28,P31)
EXPRESS(V_P31_N>,F)
V2PTS(N,F,P28,P32)
EXPRESS(V_P32_N>,F)
V2PTS(N,F,P28,P33)
EXPRESS(V_P33_N>,F)

V2PTS(N,F,P28,PVM)
VPVMX = DOT(V_PVM_N>,N1>)
VPVMY = DOT(V_PVM_N>,N2>)
VPVMZ = DOT(V_PVM_N>,N3>)

V2PTS(N,F,P28,P34)
EXPRESS(V_P34_N>,F)
V2PTS(N,F,P28,P35)
EXPRESS(V_P35_N>,F)
V2PTS(N,F,P28,P36)
EXPRESS(V_P36_N>,F)
V2PTS(N,F,P28,P37)
EXPRESS(V_P37_N>,F)
V2PTS(N,F,P28,P38)
EXPRESS(V_P38_N>,F)
V2PTS(N,F,P28,P39)
EXPRESS(V_P39_N>,F)
V2PTS(N,F,P28,P40)
EXPRESS(V_P40_N>,F)
V_P41_N> = DT(P_O_P41>,N)
EXPRESS(V_P41_N>,F)
V_P42_N> = DT(P_O_P42>,N)
EXPRESS(V_P42_N>,F)
V_P43_N> = DT(P_O_P43>,N)
EXPRESS(V_P43_N>,F)
V_P44_N> = DT(P_O_P44>,N)
EXPRESS(V_P44_N>,F)
V_P45_N> = DT(P_O_P45>,N)
EXPRESS(V_P45_N>,F)
V_P46_N> = DT(P_O_P46>,N)
EXPRESS(V_P46_N>,F)
V_P47_N> = DT(P_O_P47>,N)
EXPRESS(V_P47_N>,F)
V_P48_N> = DT(P_O_P48>,N)
EXPRESS(V_P48_N>,F)
V_P49_N> = DT(P_O_P49>,N)
EXPRESS(V_P49_N>,F)
V_P50_N> = DT(P_O_P50>,N)
EXPRESS(V_P50_N>,F)

V_CM_N> = DT(P_O_CM>,N)
VOCMX = DOT(V_CM_N>,N1>)
VOCMY = DOT(V_CM_N>,N2>)
VOCMZ = DOT(V_CM_N>,N3>)
```

```
A_O_N> = 0>
A_PO_N> = DT(V_PO_N>,N)
EXPRESS(A_PO_N>,A)
A2PTS(N,A,PO,AO)
EXPRESS(A_AO_N>,A)
A2PTS(N,A,PO,P1)
EXPRESS(A_P1_N>,A)

A2PTS(N,B,P1,BO)
A2PTS(N,B,P1,P2)

A_PE_N> = DT(V_PE_N>,N)
A2PTS(N,C,PE,CO)
A2PTS(N,C,PE,P5)

A_P3_N> = DT(V_P3_N>,N)
A2PTS(N,WB,P3,WBO)
A2PTS(N,WB,P3,P4)

A_P6_N> = DT(V_P6_N>,N)
A2PTS(N,WC,P6,WCO)
A2PTS(N,WC,P6,P7)

A_PW_N> = DT(V_PW_N>,N)
A2PTS(N,D,PW,DO)
A2PTS(N,D,PW,P9)
A2PTS(N,D,PW,P10)
A2PTS(N,D,PW,P11)
A2PTS(N,D,PW,P12)
A2PTS(N,D,PW,P13)
A2PTS(N,D,PW,P14)
A2PTS(N,D,PW,P15)
A2PTS(N,D,PW,P16)
A2PTS(N,D,PW,P17)
A2PTS(N,D,PW,P18)
A2PTS(N,D,PW,P19)
A2PTS(N,D,PW,P20)

A_PRDO_N> = DT(V_PRDO_N>,N)

APRDOE1 = DOT(A_PRDO_N>,E1>)
APRDOE2 = DOT(A_PRDO_N>,E2>)
APRDOE3 = DOT(A_PRDO_N>,E3>)

A2PTS(N,E,PRDO,P25)
A2PTS(N,E,PRDO,P26)
A2PTS(N,E,PRDO,P27)

AP26X = DOT(A_P26_N>,N1>)
AP26Y = DOT(A_P26_N>,N2>)
AP26Z = DOT(A_P26_N>,N3>)
AP27X = DOT(A_P27_N>,N1>)
AP27Y = DOT(A_P27_N>,N2>)
AP27Z = DOT(A_P27_N>,N3>)

A2PTS(N,E,PRDO,EO)
A2PTS(N,E,PRDO,P28)
A2PTS(N,E,PRDO,PU)

APU = DOT(A_PU_N>,E2>)
```

```
A2PTS(N,F,P28,FO)

A2PTS(N,F,P28,RO)
GAROX = DOT(A_RO_N>,N1>)
GAROY = DOT(A_RO_N>,N2>)
GAROZ = DOT(A_RO_N>,N3>)
LAROX = DOT(A_RO_N>,F1>)
LAROY = DOT(A_RO_N>,F2>)
LAROZ = DOT(A_RO_N>,F3>)

A2PTS(N,F,P28,P29)
A2PTS(N,F,P28,P30)
A2PTS(N,F,P28,P31)
A2PTS(N,F,P28,P32)
A2PTS(N,F,P28,P33)

A2PTS(N,F,P28,PVM)
APVMX = DOT(A_PVM_N>,N1>)
APVMY = DOT(A_PVM_N>,N2>)
APVMZ = DOT(A_PVM_N>,N3>)

A2PTS(N,F,P28,P34)
A2PTS(N,F,P28,P35)
A2PTS(N,F,P28,P36)
A2PTS(N,F,P28,P37)
A2PTS(N,F,P28,P38)
A2PTS(N,F,P28,P39)
A2PTS(N,F,P28,P40)
A_P41_N> = DT(V_P41_N>,N)
A_P42_N> = DT(V_P42_N>,N)
A_P43_N> = DT(V_P43_N>,N)
A_P44_N> = DT(V_P44_N>,N)
A_P45_N> = DT(V_P45_N>,N)
A_P46_N> = DT(V_P46_N>,N)
A_P47_N> = DT(V_P47_N>,N)
A_P48_N> = DT(V_P48_N>,N)
A_P49_N> = DT(V_P49_N>,N)
A_P50_N> = DT(V_P50_N>,N)

A_CM_N> = DT(V_CM_N>,N)
AOCMX = DOT(A_CM_N>,N1>)
AOCMY = DOT(A_CM_N>,N2>)
AOCMZ = DOT(A_CM_N>,N3>)

%----------------------------------------------------------------
% auxiliary constraints

AUXILIARY[1] = U11
AUXILIARY[2] = U12
AUXILIARY[3] = U13
AUXILIARY[4] = U14
AUXILIARY[5] = U15
AUXILIARY[6] = U16
AUXILIARY[7] = U37
AUXILIARY[8] = U38
AUXILIARY[9] = U39
AUXILIARY[10] = U40
AUXILIARY[11] = U41
AUXILIARY[12] = U42
```

```
AUXILIARY[13] = U43
AUXILIARY[14] = U44
CONSTRAIN (AUXILIARY[U11,U12,U13,U14,U15,U16,U37,U38,U39,U40,U41,U42,U43,U44])

%-----------------------------------------------------------
% forces

GRAVITY(G*N3>)

% quintic functions

W1 = (T - T0)/(T1 - T0)
W2 = 1 - (T - T0)/(T2 - T0)

% forces acting between the racket handle and thenar/hypothenar eminences

R9H = KH*(L9H0 - L9H + (RH0/KH)) - CH*L9HD*ABS(L9H0 - L9H) + R9H0*(6*W2^5 -
15*W2^4 + 10*W2^3)
R10H = KH*(L10H0 - L10H + (RH0/KH)) - CH*L10HD*ABS(L10H0 - L10H)
R11H = KH*(L11H0 - L11H + (RH0/KH)) - CH*L11HD*ABS(L11H0 - L11H) + R11H0*(6*W2^5 -
15*W2^4 + 10*W2^3)
R12H = KH*(L12H0 - L12H + (RH0/KH)) - CH*L12HD*ABS(L12H0 - L12H)
R13H = KH*(L13H0 - L13H + (RH0/KH)) - CH*L13HD*ABS(L13H0 - L13H) + R13H0*(6*W2^5 -
15*W2^4 + 10*W2^3)
R14H = KH*(L14H0 - L14H + (RH0/KH)) - CH*L14HD*ABS(L14H0 - L14H)
R15T = KT*(L15T0 - L15T + (RT0/KT)) - CT*L15TD*ABS(L15T0 - L15T) + R15T0*(6*W2^5 -
15*W2^4 + 10*W2^3)
R16T = KT*(L16T0 - L16T + (RT0/KT)) - CT*L16TD*ABS(L16T0 - L16T)
R17T = KT*(L17T0 - L17T + (RT0/KT)) - CT*L17TD*ABS(L17T0 - L17T) + R17T0*(6*W2^5 -
15*W2^4 + 10*W2^3)
R18T = KT*(L18T0 - L18T + (RT0/KT)) - CT*L18TD*ABS(L18T0 - L18T)
R19T = KT*(L19T0 - L19T + (RT0/KT)) - CT*L19TD*ABS(L19T0 - L19T) + R19T0*(6*W2^5 -
15*W2^4 + 10*W2^3)
R20T = KT*(L20T0 - L20T + (RT0/KT)) - CT*L20TD*ABS(L20T0 - L20T)

FORCE(P9/P26,R9H*UNITVEC(P_P9_P26>))
FORCE(P10/P26,R10H*UNITVEC(P_P10_P26>))
FORCE(P11/P26,R11H*UNITVEC(P_P11_P26>))
FORCE(P12/P26,R12H*UNITVEC(P_P12_P26>))
FORCE(P13/P26,R13H*UNITVEC(P_P13_P26>))
FORCE(P14/P26,R14H*UNITVEC(P_P14_P26>))
FORCE(P15/P27,R15T*UNITVEC(P_P15_P27>))
FORCE(P16/P27,R16T*UNITVEC(P_P16_P27>))
FORCE(P17/P27,R17T*UNITVEC(P_P17_P27>))
FORCE(P18/P27,R18T*UNITVEC(P_P18_P27>))
FORCE(P19/P27,R19T*UNITVEC(P_P19_P27>))
FORCE(P20/P27,R20T*UNITVEC(P_P20_P27>))

% net forces at contact points on racket handle

FHX = DOT(FORCE_P26>,E1>)
FHY = DOT(FORCE_P26>,E2>)
FHZ = DOT(FORCE_P26>,E3>)
FTX = DOT(FORCE_P27>,E1>)
FTY = DOT(FORCE_P27>,E2>)
FTZ = DOT(FORCE_P27>,E3>)
```

% net forces in springs at grip

RHX = DOT(FORCE_P9>,GRIP1>) + DOT(FORCE_P10>,GRIP1>) + DOT(FORCE_P11>,GRIP1>)
+ DOT(FORCE_P12>,GRIP1>) + DOT(FORCE_P13>,GRIP1>) + DOT(FORCE_P14>,GRIP1>)
RHY = DOT(FORCE_P9>,GRIP2>) + DOT(FORCE_P10>,GRIP2>) + DOT(FORCE_P11>,GRIP2>)
+ DOT(FORCE_P12>,GRIP2>) + DOT(FORCE_P13>,GRIP2>) + DOT(FORCE_P14>,GRIP2>)
RHZ = DOT(FORCE_P9>,GRIP3>) + DOT(FORCE_P10>,GRIP3>) + DOT(FORCE_P11>,GRIP3>)
+ DOT(FORCE_P12>,GRIP3>) + DOT(FORCE_P13>,GRIP3>) + DOT(FORCE_P14>,GRIP3>)
RTX = DOT(FORCE_P15>,GRIP1>) + DOT(FORCE_P16>,GRIP1>) + OT(FORCE_P17>,GRIP1>)
+ DOT(FORCE_P18>,GRIP1>) + DOT(FORCE_P19>,GRIP1>) + DOT(FORCE_P20>,GRIP1>)
RTY = DOT(FORCE_P15>,GRIP2>) + DOT(FORCE_P16>,GRIP2>) + OT(FORCE_P17>,GRIP2>)
+ DOT(FORCE_P18>,GRIP2>) + DOT(FORCE_P19>,GRIP2>) + DOT(FORCE_P20>,GRIP2>)
RTZ = DOT(FORCE_P15>,GRIP3>) + DOT(FORCE_P16>,GRIP3>) + OT(FORCE_P17>,GRIP3>)
+ DOT(FORCE_P18>,GRIP3>) + DOT(FORCE_P19>,GRIP3>) + DOT(FORCE_P20>,GRIP3>)

% 'string' forces as a function of length change and velocity of deformation

ST4041 = -KS3*K9*(L4041 - L20 + (ST0/(KS3*K9)))
ST4139 = -KS4*K5*(L4139 - L22 + (ST0/(KS4*K5)))
ST4144 = -KS3*(L4144 - L24 + (ST0/KS3))
ST4241 = -KS4*(L4241 - L21 + (ST0/KS4))
ST2942 = -KS1*K7*(L2942 - L19 - L20 + (ST0/(KS1*K7)))
ST4245 = -KS1*(L4245 - L24 + (ST0/KS1))
ST4342 = -KS4*(L4342 - L21 + (ST0/KS4))
ST3043 = -KS3*K9*(L3043 - L20 + (ST0/(KS3*K9)))
ST4346 = -KS3*(L4346 - L24 + (ST0/KS3))
ST3143 = -KS4*K5*(L3143 - L22 + (ST0/KS4*K5))
ST4438 = -KS2*K6*(L4438 - L22 - L23 + (ST0/(KS2*K6)))
ST4447 = -KS3*(L4447 - L25 + (ST0/KS3))
ST4544 = -KS2*(L4544 - L21 + (ST0/KS2))
ST4548 = -KS1*(L4548 - L25 + (ST0/KS1))
ST4645 = -KS2*(L4645 - L21 + (ST0/KS2))
ST4649 = -KS3*(L4649 - L25 + (ST0/KS3))
ST3246 = -KS2*K6*(L3246 - L22 - L23 + (ST0/(KS2*K6)))
ST4737 = -KS4*K5*(L4737 - L27 + (ST0/(KS4*K5)))
ST4736 = -KS3*K10*(L4736 - L28 + (ST0/(KS3*K10)))
ST4847 = -KS4*(L4847 - L21 + (ST0/KS4))
ST4835 = -KS1*K8*(L4835 - L28 - L29 + (ST0/(KS1*K8)))
ST4948 = -KS4*(L4948 - L21 + (ST0/KS4))
ST4934 = -KS3*K10*(L4934 - L28 + (ST0/(KS3*K10)))
ST3349 = -KS4*K5*(L3349 - L27 + (ST0/(KS4*K5)))

% forces between nodes/point on racket frame

FORCE(P40/P41,ST4041*UNITVEC(P_P40_P41>))
FORCE(P41/P39,ST4139*UNITVEC(P_P41_P39>))
FORCE(P41/P44,ST4144*UNITVEC(P_P41_P44>))
FORCE(P42/P41,ST4241*UNITVEC(P_P42_P41>))
FORCE(P29/P42,ST2942*UNITVEC(P_P29_P42>))
FORCE(P42/P45,ST4245*UNITVEC(P_P42_P45>))
FORCE(P43/P42,ST4342*UNITVEC(P_P43_P42>))
FORCE(P30/P43,ST3043*UNITVEC(P_P30_P43>))
FORCE(P43/P46,ST4346*UNITVEC(P_P43_P46>))
FORCE(P31/P43,ST3143*UNITVEC(P_P31_P43>))
FORCE(P44/P38,ST4438*UNITVEC(P_P44_P38>))
FORCE(P44/P47,ST4447*UNITVEC(P_P44_P47>))
FORCE(P45/P44,ST4544*UNITVEC(P_P45_P44>))
FORCE(P45/P48,ST4548*UNITVEC(P_P45_P48>))
FORCE(P46/P45,ST4645*UNITVEC(P_P46_P45>))
FORCE(P46/P49,ST4649*UNITVEC(P_P46_P49>))

```
FORCE(P32/P46,ST3246*UNITVEC(P_P32_P46>))
FORCE(P47/P37,ST4737*UNITVEC(P_P47_P37>))
FORCE(P47/P36,ST4736*UNITVEC(P_P47_P36>))
FORCE(P48/P47,ST4847*UNITVEC(P_P48_P47>))
FORCE(P48/P35,ST4835*UNITVEC(P_P48_P35>))
FORCE(P49/P48,ST4948*UNITVEC(P_P49_P48>))
FORCE(P49/P34,ST4934*UNITVEC(P_P49_P34>))
FORCE(P33/P49,ST3349*UNITVEC(P_P33_P49>))

% force acting on ball com normal to stringbed plane
% VINY is the relative velocity of the ball at contact

R45N = RSC*(((1549.1*ABS(VINY)) + 16522)*YB45 + ((1.1934*ABS(VINY)) -
3.0662)*YB45D)*(6*W1^5 - 15*W1^4 + 10*W1^3)
R49N = RSC*(((1549.1*ABS(VINY)) + 16522)*YB49 + ((1.1934*ABS(VINY)) -
3.0662)*YB49D)*(6*W1^5 - 15*W1^4 + 10*W1^3)
R46N = RSC*(((1549.1*ABS(VINY)) + 16522)*YB46 + ((1.1934*ABS(VINY)) -
3.0662)*YB46D)*(6*W1^5 - 15*W1^4 + 10*W1^3)
R48N = RSC*(((1549.1*ABS(VINY)) + 16522)*YB48 + ((1.1934*ABS(VINY)) -
3.0662)*YB48D)*(6*W1^5 - 15*W1^4 + 10*W1^3)

% force acting between ball and stringbed node

FORCE(P45/P50,R45N*(F2> + KF1*RSC*UNITVEC(P_P45_P50S>)))
FORCE(P49/P50,R49N*(F2> + KF3*RSC*UNITVEC(P_P49_P50S>)))
FORCE(P46/P50,R46N*(F2> + KF2*RSC*UNITVEC(P_P46_P50S>)))
FORCE(P48/P50,R48N*(F2> + KF2*RSC*UNITVEC(P_P48_P50S>)))

% torsional spring-damperS to model fundamental mode of vibration and stop
% racket rotation in the hand

TOREF1 = -KTOREF1*Q24 - CTOREF1*U24
TOREF2 = -KTOREF2*Q23 - CTOREF2*U23
TORE3 = -KTORE*(Q20 - RACKANG0) - CTORE*U20*ABS(Q20 - RACKANG0) + TORE30*W2

TORQUE(E/F,TOREF1*F1> + TOREF2*F2>)
TORQUE_E> += TORE3*E3>

% wobbling mass forces

RB1 = -KB*LP1P3^3 - CB*VP1P3
RB2 = -KB*LP2P4^3 - CB*VP2P4
RC1 = -KC*LP2P6^3 - CC*VP2P6
RC2 = -KC*LP5P7^3 - CC*VP5P7

FORCE(P1/P3,RB1*UNITVEC(P_P1_P3>))
FORCE(P2/P4,RB2*UNITVEC(P_P2_P4>))
FORCE(P2/P6,RC1*UNITVEC(P_P2_P6>))
FORCE(P5/P7,RC2*UNITVEC(P_P5_P7>))

% internal joint forces

FORCE(P2/PE,FEX*C1> + FEY*C2> + FEZ*C3>)
FORCE(P5/PW,FWX*D1> + FWY*D2> + FWZ*D3>)

FE = SQRT(FEX^2 + FEY^2 + FEZ^2)
FW = SQRT(FWX^2 + FWY^2 + FWZ^2)

% internal joint torques
```

```
TORQUE(A/B,TORB1*B1> + TORB2*B2> + TORB3*B3>)
TORQUE(B/C,TORC1*C1> + TORC2*C2> + TORC3*C3>)
TORQUE(C/D,TORD2*D2> + TORD3*D3>)

%----------------------------------------------------------------------
% equations of motion

ZERO = FR() + FRSTAR()
KANE(FEX,FEY,FEZ,FWX,FWY,FWZ,TORB1,TORB2,TORB3,TORC1,TORC2,TORC3,TORD2,T
ORD3)

%----------------------------------------------------------------------
% inputs

INPUT TINITIAL = 0.2392, TFINAL = 0.2392, INTEGSTP = 0.00001, PRINTINT = 10, &
    ABSERR = 1.0E-08, RELERR = 1.0E-07, T0 = 0.2392, T1 = 0.2393, T2 = 0.2492
INPUT MA = 31.884, MB = 0.426, MC = 0.295, MD = 0.401, MWB = 1.755, MWC = 1.237, &
    ME = 0.13350, MF = 0.16050, MP41 = 0.00192, MP42 = 0.00192, MP43 = 0.00192, &
    MP44 = 0.00192, MP45 = 0.00192, MP46 = 0.00192, MP47 = 0.00192, &
    MP48 = 0.00192, MP49 = 0.00192, MP50 = 0.059, &
    IA1 = 0.321, IA2 = 1.226, IA3 = 1.104, &
    IB1 = 0.0005, IB2 = 0.003, IB3 = 0.003, &
    IC1 = 0.0002, IC2 = 0.002, IC3 = 0.002, &
    ID1 = 0.0001, ID2 = 0.001, ID3 = 0.001, &
    IWB1 = 0.0025, IWB2 = 0.014, IWB3 = 0.014, &
    IWC1 = 0.0008, IWC2 = 0.008, IWC3 = 0.008, &
    IE1 = 0.0020, IE2 = 0.0020, IE3 = 0.0001, &
    IF1 = 0.0031, IF2 = 0.0039, IF3 = 0.0015, &
    L1 = 0.0, L2 = 0.145, L3 = 0.145, L4 = 0.347, L5 = 0.121, &
    L6 = 0.148, L7 = 0.288, L8 = 0.118, L9 = 0.06, L10 = 0.025, &
    L11 = 0.0, L12 = -0.03,  L13 = 0.05, L14 = 0.03, L15 = 0.1954, &
    L16 = 0.34, L17 = 0.0, L18 = 0.187, L19 = 0.019, L20 = 0.091, L21 = 0.065, &
    L22 = 0.065, L23 = 0.0075, L24 = 0.068, L25 = 0.068, L26 = 0.0055, L27 = 0.067, &
    L28 =0.089, L29 = 0.02, L30 = -0.010, L31 = 0.056, L32 = 0.29, L33 = 0.0, L34 = 0.052, &
    L35 = 0.03, L9H0 = 0.025, L10H0 = 0.025, L11H0 = 0.025, L12H0 = 0.025, &
    L13H0 = 0.025, &L14H0 = 0.025, &
    L15T0 = 0.025, L16T0 = 0.025, L17T0 = 0.025, L18T0 = 0.025, L19T0 = 0.025, L20T0 = 0.025, &
    KS1 = 1.0217E05, KS2 = 1.0338E05, KS3 = 1.1978E05, KS4 = 1.1263E05, &
    K5 = 0.4362, K6 = 0.3769, K7 = 0.9491, K8 = 0.3234, K9 = 0.3979, K10 = 0.5755, &
    G = -9.81, ST0 = 967.7, &
    RH0 = 0, RT0 = 0, RSC = -1.0, &
    R9H0 = 40.0, R11H0 = -95.0, R13H0 = -53.0, R15T0 = -51.0, R17T0 = 131.0, R19T0 = -53.0,
    TORE30 = -0.55, &
    KF1 = 0.26, KF2 = 0.30, KF3 = 0.35, RACKANG0 = -2.29, &
    KTOREF1 = 1075.0, CTOREF1 = 0.04, KTOREF2 = 1800.0, CTOREF2 = 0.1, &
    KTORE = 0.0, CTORE = 0.0, &
    KT = 0.0, CT = 0.0, KH = 0.0, CH = 0.0, &
    KB = 0.5E08, CB = 35.0, KC = 3.0E08, CC = 60.0, &
    CONST20 = -2.29, CONST21 = -0.31, CONST22 = -0.60, &
    Q1 =  0.00001, Q2 = 0.00001, Q3 = 0.0, Q4 = 0.00001, Q5 = 0.0, Q6 = 0.00001, &
    Q7 =  0.00001, Q8 = 0.0, Q9 = 0.00001, Q10 = 0.0, &
    Q11 = 0.0, Q12 = 0.0, Q13 = 0.0, Q14 = 0.0, Q15 = 0.0, &
    Q16 = 0.0, Q17 = -0.025, Q18 = 0.0, Q19 = 0.03, Q20 = -2.29, Q21 = -0.31, &
    Q22 = -0.60, Q23 = 0.0, Q24 = 0.0, &
    Q25 = 0.0, Q26 = 0.0, Q27 = 0.0, Q28 = 0.0, &
    Q29 = 0.0, Q30 = 0.0, Q31 = 0.0, Q32 = 0.0, &
    Q33 = 0.0, Q34 = -0.5809576, Q35 = 0.5651189, Q36 = -0.5678907, &
    U17 = -0.2, U18 = 3.5, U19 = 1.0, U20 = 1.42, U21 = -3.14, U22 = 0.55, &
    U35 = -9.0, VINY = -27.16, U36 = -1.35
```

```
%-----------------------------------------------------------------------
% outputs

OUTPUT T, POP45X, POP45Y, POP45Z, Q34, Q35, Q36
OUTPUT T, POP49X, POP49Y, POP49Z, Q34, Q35, Q36
OUTPUT T, POP46X, POP46Y, POP46Z, Q34, Q35, Q36
OUTPUT T, POP48X, POP48Y, POP48Z, Q34, Q35, Q36
OUTPUT T, POPVMX, POPVMY, POPVMZ, VPVMX, VPVMY, VPVMZ, APVMX, APVMY,
APVMZ
OUTPUT T, Q20, Q21, Q22, U20, U21, U22, U20', U21', U22'
OUTPUT T, Q29, Q35, YB45, YB45D, R45N
OUTPUT T, Q30, Q35, YB49, YB49D, R49N
OUTPUT T, Q33, Q35, YB46, YB46D, R46N
OUTPUT T, Q32, Q35, YB48, YB48D, R48N
OUTPUT T, U34, U35, U36
OUTPUT T, FEX, FEY, FEZ, FE
OUTPUT T, FWX, FWY, FWZ, FW
OUTPUT T, RB1, RB2, Q1, Q2, Q4
OUTPUT T, RC1, RC2, Q6, Q7, Q9
OUTPUT T, TORB1, TORB2, TORB3, TORC1, TORC2, TORC3, TORD2, TORD3
OUTPUT T, L9H, L10H, L11H, L12H, L13H, L14H
OUTPUT T, L15T, L16T, L17T, L18T, L19T, L20T
OUTPUT T, R9H, R10H, R11H, R12H, R13H, R14H
OUTPUT T, R15T, R16T, R17T, R18T, R19T, R20T
OUTPUT T, TOREF1, Q24, U24', TOREF2, Q23, U23', TORE3
OUTPUT T, POPWX, POPWY, POPWZ, VELPWX, VELPWY, VELPWZ
OUTPUT T, AP26X, AP26Y, AP26Z, AP27X, AP27Y, AP27Z
OUTPUT T, LAROX, LAROY, LAROZ, LALFENX, LALFENY, LALFENZ
OUTPUT T, GAROX, GAROY, GAROZ, GALFENX, GALFENY, GALFENZ
OUTPUT T, FHX, FHY, FHZ, FTX, FTY, FTZ
OUTPUT T, RHX,RHY,RHZ,RTX,RTY,RTZ

%-----------------------------------------------------------------------
% units

UNITS [T,T0,T1,T2] = S
UNITS [ANA1,ANA2,ANA3,AAB1,AAB2,AAB3,ABC1,ABC2,ABC3,ACD2,ACD3,
    RACKANG0] = RAD
UNITS [Q3,Q5,Q8,Q10,Q20,Q21,Q22,Q23,Q24,CONST20,CONST21,CONST22] = RAD
UNITS [ANA1',ANA2',ANA3',AAB1',AAB2',AAB3',ABC1',ABC2',ABC3',ACD2',&
    ACD3', U3,U5,U8,U10,U20,U21,U22,U23,U24,RACKANGVEL0] = RAD/S
UNITS [ANA1",ANA2",ANA3",AAB1",AAB2",AAB3",ABC1",ABC2",ABC3",ACD2",ACD3", &
U3',U5',U8',U10',U20',U21',U22',U23',U24',GALFENX,GALFENY,GALFENZ,LALFENX,LALFEN
Y,LALFENZ] = RAD/S^2
UNITS [Q1,Q2,Q4,Q6,Q7,Q9,Q11,Q12,Q13,Q14,Q15,Q16,Q17,Q18,Q19,Q25,Q26,Q27, &
    Q28,Q29,Q30,Q31,Q32,Q33,Q34,Q35,Q36,FIXX,FIXY,FIXZ,LOPO, &
    L9H,L10H,L11H,L12H,L13H,L14H,L15T,L16T,L17T,L18T,L19T,L20T, &
    L4041,L4139,L4144,L4241,L2942,L4245,L4342,L3043, &
    L4346,L3143,L4438,L4447,L4544,L4548,L4645,L4649, &
    L3246,L4737,L4736,L4847,L4835,L4948,L4934,L3349, &
    L9H0,L10H0,L11H0,L12H0,L13H0,L14H0,L15T0,L16T0,L17T0,L18T0,L19T0,L20T0, &
    POPOX,POPOY,POPOZ,POCMX,POCMY,POCMZ,POPEX,POPEY,POPEZ,POPWX,&
    POPWY,POPWZ, LP1P3,LP2P4,LP2P6,LP5P7,YB45,YB46,&
    YB49,POPVMX,POPVMY,POPVMZ,POPRDOX,POPRDOY,POPRDOZ] = M
UNITS L{1:35} = M
UNITS [POP{1:7}X,POP{1:7}Y,POP{1:7}Z] = M
UNITS [POP{9:20}X,POP{9:20}Y,POP{9:20}Z] = M
UNITS [POP{25:49}X,POP{25:49}Y,POP{25:49}Z] = M
UNITS [U1,U2,U4,U6,U7,U9,U11,U12,U13,U14,U15,U16,U17,U18,U19,U25,U26,U27, &
    U28,U29,U30,U31,U32,U33,U34,U35,U36, &
```

```
    YB45D,YB46D,YB49D,YB48D,VPVMX,VPVMY,VPVMZ,FIXX',FIXY',FIXZ',VOPO,VINY, &
    VOCMX,VOCMY,VOCMZ,VP1P3,VP2P4,VP2P6,VP5P7,VELPWX,VELPWY,VELPWZ, &
    VELPEX,VELPEY,VELPEZ,VELP1X,VELP1Y,VELP1Z, &
    L9HD,L10HD,L11HD,L12HD,L13HD,L14HD,L15TD,L16TD,L17TD,L18TD,L19TD,&
    L20TD] = M/S
UNITS [U1',U2',U4',U6',U7',U9',U11',U12',U13',U14',U15',U16',U17',U18',U19', &
    U25',U26',U27',U28',U29',U30',U31',U32',U33',U34',U35',U36', &
    AOCMX,AOCMY,AOCMZ,APVMX,APVMY,APVMZ,APRDOE1,APRDOE2,APRDOE3,&
    APU, AP26X,AP26Y,AP26Z,AP27X,AP27Y,AP27Z, &
    GAROX,GAROY,GAROZ,LAROX,LAROY,LAROZ] = M/S^2
UNITS [RB{1:2},RC{1:2}] = N
UNITS [R45N,R46N,R49N,R48N,R9H,R10H,R11H,R12H,R13H,R14H,R15T,R16T, &
    R17T,R18T,R19T,R20T, RH0,RT0,ST0,FEX,FEY,FEZ,&
    FWX,FWY,FWZ,FE,FW,FHX,FHY,FHZ,FTX,FTY,FTZ, &
    ST4041,ST4139,ST4144,ST4241,ST2942,ST4245,ST4342,ST3043, &
    ST4346,ST3143,ST4438,ST4447,ST4544,ST4548,ST4645,ST4649, &
    ST3246,ST4737,ST4736,ST4847,ST4835,ST4948,ST4934,ST3349, &
    R9H0,R11H0,R13H0,R15T0,R17T0,R19T0,RHX,RHY,RHZ,RTX,RTY,RTZ] = N
UNITS [MA,MB,MC,MD,MWB,MWC,ME,MF] = KG
UNITS MP{41:50} = KG
UNITS G = M/S^2
UNITS [KH,KT,KB,KC] = N/M
UNITS KS{1:4} = N/M
UNITS [KTORE,KTOREF1,KTOREF2] = NM/RAD
UNITS [CTORE,CTOREF1,CTOREF2] = NMS/RAD
UNITS [CB,CC,CH,CT] = NS/M
UNITS [IA{1:3},IB{1:3},IC{1:3},ID{1:3},IWB{1:3},IWC{1:3},IE{1:3},IF{1:3}] = KGM^2
UNITS [TORB1,TORB2,TORB3,TORC1,TORC2,TORC3,TORD2,TORD3, &
    TOREF1,TOREF2,TORE3,TORE30] = NM
UNITS [KF1,KF2,KF3,K5,K6,K7,K8,K9,W1,W2,RSC] = NO_UNITS

%-----------------------------------------------------------------------

SAVE C:\AL\JONO-AL\BACKHAND.ALL
CODE DYNAMICS() C:\AL\JONO-AL\BACKHAND.FOR, SUBS
```

APPENDIX 2

TENNISGOLLUM VICON BODYLANGUAGE MODEL

```
{*VICON BodyLanguage (tm) model*}
{*Start of macro section*}
{*====================*}
macro REPLACE4(p1,p2,p3,p4)
{*Replaces any point missing from set of four fixed in a segment*}
s234 = [p3,p2-p3,p3-p4]
p1V = Average(p1/s234)*s234
s341 = [p4,p3-p4,p4-p1]
p2V = Average(p2/s341)*s341
s412 = [p1,p4-p1,p1-p2]
p3V = Average(p3/s412)*s412
s123 = [p2,p1-p2,p2-p3]
p4V = Average(p4/s123)*s123
{* Now only replaces if original is missing  11-99 *}
p1 = p1 ? p1V
p2 = p2 ? p2V
p3 = p3 ? p3V
p4 = p4 ? p4V
endmacro

{*End of macro section*}

{*Initialisations*}
{*===============*}
{*
-------------------------------------------------------------
{*Define optional marker points*}
OptionalPoints(LPSI,RPSI,SACR,LTIB,RTIB)
OptionalPoints(LUPA,LFRA,LWRA,LWRB,LWRI,LWRE,LFIN)
OptionalPoints(LTHI,LSHN,LHEE,LMT5,LDOR)
OptionalPoints(RUPA,RFRA,RWRA,RWRB,RWRI,RWRE,RFIN)
OptionalPoints(RTHI,RSHN,RHEE,RMT5,RDOR)
OptionalPoints(LFHD,RFHD,LBHD,RBHD,CLAV,C7,STRN,T10)
OptionalPoints(LSHO,RSHO,LELB,RELB)

{*Set Deadband, except for static trials*}
If $Static<>1 Deadband = $Deadband EndIf
-------------------------------------------------------------
*}

OptionalPoints(LTIB,RTIB)

Gorigin = {0,0,0}
Global = [Gorigin,{1,0,0},{0,0,1},xyz]

{*KINEMATICS*}
{*==========*}

If ExistAtAll(LTHI,RTHI,LTIB,RTIB) Then
      VCM = 1
Else
      VCM = 0
```

```
EndIf

{*
----------------------------------------------------------------------
{*Pelvis, Sacrum, and Hips*}
{*======================*}

If $Static==1 Then {*Save average leg length as parameter*}
      If VCM == 1
            LLegLength = $LLegLength
            RLegLength = $RLegLength
      Else
            LLegLength = DIST(LASI,LKNE)+DIST(LKNE,LANK)
            RLegLength = DIST(RASI,RKNE)+DIST(RKNE,RANK)
      EndIf
      $LegLength = (LLegLength+RLegLength)/2
      PARAM($LegLength)
EndIf
 PELF = (LASI+RASI)/2

Pelvis = [PELF,LASI-RASI,PELF-SACR,yzx]

If ($LAsisTrocanterDistance + $RAsisTrocanterDistance) <> 0 Then
      LATD = $LAsisTrocanterDistance
      RATD = $RAsisTrocanterDistance
Else
      LATD = 0.1288*$LegLength-48.56
      RATD = LATD
EndIf

C = $LegLength*0.115-15.3
InterASISDist=DIST(LASI,RASI)
aa = InterASISDist/2
mm = $MarkerDiameter/2
COSBETA = 0.951
SINBETA = 0.309
COSTHETA = 0.880
SINTHETA = 0.476
COSTHETASINBETA = COSTHETA*SINBETA
COSTHETACOSBETA = COSTHETA*COSBETA

LHJC = {C*COSTHETASINBETA - (LATD + mm) * COSBETA,
        -C*SINTHETA + aa,
         -C*COSTHETACOSBETA - (LATD + mm) * SINBETA}*Pelvis

RHJC = {C*COSTHETASINBETA - (RATD + mm) * COSBETA,
         C*SINTHETA - aa,
         -C*COSTHETACOSBETA - (RATD + mm) * SINBETA}*Pelvis

Pelvis = (LHJC+RHJC)/2 + Attitude(Pelvis)

If $Static==1 Then {*Save pelvis size as parameter*}
      $PelvisSize = DIST(LHJC,RHJC)
EndIf
PARAM($PelvisSize)

PelvisSize = $PelvisSize
PelvisScale = {1.2,1,1}
PelvisShift = {0,0,0}
```

```
{*HipJoints (not drawn)*}
LHipJoint = LHJC+Attitude(Pelvis)
RHipJoint = RHJC+Attitude(Pelvis)

{*Sacrum (dummy; to establish relative pose of spine)*}
SAC0 = PELF + $PelvisSize*{-1,0,0}*Attitude(Pelvis)
Sacrum = SAC0+Attitude(Pelvis)

SacrumSize = PelvisSize/2
SacrumScale = {1,1,1}
SacrumShift = {0,0,0}

{*Femura*}
{*======*}
LKneeOS = ($MarkerDiameter+$LKneeWidth)/2
LAnkleOS = ($MarkerDiameter+$LAnkleWidth)/2
RKneeOS = ($MarkerDiameter+$RKneeWidth)/2
RAnkleOS = ($MarkerDiameter+$RAnkleWidth)/2

If VCM == 1 Then
      LKJC=CHORD(LKneeOS,LKNE,LHJC,LTHI)
      RKJC=CHORD(RKneeOS,RKNE,RHJC,RTHI)

      LFemur=[LKNE,LHJC-LKJC,LTHI-LKJC,zxy]
      RFemur=[RKNE,RHJC-RKJC,RKJC-RTHI,zxy]

      LFemur=ROT(LFemur,3(LFemur),-$LThighRotation)
      RFemur=ROT(RFemur,3(RFemur),$RThighRotation)

      LKJC = {0,-LKneeOS,0}*LFemur
      RKJC = {0,RKneeOS,0}*RFemur
      LFemur = LKJC + Attitude(LFemur)
      RFemur = RKJC + Attitude(RFemur)
Else
      LKneeFlexRef = LASI + {-200,0,0}*Attitude(Pelvis)
      RKneeFlexRef = RASI + LKneeFlexRef - LASI

      LFemur = [LKNE,LKneeFlexRef+LKneeOS*2(Pelvis)-LKNE,LANK-
LKNE,zyx,LTOE-LKNE]
      RFemur = [RKNE,RKneeFlexRef-RKneeOS*2(Pelvis)-RKNE,RANK-
RKNE,zyx,RTOE-RKNE]

      LKJC = CHORD(LKneeOS,LKNE,LKneeFlexRef,LKNE+500*2(LFemur))
      RKJC = CHORD(RKneeOS,RKNE,RKneeFlexRef,RKNE-500*2(RFemur))

      LAJC = CHORD(LAnkleOS,LANK,LKJC,LKJC+500*2(LFemur))
      RAJC = CHORD(RAnkleOS,RANK,RKJC,RKJC-500*2(RFemur))

      LKneeFlex = [LKJC,LKneeFlexRef-LKJC,LAJC-LKJC,zyx,LTOE-LKJC]
      RKneeFlex = [RKJC,RKneeFlexRef-RKJC,RAJC-RKJC,zyx,RTOE-RKJC]

      LFemur = [LKJC,LHJC-LKJC,-1(LKneeFlex),zyx]
      RFemur = [RKJC,RHJC-RKJC,-1(RKneeFlex),zyx]
EndIf

LFemurSize = DIST(0(LFemur),0(LHipJoint))
LFemurScale = {1,1,1}
LFemurShift = {0,0,0}

RFemurSize = DIST(0(RFemur),0(RHipJoint))
RFemurScale = {1,1,1}
```

```
RFemurShift = {0,0,0}

{*Tibiae*}
{*======*}
If VCM == 1 Then
      LAJC=CHORD(LAnkleOS,LANK,LKJC,LTIB)
      RAJC=CHORD(RAnkleOS,RANK,RKJC,RTIB)

      LTibia=[LANK,LKJC-LAJC,LTIB-LAJC,zxy]
      RTibia=[RANK,RKJC-RAJC,RAJC-RTIB,zxy]

      LTibia=ROT(LTibia,3(LTibia),-$LShankRotation)
      RTibia=ROT(RTibia,3(RTibia),$RShankRotation)

      LAJC = {0,-LAnkleOS,0}*LTibia
      RAJC = {0,RAnkleOS,0}*RTibia
      LTibia = LAJC + Attitude(LTibia)
      RTibia = RAJC + Attitude(RTibia)
Else
      LTibia = [LAJC,LKJC-LAJC,-1(LFemur),zyx,LKJC-LHJC]
      RTibia = [RAJC,RKJC-RAJC,-1(RFemur),zyx,RKJC-RHJC]
EndIf

LTibiaSize = DIST(0(LTibia),0(LFemur))
LTibiaScale = {0.9,0.93,0.93}
LTibiaShift = {0,0,-0.01}

RTibiaSize = DIST(0(RTibia),0(RFemur))
RTibiaScale = {0.93,0.93,0.93}
RTibiaShift = {0,0,-0.01}

{*Foot (and Toes) Segments*}
{*=======================*}
LFoot = [LTOE,LAJC-LTOE,LAJC-LKJC,zyx]
RFoot = [RTOE,RAJC-RTOE,RAJC-RKJC,zyx]

If $Static == 1 Then
      If $StaticFootFlat == 1 Then
            LRF = {1(LAJC),2(LAJC),3(LTOE)}
            RRF = {1(RAJC),2(RAJC),3(RTOE)}
            LFootRef = [LTOE,LRF-LTOE,LAJC-LKJC,zyx]
            RFootRef = [RTOE,RRF-RTOE,RAJC-RKJC,zyx]
      Else
            LFootRef = [LTOE,LHEE-LTOE,LAJC-LKJC,zyx]
            RFootRef = [RTOE,RHEE-RTOE,RAJC-RKJC,zyx]
      EndIf

      $LAnkleFlexOS = 1(<LFootRef,LFoot,yzx>)
      $RAnkleFlexOS = 1(<RFootRef,RFoot,yzx>)

      If ExistAtAll(LHEE,RHEE) Then
            $LFootLength = 1.1*DIST(LTOE,LHEE)-mm
            $RFootLength = 1.1*DIST(RTOE,RHEE)-mm
      Else
            $LFootLength = 1.34*DIST(LTOE,LAJC)
            $RFootLength = 1.34*DIST(RTOE,RAJC)
      EndIf

      PARAM($LAnkleFlexOS,$RAnkleFlexOS,$LFootLength,$RFootLength)
EndIf
```

```
LFoot = ROT(LFoot,2(LFoot),$LAnkleFlexOS +5)
RFoot = ROT(RFoot,2(RFoot),$RAnkleFlexOS +5)

LFootBreak = 0.24*$LFootLength
RFootBreak = 0.24*$RFootLength

ff = ($FootThickness/2+mm)
LToes = {-ff,0,-0.25*$LFootLength}*LFoot+Attitude(LFoot)
RToes = {-ff,0,-0.25*$RFootLength}*RFoot+Attitude(RFoot)
LFoot = {-ff,0,0}*LFoot+Attitude(LFoot)
RFoot = {-ff,0,0}*RFoot+Attitude(RFoot)

LFootSize = 0.76*$LFootLength
LFootScale = {1,1,1}
LFootShift = {0.13,0,0}

RFootSize = 0.76*$RFootLength
RFootScale = {1,1,1}
RFootShift = {0.13,0,0}


LToesSize = 0.24*$LFootLength
LToesScale = {1,1,1}
LToesShift = {0.42,0,0}

RToesSize = 0.24*$RFootLength
RToesScale = {1,1,1}
RToesShift = {0.42,0,0}
-----------------------------------------------------------------
*}
{*Thorax segment*}
{*==============*}
Replace4(C7,T10,CLAV,STRN)
UThorax = (C7+CLAV)/2
LThorax = (T10+STRN)/2
FThorax = (CLAV+STRN)/2
BThorax = (C7+T10)/2

TRX0 = CLAV+0.5*(C7-CLAV)
Thorax = [TRX0,LThorax-UThorax,BThorax-FThorax,zyx]

ISHO = 300
LSJC = LSHO+(ISHO*{0,0,0.2}+{0,-
$LateralShoulderOffset,0})*Attitude(Thorax)
RSJC =
RSHO+(ISHO*{0,0,0.2}+{0,$LateralShoulderOffset,0})*Attitude(Thorax)

{*Head Segment*}
{*============*}
Replace4(LFHD,RFHD,RBHD,LBHD)
LHead = (LFHD+LBHD)/2
RHead = (RFHD+RBHD)/2
BHead = (LBHD+RBHD)/2
FHead = (LFHD+RFHD)/2

If $Static ==1 Then
      $HeadSize = DIST(FHead,BHead)
      PARAM($HeadSize)
EndIf
```

```
CHead = BHead+$MarkerDiameter*(FHead-BHead)/(2*$HeadSize)
Head = [CHead,LHead-RHead,FHead-BHead,yzx]

If $Static == 1 Then
      HeadRef = [CHead,LHead-RHead,-3(Global),yxz]
      If $StaticHeadLevel == 1 Then
            $HeadFlexOS = 1(<HeadRef,Head,yzx>)
      Else
            $HeadFlexOS = 0
      EndIf
      PARAM($HeadFlexOS)
EndIf

Head = ROT(Head,2(Head),$HeadFlexOS+$HeadTilt)

HeadSize = $HeadSize
HeadScale = {1.2,1.2,1.2}
HeadShift = {0,0,-0.1}

{*Clavicle Segments*}
{*================*}
LClavicle = [LSJC,0(Thorax)-LSJC,-1(Thorax),zyx]
RClavicle = [RSJC,0(Thorax)-RSJC,-1(Thorax),zyx]

LClavicleSize = DIST(0(LClavicle),0(Thorax))
LClavicleScale = {1,1,1}
LClavicleShift = {0,0,0}

RClavicleSize = DIST(0(RClavicle),0(Thorax))
RClavicleScale = {1,1,1}
RClavicleShift = {0,0,0}

{*Humerus Segments*}
{*================*}
If ExistAtAll(LWRA,RWRA)
      LWRI = (LWRA+LWRB)/2
      RWRI = (RWRA+RWRB)/2
EndIf

ElbowOS = ($MarkerDiameter+$ElbowWidth)/2

LHumerus = [LELB,LSHO+ElbowOS*2(Thorax)-LELB,LWRI-LELB,zyx]
RHumerus = [RELB,RSHO-ElbowOS*2(Thorax)-RELB,RWRI-RELB,zyx]

LEJC = CHORD(ElbowOS,LELB,LSJC,LELB-500*2(LHumerus))
REJC = CHORD(ElbowOS,RELB,RSJC,RELB+500*2(RHumerus))

LRadius = [LWRI,LWRA-LWRB,LEJC-LWRI,xyz]
RRadius = [RWRI,RWRA-RWRB,REJC-RWRI,xyz]

WristOS = ($MarkerDiameter+$WristThickness)/2

LWJC = LWRI-$WristThickness/2*1(LRadius)
RWJC = RWRI+$WristThickness/2*1(RRadius)

{*
-------------------------------------------------------------
If ExistAtAll(LWRA,RWRA)
      {*Bar across back of wrist; A towards thumb*}
      LRadius = [LWRI,LWRA-LWRB,LEJC-LWRI,xyz]
      RRadius = [RWRI,RWRA-RWRB,REJC-RWRI,xyz]
```

```
      LWJC = LWRI-$WristThickness*2(LRadius)
      RWJC = RWRI+$WristThickness*2(RRadius)
ElsIf ExistAtAll(LWRE,RWRE)
      {*WREs above back of wrist*}
      LWJC = CHORD(WristOS,LWRI,LEJC,LWRE)
      RWJC = CHORD(WristOS,RWRI,REJC,RWRE)
Else
      LWJC = CHORD(WristOS,LWRI,LEJC,LEJC-500*2(LHumerus))
      RWJC = CHORD(WristOS,RWRI,REJC,REJC+500*2(RHumerus))
EndIf
-----------------------------------------------------------------
*}
Jono = [RSJC,RSJC-TRX0,UThorax-LThorax,zxy]
LHumerus = [LEJC,LEJC-LSJC,LEJC-LELB,zxy] {* y towards centre *}
RHumerus = [REJC,REJC-RSJC,RELB-REJC,zxy]

{*Radius (and Ulnar) Segments*}
{*=========================*}
LRadius = [LWJC,LWJC-LEJC,LWRB-LWRA,zxy] {* y towards centre *}
RRadius = [RWJC,RWJC-REJC,RWRA-RWRB,zxy]

{*
-----------------------------------------------------------------

{*Wrist Segments (dummy)*}
{*====================*}
If ExistAtAll(LWRA,RWRA)
      {*Bar across back of wrist; A towards thumb*}
      LWrist = [LWJC,3(LRadius),LWRB-LWRA,zxy]
      RWrist = [RWJC,3(RRadius),RWRA-RWRB,zxy]
ElseIf ExistAtAll(LWRE,RWRE)
            {*WREs above back of wrist*}
      LWrist = [LWJC,3(LRadius),LWJC-LWRE,zyx]
      RWrist = [RWJC,3(RRadius),RWJC-RWRE,zyx]
Else
      LWrist = LWJC+Attitude(LRadius)
      RWrist = RWJC+Attitude(RRadius)
      LWrist = ROT(LWrist,3(LWrist),-50)
      RWrist = ROT(RWrist,3(RWrist),50)
EndIf

-----------------------------------------------------------------
*}

{*Hand Segments*}
{*============*}

{*
-----------------------------------------------------------------
If $Static == 1 Then
      $HandSize = 0.35*(DIST(LWJC,LEJC)+DIST(RWJC,REJC))
      PARAM($HandSize)
EndIf
-----------------------------------------------------------------
*}

If ExistAtAll(LFIN,RFIN)
      HandOS = ($MarkerDiameter + $HandThickness)/2
      LHND = CHORD(HandOS,LFIN,LWJC,LWJC-500*1(LRadius))
      RHND = CHORD(HandOS,RFIN,RWJC,RWJC-500*1(RRadius))
{*    LHand = [LWJC,LWJC-LHND,-1(LWrist),zyx]
```

```
        RHand = [RWJC,RWJC-RHND,-1(RWrist),zyx]
Else
        LHand = LWrist
        RHand = RWrist
*}
EndIf

LHand = [LWJC,LHND-LWJC,LWRB-LWRA,zxy] {* y towards body centre *}
RHand = [RWJC,RHND-RWJC,RWRA-RWRB,zxy]

{*Tennis Racket*}
{*============*}
Replace4(TRHDA,TRHDB,TRHDC,TRHDD)
Mid1=(TRHDB+TRHDC)/2
Mid2=(TRHDA+TRHDD)/2
MidHead=(Mid1+Mid2)/2
TennisRacket=[MidHead,Mid1-Mid2,Mid1-TRHDA,yxz]

OUTPUT(RSJC,REJC,RWJC,TRX0,TRHDA,TRHDB,TRHDC,TRHDD,TRHNA,TRHNB)

{*Joint Angles*}
{*============*}
{* See Euler Angles document for a detailed explanation *}
{* of the use of the <> angle function *}

{* First, find the general progression direction of the subject *}
{*=============================================================*}
{*
-------------------------------------------------------------
PelvisDirection = AVERAGE( SACR-PELF )
If $Static == 1 Then
      Anatomy = [0(Global),3(Global),PelvisDirection,zyx]
Else
      Progress = (PELF[7] + PELF[6] + PELF[5] + PELF[4] + PELF[3]
            - PELF[-7]- PELF[-6]- PELF[-5]- PELF[-4]- PELF[-3])/5
      Anatomy = [0(Global),3(Global),-Progress,zyx]
EndIf
If VCM == 1 Then
      Fwd = 3(<Anatomy,Global>)
      {*align to +X*} Anatomy = Global
      If (Fwd > -135) AND (Fwd <= -45) Then {*align to -Y*}
            Anatomy = ROT(Anatomy, 3(Anatomy),-90)
      ElseIf (Fwd > 45) AND (Fwd <= 135) Then {*align to +Y*}
            Anatomy = ROT(Anatomy, 3(Anatomy),90)
      ElseIf (Fwd > 135) OR (Fwd <= -135) Then {*align to -X*}
            Anatomy = ROT(Anatomy, 3(Anatomy),180)
      EndIf
EndIf

{*Anatomical Planes >> Head*}
RHeadAngles = <Anatomy,Head,yxz>(-3)
LHeadAngles = -RHeadAngles(-1)

{*Anatomical Planes >> Thorax*}
RThoraxAngles = -<Anatomy,Thorax,yxz>
RThoraxAngles = <-180-RThoraxAngles(1), RThoraxAngles(2), 180-
RThoraxAngles(3)>
LThoraxAngles = -RThoraxAngles(-1)

{*Anatomical Planes >> Pelvis (VCM)*}
RPelvisAngles = -<Anatomy,Pelvis,yxz>(-2)
```

```
LPelvisAngles = -RPelvisAngles(-1)

{*Foot Progression: Anatomical Planes >> Feet (VCM)*}
LFootProgressAngles = -<Anatomy,LFoot,yxz>(-2)
RFootProgressAngles = -<Anatomy,RFoot,yxz>(-3)

{*Neck: Head >> Thorax *}
RNeckAngles = -<Head,Thorax,yxz>
RNeckAngles  = < -180-RNeckAngles(1), RNeckAngles(2) , 180-
RNeckAngles(3) >
LNeckAngles = -RNeckAngles(-1)
-------------------------------------------------------------
*}

{*Thorax: Global >> Thorax*}
ThoraxAngles = -<Global,Thorax,yxz>
JonoAngles = -<Global,Jono,zyx>
JSA = -<Jono,RHumerus,yxz>

{*Shoulders: Thorax >> Humeri*}
LShoulderAngles = -<Thorax,LHumerus,yxz>
RShoulderAngles = <Thorax,RHumerus,yxz>(-1)
AbsRSA = -<Thorax,RHumerus,yxz>

{*Elbows: Humeri >> Radii*}
LElbowAngles = -<LHumerus,LRadius,yxz>
RElbowAngles = <RHumerus,RRadius,yxz>(-1) {* all joint angles wrt
flexion/pronation/int. rot. *}
AbsREA = -<RHumerus,RRadius,yxz>

{*Wrists: Radii >> Hands*}
LWristAngles = -<LRadius,LHand,yxz>
RWristAngles = <RRadius,RHand,yxz>(-1)
AbsRWA = -<RRadius,RHand,yxz>

{*Tennis Racket: RRadius >> Racket)*}
RacketAngles= -<RHand,TennisRacket,yxz>
RacketGlobal= -<Global,TennisRacket,yxz>

{*
-------------------------------------------------------------
{*Lumbar Spine (Pelvis >> Thorax)*}
RSpineAngles = -<Pelvis,Thorax,yxz>
RSpineAngles = <-180+RSpineAngles(1),-RSpineAngles(2), -
180+RSpineAngles(3)>
LSpineAngles = -RSpineAngles(-1)

{*Hips: Pelvis >> Femora (VCM)*}
LHipAngles = <Pelvis,LFemur,yxz>
RHipAngles = -<Pelvis,RFemur,yxz>(-1)

{*Knees: Femora >> Tibiae (VCM)*}
LKneeAngles = <LFemur,LTibia,yxz>(-1)
RKneeAngles = -<RFemur,RTibia,yxz>

{*Ankles: Tibiae >> Feet (VCM)*}
LAA = -<LTibia,LFoot,yxz>
LAnkleAngles = < -90 - 1(LAA),-3(LAA),-2(LAA)>
RAA = -<RTibia,RFoot,yxz>
RAnkleAngles = < -90 - 1(RAA),3(RAA),2(RAA)>
```

```
{*Forefoot: Feet >> Toes)*}
LFFootAngles = <LFoot,LToes,yxz>(-1)
RFFootAngles = -<RFoot,RToes,yxz>
-----------------------------------------------------------------
*}

OUTPUT(ThoraxAngles,AbsRSA,RShoulderAngles,AbsREA,RElbowAngles,AbsRWA
,RWristAngles,JonoAngles,JSA)
OUTPUT(RacketAngles,RacketGlobal)
```

APPENDIX 3

VICON MOTION ANALYSIS DATA

The following graphs show the shoulder, elbow and wrist joint angle-time histories for the selected trials. The raw vicon motion data and the splined joint angle time histories are shown for 50 ms either side of ball impact.

Trial 1 – one-handed backhand topspin groundstroke

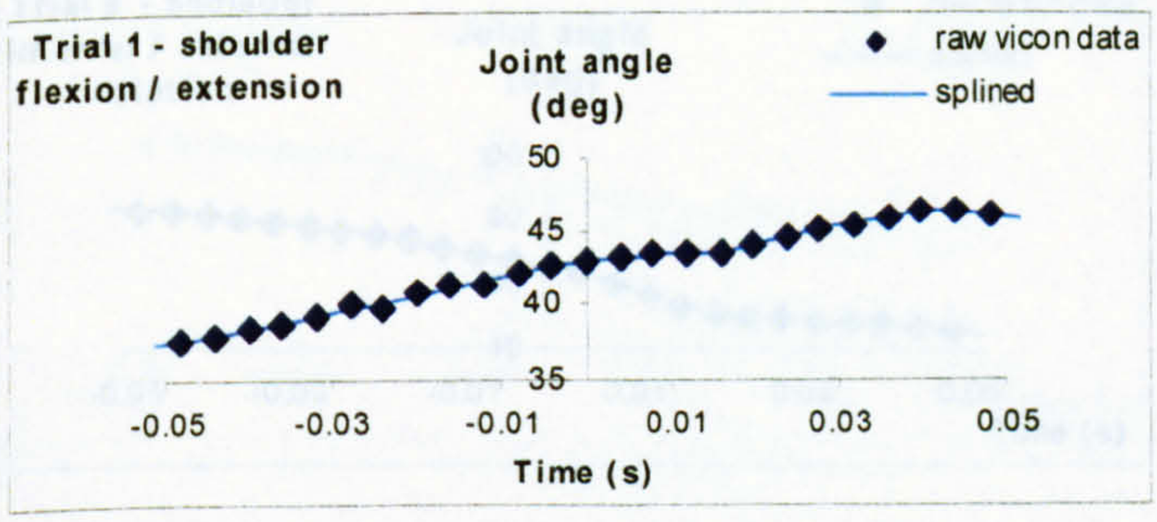

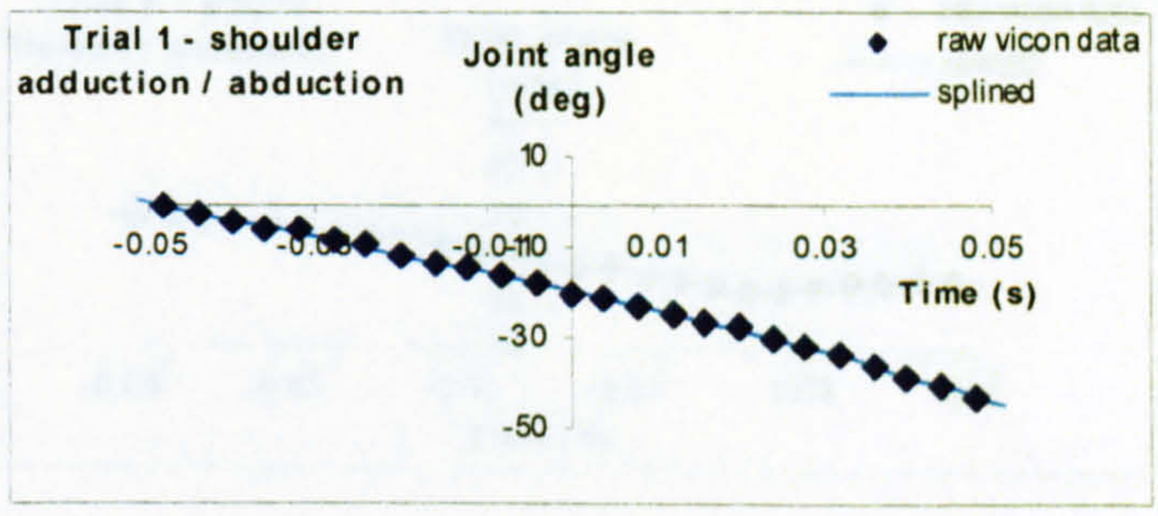

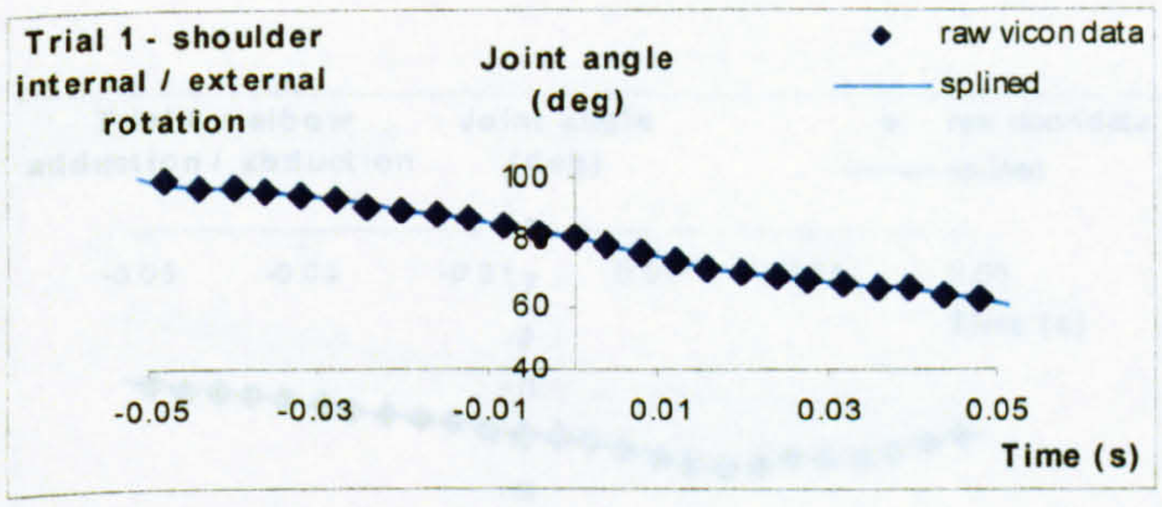

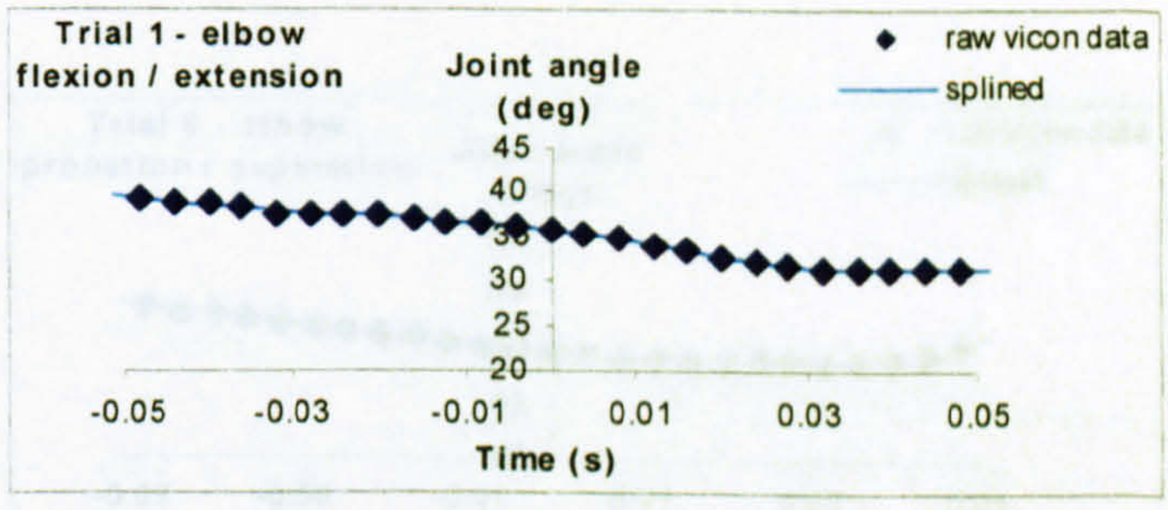

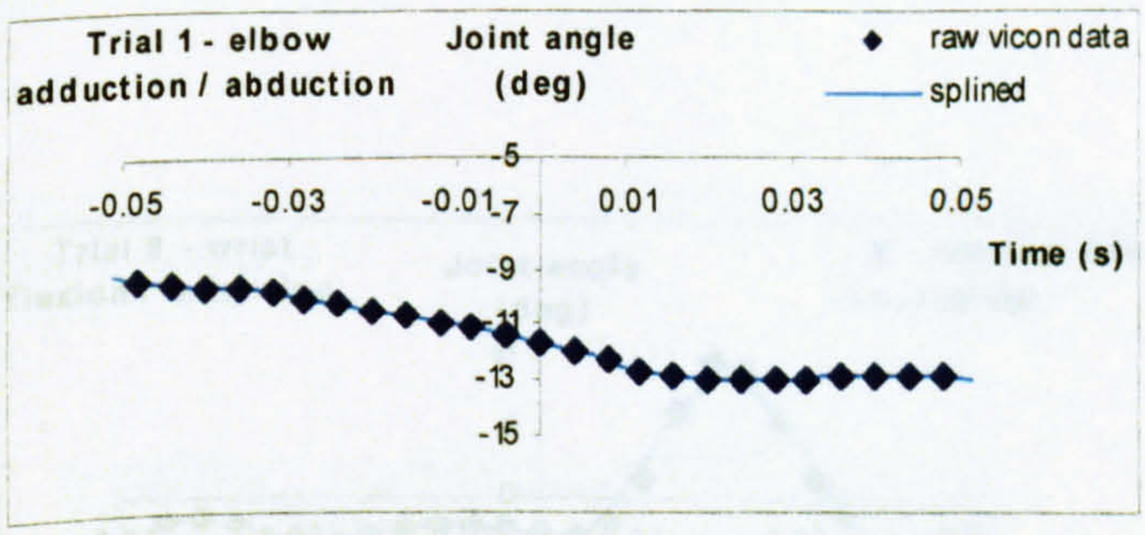

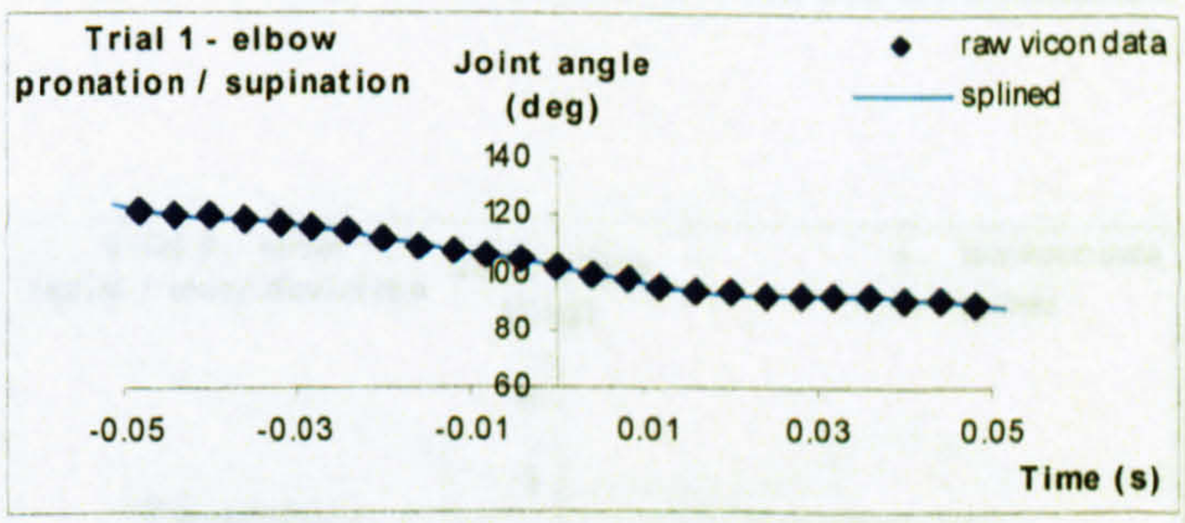

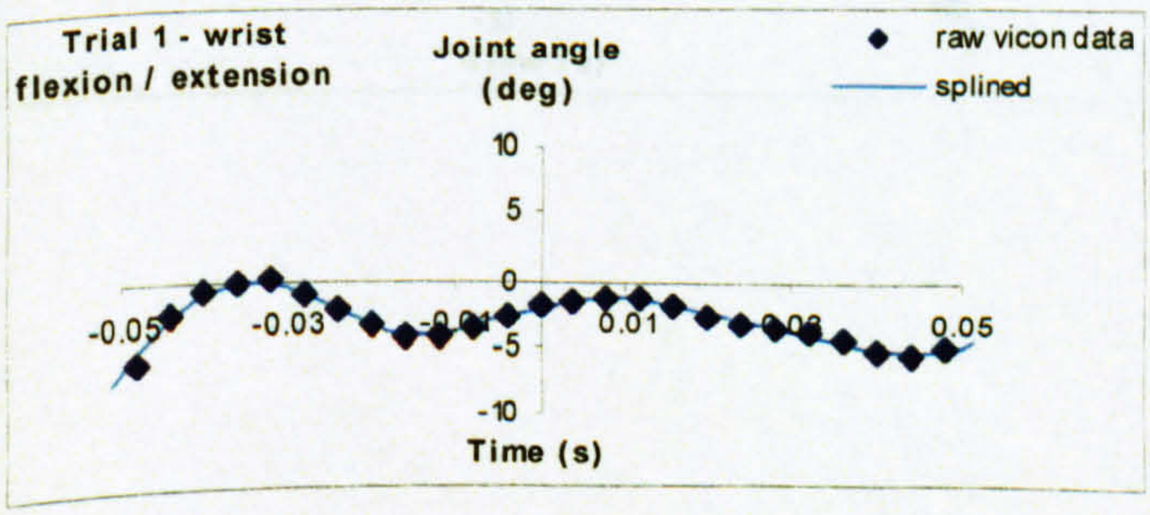

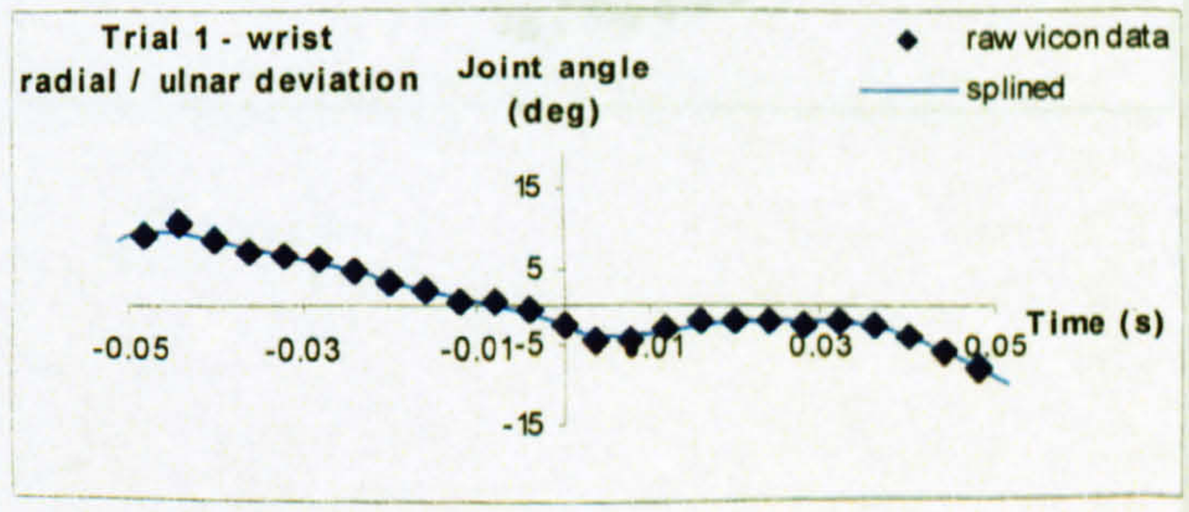

Trial 8 – one-handed backhand topspin groundstroke

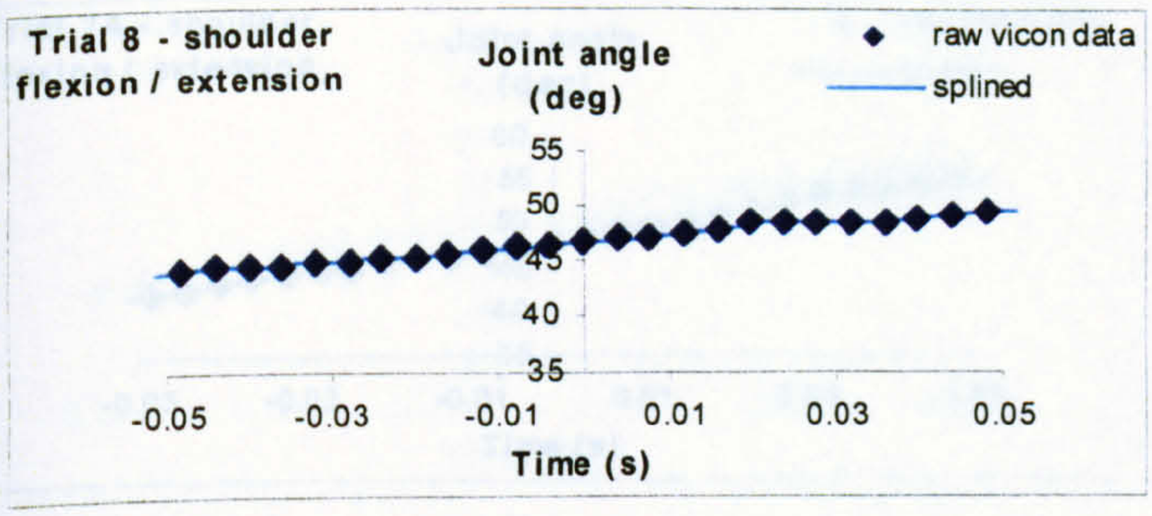

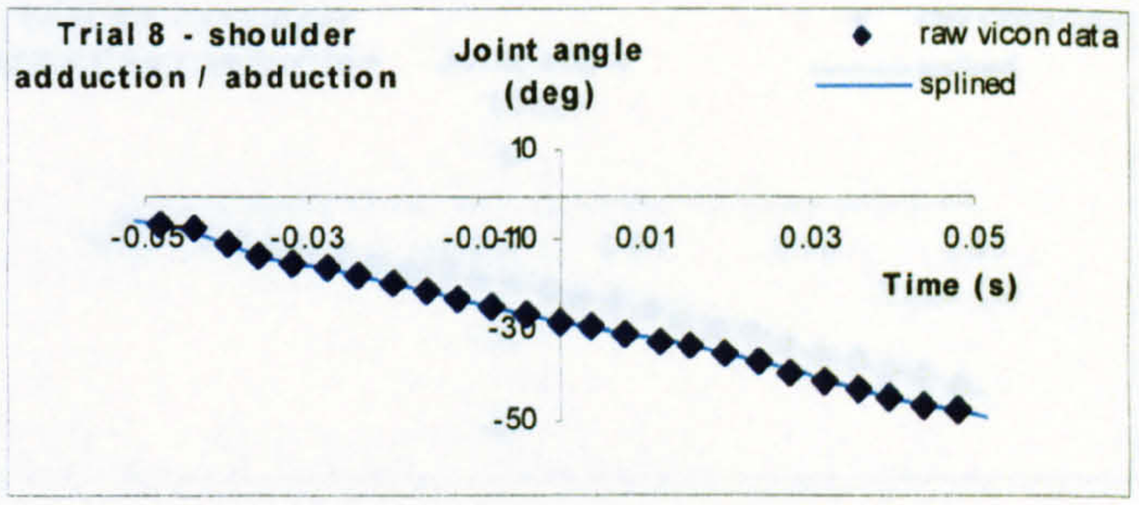

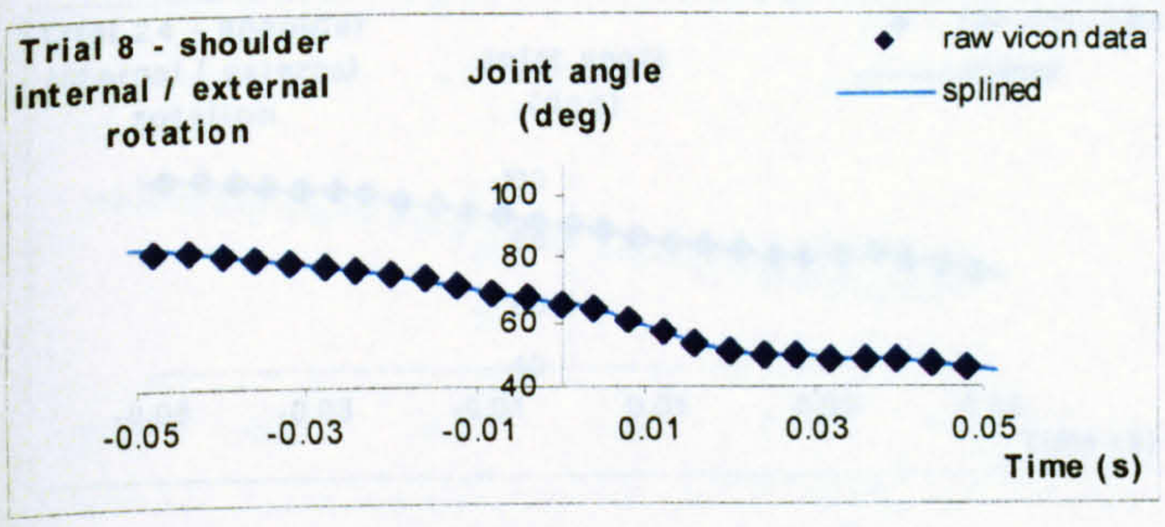

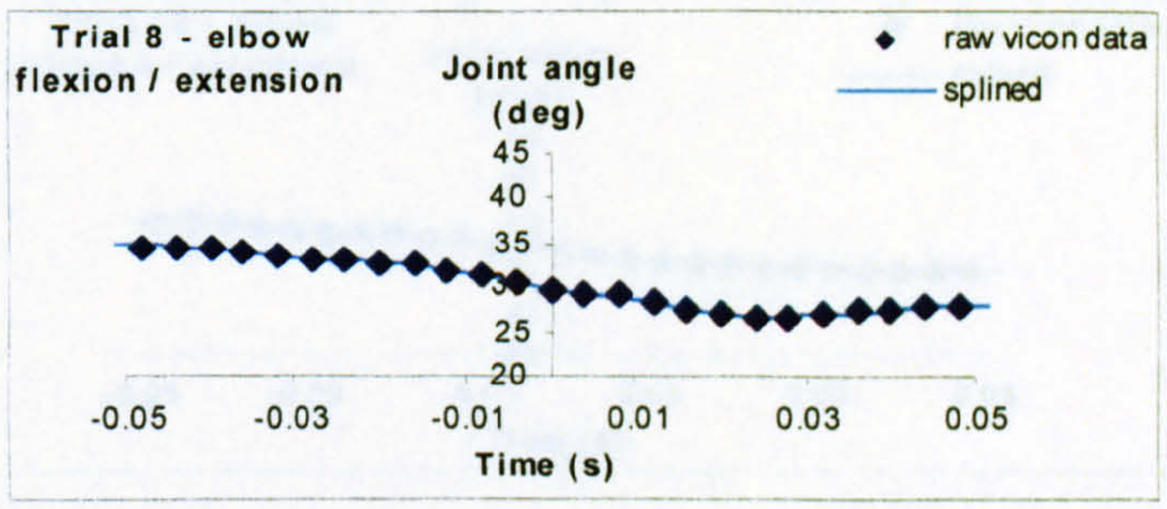

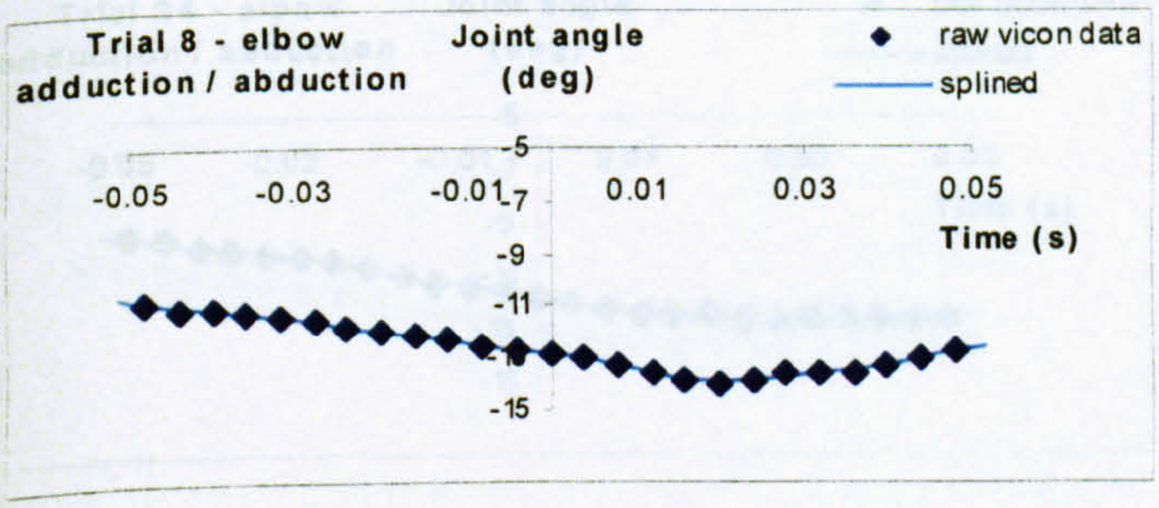

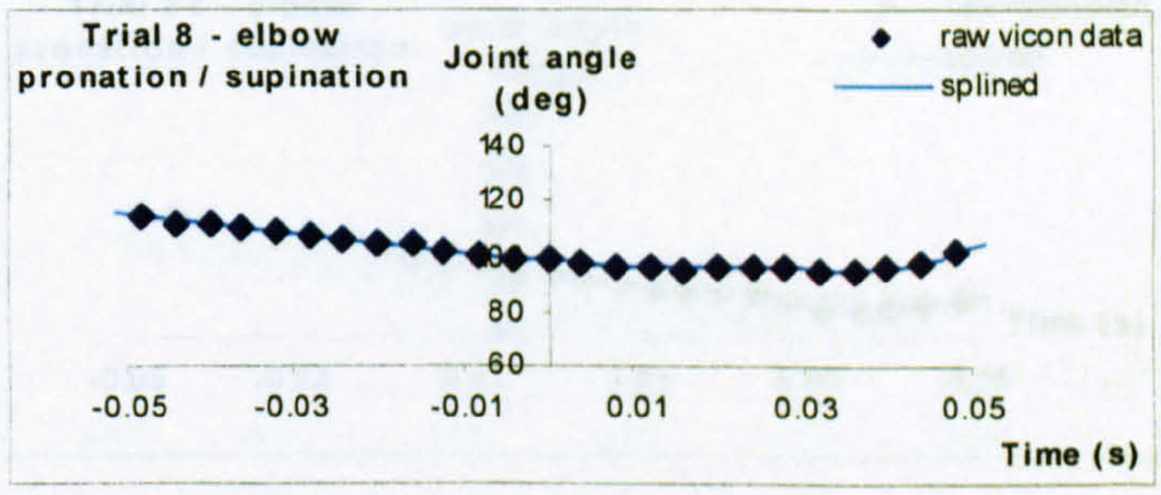

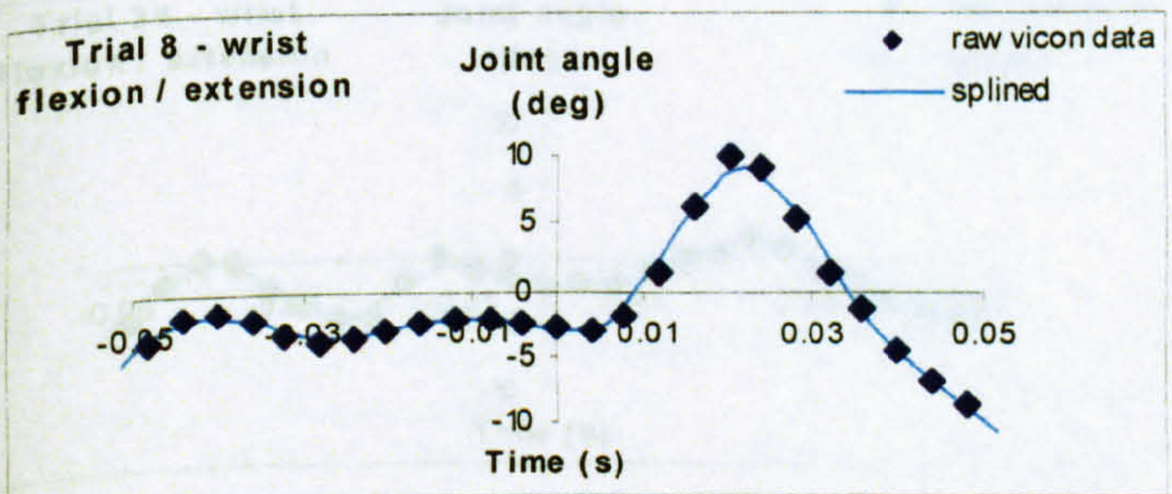

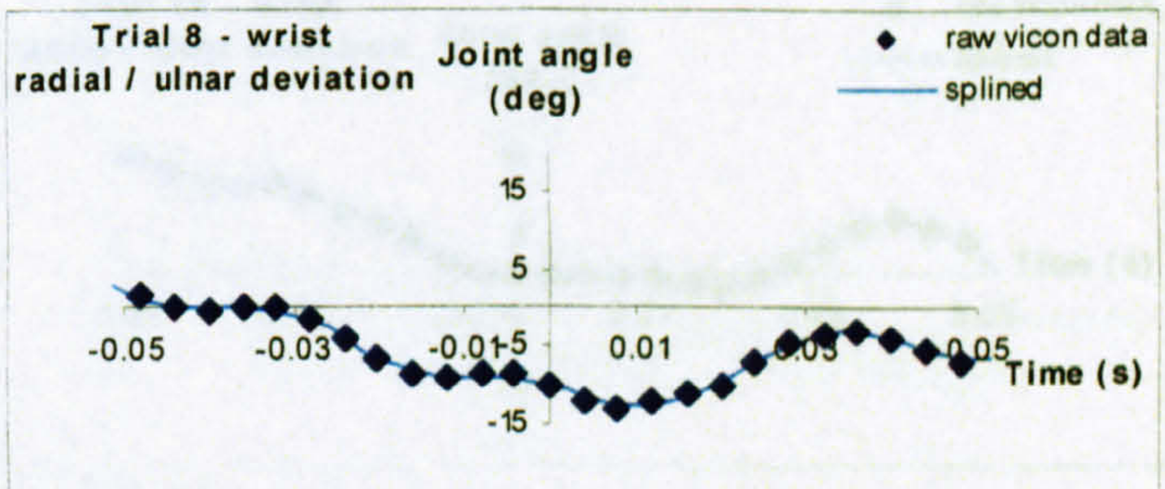

Trial 24 – one-handed backhand topspin groundstroke

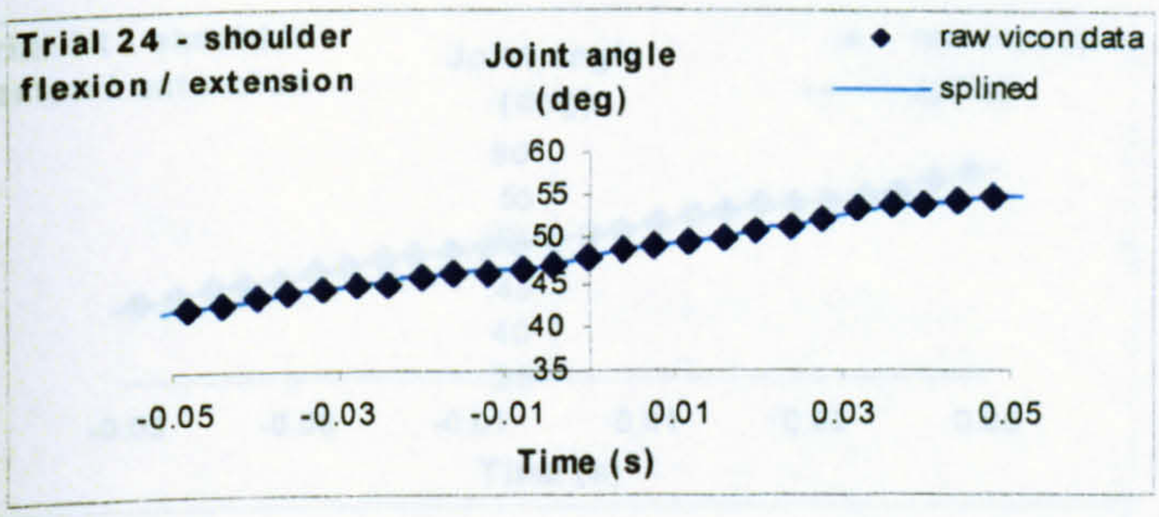

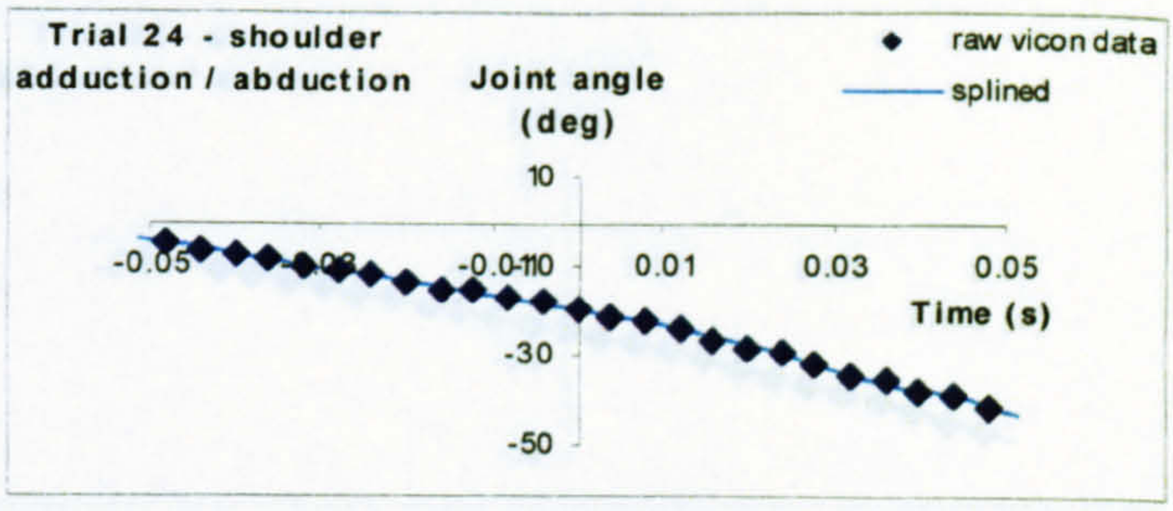

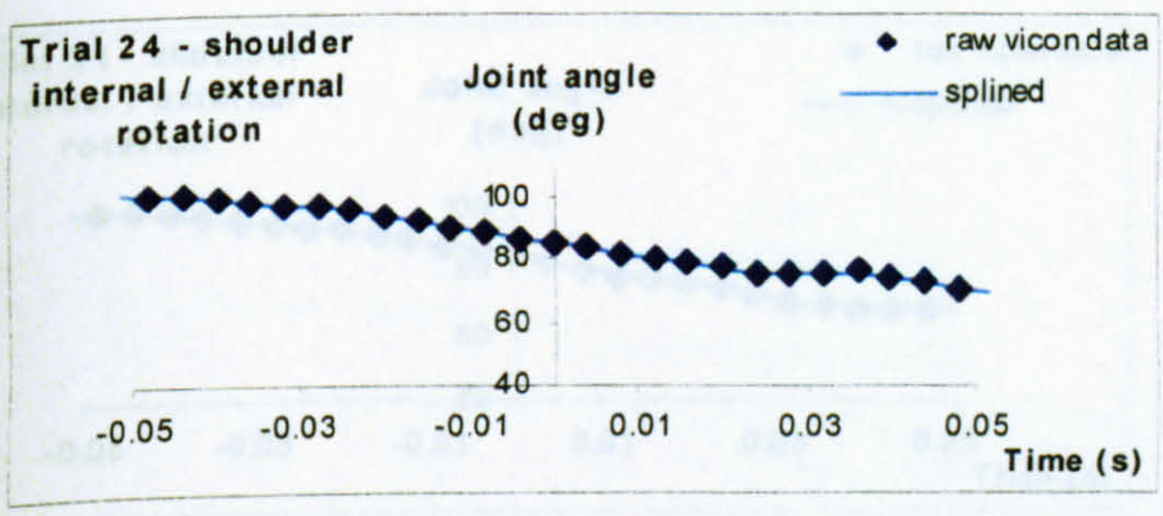

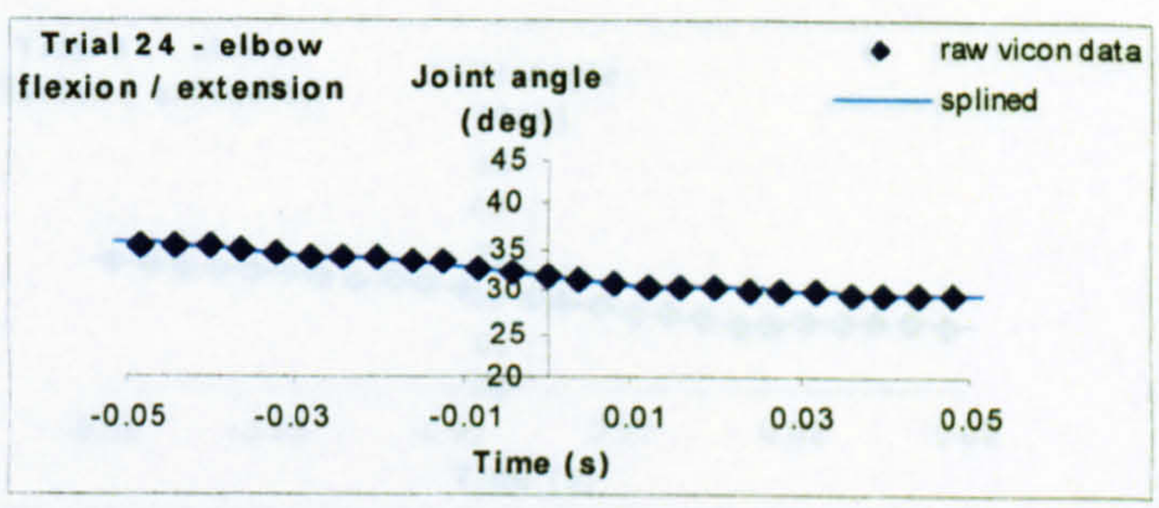

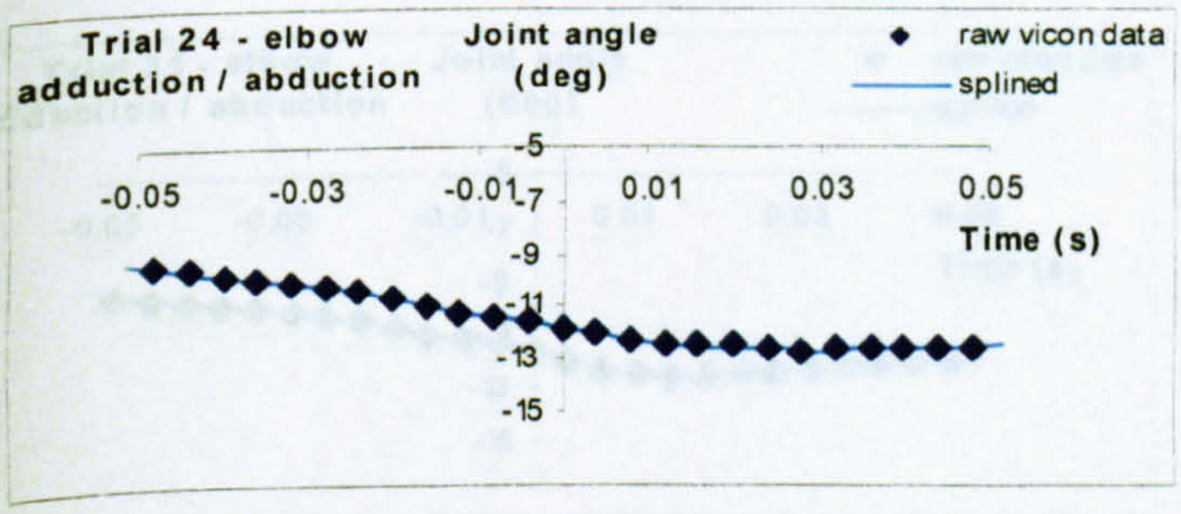

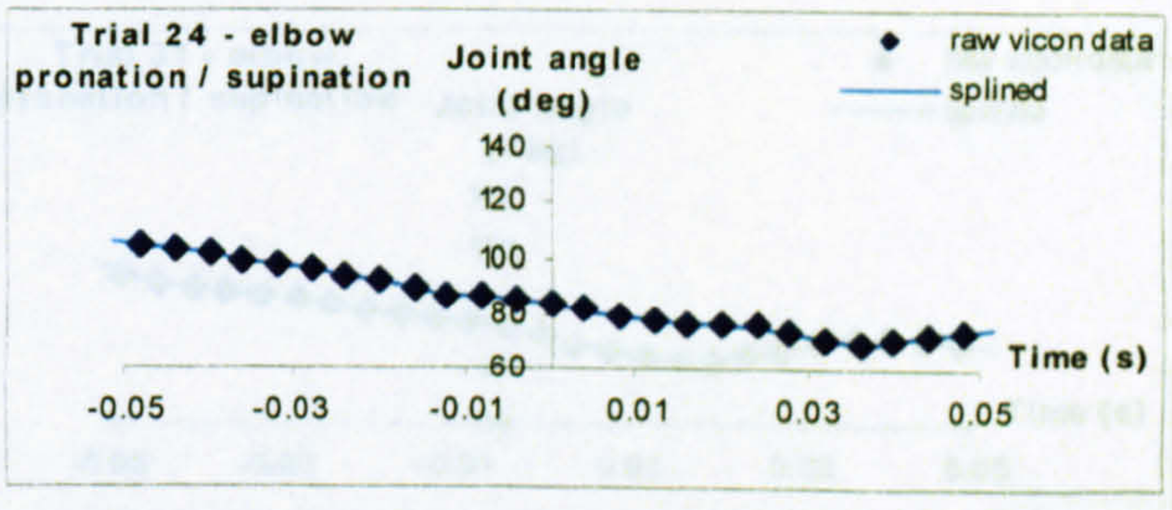

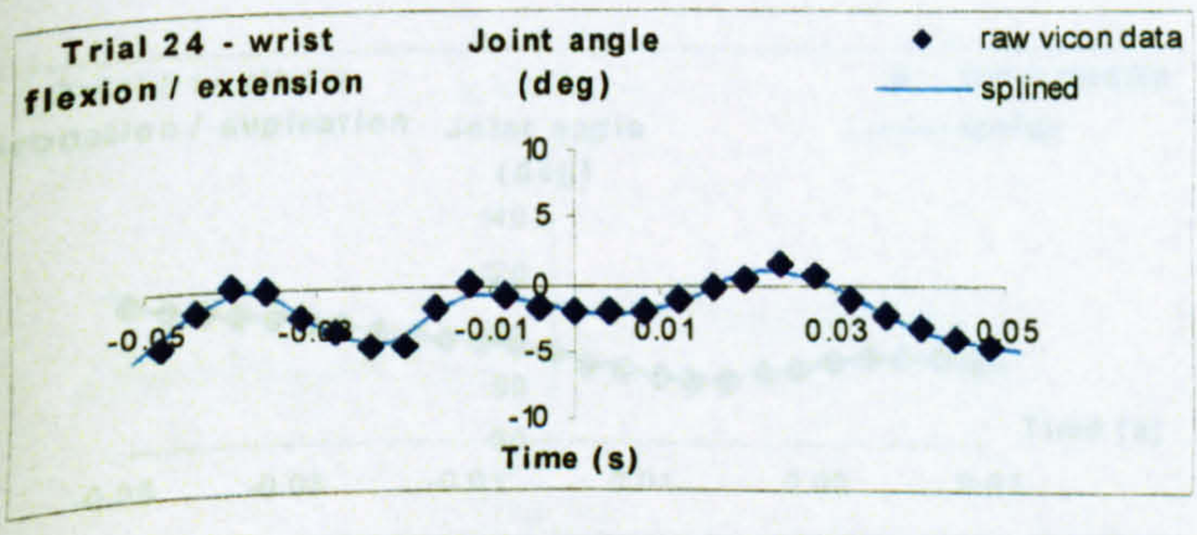

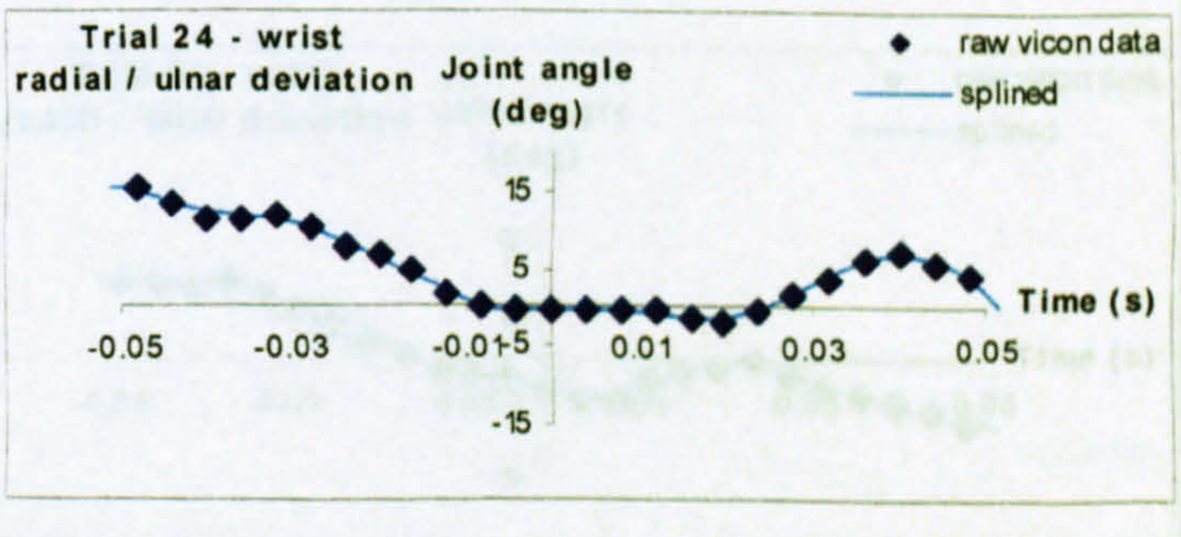

Trial 31 – one-handed backhand topspin groundstroke

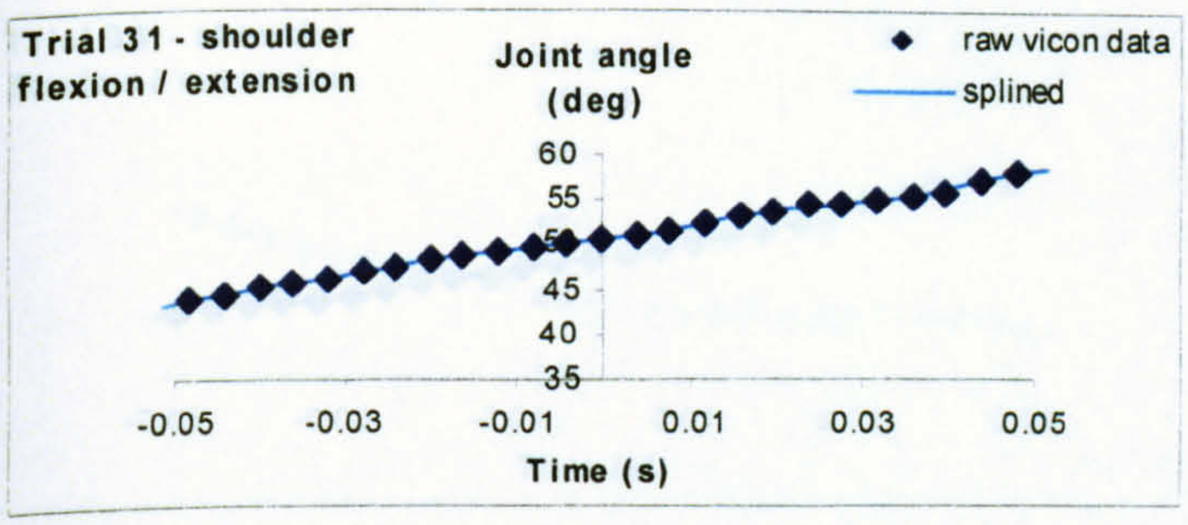

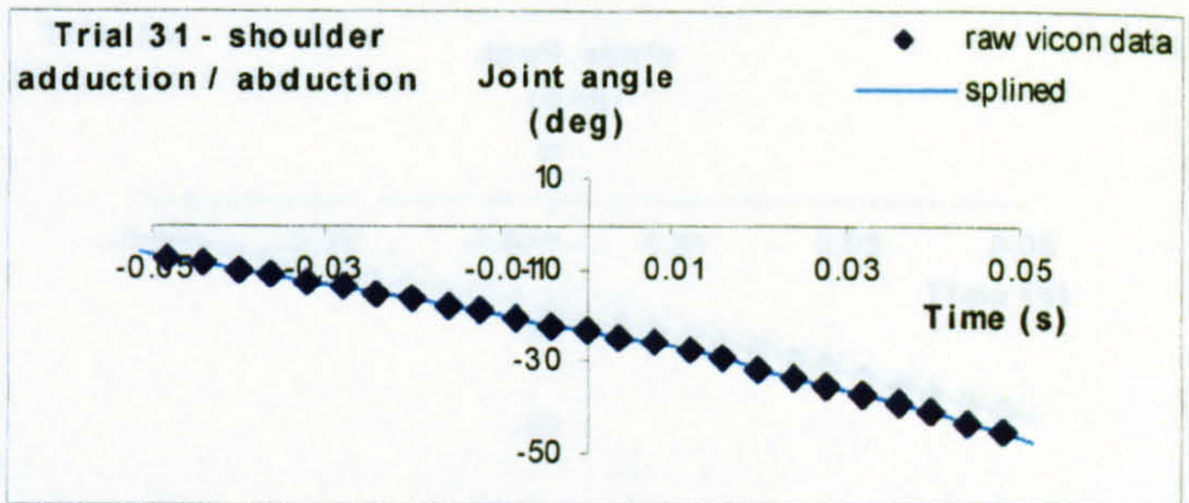

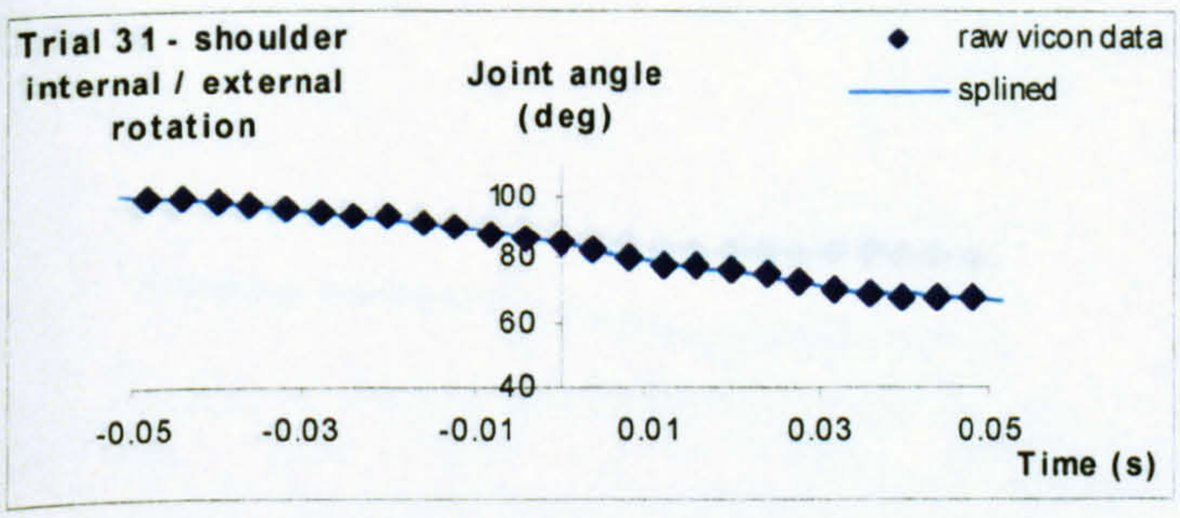

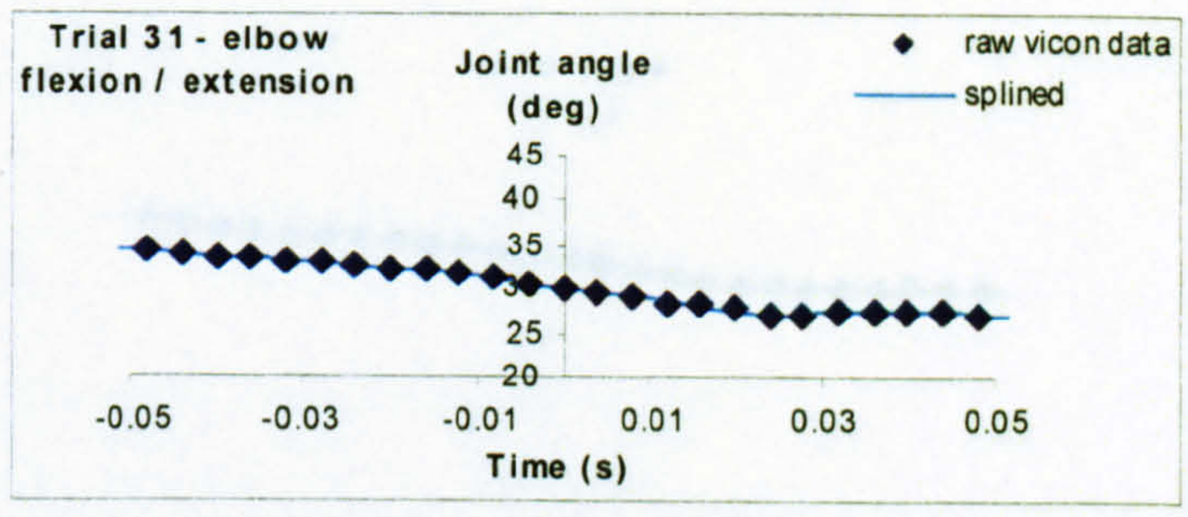

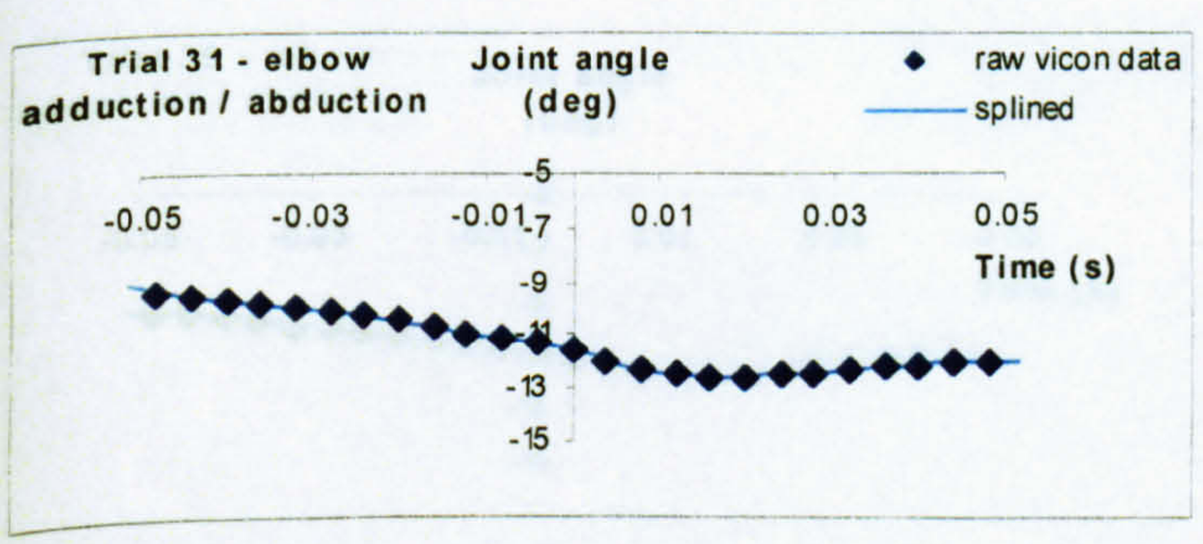

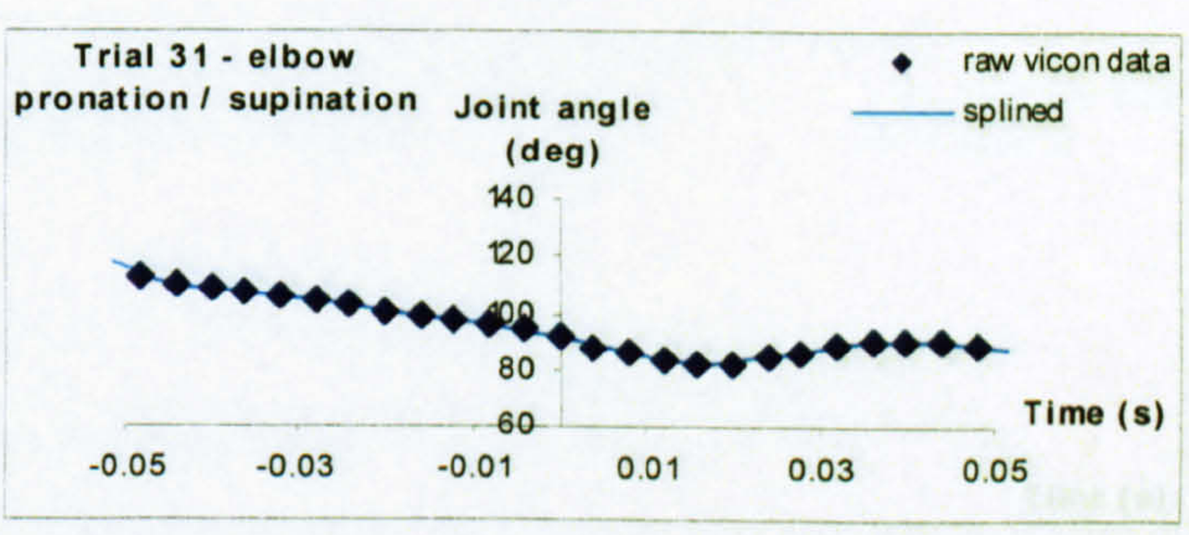

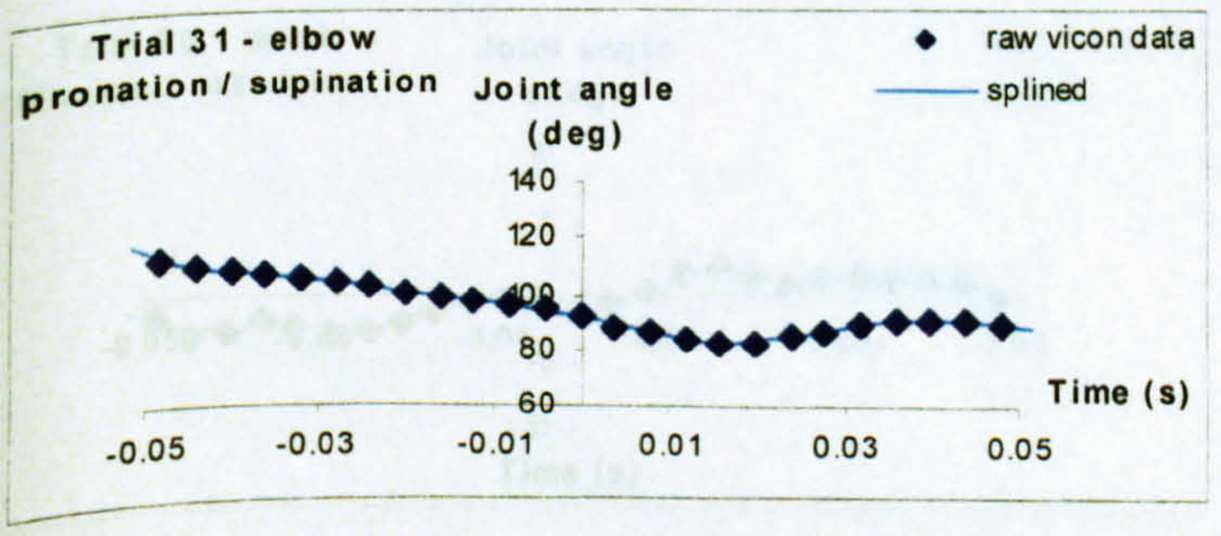

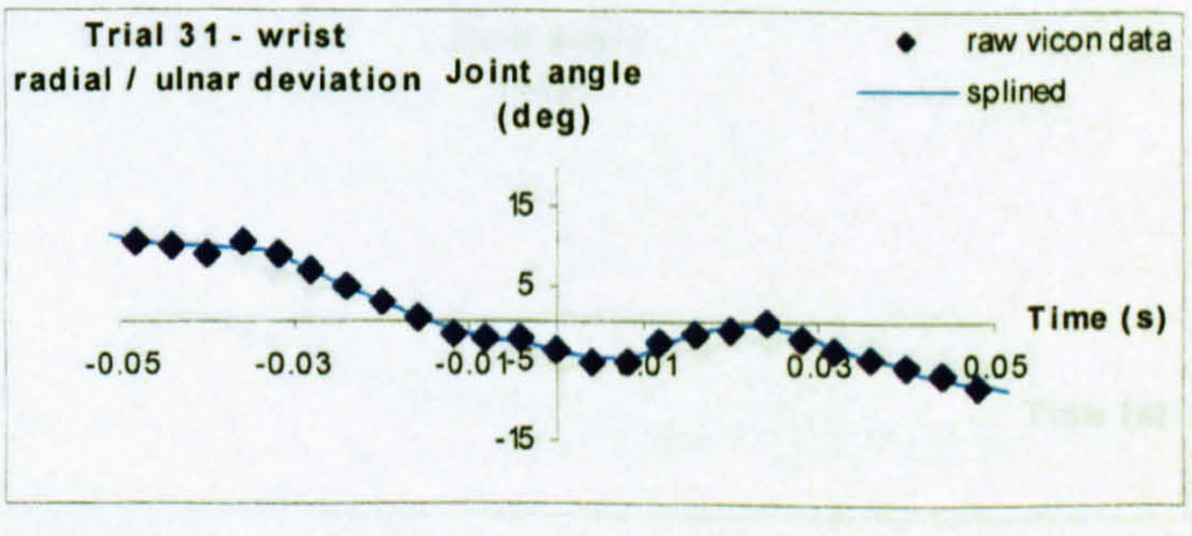

Trial 36 – one-handed backhand topspin groundstroke

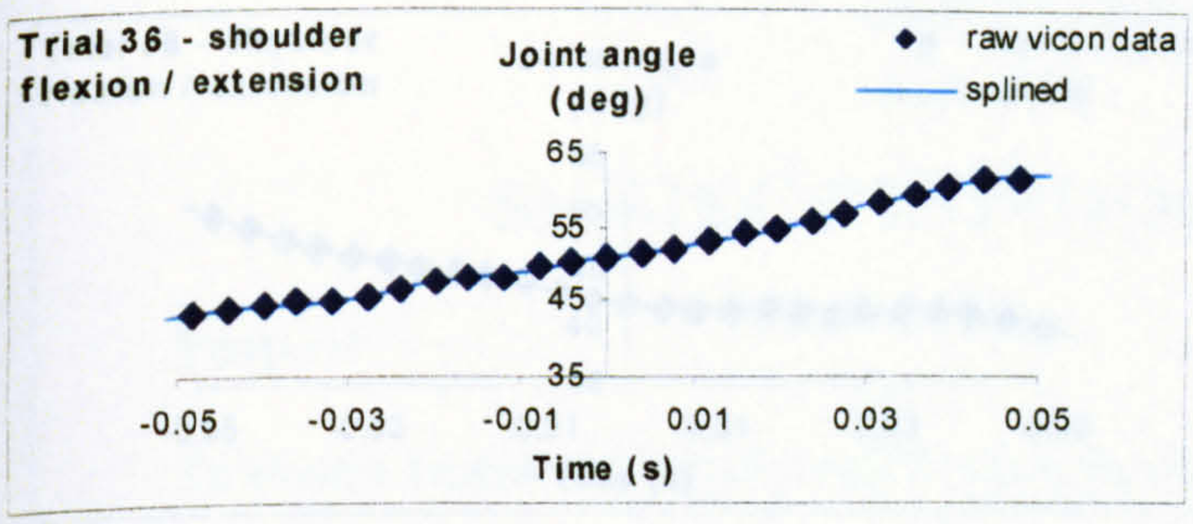

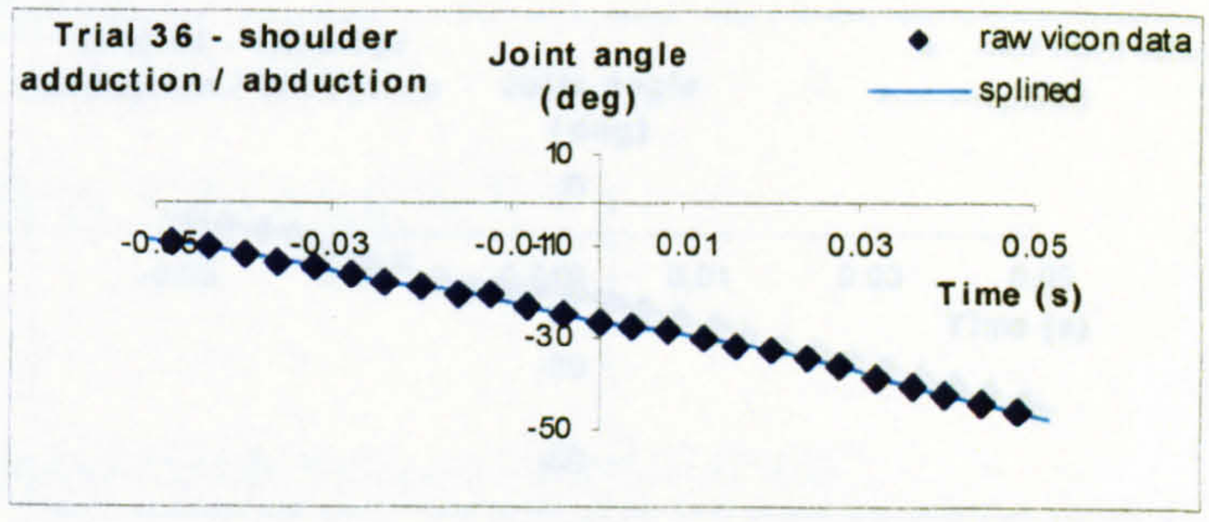

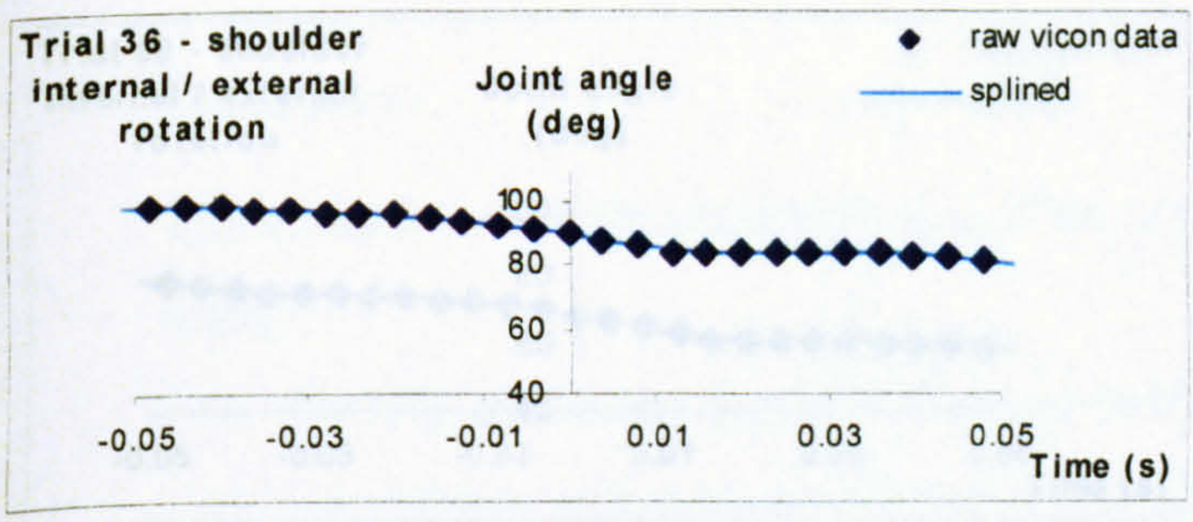

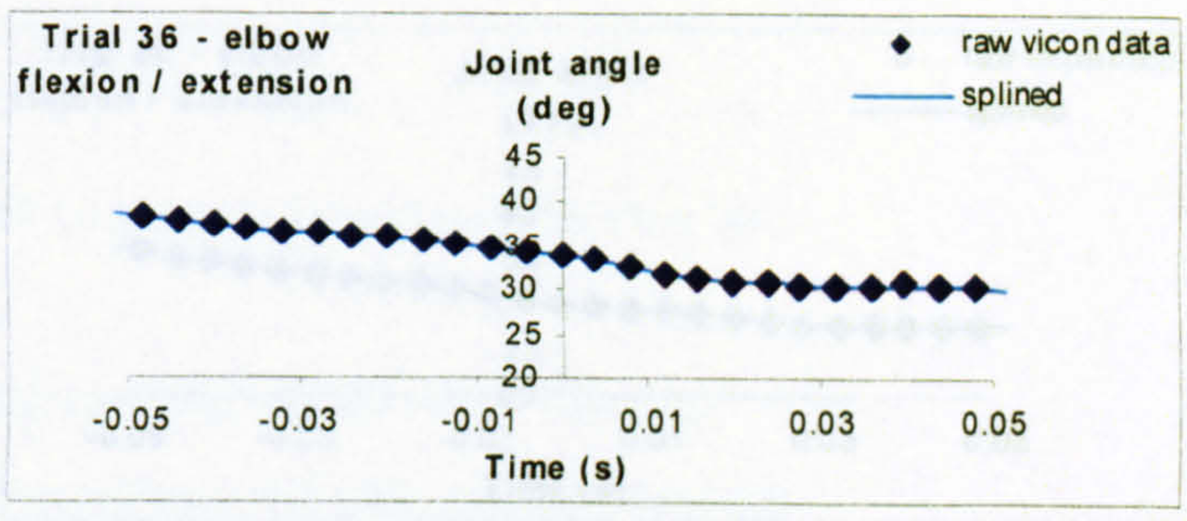

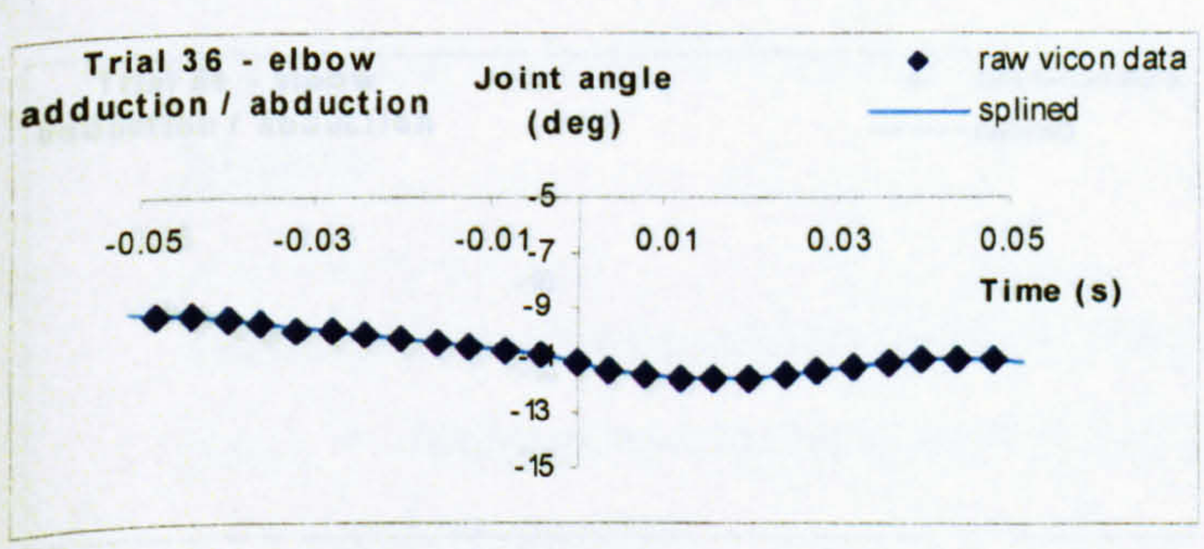

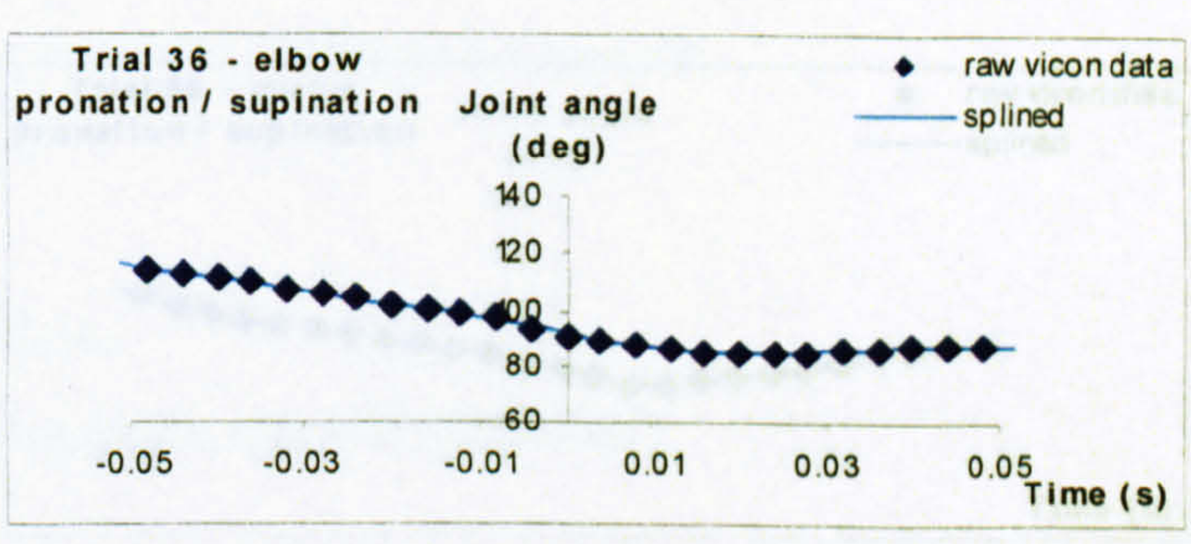

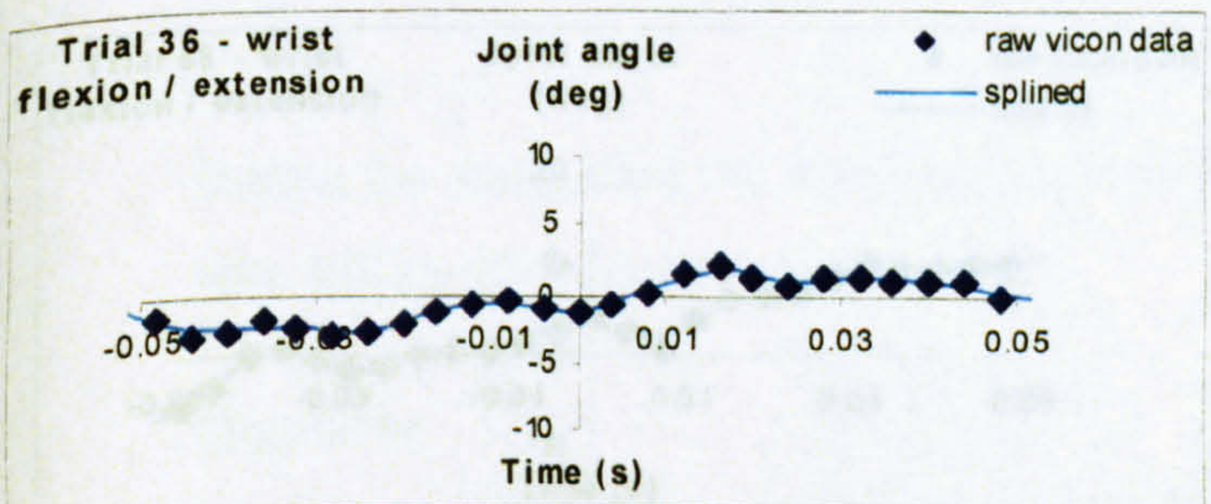

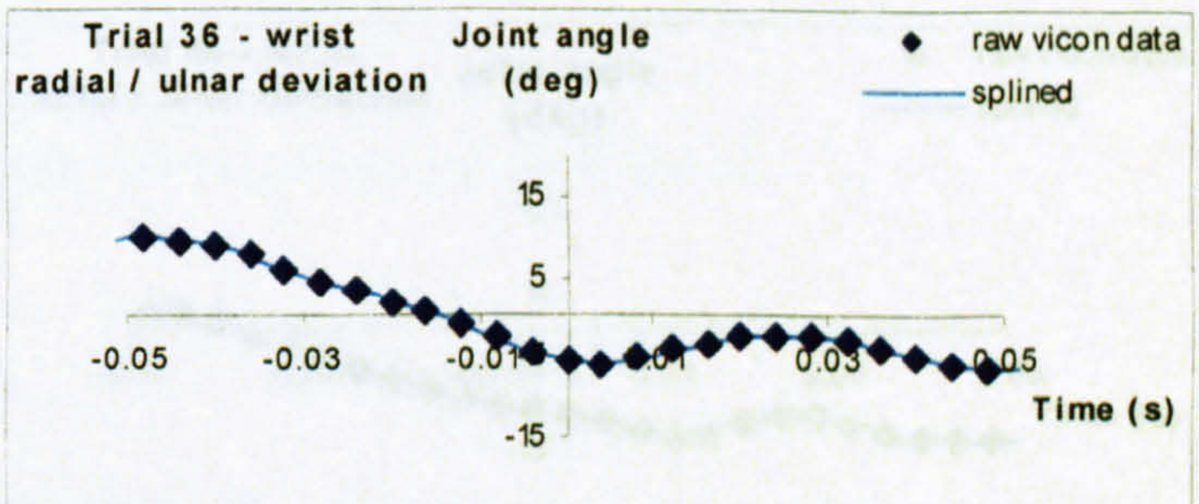

Trial 56 – one-handed backhand slice groundstroke

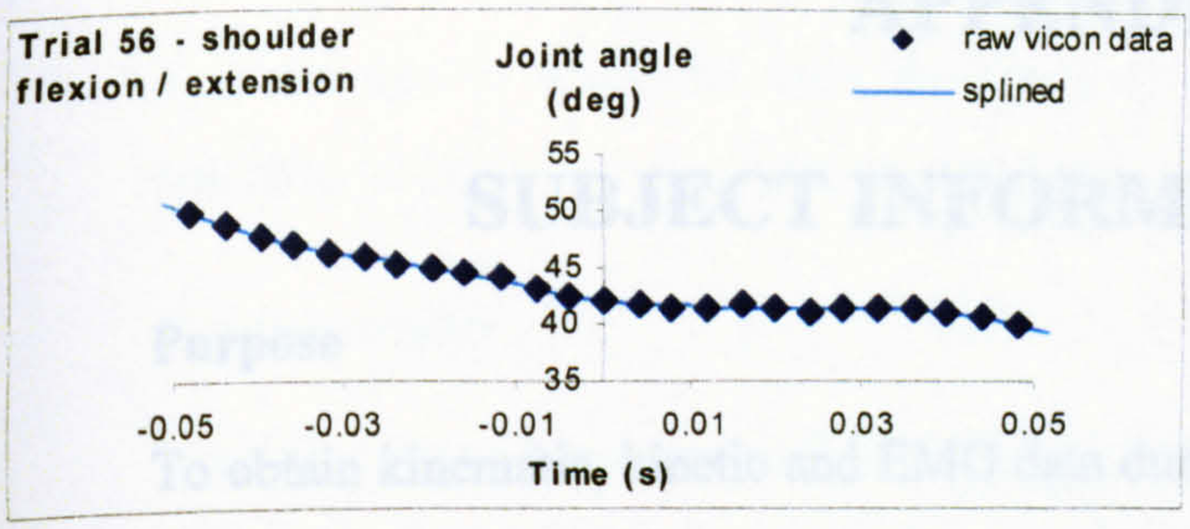

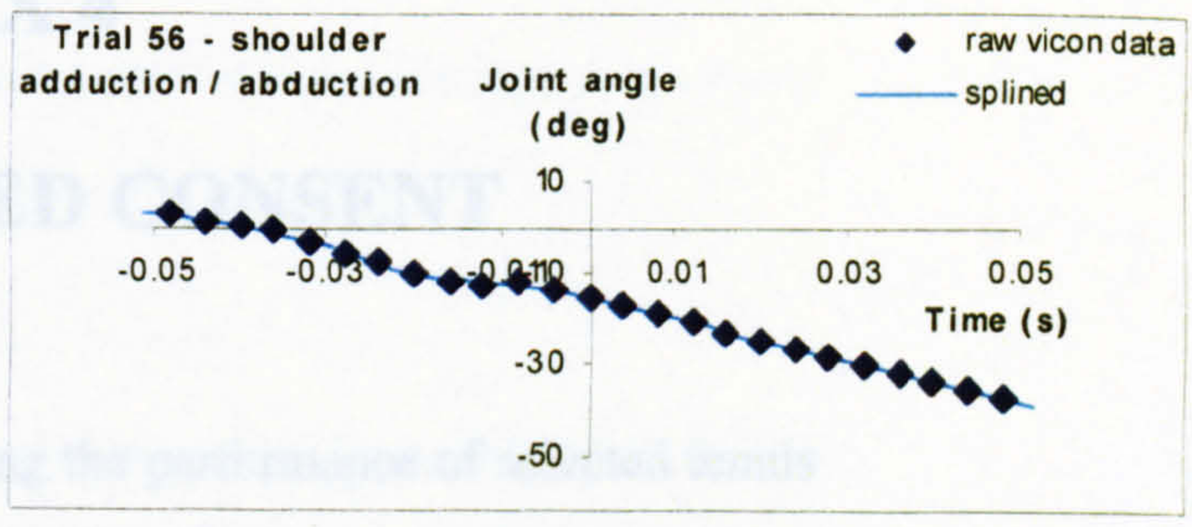

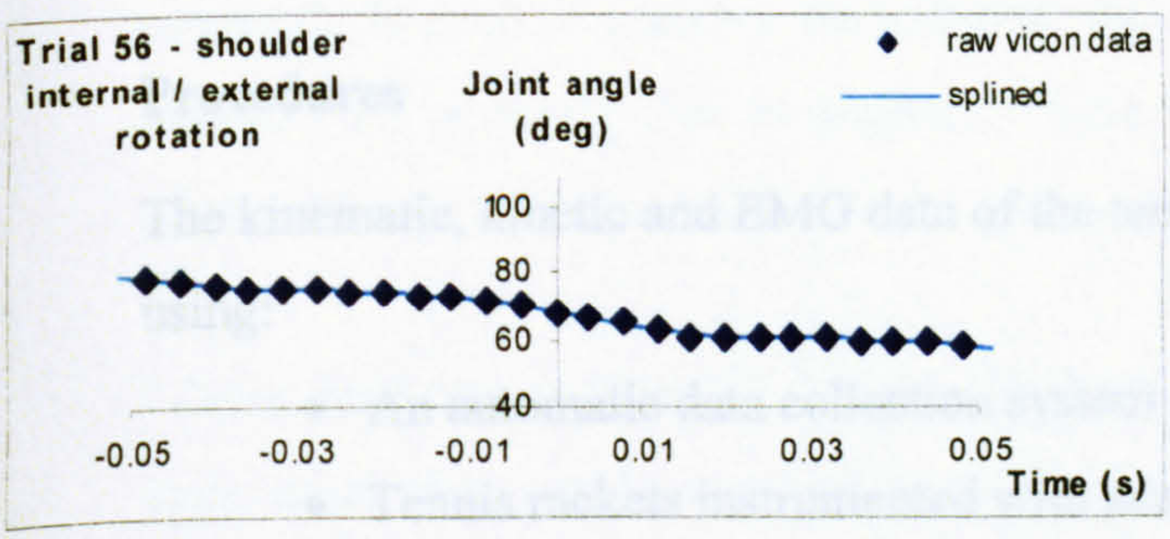

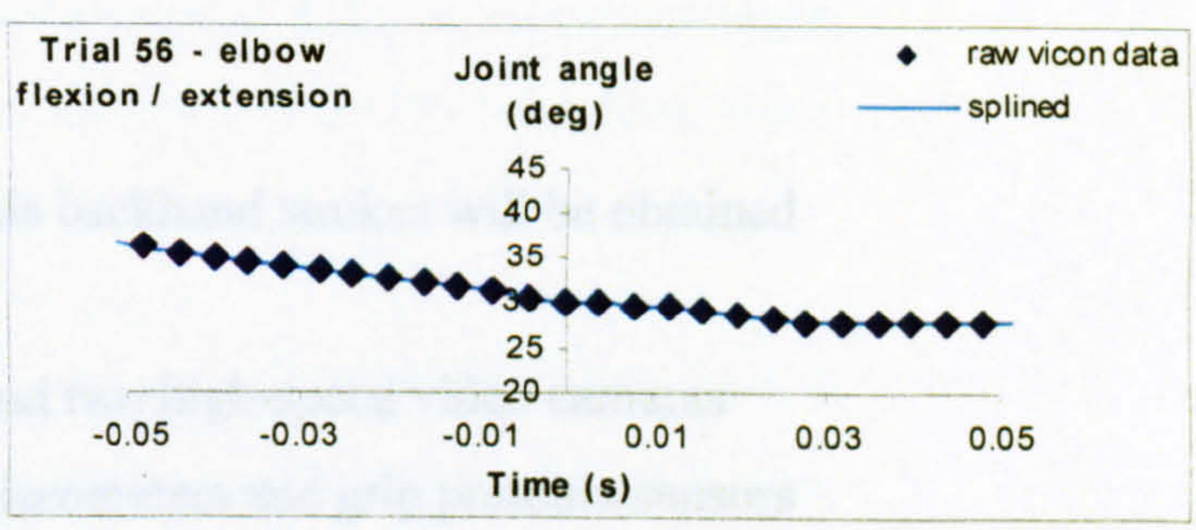

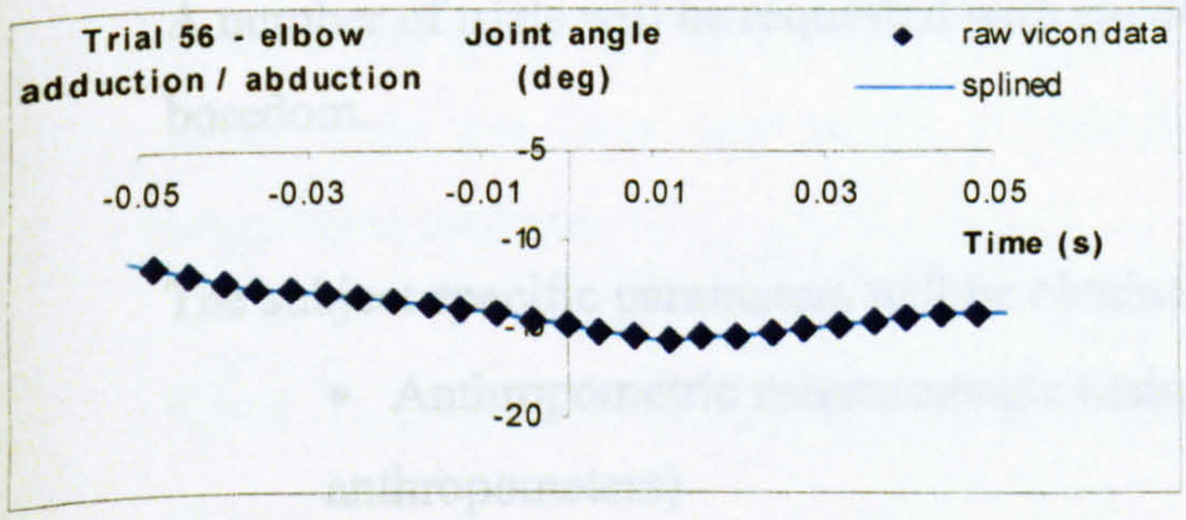

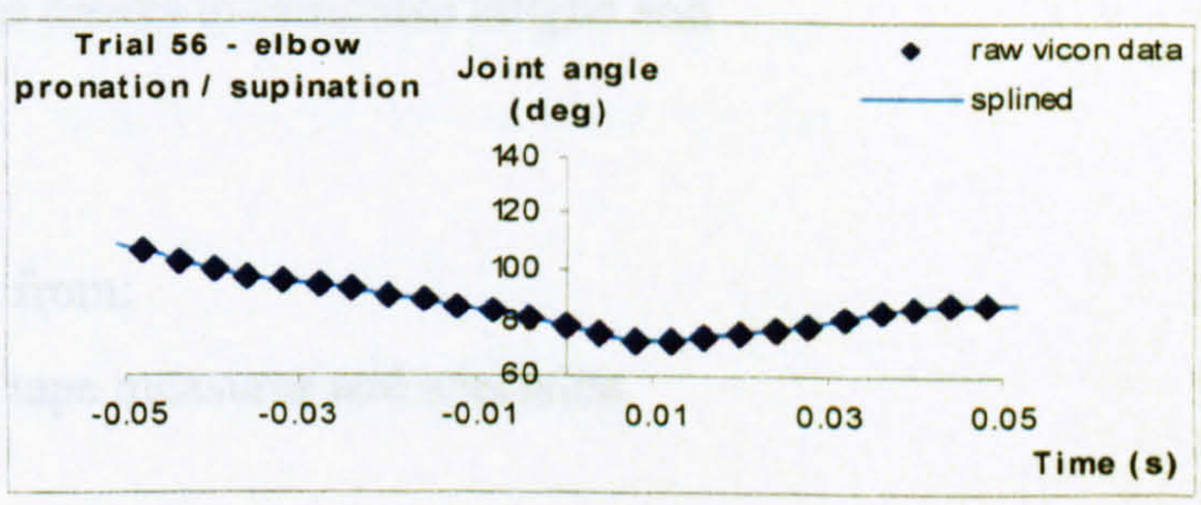

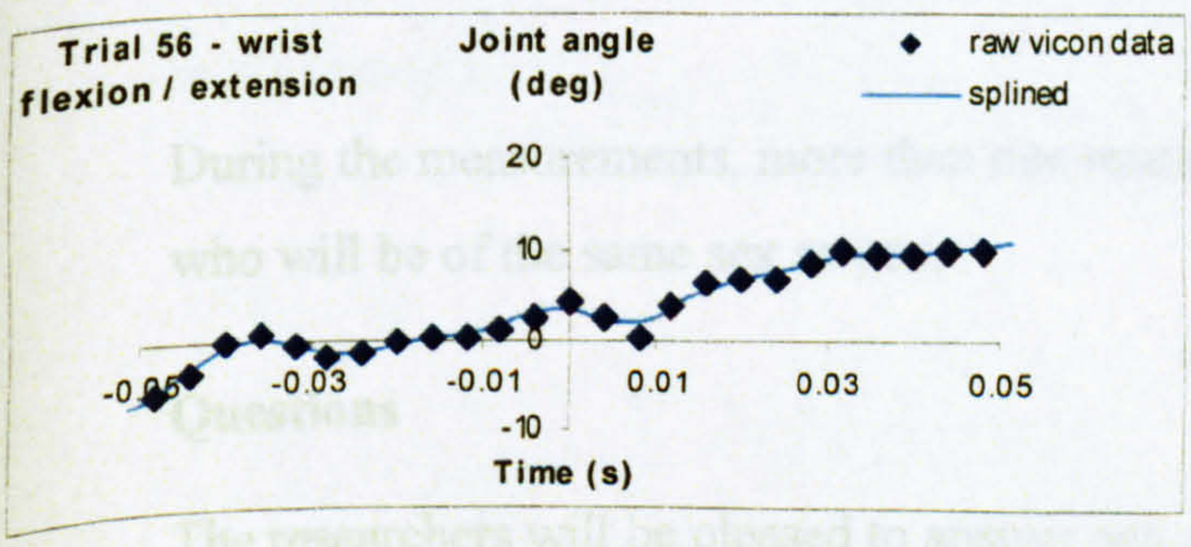

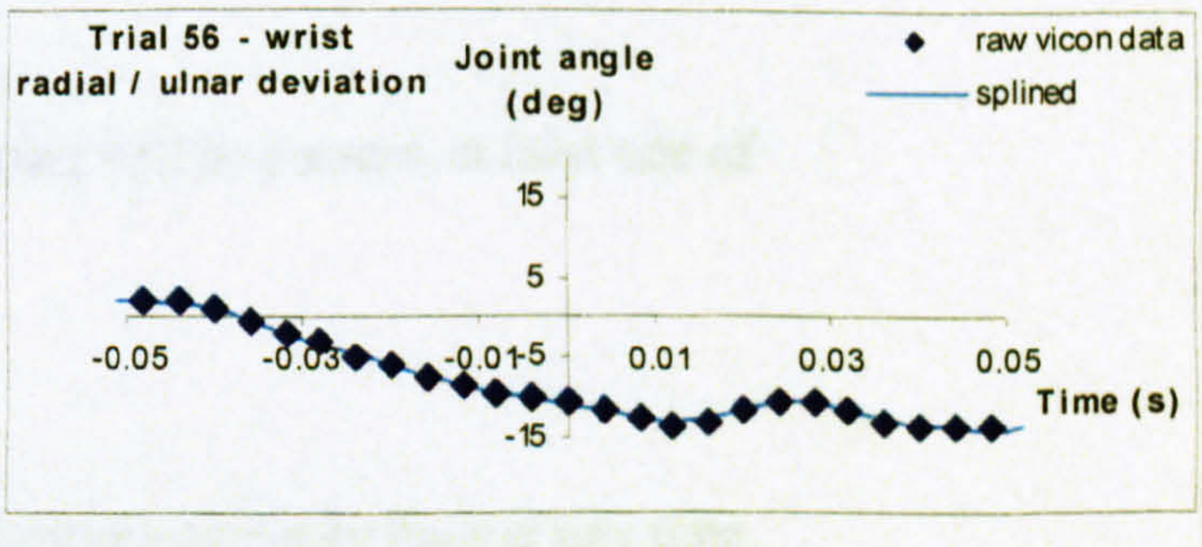

APPENDIX 4

SUBJECT INFORMED CONSENT

Purpose

To obtain kinematic, kinetic and EMG data during the performance of selected tennis backhand strokes. To obtain subject specific inertia, body composition and joint torque parameters.

Procedures

The kinematic, kinetic and EMG data of the tennis backhand strokes will be obtained using:

- An automatic data collection system and two high-speed video cameras
- Tennis rackets instrumented with accelerometers and grip pressure sensors
- EMG data using surface electrodes attached to the arm holding the racket

A number of trials will be requested with suitable breaks to minimise fatigue and boredom.

The subject specific parameters will be obtained from:

- Anthropometric measurements (using tape measures and specialist anthropometers)
- Body composition measurements (using skinfold callipers)
- Joint torque profiles (using an isovelocity dynamometer)

During the measurements, more than one researcher will be present, at least one of who will be of the same sex as you.

Questions

The researchers will be pleased to answer any questions you may have at any time.

Withdrawal

You are free to withdraw from the study at any stage without having to give any reasons.

Confidentiality

Your identity will remain confidential in any material resulting from this work. Video recordings will be stored in the video analysis room to which access is restricted to members of the biomechanics research team. On occasion video images may be required. In such an instance we will seek your written permission to use such images and you are perfectly free to decline. Video recordings will be kept for three years after publication of the study.

I have read the outline of the procedures that are involved in this study, and I understand what will be required by me. I have had the opportunity to ask for further information and for clarification of the demands of each of the procedures and understand what is entailed. I am aware that I have the right to withdraw from the study at any time with no obligation to give reasons for my decision. As far as I am aware I do not have any injury or infirmity, which would be affected by the procedures outlined.

Name .....

Signed .....(subject) Date.....

In the presence of: Name .....

APPENDIX 5

ANTHROPOMETRIC MEASUREMENTS FOR SEGMENTAL INERTIA PARAMETERS

NAME Jim May AGE 22 DATE 14/05/04

All measurements in millimetres

TORSO

Level	hip	umbilicus	ribcage	nipple	shoulder	neck	→	nose	ear	top
Length	0	173	221	403	549	620	0	73	139	246
Perimeter	946	840	815	910		380		476	586	
Width	348	296	296	319	350					
Depth					181					

LEFT ARM

Level	shoulder	midarm	elbow	forearm	wrist	→	thumb	knuckle	nails
Length	0		308	376	587	0	52	94	186
Perimeter	367	272	262	260	179		253	205	101
Width					62		105	85	47

RIGHT ARM

Level	shoulder	midarm	elbow	forearm	wrist	→	thumb	knuckle	nails
Length	0		289	371	585	0	52	91	185
Perimeter	375	272	265	281	171		261	215	105
Width					64		109	87	49

LEFT LEG

Level	hip	crotch	midthigh	knee	calf	ankle	→	heel	arch	ball	nails
Length	0	80		451	643	912	0	33		155	231
Perimeter		558	488	364	378	233		325	252	247	134
Width										102	61
Depth								129			

RIGHT LEG

Level	hip	crotch	midthigh	knee	calf	ankle	→	heel	arch	ball	nails
Length	0	78		461	655	919	0	34		152	234
Perimeter		555	480	361	359	229		324	248	238	148
Width										100	63
Depth								131			

Height (mm) 1860 Weight (N) 740.7